Stationary Properties and Dynamical Response of One-Dimensional Multi-Component Quantum Droplets

Dissertation

zur Erlangung des Doktorgrades

an der Fakultät für Mathematik,Informatik und Naturwissenschaften,

Fachbereich Physik

der Universität Hamburg

vorgelegt von

Ilias ENGLEZOS

geboren am 03.11.1994 in Athen

Hamburg
2026

Gutachter/innen der Dissertation:	Prof. Dr. Peter Schmelcher Prof. Dr. Konstantinos Nikolopoulos
Zusammensetzung der Prüfungskommission:	Prof. Dr. Michael Potthoff Prof. Dr. Peter Schmelcher Prof. Dr. Konstantinos Nikolopoulos Prof. Dr. Henning Moritz Dr. Thore Posske
Vorsitzende der Prüfungskommission:	Prof. Dr. Michael Potthoff
Datum der Disputation:	18/06/2026
Vorsitzender Fach-Promotionsausschusses PHYSIK:	Prof. Dr. Johannes Haller
Leiter des Fachbereichs PHYSIK:	Prof. Dr. Markus Drescher
Dekan der Fakultät MIN:	Prof. Dr.-Ing. Norbert Ritter

"Rest is not idleness, and to lie sometimes on the grass under trees on a summer's day, listening to the murmur of the water, or watching the clouds float across the sky, is by no means a waste of time. "

- John Lubbock, 1st Baron Avebury

To my family...

Abstract

Ultracold atomic gases provide versatile platforms for exploring quantum many-body (MB) phenomena, while offering an unprecedented level of control of the external geometry, inter-atomic interactions and number of particles. In particular, several fundamental aspects of quantum MB physics such as collective excitations, correlation effects in both the ground state and non-equilibrium dynamics, as well as dimensional crossovers and quantum phase transitions, can be cleanly induced and observed in the laboratory. From the theoretical side, understanding these phenomena and novel correlated phases of matter beyond the standard Mean-Field (MF) approach, is a formidable task.

The present cumulative thesis aims to contribute to the understanding of the influence of quantum fluctuations in weakly interacting bosonic mixtures, by studying the recently discovered self-bound quantum droplets in one spatial dimension (1D). They are studied in terms of their ground state configurations and in terms of their dynamical response following a quench. To this end, a combination of numerical and analytical techniques is employed. The time-dependent MB Schrödinger equation is numerically solved utilizing the sophisticated *ab-initio* method: Multi-Layer Multi-Configuration Time-Dependent Hartree Method for Atomic Mixtures (ML-MCTDHX). Moreover, the perturbative Bogoliubov theory is employed to derive analytical results. Finally, effective models which provide qualitative and quantitative insights into the observed phenomenology are derived and their predictions are compared to suitable numerical simulations.

The first part of this thesis is focused on exact numerical simulations of the ground state and non-equilibrium quantum dynamics of 1D two-component bosonic mixtures, using the ML-MCTDHX approach, in regimes slightly outside the formal validity region of the standard Lee-Huang-Yang (LHY) theory for quantum droplets. Namely, a weak harmonic trap is imposed to emulate usual experimental conditions and test the robustness of droplet configurations beyond flat geometries. Indeed, droplet configurations are revealed to persist in both homonuclear and heteronuclear settings, while characteristic patterns are found in higher-order observables such as their two-body correlation functions and inter-component entanglement. Quenches of the position and frequency of the harmonic trap result in a dipole motion independent of the system parameters and an interaction-dependent breathing mode respectively. The latter leads to delocalization characterized by enhanced inter-component entanglement and long-range two-body intra-component correlations, as well as correlation-induced dephasing for species selective quenches. Moreover, droplet configurations of the bath were found to persist also in highly particle imbalanced mixtures, while their phenomenology was shown to be adequately explained by an effective model derived within the context of the LHY theory. Interestingly, this particle imbalanced setting exhibits droplet to soliton transitions, while it

indicates a strong connection between the phenomenology of quantum droplets and that of few interacting impurities.

The second part of this thesis is devoted on the analytical derivation, and subsequent study, of the equations of motion for multi-component 1D droplets, which are valid across the entire MF stability regime. Motivated by the robustness of the LHY phenomenology, in regimes where the theory is not formally valid as discussed in the first part of this thesis, the perturbative Bogoliubov theory for 1D bosonic mixtures was applied, while focusing on requiring minimal assumptions. This allowed the derivation of the LHY energy and generalized extended Gross-Pitaevskii Equations (eGPEs) for quantum droplets consisting of two, three, and four components. The original eGPEs for two-component droplets were shown to be obtained from these new exact equations as the first order approximation at the edges of the MF stability regime. For repulsive interactions a previously unseen early onset of phase-separation was found to occur for both homonuclear and heteronuclear two-component mixtures. The investigation was thereafter concentrated on three-component particle imbalanced settings, revealing a multitude of mixed droplet configurations characterized also by distinct elementary excitation spectra.

Zusammenfassung

Ultrakalte atomare Gase bieten vielseitige Plattformen zur Erforschung quantenmechanischer Vielteilchenphänomene (MB) und ermöglichen dabei ein bislang unerreichtes Maß an Kontrolle über die äußere Geometrie, die zwischenatomaren Wechselwirkungen und die Teilchenzahl. Insbesondere lassen sich mehrere grundlegende Aspekte der quantenmechanischen Vielteilchenphysik — wie kollektive Anregungen, Korrelationseffekte sowohl im Grundzustand als auch in Nichtgleichgewichtsdynamiken, sowie dimensionsabhängige Übergänge und Quantenphasenübergänge — im Labor sauber erzeugen und beobachten. Auf theoretischer Seite stellt das Verständnis dieser Phänomene und neuartiger korrelierter Materiezustände jenseits des Standard-Mean-Field-(MF)-Ansatzes eine anspruchsvolle Aufgabe dar.

Die vorliegende kumulative Dissertation zielt darauf ab, zum Verständnis des Einflusses quantenmechanischer Fluktuationen in schwach wechselwirkenden bosonischen Mischungen beizutragen, indem die kürzlich entdeckten selbstgebundenen Quantentröpfchen in einer räumlichen Dimension (1D) untersucht werden. Sie werden sowohl hinsichtlich ihrer Grundzustandskonfigurationen als auch bezüglich ihrer dynamischen Antwort nach einem Quench analysiert. Zu diesem Zweck wird eine Kombination numerischer und analytischer Methoden eingesetzt. Die zeitabhängige Vielteilchen-Schrödinger-Gleichung wird numerisch mithilfe der hochentwickelten ab-initio-Methode Multi-Layer Multi-Configuration Time-Dependent Hartree for Atomic Mixtures (ML-MCTDHX) gelöst. Darüber hinaus wird die perturbative Bogoliubov-Theorie verwendet, um analytische Ergebnisse abzuleiten. Schließlich werden effektive Modelle entwickelt, die qualitative und quantitative Einblicke in die beobachtete Phänomenologie liefern, und deren Vorhersagen werden mit geeigneten numerischen Simulationen verglichen.

Der erste Teil dieser Dissertation konzentriert sich auf exakte numerische Simulationen des Grundzustands und der Nichtgleichgewichts-Quantendynamik von 1D-Zweikomponenten-Bosonenmischungen mithilfe des ML-MCTDHX-Ansatzes, in Bereichen, die leicht außerhalb des formalen Gültigkeitsbereichs der Standard-Lee-Huang-Yang-(LHY)-Theorie für Quantentröpfchen liegen. Es wird insbesondere eine schwache harmonische Falle eingeführt, um typische experimentelle Bedingungen zu emulieren und die Robustheit von Tröpfchenkonfigurationen jenseits flacher Geometrien zu testen. Tatsächlich zeigt sich, dass Tröpfchenkonfigurationen sowohl in homonuklearen als auch in heteronuklearen Systemen bestehen bleiben, während charakteristische Muster in höhergeordneten Observablen wie Zwei -Teilchen - Korrelationsfunktionen und der Verschränkung zwischen den Komponenten auftreten. Quenches der Position bzw. Frequenz der harmonischen Falle führen zu einer Dipolbewegung, die unabhängig von den Systemparametern ist, bzw. zu einem wechselwirkungsabhängigen Atmungsmodus. Letzterer führt zu einer Delokalisierung, die sich durch verstärkte interkomponentielle Verschränkung und langreichweitige Zwei - Teilchen - Intra - Komponenten - Korrelationen auszeichnet, sowie zu korrelationsinduziertem

Dephasing bei komponentenselektiven Quenches. Zudem wurde festgestellt, dass Tröpfchenkonfigurationen des Bades auch in stark teilchenungleichgewichtigen Mischungen bestehen bleiben, während ihre Phänomenologie durch ein innerhalb der LHY-Theorie abgeleitetes effektives Modell hinreichend erklärt werden kann. Interessanterweise zeigt dieses Szenario mit Teilchen-Ungleichgewicht Übergänge von Tröpfchen zu Solitonen, was auf eine enge Verbindung zwischen der Phänomenologie von Quantentröpfchen und der von wenigen wechselwirkenden Verunreinigungen hinweist.

Der zweite Teil dieser Dissertation widmet sich der analytischen Herleitung und anschließenden Untersuchung der Bewegungsgleichungen für mehrkomponentige 1D-Tröpfchen, die im gesamten MF - Stabilitätsbereich gültig sind. Motiviert durch die Robustheit der LHY-Phänomenologie in Bereichen, in denen die Theorie formal nicht gültig ist — wie im ersten Teil diskutiert — wurde die perturbative Bogoliubov - Theorie für 1D - bosonische Mischungen angewandt, wobei der Fokus auf minimalen Annahmen lag. Dies ermöglichte die Herleitung der LHY-Energie und verallgemeinerter erweiterter Gross - Pitaevskii - Gleichungen (eGPEs) für Quantentröpfchen bestehend aus zwei, drei und vier Komponenten. Es wurde gezeigt, dass die ursprünglichen eGPEs für zweikomponentige Tröpfchen als erste Ordnungsnäherung dieser neuen exakten Gleichungen an den Rändern des MF - Stabilitätsbereichs erhalten werden. Für repulsive Wechselwirkungen wurde ein zuvor nicht beobachteter, frühzeitiger Beginn der Phasentrennung festgestellt, der sowohl bei homonuklearen als auch bei heteronuklearen Zweikomponenten-Mischungen auftritt. Die Untersuchung konzentrierte sich anschließend auf dreikomponentige, teilchenungleichgewichtige Systeme, in denen eine Vielzahl gemischter Tröpfchenkonfigurationen mit jeweils unterschiedlichen Spektren elementarer Anregungen aufgedeckt wurde.

Contents

List of Figures

List of Abbreviations

BEC	**B**ose **E**instein **C**ondensate
MF	**M**ean **F**ield
MB	**M**any **B**ody
GPE	**G**ross-**P**itaevskii Equation
eGPE	**e**xtended **G**ross-**P**itaevskii Equation
LHY	**L**ee-**H**uang-**Y**ang
BdG	**B**ogoliubov **d**e **G**ennes
MCTDH	**M**ulti-**C**onfiguration **T**ime-**D**epetended **H**artree
MCTDHB	**M**ulti-**C**onfiguration **T**ime-**D**epetended **H**artree for **B**osons
MCTDHF	**M**ulti-**C**onfiguration **T**ime-**D**epetended **H**artree for **F**ermions
ML-MCTDH	**M**ulti **L**ayer **M**ulti-**C**onfiguration **T**ime-**D**ependent **H**artree
ML-MCTDHX	**M**ulti **L**ayer **M**ulti-**C**onfiguration **T**ime-**D**ependent **H**artree for atomic mi**X**tures
DMRG	**D**ensity **M**atrix **R**enormalization **G**roup
1D	**1 D**imensional or **1 D**imension
2D	**2 D**imensional or **2 D**imension
3D	**3 D**imensional or **3 D**imension
FT	**F**lat **T**op

Physical Constants

Plank's constant	$h = 6.626\,070\,15 \times 10^{-34}\,\mathrm{J\,s}$
Reduced Plank's constant	$\hbar = 1.054\,571\,817 \times 10^{-34}\,\mathrm{J\,s}$
Boltzmann constant	$k_B = 1.380\,649 \times 10^{-23}\,\mathrm{J\,K^{-1}}$
Bohr radius	$a_0 = 5.291\,772\,105\,44(82) \times 10^{-11}\,\mathrm{m}$
Speed of Light	$c_0 = 2.997\,924\,58 \times 10^{8}\,\mathrm{m\,s^{-1}}$

Preface

The present cumulative thesis is based on the following publications:

Publications covered by this thesis

[IE1] I. A. Englezos, S. I. Mistakidis, and P. Schmelcher, Phys. Rev. A **107**, 023320 (2023).

[IE2] I. A. Englezos, P. Schmelcher, and S. I. Mistakidis, Phys. Rev. A **110**, 023324 (2024).

[IE3] I. A. Englezos, P. Schmelcher, and S. I. Mistakidis, SciPost Phys. **19**, 133 (2025).

[IE4] I. A. Englezos, E. G. Charalampidis, P. Schmelcher, and S. I. Mistakidis, arxiv: 2601.04950 (Submitted to PRA), 10.48550/arXiv.2601.04950 (2026).

Note that the reference indices [IE1–IE4] employed in this thesis refer to the above publications. Additional publications not covered in this thesis are indicated by indices [E1, E2].

Outline of this thesis

Chapter 1 provides a brief but general overview to the field of ultracold atomic gases. It focuses primarily on bosonic gases, their correlation or entanglement properties and their dynamical response. Collective phenomena emerging in interacting bosonic gases and mixtures, as a consequence of their correlation properties are addressed. A particular emphasis is placed on one-dimensional settings where correlation effects are generally enhanced. The topic of impurities immersed in a macroscopic or messoscopic ultracold many-body bosonic system is also briefly discussed. In Chapter 2, the necessary theoretical background regarding the settings, concepts and techniques employed in the ensuing scientific contributions is provided. In particular, the main techniques employed to cool, confine, and control the atoms in order to realize the systems which are theoretically investigated in the scientific contributions are briefly summarized. Some key elements of scattering theory at low energy, or equivalently low temperature, are presented. Subsequently, a brief summary of the mean-field theory is given. Then, the perturbative extension to the mean-field theory, which captures the impact of quantum fluctuation to first order, known as the Lee-Huang-Yang correction, which is a central theme of the present

thesis, is presented. The chapter concludes with a short introduction to the *ab initio* many-body variational method employed in some of the scientific contributions included in this thesis. In Chapter 3, details are provided regarding every scientific contribution, summarizing the key questions being addressed, as well as outlining the main results. In the next chapter (Chapter 4), the scientific contributions [[IE1]-[IE4]] are provided in their published format. Finally, Chapter 5 briefly outlines the main results and conclusions stemming from all the scientific contributions covered by this thesis, offering also some suggestions for future extensions.

Declaration of Personal Contributions to the Publications

The project [IE1] has been conceptualized by Dr. Simeon I. Mistakidis. I have carried out all analytical and numerical computations. Template scripts to assist with some of the data analysis and simulations were developed by Dr. Simeon I. Mistakidis and adapted or extended by me as needed. Together with Dr. Simeon I. Mistakidis we interpreted the results and decided on the optimal way to present them. The first draft of this work was written by myself and was subsequently substantially optimized and rewritten by Dr. Simeon I. Mistakidis. Prof. Dr. Peter Schmelcher supervised the project and offered helpful comments towards the interpretation and final presentation of the results.

The project [IE2] was conceptualized by Dr. Simeon I. Mistakidis and myself based on our discussions regarding the insights obtained from our previous work and on the observations drawn from the initial results. Dr. Simeon I. Mistakidis developed the code for the extension to fermionic impurities. I have written the rest of the necessary code and performed the analytical and numerical calculations. The first draft was written by myself. Dr. Simeon I. Mistakidis substantially improved and partially rewrote it. Prof. Dr. Peter Schmelcher contributed in the discussion while supervising the project and added helpful remarks for the improvement of the manuscript.

The project on the extension of the standard Lee-Huang-Yang theory to multi-component mixtures and unconstrained inter-component interactions [IE3] has been conceptualized by myself. I have written all the necessary code and performed all the analytical and numerical calculations. The interpretations of the results was conducted by Dr. Simeon I. Mistakidis and myself. Dr. Simeon I. Mistakidis and I also decided on the best way to present our results. The first draft was written by myself, while Dr. Simeon I. Mistakidis significantly improved the presentation and partially rewrote the text. Prof. Dr. Peter Schmelcher also contributed to the improvement of the manuscript and supervised the project.

The project on particle imbalanced three-component droplets [IE4] was conceptualized by Dr. Simeon I. Mistakidis and Dr. E. G. Charalampidis, based also on the effective model approach developed in [IE2]. The code and analytical calculations

required for the implementation of the Newton method was done by Dr. E. G. Charalampidis. Dr. E. G. Charalampidis and myself derived the BdG equations for the three-component droplet. The analytical derivations and the codes for the effective model were done by myself. I have carried out all numerical computations to obtain, analyze, and visualize the data included in the manuscript. I wrote the first draft. Dr. Simeon I. Mistakidis and Dr. E. G. Charalampidis significantly improved the presentation and rewrote parts of the text. Prof. Dr. Peter Schmelcher supervised the project and offered useful comments to improve the manuscript.

Further List of Publications

[E1] A. Katsaris, I. A. Englezos, C. Weitenberg, F. K. Diakonos, and P. Schmelcher, Phys. Rev. A **110**, 013316 (2024).

[E2] A. Katsaris, I. A. Englezos, C. Weitenberg, F. K. Diakonos, and P. Schmelcher, arxiv: 2602.04395 (Submitted to PRA), 10.48550/arXiv.2602.04395 (2026).

Chapter 1

Introduction

Ultracold bosonic gases have become the paradigmatic engineered quantum system, ever since the first realization of Bose-Einstein Condensate (BEC) [1–3], which was soon followed by the direct observation of Fermi degeneracy [4, 5]. These pioneering achievements, along with subsequent successes, were the culmination of the constantly improving techniques for loading [6–18], cooling [19–22], imaging [23, 24] and controlling atomic gases, leading to the establishment of the field of ultracold quantum gases [25, 26]. These advances in experimental techniques have made it possible to control a plethora of parameters, resulting in pristine configurations [27–30]. One particularly key aspect is the capability to precisely tune both the sign and the strength of interparticle interactions by exploiting magnetic, optical or confinement-induced Fano-Feshbach resonances [31–35]. Interatomic interactions enable the development of entanglement in the system leading to novel inherently quantum phases, as well as playing a crucial role in the formation of few-body bound states [36, 37], recombination processes [38], Cooper pairing [39], and superfluidity [40, 41].

Utilizing optical techniques, arbitrary potential landscapes can be designed and even dynamically controlled in a time-dependent manner [25, 30, 42]. Such optical potentials have enabled, for instance, the observation of the superfluid–Mott insulator transition in a Bose gas [43, 44] in optical lattices [45]. In addition, they also provide access to few-body physics [46–50], by controlling the atom number confined in them, along with optical tweezers and arrays [51, 52] which can confine single atoms or molecular states [53, 54]. This level of control has provided, for example, access to the study of complex discrete geometries such as those exhibiting topological phases [55–57]. Moreover, the use of artificial dimensions stemming from internal states of single atoms can also be achieved [58–62], granting further access to genuinely discrete degrees of freedom. Finally, different trapping frequencies along each of the three spatial dimensions can be generated, enabling highly anisotropic configurations, where the atoms are kinematically constrained in two or one spatial direction [63–65]. Thus, low dimensional ultracold quantum systems can be realized, giving rise to novel phases and further enabling the emergence of strong correlations [66–68].

As the field continued to rapidly evolve and mature, the first realizations of single - component BECs were quickly followed by explorations of systems composed of multiple atomic elements or internal states. These mixtures opened the door to a far richer landscape of interactions, phases, and dynamical phenomena than could be accessed with a single component alone [69]. In particular, bose-bose mixtures [70–74] and bose-fermi [75] mixtures have been realized. Fermionic mixtures of different spin states have enabled the observation of the BEC–BCS crossover in Fermi gases [76, 77]. These significant advantages lead to the establishment of a multitude of intriguing phenomena such as the development of phase separation in repulsively interacting components [78–80], the emergence of solitonic [81–89] and vortex [90–92] states, including exotic configurations such as Peregrine [93] or symbiotic solitons [94]. At the same time, questions such as the impact of intercomponent entanglement [95–102] and bound state formation [103–110] became increasingly relevant in the study of these mixtures. Moreover, dipolar quantum gases involving magnetic atoms can be realized enabling, for example, the study [111, 112] of exotic phases of matter such as droplets [113] and supersolids [114]. Additionally, electrically polarized settings using Rydberg [115, 116] or molecular states [117, 118], featuring enhanced long-range interactions, have been observed [119].

The above - mentioned characteristics make systems of ultracold atoms powerful quantum many-body platforms for simulating diverse physical phenomena. Indeed, various systems inspired from the fields of condensed matter physics [29, 120], high energy physics [121–124], or quantum information and computation theory [53, 125–128] can be emulated in the laboratory. Beyond the ideal quantum gas limit, interactions between the atoms give rise to correlated quantum many-body states, which can be designed and experimentally prepared [29], allowing us to probe novel phenomena and even new phases of matter. Developing a deeper understanding of these correlated quantum systems is of central importance, both from the perspective of fundamental research and in the pursuit of applications relying on engineered quantum properties [27–29]. From the theoretical side, many of the phenomena occurring in ultracold atomic gases can be described by the so-called Mean-Field (MF) approximation [or the Hartree-Fock approach for fermions], which entirely neglects the correlations present in the system [25, 26]. In spite of its simplicity, the MF approach is often adequate in describing observables at the single-particle level including, for instance, non-linear excitations in the form of solitary waves and vortices [83, 85], although it obviously cannot predict higher order observables such as correlation functions [44, 129–131]. However, there are cases where the MF approach fails even for the lower-order observables and the system exhibits not only quantitative differences but also a qualitatively distinct behavior.

These cases usually refer to the strong interaction regime where correlation effects are enhanced. An early characteristic example is the Tonks-Girardeau gas, which occurs for strongly repulsive interactions in one-dimensional (1D) single-component

gases [67, 132, 133]. In this interaction regime, bosons behave similarly to fermions in their spatial profile (not in their momentum space representation however [134]), preferring to minimize their spatial overlap. This phenomenon was later extended to the strongly attractive case, realizing the so called super-Tonks-Girardeau phase [68, 135]. Prototypical examples of correlated many-body states naturally emerging even in weakly interacting gases are quasiparticles such as polarons [136–138] and macroscopic structures such as self-bound quantum droplets [113, 139–142]. The experimental observation of Bose [143–147] and Fermi polarons [148–150] highlighted the important role of correlations in these systems, spawning significant theoretical interest [151, 152] in the investigation of correlation effects in the stationary [153–157] as well as the out-of-equilibrium quantum dynamics [158–161] of quasiparticles.

On the other hand, self-bound quantum droplets, which constitute the main focus of this thesis and are addressed with various approaches in [IE1–IE4], have in particular gained a lot of interest, as they were quickly found to host a wide range of novel phenomenology [141, 142]. Interestingly, quantum droplets were first predicted to emerge in two-component bosonic mixtures, with contact interactions in three-dimensions [139] and soon extended to the corresponding 2D and 1D systems [162]. However, they were essentially simultaneously and independently discovered experimentally in a single-component dipolar gas of dysprosium (^{164}Dy) atoms [113]. In both settings the formation of quantum droplets stems from a conceptually similar mechanism, albeit the underlying systems have significant differences. Namely, droplet states manifest when quantum fluctuations, accounted to first order by the Lee-Huang-Yang (LHY) correction term [163], stabilize the system against wave collapse originating from mean-field interaction effects [139, 164]. In both contact interacting and dipolar gases in 3D this is owed to the repulsive nature of the LHY contribution, allowing the system to remain stable in parametric regions where attractive interactions would lead the system to collapse within the MF framework [25]. In the case of contact interacting bosonic mixtures, this instability refers to the so-called MF collapse, occurring when the intercomponent attraction overcomes the intracomponent repulsion [25, 139]. Instead, for dipolar bosonic gases, the instability refers to the roton instability which occurs when the long range dipolar attraction overcomes the short-range repulsion between the atoms [25, 113, 165]. It is important to emphasize that, although the phenomenology is conceptually similar, the LHY correction is not identical in each case [139, 164]. In addition, the differences in the underlying instability mechanisms have profound consequences such as the emergence of supersolid or more involved mixed states in dipolar gases, owing to the interplay between the length-scales of the confinement and the long-range dipolar interaction [114, 119, 140].

For completeness, it is worth to mention that droplet states can also emerge in two-component mixtures involving dipolar gases [166, 167]. Additionally, theoretical studies have proposed droplet structures emerging in Bose-Fermi mixtures, both

with [168] and without spin-orbit coupling [169, 170]. Interestingly, other theoretical works, aiming to explore beyond standard MF phenomenology, have also suggested that droplet states may occur in the presence of three-body interactions [171, 172]. Overall, quantum droplets and related LHY structures have emerged as rather general and ubiquitous states in the field of weakly interacting bosonic gases, which manifest quantum fluctuations at macroscopic systems.

Focusing on short-range interacting bosonic mixtures, experimental observation of quantum droplets soon followed their theoretical proposal [173–175]. Quantum droplets were confirmed to exhibit features of a dilute liquid - like state [139]. A characteristic feature, associated with their presence, is the development of a flat-top (FT) profile in their spatial density configuration. In three dimensions, this quantum liquid character can be understood in terms of their surface tension [139, 176] and incompressibility [177]. However, further study of 3D droplets, and in particular their dynamical response, is hindered by their three-body losses, which crucially reduces their lifetime [139, 178]. These three-body losses are expected to be significantly suppressed in one-dimensional systems [162, 179–182]. Hence, one-dimensional configurations, which are the main focus of this thesis, provide an ideal setting to explore long lived and stable quantum droplets.

The majority of early investigations on quantum droplets were focused on studying them, within the perturbative LHY treatment, via the corresponding coupled set of extended Gross-Pitaevskii equations (eGPEs) for each component [139, 141, 142]. Moreover, it is common to impose a fixed ratio condition between the densities of the two components determined by their intracomponent interaction strengths. The reason for this condition is twofold. Namely under this condition, 3D droplets tend to be more stable [139, 183], while the two-component setting reduces to an effective single-component description simplifying their treatment. In [IE1, IE2], we aim to provide further insight on both the genuinely two-component nature of 1D quantum droplets and on the beyond MF features of quantum droplets. To this end, the two-component mixture is investigated with an *ab-initio* many-body method, namely the Multi-Layer Multi-Configuration Time-Dependent Hartree Method for Atomic Mixtures (ML-MCTDHX). In addition, intercomponent imbalance violating the fixed density ratio condition is imposed with respect to the interaction strengths, the mass ratio between the atoms in each component, and the number of particles in each component. We note also that, at the time, the LHY treatment and resulting eGPEs for heteronuclear 1D droplets had not been reported in the literature, making them addressable only via *ab-initio* methods [184]. The correlation properties of quantum droplets are investigated for a wide range of system parameters. Furthermore, it is shown that the emergence of quantum droplets remains robust, in-spite of quantitative differences, also under harmonic confinement where the LHY theory is not formally valid. Moreover, their dynamical response to quenches of the external geometry is demonstrated. Finally, intriguing phases where droplet and soliton

structures can coexist are unveiled in the presence of significant particle imbalance.

The effective single-component description has also been studied from an *ab-initio* perspective [184–186] in order to benchmark the LHY approach, finding excellent qualitative agreement and some quantitative differences especially for increasing interaction strength. The genuine two-component nature of quantum droplets has been addressed by employing mass imbalance in 3D systems [175, 187, 188] and in 1D systems with an ab-initio treatment [184], as well as by exploiting different intracomponent interactions and particle numbers within the 1D LHY approach [189–191]. Interestingly, an 1D system of strongly interacting lattice trapped bosonic mixtures, was shown to also host symmetric and particle imbalanced droplets, using the density matrix renormalization group (DMRG) method [192, 193]. In all cases, the 1D droplet structures were shown to be remarkably stable under the violation of the fixed density ratio condition as well as under confinement. In 3D, quantum droplets in particle imbalanced configurations were also explored [183, 194–196] within the context of the LHY theory. A somewhat extended stability region was found beyond the threshold of fixed density ratio condition, characterized also by mixed droplet-gas phases. However, the 3D system was confirmed to be primarily robust and stable when this condition is satisfied, in sharp contrast to its 1D counterpart.

These significant differences between the 3D and 1D quantum droplets demand further attention. In [IE3] we analytically explore 1D weakly interacting mixtures, aiming to derive the LHY correction for the most general system. In particular, the initial derivation of the LHY correction for the 1D system was strongly motivated by the early observations regarding 3D quantum droplets [139, 162]. However, a fundamental difference between the 3D and 1D settings becomes evident from the fact that the LHY correction is repulsive in the former systems and attractive in the latter. As a result, while 3D quantum droplets emerge only just outside the attractive MF stability threshold, where the repulsive quantum fluctuations can stabilize the collapsing gas, in 1D this restriction is found to be unnecessary and droplet states are found to exist throughout the MF stability regime. Removing this assumption yields quantitative corrections from the original derivation in the effective single-component description, and qualitative differences in the presence of intercomponent imbalance giving rise to mixed droplet phases and an early onset of phase separation. Moreover, the derivation of the LHY correction is extended to three- and four-component 1D mixtures, the latter being the maximum number of components which allow an analytic derivation in the general case. Three- and four-component 1D mixtures are also shown to feature droplet ground state configurations, focusing primarily in the cases where the multi-component systems can be reduced to an effective single-component description. The three-component mixture was further studied in [IE4] with respect to particle imbalanced configurations and the elementary excitations they can host. Several regimes in terms of the ground state droplet configurations

and the excitation spectrum, inaccessible by lower component mixtures, were identified indicating the rich and largely still unexplored phenomenology of genuinely multi-component 1D droplets.

It is worth noting, that three-component 3D mixtures were also addressed in [197, 198] revealing distinct phases from the 1D case, such as mixed stability regimes, further highlighting the strong dependence of these many-body states on the dimensionality. The case of a single impurity immersed in a two-component droplet was also studied [199–202]. For the 1D case, the system was studied within a self consistent LHY and Fróhlich Hamiltonian framework, emphasizing the role of quasiparticles in droplet environments [202]. Moreover, early indications for a modification of the phase separation regime due to the quantum fluctuations captured by the LHY term, also referred to as bubble formation, were also found for the 3D two-component system [203]. However, due to the repulsive nature of all interaction strengths as well as the LHY term, the system required external confinement from a harmonic trap, making its treatment within the LHY framework formally invalid. Finally, the study of mixed phases in quantum droplets is rapidly receiving significant interest for example in terms of their coexistence with nonlinear soliton [204, 205] and vortex [206–210] states.

1.1 Objectives Of This Thesis

In this cumulative thesis, our main goal is to theoretically study one dimensional multi-component bosonic mixtures under the impact of quantum fluctuations, particularly in the regime of attractive inter-component interactions, where quantum droplet states are known to emerge. This is examined with two methods. First an *ab-initio* many-body method is employed to study the ground state and the dynamical response of the system following quenches of the external geometry. This allows for the characterization of higher-order observables, such as one- and two-body correlation functions or the entanglement entropy between the components of the mixture. Furthermore, insights on the formation and subsequent behavior of quantum droplets are drawn in the presence of harmonic confinement, where exact analytical treatments are lacking. Additionally, a transition between the mesoscopic regime and the few-body limit is realized on one of the two-components, evincing droplet to soliton transitions, as well as intriguing connections between droplet and polaron physics. Secondly, an analytical treatment based on the LHY framework is utilized to derive exact perturbative results for 1D bosonic mixtures of two, three, and four components, valid for both attractive and repulsive intercomponent interactions. Effective models, based on the LHY framework, are also derived to characterize the transition from particle balanced to highly particle imbalanced mixtures from the macroscopic perspective in both two- and three-component mixtures. In particular, we aim to:

- examine the existence and stability of quantum droplets in 1D harmonically trapped two-component bosonic mixtures.
- characterize the corresponding structures from many-body observables, such as their one- and two-body coherence functions.
- exploit these measures to monitor transitions, such as between droplet-like and soliton-like many body states.
- revisit and extend the LHY theory with the aim of restricting it to 1D settings under minimal assumptions.
- derive generalized LHY corrections for multi-component 1D mixtures, beyond the attractive edge of the MF stability region and the two-component mixture.
- explore the transition from a balanced droplet, to heavily particle imbalanced configurations in two- and three-component mixtures.
- extract and characterize the excitation spectrum and phases of droplets in three-component mixtures

The first three of these goals and the two-component case of the sixth goal are achieved by utilizing the Multi-Layer Multi-Configuration Time-Dependent Hartree method for atomic mixtures (ML-MCTDHX). This is an *ab-initio* variational method for tackling the ground state and importantly out-of-equilibrium dynamics of multi-component systems of bosons, fermions, or distinguishable degrees of freedom [Sec. 2.3.1]. The remaining goals rely on the application of the perturbative Bogoliubov theory to 1D mixtures, in order to analytically derive the energy corrections stemming from quantum fluctuations in the system and the corresponding extended Gross-Pitaevskii equations [Sec. 2.2.3]. These are subsequently solved with imaginary propagation, using either a finite-difference or a split operator approach to handle the kinetic terms, or with a Newton method.

Chapter 2

Theoretical Framework

2.1 Quantum Gases

Quantum gases refer to ensembles of neutral atoms cooled down to ultra-low temperatures near absolute zero (usually of the order of nanokelvin). In this regime, often termed quantum degeneracy regime, the thermal de Broglie wavelength becomes comparable to or larger than the other length scales of the system. Hence, thermal effects are almost completely suppressed and the atomic ensemble exhibits macroscopic phase coherence and quantum correlations. Cooling, confining, and controlling the atoms to this ultra-cold regime requires a combination of techniques relying on optical and magnetic effects.

In the following, we briefly present the main aspects of the experimental techniques employed to prepare ultra-cold quantum gasses in precisely tailored potentials and tune their interactions [25, 30, 119]. First we address the strongly interconnected topics of cooling and trapping neutral atoms, utilizing lasers and magnetic fields. Moreover, we highlight the ability to control the internal states of the atoms in the ensemble. Then we discuss the main elements of scattering theory at low energies, illustrating how the scattering length emerges as the crucial factor, which can be tuned via external magnetic fields.

The combination of all these techniques enables the realization of settings featuring mixtures of atomic species, either of the same element in different internal states, or of different elements, in effectively 1D geometries [50, 211]. At the same time, the population of atoms in each component of the mixture, as well as the strength and sign of their intra- and inter-component interactions, can be precisely tuned. These settings will be the starting point for the works included in this thesis.

2.1.1 Cooling and Trapping the Atoms

2.1.1.1 Laser Cooling

To cool atomic gases to the mikrokelvin temperatures, the most widely used technique is laser cooling, also known as Doppler-cooling, or "Optical Molasses" [19–

22]. A simple description of this method can be given by considering the atom in a simple two-level system, with a transition energy $\hbar\omega_0$, and velocity $\mathbf{v}$, experiencing monochromatic radiation of frequency ω and wave vector $\mathbf{k}$. In the frame of the atom, the frequency is shifted by the Doppler effect, resulting in the effective frequency $\omega' = \omega - \mathbf{kv}$. If the laser is red-detuned ($\omega < \omega_0$) the atoms moving towards the laser will see the light as closer to resonant and will have a larger probability to absorb photons, while those moving away from the laser will have a reduced probability. The absorption of the photon transfers momentum $\hbar\mathbf{k}$, while the subsequent spontaneous emission, returning the atom in the ground state, emits a photon with momentum $\hbar k$ in a random direction. The net result of this emission and absorption sequence is an average force along the direction of $\mathbf{k}$ or equivalently $-\mathbf{v}$. Adding a second, counter-propagating beam, (or three orthogonal pairs of counter propagating beams along each axis) results in a total force proportional to $-\mathbf{v}$, resembling a friction force, which reduces the kinetic energy and hence the temperature of the atoms.

Similar to friction however, this method also introduces heating in the system via the spontaneous emission, which imparts a recoil momentum to the atom at a random direction. Due to the finite lifetime τ of the excited-state, the lowest temperature that can be reached with this method is the Doppler temperature $T_D = \frac{\hbar}{2k_B\tau}$ [12]. The internal structure of real atoms is of course more complex than the simple two-level system considered here. The rich internal spectrum of the atoms can either increase the minimum temperatures reached [212–215], or even reduce it in some cases [13, 216–220] owing to polarization effects usually referred to as Sisyphus cooling[12, 216, 221]. Thus a more realistic cooling procedure requires re-pumping schemes [7, 8, 215, 222–233] to additional levels known as sub-Doppler cooling. In addition, for tight optical lattices or optical tweezers a different technique, exploiting the well resolved motional states, known as Raman sideband cooling can be employed [126, 234–238].

During the cooling process, the atoms remain in a gas phase. The target quantum degenerate phase is also gaseous in many cases, although liquid- or solid-like phases can also occur. In any case, a confining mechanism is required to trap the thermal cloud during the cooling process and in many cases to hold and manipulate the resulting ultracold quantum ensemble. The most widely used confining configuration is the Magneto-Optical Trap (MOT) [6–18]. As its name suggests, it combines magnetic and optical effects to simultaneously cool and confine the atoms. The magnetic part of its operation relies on the Zeeman effect, which causes a spatially dependent shift to the atomic energy levels in the presence of a (usually weak) magnetic field gradient. The Zeeman effect creates a trapping potential experienced by the atoms, however it is usually rather shallow. To enhance the trapping effect, the MOT combines the magnetic Zeeman effect with the optical means, namely the radiation pressure already discussed in the context of cooling. The Zeeman shift further enhances

the preferential absorption of (red-detuned) photons propagating opposite to the velocity of the atoms, resulting in an approximately harmonic potential experienced by the atoms while also cooling them via the Doppler effect. As in the case of laser cooling, pairs of counter-propagating beams along each axis are combined to realize a 3D MOT, as well as pairs of quadrupole coils in the plane orthogonal to the direction of the thermal atomic beam. Moreover, a single near resonant laser beam directed opposite to the propagation direction of the thermal atomic beam, combined with a linearly decreasing magnetic field $B = B_0 - bx$ along the same direction can be employed to initially slow the atoms and facilitate capture in the MOT [20, 239]. This configuration is called the Zeeman slower, where the Zeeman shift compensates for the reducing Doppler shift as the atoms lose their velocity improving efficiency.

2.1.1.2 Trapping Techniques

Magnetic traps were integral in the first realizations of BEC [1–3, 119, 240–243]. However, they are also burdened by certain challenges and limitations. These limitations can often be counterbalanced, at least in part, by various smart solutions making the study and development of magnetic traps a paradigmatic case-study in problem solving. One important limitation is on the maximum densities they are able to effectively confine, owing to the outward pressure stemming from the spontaneous emission from the atoms. For high enough densities, this pressure can balance the trapping force preventing further density increase. One way to overcome this issue, called dark spontaneous-force optical trap (SPOT), is to pump atoms in the center of the MOT to a so called dark state, which suppresses the outward radiation pressure [244, 245]. A more foundational limitation, is that only atoms possessing a permanent magnetic dipole moment (μ) can be trapped in a static, spatially dependent, magnetic field $\mathbf{B}(\mathbf{r})$. Most atoms exhibit relatively weak magnetic dipole moments, which in combination with the difficulty in creating strong magnetic fields, results in rather shallow trap configurations. However, certain atomic species such as *Dy* or *Er* posses appreciable magnetic dipole moments making them ideal for magnetic trapping.

A further limitation, stems from the magnetic Earnshaw's theorem stating that a local maximum of the magnetic field cannot be created in free space using only static magnetic fields. Considering a magnetic field along the z-axis $\mathbf{B}(\mathbf{r}) = B_z\hat{\mathbf{z}}$, an atom with magnetic dipole moment $\mu = -\mu_B \mathrm{g}\mathbf{F}/\hbar$, where μ_B the Bohr magneton, g the gyromagnetic moment, and $\mathbf{F}$ the total angular momentum of the atom, experiences an energy contribution $H_B = -\mu\mathbf{B}(\mathbf{r}) = \mu_B \mathrm{g}\mathrm{F}_z\mathrm{B}_z/\hbar$ from its interaction with the magnetic field. This means that only states with $\mathrm{gF}_z > 0$ can be confined by a minimum in the magnetic field, hence termed low-field seeking states, while high-field seeking states ($\mathrm{gF}_z < 0$) are expelled from the trap [246]. Compounding the issue, if the minimum of the magnetic field at the trap center is $B = 0$, then the atom can undergo a so-called Majorana spin-flip, transforming into a high-field seeking state

and becoming expelled from the trap [242, 247]. The most common magnetic trap configuration is the quadrupole trap, which indeed creates a magnetic field which vanishes at the center, making it vulnerable to Majorana spin-flip loses. To mitigate these losses, a common strategy is to "plug the hole" using a repulsive optical potential at the center of the trap to prevent the atoms from reaching the problematic low-field region. Another solution is to implement an Ioffe-Pritchard trap or its many variances [241, 248–251], which produces a non-vanishing magnetic field minimum at the trap center. Finally, another solution is to combat the magnetic Earnshaw's theorem directly, by employing time-dependent magnetic fields [1, 252].

An exciting advancement in recent years has been the staggering improvement in laser technology, and correspondingly in the optical techniques, which can be employed to produce highly versatile and controllable optical potential landscapes. The main building blocks of these optical dipole traps are again the two level system and the external field it responds to, which is now the electric field inducing an AC Stark shift to the atom, similar to the magnetic fields causing a Zeeman shift in the magnetic traps. Subject to a laser beam with intensity profile $I(r)$ and frequency ω, the atom in a two-level system with transition frequency ω_0 and natural linewidth $\gamma = 1/\tau$ experience an optical dipole potential $V \propto \gamma I(r)/(\omega - \omega_0)$, which is repulsive for blue detuning ($\omega > \omega_0$) and attractive for red detuning ($\omega < \omega_0$) [12, 253, 254]. For realistic atoms, which have a more complex structure, the potential also depends on the polarization and the magnetic quantum number of the ground state. The main advantages of optical dipole traps stem from the ability to construct high intensity, shapeable beams allowing for a nearly arbitrary spatial profile of the intensity $I(r)$. Importantly, the heating owed to the dissipative radiation pressure is proportional to $I(r)/(\omega - \omega_0)^2$, hence it can be strongly suppressed by tuning the laser to a large detuning, at the cost of requiring higher intensity to realize deep trapping potentials. For this reason the name Far Off-Resonance Trap (FORT) is often used.

Shaping the laser intensity in the vicinity of the atomic cloud enables an exceptional tunability of the potential experienced by the atoms. This precise shaping is achieved by combining multiple lasers and utilizing advanced optical devices called spatial light modulators (SLMs). These devices include intensity SLMs, namely Digital Micromirror Devices (DMDs), Acousto- and Electro-Optic Deflectors (AODs and EODs), and acoustic-optic modulators (AOMs) which are used to shape the spatial profile of the laser intensity, as well as phase SLMs which allow for the local modification of the phase of the laser beam such as Liquid Crystal on Silicon SLMs (LCOS-SLM) [255–265]. These techniques, along with various other advancements, have also enabled the creation of a variety of highly tunable potential landscapes, most notably optical lattices and optical tweezers.

Optical lattices are, in essence, artificial crystals formed by the interference of two (or more) counter-propagating laser beams. In contrast to the naturally occurring

crystals in solids, they can be constructed to be defect free, easily tunable, and importantly to posses long coherence time allowing for the direct observation of the transport of atoms (or excitations) operating as a direct analog to the electrons in solids. The simplest implementation consists of a one-dimensional lattice generated by a retro-reflected laser beam resulting in a standing wave potential. However, more complex settings corresponding to cubic, square, triangular geometries as well as supper-latices and quasi-crystals can also be obtained by adjusting the relative angles of multiple beams [27, 266, 267]. Atoms in optical lattices can be directly mapped to various Hubbard models (bosonic or fermionic) making them one of the first templates for quantum simulations of condensed matter models. For example they led to the realization of the superfluid–Mott insulator transition for bosons as well as the study of fermionic Mott insulators [43, 44, 268–278]. Moreover, the advances in quantum gas microscopy have enabled single-site detection and manipulation of atoms allowing the direct observation of local observables and correlation functions. Thus, they provide unprecedented access to the study of strongly correlated systems, synthetic fields, and topological models both in the ground state and with regards to their out-of-equilibrium many-body dynamics [269, 279].

Optical tweezers, on the other hand, are essentially tightly focused optical dipole traps which are able to trap single atoms and cool them very close to their motional ground state [51, 52, 126, 280–291]. Once loaded with atoms, arrays or grids of optical tweezers can be rearranged dynamically, allowing for highly flexible and programmable configurations in all three dimensions, making them a promising platform for quantum simulations of discrete systems. Indeed, combining optical tweezers with Rydberg excitations of the atoms, which provide strong and controllable long range interactions to couple the individual atoms, has enabled the realization of various spin Hamiltonians [53, 54, 120, 292–321]. Such systems can be highly relevant both for fundamental research, such as, in quantum magnetism and critical dynamics [322–327], as well as in technological applications including quantum sensors and neutral-atom quantum computers [127, 328–330].

2.1.1.3 Evaporative Cooling

These advancements in the magnetic and optical trapping of atoms have lead to experimental configurations capable of confining sufficiently high densities of atoms, which as mentioned was one of the main limitations of a MOT. However, still lower temperatures than those achieved by Doppler cooling (usually being of the order of $100\mu K$) are required to achieve quantum degeneracy. The final step in this process, which brings the Doppler-cooled trapped atomic gas to temperatures of the order of $100nK$ where quantum degeneracy usually sets in, is called evaporative cooling [331–334]. The main idea behind evaporative cooling consists of selectively expelling the most energetic atoms from the thermal (Boltzmann) distribution. Subsequently, the remaining atoms are allowed to equilibrate, effectively re-normalizing

their distribution at a lower temperature. The key to efficient evaporating cooling is to balance the evaporation rate, the elastic collision rate, and the trap loss rate. The goal is to ensure that, the elastic collision rate doesn't decrease with each evaporation sequence, thus preventing the evaporation from slowing down, and resulting in the so-called runaway evaporation regime. The exact implementation of the method crucially depends on the trap geometry and type. Namely, in a magnetic trap a radio-frequency (RF) pulse is usually applied. If the frequency of this pulse is close to the Zeeman-shifted transition frequency of the most energetic atoms, it can cause those atoms to spin-flip and thus to be expelled from the trap [1, 3, 90–92, 335–342]. Meanwhile, in optical dipole traps, the laser intensity can be reduced, decreasing the depth of the potential experienced by the atoms, until the most energetic atoms can escape or tunnel out of the trap. Finally, a particular benefit of optical dipole traps is that, unlike magnetic traps, it is possible to cool simultaneously different spin projections of the atomic ensemble [343–348].

As we have already alluded to throughout this brief description of the cooling and trapping process, a central tool in many of the steps is the ability to couple the internal spin states of the atoms and drive transitions between them. Considering a two-level quantum system driven by a near-resonant field, the probability of finding the system in either of the two states oscillates at the so-called Rabi frequency [349–354]. The probability of an atom initially prepared at the ground state, to be found occupying the excited state at time t is $P_e(t) = \frac{\Omega_R^2}{\Omega_R^2+\Delta^2}\sin^2(\frac{\sqrt{\Omega_R^2+\Delta^2}}{2}t)$ [30, 352]. This phenomenon of coherent population transfer between the two-state is called Rabi oscillation or Rabi flopping. In practice Rabi oscillations become dumped owing to various decoherence mechanisms, especially if the excited state has a relatively small lifetime.

A more stable way of inducing transitions between the two levels is to employ two-photon processes known as Raman transitions, which employ an additional field to couple the two long lived states via an intermediate off-resonant excited state. This results in a tunable effective Rabi frequency $\Omega_{eff} \propto \Omega_{R1}\Omega_{R2}/\Delta$, where Ω_{Ri} is the respective single-photon Rabi frequencies and Δ is the detuning with respect to the intermediate state [126, 355–359]. Rabi oscillations and Raman transitions are used in a wide range of applications, from the cooling of the atoms, as mentioned already, to atom interferometry and spectroscopy [355, 356]. One application, which is particularly relevant for the works included in this thesis [IE1–IE4], is the ability to engineer mixtures of different hyperfine states with controllable particle number ratios. Namely, the atomic gas can first be prepared in a single hyperfine state, such as a low-field seeking state in a MOT. Then the gas can be loaded in an optical dipole trap shaped in a desirable geometry. Finally, a microwave Raman transition can be used to transfer part of the atoms to a different hyperfine state, thus creating a mixture of the two states. The percentage of atoms transferred to the target hyperfine state can be precisely controlled via the duration of the laser pulses. This can result

in particle balanced mixtures, with equal number of particles occupying the two or more hyperfine levels. But it can also produce highly particle imbalanced mixtures, consisting a small fraction of the atoms occupying the second (or additional) hyperfine level(s) acting as impurities, or anything in-between [89, 173, 174, 183].

2.1.2 Interactions Between the Atoms

Some key aspects of quantum degeneracy, such as the formation of BECs or Fermi liquids, are evident even for systems of non-interacting particles. However, the interparticle interactions are integral for the development of collective excitations in the quantum gas, as well as for the emergence of correlated phases such as Mott insulating states, quantum droplets, few-particle bound states, quantum magnetism and much more [25–29, 50, 85, 142, 360]. In the following we briefly discus the main aspects of scattering theory concerning the interactions between neutral unpolarized atoms.

2.1.2.1 Scattering Length

Let us consider two neutral atoms in free space interacting via a central potential. The motion of the particle can be separated to the center of mass motion and the relative motion characterized by energy $E = \frac{\hbar^2 k^2}{2\mu}$, with μ being the reduced mass and k the relative momentum of the two atoms. The interaction properties of the system are captured by the relative motion, which is described by the relative Schrödinger equation [25, 26, 361]:

$$\left[-\frac{d^2}{dr^2} - \frac{2}{r}\frac{d}{dr} + \frac{l(l+1)}{r^2} + \frac{2\mu}{\hbar^2}V_{int}(r)\right]\Psi_{k,l}(r) = k^2\Psi_{k,l}(r), \tag{2.1}$$

where $\Psi_{k,l}(r)$ the radial wavefunction, l the angular momentum, and $V_{int}(r)$ the central interaction potential depending only on the distance r between the two atoms. Due to the exchange symmetry of the atoms, only even values of l enter the equation for bosonic particles and only odd values of l for fermions.

As mentioned, our focus is on neutral unpolarized bosonic atoms at low temperatures. This regime is specified by the assumptions that the atoms interact via the short-range van der Waals potential, l is even, and the relative momentum k is small (since the individual momenta must also be small) [83, 362–364]. To make these more concrete, the van der Walls interaction is characterized by a repulsive core, usually modeled by an infinite barrier or by a sharply diverging one $\propto C_{12}/r^{12}$ for $r < r_0$ and an attractive rapidly decaying tail $\propto -C_6/r^6$ for $r > r_0$. Focusing on $r > r_0$, the characteristic length scale of the system is given by $r_c = (\frac{2\mu C_6}{\hbar^2})^{1/4}$, which is usually much larger that the location of the minimum of the interaction potential ($\approx r_0$) for atoms with weak magnetic dipole moments and no induced electric dipole. This allows us to ignore the details of the inner core and approximate the wavefunction by

its asymptotic value, which for $l = 0$, called the s-wave interaction, is given by [365]:

$$\Psi_{k,0}(r) \xrightarrow{r \gg r_0} \frac{1}{r} \sin\left[kr + \delta_0(k)\right]. \tag{2.2}$$

Essentially, all the information regarding the scattering process becomes imprinted only in the phase shift $\delta_0(k)$, which the wavefunction accumulated during the interaction between the atoms at short interatomic distances.

Finally, our last assumption is that the temperature is sufficiently small such that the relative momentum k is small compared to the momentum scale given by the characteristic length scale of the system $1/r_c$, i.e. $k \cdot r_c \ll 1$. In this limit, the relative energy of the atoms ($\hbar^2 k^2/2\mu$) is much smaller than the centrifugal potential barrier, which is created by the combination of the van der Waals interaction and the angular momentum terms ($\frac{\hbar^2}{2\mu}\frac{1l(l+1)}{3r_c^2}$). Hence, the tunneling probability is heavily suppressed and the contribution of higher angular momentum states to the total cross-section vanishes, since these states cannot experience the van der Waals interaction. In particular, it can be shown that the cross section in the limit we are interested in becomes $\lim_{k\to 0} \sigma_{l=0} = 8\pi a$, with the scattering length $a = -\lim_{k\to 0} \tan\delta_0(k)/k$ or $\Psi_{k,0}(r) \xrightarrow{r \gg r_0} \frac{\sin k(r-a)}{r}$. Hence, the interactions between ultracold bosonic atoms (neglecting dipolar interactions) are dominated by the s-wave regime, which can be fully characterized by a single parameter, namely the scattering length a [35, 40, 365–368].

2.1.2.2 Contact Pseudopotential

Working with the van der Waals potential in the treatment of many-body atomic systems is challenging, therefore it is common to replace it with a so-called contact pseudopotential. As discussed in the previous section, the s-wave regime can be fully characterized via the scattering length a, meaning that it is insensitive to the details of the interaction potential at short distances. As such, one can extent the asymptotic wavefunction to all interparticle distances, subject to the Bethe-Peierls condition $\frac{[r\Psi_{k,0}(r)]'}{r\Psi_{k,0}(r)} \xrightarrow{r\to 0} = -\frac{1}{a}$ [369]. The contact pseudopotential is an artificial potential, assumed to be valid at all interatomic distances, which results in the same s-wave scattering length as the actual van der Waals interaction, while being more practical to work with. Such a pseudopotential is the Fermi-Huang pseudopotential [370, 371]:

$$V(r) = \frac{2\pi\hbar^2 a}{\mu}\delta^{(3)}(r)\frac{\partial}{\partial r}(r\cdot), \tag{2.3}$$

where $\delta^{(3)}(r)$ is the 3D Dirac delta function, while the regularization operator $\frac{\partial}{\partial r}(r\cdot)$ is chosen to lift the divergence at small distances. It is worth noting that, although the contact pseudopotential reproduces the correct scattering length, it can be shown that it only supports a single bound state with energy $-\frac{\hbar^2}{2\mu a^2}$, while the actual van der Waals potential can in general support many two-body bound states [372]. This

single bound state is usually associated with the least bound state of the van der Waals potential, which tends to be the most relevant state in most cases. Note finally, that the scattering length can take also negative values (in-spite of what the term "length" might suggest), in which case it describes an overall attractive interaction between the atoms.

This thesis is focused in 1D systems, where the asymptotic wavefunction takes the form $\Psi_k(x) = \sin(k(|x| - a_{1D}))$, where a_{1D} is the corresponding 1D scattering length and the Bethe-Peierls condition becomes $\frac{\Psi_k'(x)}{\Psi_k(x)} \xrightarrow{x\to 0^{\pm}} = \mp\frac{1}{a}$. An appropriate contact pseudopotential, hence, is [373–376]:

$$V(x) = \frac{\hbar^2}{\mu a_{1D}}\delta(x). \tag{2.4}$$

This form of the potential suggests, somewhat counterintuitively, that positive scattering lengths correspond to attraction and negative ones to repulsion, while the non-interacting limit is found for $a_{1D} \to \pm\infty$. Moreover, this 1D contact pseudopotential supports a single two-body bound state, which emerges only for attractive interactions $a_{1D} > 0$ [103]. To avoid confusion, it is often more convenient to define the strength of the interaction as the multiplicative factors in front of the delta-functions in the contact pseudopotentials, i.e. $g_{3D} = \frac{2\pi\hbar^2 a}{\mu}$ and $g_{1D} = -\frac{\hbar^2}{\mu a_{1D}}$ for the 3D and 1D cases respectively. With these definitions we can refer consistently to repulsive [attractive] interactions having positive [negative] interaction strengths. Furthermore, a larger absolute value of the interaction strength corresponds to stronger interactions (either repulsive or attractive) and a smaller one to weaker interactions.

Although nature insists on being genuinely 3D, regardless of how inconsiderate that is to computational scientists, it is possible to experimentally realize artificial effectively low-dimensional settings, termed quasi-low dimensional systems. This is usually accomplished by confining the atomic gas in a highly anisotropic harmonic oscillator, effectively freezing the dynamics of the atoms in the strongly confined dimensions. As a result, such configurations allow the low dimensional properties to emerge along the weakly confined direction (or directions for quasi-2D systems [103, 374, 377–383]). In particular, considering a system with high trapping frequency $\omega_\perp$ along two strongly confined directions, the remaining weakly confined transverse direction constitutes a quasi-1D system with effective scattering length [384–391]:

$$a_{1D} = -\frac{a_\perp^2}{2a}\left[1 + \zeta(1/2)\frac{a}{a_\perp}\right], \quad \text{or} \quad g_{1D} = -\frac{\hbar^2}{\mu a_{1D}} = \frac{\hbar^2}{\mu a_\perp}\frac{2}{\frac{a_\perp}{a} + \zeta(1/2)}, \tag{2.5}$$

where $a_\perp = \sqrt{\frac{\hbar}{\mu\omega_\perp}}$ the oscillator length along the strongly confined directions and $\zeta(1/2) \approx -1.4603$ the Riemann zeta function [392]. Note that, this form of the potential suggests that the effective 1D interaction is relatively weakly attractive for

$a \to \pm\infty$. Moreover, it features a resonance around the critical value of the 3D scattering length $a_{cr} = -\frac{a_\perp}{\zeta(1/2)}$, with large repulsive 1D interactions for $a \lessapprox a_{cr}$ (eg. Tonks-Girardeau regime [67, 393]) and strongly attractive 1D interactions for $a \gtrapprox a_{cr}$ (eg. super-Tonks-Girardeau regime [68, 135]). As such, the value of the quasi-1D effective interaction strength can be controlled via tuning either the oscillator length or the 3D scattering length [67, 394–398].

2.1.2.3 Fano-Feshbach Resonances

In realistic atomic gasses, depending on the internal state of the atoms involved (eg. singlet, triplet, etc.), there can be multiple different potentials active. This fact does not invalidate our previous discussion, since most of these potentials exhibit van der Waals tails at large relative distances, however, they asymptotically tend to a finite energy E_a caused by the total spin of the atoms [28, 35, 366]. By convention, the nomenclature employed to describe the resulting phenomenology classifies the potentials with asymptotic energy below the collision energy E as "open channels" ($E > E_a$) and accordingly as "closed channels" those with energy above the collision energy ($E < E_a$). The terms “open” and “closed” refer to the fact that, from a classical perspective, these channels are energetically accessible and inaccessible, respectively. However, quantum-mechanically, the hyperfine interactions, in general, couple all those interaction potentials [366, 399]. Since those potentials are differentiated by the total spin of the states involved, their asymptotic energy can be Zeeman-shifted by applying external magnetic fields. At certain values of the magnetic field B_{res}, the energies of the bound states of a closed channel can (almost) coincide with the collision energy E, causing the atoms to resonantly couple with the two-body bound state of this closed channel. This resonant coupling has a profound effect on the 3D scattering length, which in the vicinity of such a resonance responds as [33, 34]:

$$a(B) \approx a_{bg}\left(1 - \frac{\Delta B}{B - B_{res}}\right), \tag{2.6}$$

where a_{bg} is the value of the scattering length far from the resonance (without coming close to a different resonance), ΔB is the width of the resonance, and B is the value of the magnetic field. Utilizing this mechanism, known as a Fano-Feshbach resonance [399–402], the scattering length can be tuned from the non-interacting limit at $B = \Delta B + B_{res}$ to the strongly interacting regime when $B \approx B_{res}$ and to any value in between. This extraordinary controllability of microscopic interactions is one of the cornerstones of the advances in the field of ultracold atoms [23, 31, 33, 34, 403–406]. It is worth mentioning, that Feshbach resonances can also be realized with optical fields [407].

2.2 Analytical Approaches

Let us consider a macroscopic ensemble of $N \gg 1$ neutral bosonic atoms of mass m. The atoms are assumed to be cooled to temperatures close to absolute zero. Under this assumption the system may be described accurately by a wavefunction. In contrast, at finite temperatures the systems should generally be considered as occupying a thermal ensemble, which would require a description in terms of a density matrix. Moreover, we assume that the interatomic interactions can be approximated by a contact pseudopotential. As discussed in the previous section, this assumption is consistent with the assumption of zero temperature, when considering atoms, which have no inherent magnetic dipole moment and are not subject to polarizing electric fields. These assumptions may appear at first glance to be very restrictive. However, as already discussed, they are not only readily realizable to an excellent approximation in experiments, but they are also sufficiently broad to produce a theoretical framework featuring rich phenomenology.

In particular, below we shall show, how the celebrated Gross-Pitaevskii equation (GPE) can be derived by further neglecting quantum fluctuations in the system. Recall that thermal fluctuations have also been neglected through the assumption of zero temperature [25, 26, 83]. The GPE, in spite of its simplicity, already provides a fairly accurate description of such ultracold bosonic gases in a wide range of conditions in terms of the interatomic interaction strength and the external geometry imposed on the system. This highly successful treatment, providing a fairly simple description of the interacting bosonic gas, is also called Mean-Field Theory or Mean-Field Approximation (MF). Interestingly, the MF treatment provides a description of the bosonic cloud in terms of a non-linear quantum fluid. This non-linearity gives rise to intriguing dynamical behaviors including various collective excitation modes as well as the emergence of localized solitonic excitations with topological character such as kinks in 1D, or vortices in higher dimensions [83]. In particular, 1D systems can also host stable bright solitons in the presence of attraction.

Subsequently, we shall take one more step in increasing complexity and accuracy, to illustrate how the quantum fluctuations of the system can be re-introduced perturbatively within the Bogoliubov theory framework [50, 139, 141, 142, 371]. This approach allows us to analytically derive the first-order correction to the MF energy of the system known as Lee-Huang-Yang (LHY) energy, as well as the corresponding extended Gross-Pitaevskii equation (eGPE). Aside from providing a quantitative correction to the energy derived within the simpler MF approximation, the LHY correction was recently found to lead to remarkable qualitatively different phases under certain conditions. Namely, the quantum fluctuations lead to the formation of quantum droplets, which are liquid-like self-bound structures, in contrast to the gas-like structures predicted within the MF approximation. Quantum droplets have garnered wide interest, as they directly manifest the impact of quantum fluctuations

not only in their dynamical behavior, but strikingly also in their ground state density configurations [113, 183].

The main conditions, under which quantum droplets (or related structures such as LHY supersolids [140]) emerge, can be summarized by the requirement that the energy due to the "averaged", "classical", or "direct" interatomic interactions has the opposite sign compared to the LHY energy accounting for the quantum fluctuations. Under this condition, the competition between those two contributions results in the energy minimum being shifted to finite density values, thus giving rise to liquid-like self-bound configurations as opposed to a gas phase. Note that, the terms "classical" or "direct" interatomic interactions are used here to emphasize that they can be understood as classical forces of electromagnetic nature acting between the atoms. This is in contrast to the LHY term, which manifests the impact of quantum fluctuations and cannot be directly associated with any classical force, even though in practice, it results in an additional non-linear interaction term. Although not strictly necessary, if conditions can be engineered, such that, these "averaged" "classical" interatomic interactions are sufficiently weak causing their energy contribution to become comparable to the perturbative LHY energy, then quantum droplets become more pronounced and more easily observable. Such conditions are exemplary realized in two-component 3D bosonic gases, when their contact intercomponent interaction strength is tuned slightly past the attractive edge of the MF stability threshold. In this case, the "averaged" interatomic interactions provide a small negative energy contribution, while the LHY energy is positive and has comparable magnitude [139, 183]. A similar scenario occurs in the case of dipolar bosons (occupying singular or multiple components), where the combination of contact and dipolar interactions is tuned towards small attraction to compete the positive LHY energy [140]. It is worth noting that this setting can host not only quantum droplets, but also supersolid and more complex mixed structures, owing to the long-range nature of the dipolar interactions and their interplay with the external confinement [114]. Finally, as we shall emphasize below and in the works included in this thesis [IE1–IE4], quantum droplets may be present throughout the MF stability regime in single- and multi-component bosonic mixtures in 1D, where the positive energy stemming from the ("averaged") interatomic interaction(s) competes with the negative LHY energy.

below we present all the relevant theory by employing the simpler case of a single-component 1D gas of bosonic atoms featuring contact interaction, while the case of multi-component bosonic mixtures can be found in [IE3]. In Fig. 2.1 we also present schematic representations of harmonically confined bosonic mixtures consisting of one [Fig. 2.1(a)], two [Fig. 2.1(b)] or three [Fig. 2.1(c)] components. It is evident that the complexity of the system quickly increases upon increasing the number of components, hence below we restrict our analysis to the less involved single-component system. We shall also address briefly the 3D case, which served as a crucial motivation to the original formulation of the droplet theory, in order to emphasize certain

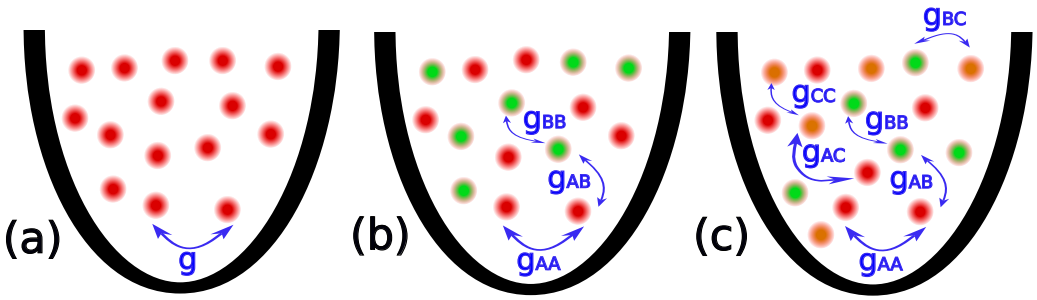

FIGURE 2.1: Schematic representation of a harmonically confined atomic mixture consisting of (a) a single component (b) two components (c) three components.

key differences to the 1D setting.

2.2.1 The Many-Body Problem

Let us start making the above discussion more concrete, by writing the many-body Hamiltonian for N identical bosonic atoms in 1D in the low energy regime, where their scattering properties are dominated by the s-wave contact interaction [25, 26, 50]:

$$H = -\frac{\hbar^2}{2m}\sum_{i=1}^{N}\frac{\partial^2}{\partial x_i^2} + \sum_{i=1}^{N} V(x_i) + g\sum_{i<j}^{N}\delta(x_i - x_j). \tag{2.7}$$

Here x_i corresponds to the position of the $i-$th boson, m is the common mass of each atom, $V(x_i)$ represents the external potential experienced by the bosons, g quantifies the interatomic interaction strength, $\hbar$ is Plank's reduced constant, and Dirac's delta function is given by δ.

In principle one could solve the resulting many-body Schrödinger equation:

$$H\left|\Psi\right\rangle = E\left|\Psi\right\rangle, \tag{2.8}$$

to derive not only the ground state of the system, but also the entire excitation spectrum and corresponding eigenstates of the system. However, this is not possible to do analytically in all but the simplest cases. Advanced numerical methods can, in some cases, simulate the ground state or even a few low-lying states for fairly large systems, consisting e.g. of up to $N \approx 100$ particles. We will discuss one such numerical approach in more detail in Sec. 2.3. For now we only mention that the difficulty in solving the Schrödinger equation for large systems stems from the so-called "curse of dimensionality".

To understand the "curse of dimensionality", let us attempt to construct a basis in which we aim to solve the many-body Schrödinger equation, for a system described

by the Hamiltonina of Eq. (2.7), and consisting of N bosonic atoms. A fairly natural choice would be to use the eigenstates of the single particle problem, given by the single-particle Hamiltonian $h_0 = -\frac{\hbar^2}{2m}\frac{\partial^2}{\partial x^2} + V(x)$, which results in the single-particle Schrödinger equation $h_0 |\phi_k\rangle = e_k |\phi_k\rangle$. The single-particle states $|\phi_k\rangle$ are often referred to as orbitals in this context. Then a many-body basis state can be written as $|i\rangle = \prod_k |n_{i_k}\rangle$, where $|n_{i_k}\rangle$ describes a configuration with n_{i_k} particles occupying the single-particle state $|\phi_k\rangle$ and $N = \sum_k n_{i_k}$, for each i numbering the many-body basis states. One problem appearing already is the fact that the single-particle Hamiltonian has an infinite number of single-particle eigenstates. However, one can circumvent this issue by truncating the problem and keeping only a sufficiently large number of eigenstates, which we set as $\mathcal{K}$. Even with this truncation, however, another, not so easily addressed, issue remains. The number of many-body basis states derived from the single-particle eigenstates, is given by the combinatorial problem of distributing N indistinguishable bosons in $\mathcal{K}$ single-particle states, i.e. $i_{max} = \frac{(N+K-1)!}{N!(K-1)!}$. If the atoms were distinguishable, then the number of many-body basis states required would scale exponentially as $\sim \mathcal{K}^N$. The bosonic exchange symmetry reduces somewhat the number of required many-body basis states, but in most cases the scaling remains close to exponential for practical purposes. This exponential (or almost exponential) growth in the required number of many-body basis states, or equivalently in the number of "dimensions" of the many-body Hilbert space, is what is referred to as the "curse of dimensionality". The direct consequence of this exponential scaling is that, when attempting to numerically solve either larger (increasing N) or more correlated systems (increasing $\mathcal{K}$), the computation time and memory required increase very rapidly. This increase in the required resources, eventually, makes such a numerical solution impractical or even impossible to obtain. Moreover, during the out-of-equilibrium dynamics of the system, correlations tend to increase over time requiring an increasing number ($\mathcal{K}$) of single-particle states to be considered.

2.2.2 Mean-Field Approach

As mentioned, in Sec. 2.3 we will discuss an advanced numerical method for circumventing the "curse of dimensionality", when the physics of the problem in question allows for an accurate low-dimensional treatment in some basis. However, the simplest way to avoid the "curse of dimensionality" is given by the MF approximation. Under this approximation we reduce the exponentially large dimension of the many-body Hilbert space to exactly one! Namely, we assume that there exists an orbital $|\Phi\rangle$ such that the many-body ground state $|\Psi\rangle$ can be expressed to a good accuracy as a product state [25, 26]:

$$|\Psi\rangle = \prod_i^N |\Phi\rangle_i . \tag{2.9}$$

Here $|\Phi\rangle_i$ describes the particle i occupying the orbital $|\Phi\rangle$. Hence the MF Ansatz of Eq. (2.9) assumes that all N particles occupy a single orbital $|\Phi\rangle$. Note also that, both the many-body ground state $|\Psi\rangle$ and the MF orbital are assumed to be normalized to unity $\langle\Psi|\Psi\rangle = \langle\Phi|\Phi\rangle = 1$.

The MF approximation is arguably a rather extreme approximation. However, there are several subtle ideas and physical intuition to justify and motivate such an assumption. First, the main physical intuition stems from the physics of the BEC of a non-interacting ensemble of atoms in 3D. In the case of a non-interacting system of particles in 3D, it is well known that at zero temperature, the atoms will all condense to a single energy level corresponding to the ground state of the single-particle problem $|\phi_0\rangle$. The idea concerning the MF approximation is then that, if we start increasing the interaction strength to a non-zero, but sufficiently small value, we can expect that the condensate will not rapidly deplete. Instead, we imagine that its initial many-body state at zero interaction, in which all particles occupy the ground state of the single-particle problem $|\phi_0\rangle$, will gradually shift towards the state in which all particles occupy the MF orbital $|\Phi\rangle$. In reality, some depletion of the condensate is expected to occur. However, to a rather good accuracy we may ignore this depletion, as long as the number of "condensed" particles is much larger than the number of particles which "escape" the condensate. A second argument in favor of the usefulness MF approximation, stems from the variational principle. It states that the ground state energy of a system is always smaller than the expectation value of its Hamiltonian calculated at any arbitrary state, i.e. $E_{GS} \leq \langle\Psi'|H|\Psi'\rangle$, where $|\Psi'\rangle$ can be an arbitrary many-body state acting as a trial function. Hence, the MF Ansatz provides a comparatively easy way to derive a reasonable trial function, which can be used to obtain an upper bound estimate for the exact ground state energy of the many-body system. Comparisons with experimental measurements, or with numerical calculations using advanced numerical methods, have shown that the MF approximation results in decent estimations for observables such as the energy and the single-particle density ($\rho(x) = \langle x|\, Tr^{N-1}(|\Psi\rangle\langle\Psi|)\,|x\rangle = |\Phi(x)|^2$) of the many-body state, under certain conditions [25, 50, 83].

Substituting the MF Ansatz of Eq. (2.9) to the many-body Schrödinger equation governed by the Hamiltonian (2.7), we obtain the expectation value:

$$\langle\Psi|H|\Psi\rangle = N\int dx\left[\frac{\hbar^2}{2m}\left|\frac{\partial\Phi(x)}{\partial x}\right|^2 + V(x)|\Phi(x)|^2 + \frac{(N-1)}{2}g|\Phi(x)|^4\right]. \quad (2.10)$$

It is customary to work with wavefunctions normalized to the particle number instead of unity i.e. $\Phi(x) \to \sqrt{N}\Phi(x)$. Moreover, since we have already assumed that the total number of particles is large enough to ignore any depletion, we also usually approximate $N-1 \approx N$ i.e. $N \gg 1$. Note that so far the orbital $\Phi(x)$ has really been just a placeholder. We have only assumed that such an orbital exists and

we have provided some physical arguments that it can provide a decent approximation to the true solution. In particular, it is important to emphasize here that the MF orbital has no connection to the eigenstates of the single-particle problem, which we discussed before. The MF orbital $|\Phi\rangle$ is a state of the Hilbert space spanned by the eigenstates $|\phi_k\rangle$ of the single particle problem and in this sense we identify it as a valid single-particle state or orbital. However, in general, it can correspond to an arbitrary superposition of these eigenstates $|\Phi\rangle = \sum_k a_k |\phi_k\rangle$ and it should not be confused with eg. the ground state of the single-particle problem $|\phi_0\rangle$.

To determine the desired MF wavefunction we exploit the variational principle. In Eq.(2.10), we have essentially calculated the expectation value of the many-body Hamiltonian (or the average energy) for an arbitrary many-body state, characterized by all the particles occupying a single orbital. For instance, we could substitute Φ in Eq.(2.10) with one of the single-particle eigenstates (or really any function of our choosing as long as it satisfies the boundary conditions) and calculate the resulting average energy of the corresponding system. Note, that in deriving Eq.(2.10), we have implicitly assumed that the boundary conditions are such that $\int \frac{\partial}{\partial x}[\Phi^* \frac{\partial \Phi}{\partial x}]dx = 0$, which is true for most boundary conditions commonly employed in physical systems. In this context, we define the MF orbital as the wavefunction which minimizes the many-body energy functional:

$$E(\Phi) = \int dx \left[\frac{\hbar^2}{2m} \left| \frac{\partial \Phi(x)}{\partial x} \right|^2 + V(x)|\Phi(x)|^2 + \frac{g}{2}|\Phi(x)|^4 \right], \tag{2.11}$$

for a fixed number of particles $N = \int dx |\Phi(x)|^2$. This is achieved if the variation $\delta E - \mu \delta N = 0$ with respect to Φ^* vanishes to first order, resulting in the celebrated GP equation [25, 26]:

$$-\frac{\hbar^2}{2m}\frac{\partial^2 \Phi(x)}{\partial x^2} + V(x)\Phi(x) + g|\Phi(x)|^2\Phi(x) = \mu\Phi(x), \tag{2.12}$$

where the Lagrange multiplier μ is the chemical potential of the system ($\mu = \frac{\partial E}{\partial N}$). Solving the GP equation we can derive the MF wavefunction/orbital and the MF energy, which as mentioned serves as an (upper bound) approximation for the exact many-body energy.

2.2.2.1 The 3D Case

The MF energy functional and the resulting GP equation can readily be generalized to the 3D case. We simply replace the spatial coordinate x and the spatial derivative $\frac{\partial}{\partial x}$, with the 3D position vector $\mathbf{r}$ and the 3D gradient ∇ respectively. With that, the energy functional becomes [25, 26]:

$$E(\Phi) = \int d\mathbf{r} \left[\frac{\hbar^2}{2m} |\nabla \Phi(\mathbf{r})|^2 + V(\mathbf{r})|\Phi(\mathbf{r})|^2 + \frac{g}{2}|\Phi(\mathbf{r})|^4 \right], \tag{2.13}$$

resulting in the corresponding 3D GP equation:

$$-\frac{\hbar^2}{2m}\nabla^2\Phi(\mathbf{r}) + V(\mathbf{r})\Phi(\mathbf{r}) + g|\Phi(\mathbf{r})|^2\Phi(\mathbf{r}) = \mu\Phi(\mathbf{r}), \tag{2.14}$$

where g now represents the 3D interaction strength as discussed in Sec. 2.1.2.

It can be shown [408] that for attractive interactions (even extremely small) the MF energy of the 3D system in free space diverges to $-\infty$ as the width of the density tends to zero. In the presence of an isotropic harmonic potential, for very weak attraction and small particle number, the density of the 3D system quickly becomes highly localized at the center. This results in a metastable state featuring finite density width, as the kinetic energy tries to balance the attractive interaction energy. However, this metastable state vanishes at a critical number of atoms given by $N_{cr}\,|a|\,/a_{ho} \approx 0.575$, where a the 3D scattering length and a_{ho} the oscillator length of the trap [25, 83]. When the number of atoms in the system exceeds the critical number of atoms the system is said to collapse, since it cannot support any long lived states with finite density width.

Recently, it was shown that in multi-component systems it is possible to exploit quantum fluctuations in order to arrest this collapse [139, 197]. For a symmetric two - component mixture, the MF approximation results in a GP equation identical to the one of the single-component case except that the interaction strength has to be replaced by $\delta g = g + g_{AB}$. Here g is the intra-component interaction strength (identical for both components) and g_{AB} is the inter-component interaction strength. Thus from a MF perspective, if the interactions are tuned such that the effective interaction $g_{AB} < -g \Rightarrow \delta g < 0$, the two-component mixture is expected to collapse, just as the single-component system collapses for $g < 0$. The main idea, originally proposed in [139], is based on the fact that quantum fluctuations, accounted to first order in perturbation theory, result in an additional positive/repulsive term in the energy functional, known as the Lee-Huang-Yang (LHY) energy. Note that, an important complication is that the LHY energy becomes imaginary when $\delta g < 0$, so its value at $\delta g = 0$, which scales as $(gn)^{5/2}$ in 3D, is usually used instead, under the assumption that the unstable modes do not meaningfully contribute. The result of the competition, between the attractive MF interaction term and the LHY term, accounting for quantum fluctuations, is that the mixture minimizes its energy at a state with finite density and density-width even in the absence of external confinement. As a result, the system does not collapse as predicted by the MF theory, but arranges into a self-bound configuration exhibiting a finite size. These self-bound structures, manifesting directly the impact of quantum fluctuations, are called quantum droplets. In the next section, we will address in detail the 1D case, and we will show that quantum droplet structures are always supported in the repulsive regime (or more generally the MF stability regime), even for the single-component system, owing to the LHY energy being negative. The case of two-component 1D mixtures

close to the limit $\delta g \approx 0$ was addressed originally in [162], while the case of two- or higher-component mixtures at arbitrary interaction strengths within the MF stability regime was addressed in [IE3].

Finally, let us mention that, to obtain the time-dependent GP equation we augment the functional as:

$$S[\Phi(\mathbf{r},t)] = \int d\mathbf{r}dt \left[i\hbar\Phi^*(\mathbf{r},t)\frac{\partial\Phi(\mathbf{r},t)}{\partial t} - \mathcal{E}_{MF} \right], \tag{2.15}$$

where $\mathcal{E}_{MF} = \frac{\hbar^2}{2m}|\nabla\Phi(\mathbf{r})|^2 + V(\mathbf{r})|\Phi(\mathbf{r})|^2 + \frac{g}{2}|\Phi(\mathbf{r})|^4$ is the MF energy density which enters into the time-independent functional of Eq. 2.13. The resulting time-dependent GP equation is:

$$i\hbar\frac{\partial\Phi(\mathbf{r},t)}{\partial t} = -\frac{\hbar^2}{2m}\nabla^2\Phi(\mathbf{r},t) + V(\mathbf{r})\Phi(\mathbf{r},t) + g|\Phi(\mathbf{r},t)|^2\Phi(\mathbf{r},t). \tag{2.16}$$

Note that, the solutions ($\Phi(\mathbf{r},0)$) of the time-independent GPE correspond to stationary solutions of the time-dependent GPE, with a time-dependent phase given by the chemical potential $\Phi(\mathbf{r},t) = e^{-i\mu/\hbar}\Phi(\mathbf{r},0)$.

2.2.3 Bogoliubov Theory

As mentioned already, albeit highly successful, the MF approximation is a rather simplistic one, reducing the genuinely many-body problem to one concerning only a single orbital. In order to take into account the impact of quantum fluctuations involving the contributions from higher orbitals, one can employ the perturbative Bogoliubov theory. In this perturbative treatment, the MF approximation emerges as the zeroth-order contribution to the energy of the system, while the first-order correction is given by the LHY energy. In Sec. 2.2.3.1 we provide a general description of the Bogoliubov transformation. Then in Sec. 2.2.3.2, we apply it to the case of an 1D single-component bosonic gas, deriving the MF and LHY contributions. Finally, in Sec. 2.2.3.3 and Sec. 2.2.3.4 we derive the corresponding eGPE and the Bogoliubov de Gennes (BdG) equations respectively, which describe the ground state and dynamical properties of the system under the influence of quantum fluctations. As mentioned, the same methods are used in [IE3] and [IE4] in order to derive the LHY correction for multi-component 1D bosonic mixtures and the corresponding BdG equations for the three-component case.

2.2.3.1 The Bogoliubov Transformation

We consider a set of bosonic operators $A^\dagger = (\hat{a}^\dagger,\ \hat{a})$, satisfying the bosonic commutation conditions $[\hat{a},\hat{a}^\dagger] = 1$ and $[\hat{a},\hat{a}] = [\hat{a}^\dagger,\hat{a}^\dagger] = 0$. We want to define a new set of bosonic operators $B^\dagger = (\hat{b}^\dagger,\ \hat{b})$ as a linear combination of the bosonic operators in A, i.e. $A = UB$, such that the commutation conditions $[\hat{b},\hat{b}^\dagger] = 1$ and $[\hat{b},\hat{b}] = [\hat{b}^\dagger,\hat{b}^\dagger] = 0$ hold. It is instructive to calculate explicitly the transformation

matrix U, for this simple case, to illustrate the properties it must satisfy in order to preserve the bosonic commutation relations.

$$A = UB \iff \begin{pmatrix} \hat{a} \\ \hat{a}^\dagger \end{pmatrix} = \begin{pmatrix} u_{11} & u_{12} \\ u_{21} & u_{22} \end{pmatrix} \begin{pmatrix} \hat{b} \\ \hat{b}^\dagger \end{pmatrix} = \begin{pmatrix} u_{11}\hat{b} + u_{12}\hat{b}^\dagger \\ u_{21}\hat{b} + u_{22}\hat{b}^\dagger \end{pmatrix} \tag{2.17}$$

Since $\hat{a}^\dagger$ is the adjoined of $\hat{a}$ we can readily see from Eq. (2.17) that $u_{21}^* = u_{12} := v$ and $u_{22}^* = u_{11} := u$. It is easy to see that the commutation relations $[\hat{a}, \hat{a}] = [\hat{a}^\dagger, \hat{a}^\dagger] = 0$ are satisfied trivially if $[\hat{b}, \hat{b}] = [\hat{b}^\dagger, \hat{b}^\dagger] = 0$. Instead, for the commutation relations $[\hat{a}, \hat{a}^\dagger] = 1$ and $[\hat{b}, \hat{b}^\dagger] = 1$ to be simultaneously satisfied, we obtain an additional constraint on the elements of the transformation matrix U, namely

$$U = \begin{pmatrix} u & v \\ v^* & u^* \end{pmatrix}, \quad \text{with} \quad \det U = 1 \Leftrightarrow |u|^2 - |v|^2 = 1. \tag{2.18}$$

It is important to note that the inverse matrix: $U^{-1} = \begin{pmatrix} u^* & -v \\ -v^* & u \end{pmatrix} \neq U^\dagger$, meaning that U is not a unitary matrix, and hence the Bogoliubov transformation is not a unitary transformation. Instead, the property $U^T \Omega U = U$, with $\Omega = \begin{pmatrix} 0 & 1 \\ -1 & 0 \end{pmatrix}$ and U^T the transpose matrix of U holds. Mathematically, Ω is called a nonsingular, skew-symmetric matrix and the above property defines U as a symplectic matrix. However, for our purposes it is more useful to express this condition in the following equivalent formulation:

$$UGU^\dagger = G, \tag{2.19}$$

where

$$G = [A, A^\dagger] := AA^\dagger - ((A^\dagger)^T A^T)^T = \begin{pmatrix} 1 & 0 \\ 0 & -1 \end{pmatrix} \tag{2.20}$$

is the Bosonic metric [409]. This property is a direct consequence of the requirement that both A and B correspond to sets of bosonic creation and annihilation operators. Furthermore, it does not depend on the exact form of U or on the number of bosonic fields we consider.

Indeed, we can generalize the above treatment to an arbitrary set of n bosonic operators $A^\dagger = (\hat{a}_1^\dagger,\ \hat{a}_2^\dagger,\ ...,\ \hat{a}_n^\dagger\ , \hat{a}_1,\ \hat{a}_2,\ ,...,\ \hat{a}_n)$, and define a Bogoliubov transformation $A = UB$, with $B^\dagger = (\hat{b}_1^\dagger,\ \hat{b}_2^\dagger,\ ...,\ \hat{b}_n^\dagger\ , \hat{b}_1,\ \hat{b}_2,\ ,...,\ \hat{b}_n)$ and $U = \begin{pmatrix} M & N \\ N^* & M^* \end{pmatrix}$, where M, N are $n * n$ matrices. Then, if we demand that both A and B satisfy bosonic commutation relations, we can write them compactly in matrix form, using the Bosonic metric, as $G = [A, A^\dagger] = [B, B^\dagger] = \begin{pmatrix} I_n & 0 \\ 0 & -I_n \end{pmatrix}$, where I_n is the n-dimensional identity matrix. We can then show explicitly, using the definition of the Bosonic metric, given in Eq. (2.20), that the property of Eq. (2.19) holds for the arbitrary Bogoliubov

transformation:

$$\begin{aligned} G =& [A, A^\dagger] := AA^\dagger - ((A^\dagger)^T A^T)^T = UBB^\dagger U^\dagger - ((B^\dagger U^\dagger)^T (UB)^T)^T \\ =& UBB^\dagger U^\dagger - U((B^\dagger)^T B^T)^T U^\dagger = U[B, B^\dagger]U^\dagger \\ =& UGU^\dagger. \end{aligned}$$

Hence, demanding that Eq. (2.19) holds is equivalent to imposing that the Bogoliubov transformation preserves the commutation relations of the set of bosonic operators, without having to explicitly derive the constraints on the elements of the transformation matrix U.

As a final step, we explicate how the Bogoliubov transformation can be used to diagonalize an operator written in bilinear form in terms of the arbitrary set of bosonic operators A. Namely, we consider $\hat{H} = A^\dagger H A$, where $\hat{H}$ is an One-Body-Operator written in second quantization form in terms of the operators $\hat{a}_i$, $\hat{a}_i^\dagger$ and H is the corresponding matrix representation. It is important to note that the Bogoliubov transformation matrix U is not unique (see e.g. Eq. (2.18)), therefore we can exploit the remaining degrees of freedom (after the constraints required to preserve the bosonic symmetry have been applied) to impose additional constraints.

First, we can write

$$\hat{H} = A^\dagger H A = B^\dagger U^\dagger H U B = B^\dagger G U^{-1} G H U B.$$

Then we can demand that the Bogoliubov transformation diagonalizes $\hat{H}$ in term of the bilinear form with respect to B, i.e.

$$G U^{-1} G H U = D \iff U^{-1} G H U = G D, \tag{2.21}$$

where D is a diagonal matrix. Explicitly then, we demand that the Bogoliubov transformation matrix diagonalizes the matrix $\mathcal{H}_G = GH$, as $U^{-1}\mathcal{H}_G U = GD$. If we now calculate the eigenvalues of $\mathcal{H}_G$ by solving the characteristic equation

$$\det\left(GH - \lambda I_{2*n}\right) = 0, \tag{2.22}$$

we can write $D = \mathrm{diag}(\lambda_1, ..., \lambda_n, -\lambda_{n+1}, ..., -\lambda_{2n})$. Then the operator $\hat{H}$ can be written as:

$$\hat{H} = B^\dagger D B = \sum_{i=1}^{n} \left(\lambda_i \hat{b}_i^\dagger \hat{b}_i - \lambda_{n+i} \hat{b}_i \hat{b}_i^\dagger\right) = \sum_{i=1}^{n} (\lambda_i - \lambda_{n+i}) \hat{b}_i \hat{b}_i^\dagger - \sum_{i=1}^{n} \lambda_i \tag{2.23}$$

where in the last step we have used the commutation relation $[\hat{b}_i, \hat{b}_i^\dagger] = 1$. In this sense, $h_0 = -\sum_{i=1}^{n} \lambda_i$ is the eigenvalue of $\hat{H}$ corresponding to the quasi-particle vacuum in terms of the bosonic quasi-particle operators $(\hat{b}_i,\ \hat{b}_i^\dagger)$, while $h_i = \lambda_i - \lambda_{n+i}$ are the eigenvalues corresponding to the quasi-particle excitations.

2.2.3.2 Derivation of the Lee-Huang-Yang Energy in 1D

The Hamiltonian density for a single component bosonic gas in a periodic box of length L, with contact interactions between the bosons $V(x,x') = g\delta(x-x')$, where g is the 1D interaction strength, can be written in second quantization form as [25, 26]:

$$\hat{\mathcal{H}}(x) = \hat{\Psi}^\dagger(x)\big(-\frac{\hbar^2}{2m}\frac{\partial^2}{\partial x^2}\big)\hat{\Psi}(x) + \frac{g}{2}\hat{\Psi}^\dagger(x)\hat{\Psi}^\dagger(x)\hat{\Psi}(x)\hat{\Psi}(x). \tag{2.24}$$

Here $\hat{\Psi}(x)$ [$\hat{\Psi}^\dagger(x)$] is the bosonic field operator annihilating [creating] a boson at position x, and m the mass of the bosons. Note that $H = \langle x|\, \hat{\mathcal{H}}(x)\, |x'\rangle$ results in the many-body Hamiltonian of (2.7) for $V(x) = 0$.

To proceed we transform to the momentum space, by writing the field operator as:

$$\hat{\Phi}(x) = \frac{1}{\sqrt{L}}\hat{a}_0 + \sum_{k\neq 0}\frac{e^{ikx}}{\sqrt{L}}\hat{a}_k, \tag{2.25}$$

where $\hat{a}_k$ ($\hat{a}_k^\dagger$) the bosonic operator annihilating (creating) a boson with momentum k. Substituting the Ansatz of Eq. (2.25) into the Hamiltonian density (Eq. (2.24)), keeping terms up to bilinear order in the bosonic operators at finite momentum ($\hat{a}_{k\neq 0}$), and integrating over the length of the box, we obtain the Hamiltonian:

$$\begin{aligned}\hat{H} = \int \hat{\mathcal{H}}(x)dx = \frac{g}{2L}\hat{a}_0^\dagger\hat{a}_0^\dagger\hat{a}_0\hat{a}_0 + \\ \sum_{k\neq 0}\left[\frac{\hbar^2k^2}{2m}\hat{a}_k^\dagger\hat{a}_k + \frac{g}{2L}\left(\hat{a}_0^\dagger\hat{a}_0^\dagger\hat{a}_k\hat{a}_{-k} + \hat{a}_0\hat{a}_0\hat{a}_k^\dagger\hat{a}_{-k}^\dagger + 4\hat{a}_0^\dagger\hat{a}_0\hat{a}_k^\dagger\hat{a}_k\right)\right] \\ + \mathcal{O}(\hat{a}_k^3).\end{aligned} \tag{2.26}$$

In this formulation, the MF approximation is realized by taking into account only the zeroth order terms in the momentum excitations. Namely, we set $\hat{a}_0 = \sqrt{N}$, where N the number of particles, and neglect all higher terms. Hence the Hamiltonian reduces to the MF energy for a uniform gas $\hat{H}^{(0)} = E_{MF} = \frac{gN^2}{2L} = \frac{Ngn}{2} = \frac{gn^2L}{2}$, where $n = \frac{N}{L}$ the density of the uniform bosonic gas. This energy captures the contribution of the interparticle interaction at the MF level. To obtain the usual GP equation in this approach we define the energy functional

$$E(\Phi) = \int \left(\mathcal{E}_{SP}(\Phi) + \mathcal{E}_{MF}(\Phi)\right) dx,$$

where the single particle energy density

$$\mathcal{E}_{SP}(\Phi) = i\hbar\Phi^*\frac{\partial\Phi}{\partial t} + \frac{\hbar^2}{2m}\left|\frac{\partial\Phi}{\partial x}\right|^2 + V(x)\,|\Phi|^2$$

is the energy functional which produces the single particle time dependent Schrödinger equation, and

$$\mathcal{E}_{MF}(\Phi) = \frac{E_{MF}}{L} = \frac{gn^2}{2}$$

is the MF energy density. Finally, a variational treatment with respect to Φ^*, results in the time-dependent 1D GP equation:

$$i\hbar\frac{\partial\Phi}{\partial t} = -\frac{\hbar^2}{2m}\frac{\partial^2\Phi}{\partial x^2} + V(x)\Phi + \frac{\partial\mathcal{E}_{MF}}{\partial n}\Phi = -\frac{\hbar^2}{2m}\frac{\partial^2\Phi}{\partial x^2} + V(x)\Phi + g\left|\Phi\right|^2\Phi, \quad (2.27)$$

in agreement with the GP equation we derived in Sec. 2.2.2.

To obtain the higher order correction we have to take into account the depletion of the condensate due to quantum fluctuations, by setting the particle number $N = \hat{a}_0^\dagger\hat{a}_0 + \sum_{k\neq 0}\hat{a}_k^\dagger\hat{a}_k \Rightarrow \hat{a}_0^\dagger\hat{a}_0^\dagger\hat{a}_0\hat{a}_0 = N^2 - 2N\sum_{k\neq 0}\hat{a}_k^\dagger\hat{a}_k + \mathcal{O}(\hat{a}_k^4)$. Then substituting into the Hamiltonian of Eq. (2.26) we obtain:

$$H = \frac{gN^2}{2L} + \sum_{k\neq 0}\left(\frac{\hbar^2k^2}{2m} + \frac{gN}{L}\right)\hat{a}_k^\dagger\hat{a}_k + \frac{gN}{2L}\sum_{k\neq 0}\left(\hat{a}_k\hat{a}_{-k} + \hat{a}_k^\dagger\hat{a}_{-k}^\dagger\right) \quad (2.28)$$

To employ the techniques discussed in Sec. 2.2.3.1 towards the calculation of the 1st order correction to the energy, known as LHY energy, we first have to rewrite Eq. (2.28) in bilinear form. To this end, one has to notice that we can identify the operators creating a boson with positive and negative momentum as two different bosonic operators, i.e. $\hat{a}_1 = \hat{a}_k$ and $\hat{a}_2 = \hat{a}_{-k}$, since $[\hat{a}_k, \hat{a}_{-k}^\dagger] = 0$ for every $k \neq 0$. With that we can write the set of operators $A^\dagger = (\hat{a}_k^\dagger, \hat{a}_{-k}^\dagger, \hat{a}_k, \hat{a}_{-k})$. However, since the Hamiltonian of Eq. (2.28) only includes terms that preserve the total momentum [i.e. there are no terms $\propto \hat{a}_k\hat{a}_k$, etc.], we can reduce the matrix dimensions by half and use the set of operators $\Phi^\dagger = (\hat{a}_k^\dagger, \hat{a}_{-k})$ instead of A. Note that the reduced set of operators satisfies the bosonic commutation condition $G = [\Phi, \Phi^\dagger] = \begin{pmatrix} 1 & 0 \\ 0 & -1 \end{pmatrix}$.

We can now write the Hamiltonian of Eq. (2.28) in bilinear form as:

$$\hat{H} = \sum_{k>0}\Phi^\dagger H\Phi + \frac{gN^2}{2L} - \sum_{k>0}\left(\frac{\hbar^2k^2}{2m} + gn\right) \quad (2.29)$$

with the hamiltonian matrix

$$H = \begin{pmatrix} \frac{\hbar^2k^2}{2m} + gn & gn \\ gn & \frac{\hbar^2k^2}{2m} + gn \end{pmatrix}.$$

Note that the sums in Eq. (2.29) are now over positive momenta. As shown in Sec. 2.2.3.1 we can diagonalize the Hamiltonian of Eq. (2.29), by solving the characteristic equation (Eq. (2.22)):

$$\det\left(GH - \epsilon(k)I_2\right) = 0 \Rightarrow$$

$$\Big(\frac{\hbar^2k^2}{2m}+gn-\epsilon(k)\Big)\Big(-\frac{\hbar^2k^2}{2m}-gn-\epsilon(k)\Big)+(gn)^2=0\Rightarrow$$
$$\epsilon(k)^2=\Big(\frac{\hbar^2k^2}{2m}\Big)^2+2\frac{\hbar^2k^2}{2m}gn,$$

which is called the Bogoliubov dispersion relation. Then using Eq. (2.23) and collecting the constant terms in Eq. (2.29), we find that the ground state energy corresponding to the quasi-particle vacuum is:

$$E_0=\frac{gn^2L}{2}+\sum_{k>0}\Big(\epsilon(k)-\frac{\hbar^2k^2}{2m}-gn\Big). \tag{2.30}$$

2.2.3.3 Closed Forms and Extended Gross-Pitaevskii Equation

We now move to explicitly calculate the sum in Eq. (2.30) and to write the ground state energy including the LHY correction in closed form. To this end, we substitute the sum with an integral over k according to $\sum_{k>0}\rightarrow\frac{L}{2\pi}\int_0^{+\infty}dk$, resulting in the energy density:

$$\mathcal{E}=\frac{E_0}{L}=\frac{gn^2}{2}+\frac{1}{2\pi}\int_0^{+\infty}\big(\epsilon(k)-\frac{\hbar^2k^2}{2m}-gn\big)dk. \tag{2.31}$$

The integral can be calculated analytically by setting $\hbar k=\sqrt{mgn}y\Rightarrow\hbar dk=\sqrt{mgn}dy$, then

$$\begin{aligned}\mathcal{E}=&\frac{gn^2}{2}+\frac{\sqrt{mg^3n^3}}{2\pi\hbar}\int_0^{+\infty}\big(\sqrt{y^2+\frac{y^4}{4}}-\frac{y^2}{2}-1\big)dy\\ =&\frac{gn^2}{2}-\frac{2\sqrt{mg^3n^3}}{3\pi\hbar},\end{aligned} \tag{2.32}$$

where the definite integral with respect to y is simply $-4/3$.

Note that already at the single species level, the ground state energy (including the LHY correction) predicts a liquid-like state with saturation density $n_s=\frac{4mg}{9\pi^2\hbar^2}$, which is the density that minimizes the energy per particle $\frac{\mathcal{E}}{n}=\frac{E_0}{N}$. However, this density is in general significatly smaller than the usual density in 1D BECs [63], and typically predicts a very dilute liquid spread over a large length scale.

Having found the ground state energy including the LHY correction, we can also derive the corresponding extended Gross-Pitaevskii equation (eGPE) as:

$$i\hbar\frac{\partial\Psi}{\partial t}=-\frac{\hbar^2}{2m}\frac{\partial^2\Psi}{\partial x^2}+\frac{\partial\mathcal{E}}{\partial n}\Psi=-\frac{\hbar^2}{2m}\frac{\partial^2\Psi}{\partial x^2}+g\left|\Psi\right|^2\Psi-\frac{\sqrt{mg^3}}{\pi\hbar}\left|\Psi\right|\Psi \tag{2.33}$$

Note that the usual GP equation, corresponding to the MF approximation, is derived in the exact same way, by simply neglecting the first order correction to the ground state energy density, i.e. the LHY correction $\mathcal{E}_{LHY}=-\frac{2\sqrt{mg^3n^3}}{3\pi\hbar}$. An interesting consequence of taking into account the LHY correction is that the attractive

regime ($g < 0$) becomes unstable even in one dimension. Indeed, while at the MF limit the usual GP equation allows for bright-soliton stationary solutions in one dimension, within the LHY approach, the ground state energy obtains an imaginary part for $g < 0$ and no stationary solutions exist [i.e. every solution would decay with lifetime $\tau \approx \hbar / Im(\mathcal{E}_{LHY})$]. Of course, bright solitons do indeed occur in attractive 1D systems [83], which suggests that the LHY treatment is not appropriate for the attractive regime. Indeed, a basic assumption, in the derivation of the LHY energy, is that the quantum fluctuations emerge on top of a uniform density distribution such that $\Phi \approx \sqrt{\frac{N}{L}} = const.$, when neglecting quantum fluctuations. This assumption is justified when treating the repulsive system in free space, where indeed the MF solution corresponds to a uniform density under periodic boundary conditions. At the mean field level, an external potential can be introduced under the so called Local Density Approximation (LDA). LDA assumes that the external potential varies slowly enough in space, such that at each point it can be considered as an effectively constant shift to the energy corresponding to the uniform density. Thus, under this assumption, the non-uniform case is addressed, by assuming that at each point in space the MF energy maintains its free space form, but with a space dependent density. This situation becomes more complicated when treating the system within the LHY theory, since we cannot as easily assume that the quasi-particle vacuum energy experiences only a local shift in the presence of an external potential. Similarly, when the MF solution takes a soliton form, the assumption of a uniform zeroth-order solution is violated and we cannot assume that the eGPE of Eq. (2.33) holds. Extending the above-described LHY treatment to arbitrary external geometries and zeroth-order density configurations is a highly desirable, but far from trivial theoretical challenge, that remains open.

2.2.3.4 Bogoliubov de Gennes Equations

One important question is the ability to distinguish droplets from other MF configurations, especially when the saturation density of the droplet is either too high or too low rendering the observation of the FT profile somewhat impractical. The inelastic collisions of quantum droplets [177, 180] can be a useful probe, although aside from being more involved to realize experimentally, the inelasticity is also more significant deep in the FT regime. A useful measure, which can be experimentally accessed, is the low-amplitude excitation spectrum of 1D droplet configurations. In particular, 1D solitons do not support any discrete modes but only continuum excitations [83, 85], hence the observation of discrete droplet modes in the low-amplitude excitation spectrum could serve as a valuable probe in the effects of quantum fluctuations in the bosonic system. Moreover, differences in the spectrum of quantum droplets depending on the dimensionality can offer significant insights in the dimensional crossover, which has a crucial impact on the development of correlations [139, 162, 182].

Let Ψ be a stationary solution of the eGPE of Eq. (2.33) corresponding to chemical potential μ. Our aim is to determine the response of the system following a perturbation by a low amplitude excitation. The perturbation can be described by the following ansatz:

$$\tilde{\Psi} = e^{-i\mu t/\hbar}[\Psi + \epsilon(ae^{i\omega t} + b^* e^{-i\omega^* t})], \tag{2.34a}$$

$$\tag{2.34b}$$

where $a = a(x)$ and $b = b(x)$ are arbitrary (smooth) space depended complex functions and ω is an in-general complex phase.

Working to order $\mathcal{O}(\epsilon)$ the derivative terms become:

$$i\hbar \frac{d}{d\epsilon}\frac{\partial \tilde{\Psi}}{\partial t}\Big|_{\epsilon=0} = \left[(\mu - \hbar\omega)ae^{i\omega t} + (\mu + \hbar\omega^*)b^* e^{-i\omega^* t}\right] e^{-i\mu t}, \tag{2.35a}$$

$$-\frac{\hbar^2}{2m}\frac{d}{d\epsilon}\frac{\partial^2 \tilde{\Psi}}{\partial x^2}\Big|_{\epsilon=0} = -\frac{\hbar^2}{2m}\left[\frac{\partial^2 a}{\partial x^2}e^{i\omega t} + \frac{\partial^2 b^*}{\partial x^2}e^{-i\omega^* t}\right] e^{-i\mu t}. \tag{2.35b}$$

The density dependent terms have a somewhat more complicated form. Using the fact that the general form of these terms stem from the derivative $\frac{\partial \mathcal{E}}{\partial n}\Psi$, we can write the impact of the perturbation to first order in the perturbation $\mathcal{O}(\epsilon)$ in the general form:

$$\frac{d}{d\epsilon}\left(\frac{\partial \mathcal{E}(\tilde{n})}{\partial n}\tilde{\Psi}\right)\Big|_{\epsilon=0} = \frac{\partial \mathcal{E}}{\partial n}\frac{d\tilde{\Psi}}{d\epsilon}\Big|_{\epsilon=0} + \frac{\partial^2 \mathcal{E}}{\partial n^2}\frac{d\tilde{n}}{d\epsilon}\Big|_{\epsilon=0}\Psi, \tag{2.36}$$

where $\tilde{n} = \left|\tilde{\Psi}\right|^2$ is the particle density associated with the perturbed solution of our ansatz. Hence, we only need to calculate the derivatives:

$$\begin{aligned}
\frac{d\tilde{\Psi}}{d\epsilon}\Big|_{\epsilon=0} &= ae^{i\omega t} + b^* e^{-i\omega^* t}, \\
\frac{d\tilde{n}}{d\epsilon}\Big|_{\epsilon=0} &= (\Psi^* a + \Psi b)e^{i\omega t} + (\Psi^* b^* + \Psi a^*)e^{-i\omega^* t}, \\
\frac{\partial^2 \mathcal{E}}{\partial n^2} &= g - \frac{\sqrt{mg^3}}{2\pi\hbar\sqrt{n}}.
\end{aligned} \tag{2.37}$$

Collecting all the terms and separating the terms $\propto e^{i\omega t}$ and $\propto e^{-i\omega^* t}$, we arrive at a coupled system of two eigenvalue equations for the two amplitudes and the common phase ω.

$$\begin{aligned}
\hbar\omega a &= \left[\mu + \frac{\hbar^2}{2m}\frac{\partial^2}{\partial x^2} - \left(2gn - \frac{3\sqrt{mg^3}}{2\pi\hbar}\sqrt{n}\right)\right] a - \left(g - \frac{3\sqrt{mg^3}}{2\pi\hbar\sqrt{n}}\right)\Psi^2 b, \\
\hbar\omega b &= \left[-\mu - \frac{\hbar^2}{2m}\frac{\partial^2}{\partial x^2} + \left(2gn - \frac{3\sqrt{mg^3}}{2\pi\hbar}\sqrt{n}\right)\right] b + \left(g - \frac{3\sqrt{mg^3}}{2\pi\hbar\sqrt{n}}\right)\Psi^{*2} a.
\end{aligned} \tag{2.38}$$

Setting the amplitude vector $u = (a, b)$ we can write the above equations in matrix form as $Au = \hbar\omega u$, with the so-called stability matrix A:

$$A = \begin{pmatrix} \mu + \frac{\hbar^2}{2m}\frac{\partial^2}{\partial x^2} - \left(2gn - \frac{\sqrt[3]{mg^3n}}{2\pi\hbar}\right) & -\left(g - \frac{\sqrt[3]{mg^3}}{2\pi\hbar\sqrt{n}}\right)\Psi^2 \\ \left(g - \frac{\sqrt[3]{mg^3}}{2\pi\hbar\sqrt{n}}\right)\Psi^{*2} & -\mu - \frac{\hbar^2}{2m}\frac{\partial^2}{\partial x^2} + \left(2gn - \frac{\sqrt[3]{mg^3n}}{2\pi\hbar}\right) \end{pmatrix}. \quad (2.39)$$

By solving the resulting eigenvalue problem, we can derive the energy spectrum and corresponding eigenmodes of the elementary small-amplitude excitations on top of the stationary solution Ψ. Eigenmodes associated with complex eigenvalues correspond to dynamical instabilities of said solutions, while real eigenvalues describe stable excitation modes available to the system following a weak perturbation.

2.3 Numerical Approach

The MF approach and the beyond MF, LHY theory, have proven to be extremely successful in describing the physics of weakly interacting ultracold bosonic mixtures. Some analytical approaches have also been successful in addressing the opposite, so called universality limit, of very strong interactions [28, 50]. However, these analytical methods face many challenges in extending their validity beyond these limits, to arbitrary interaction strengths, as well as to various external geometries, particle numbers, dimensions, and compositions of the atomic mixture. For this reason, highly sophisticated computational methods have been developed aiming to explore the ground state properties and out-of-equilibrium quantum dynamics of a wide variety of many-body systems. We cannot provide a comprehensive review of all such methods, nor of the wide range of beyond MF physics they have unveiled [410]. Instead, we will simply mention a few of them, namely the exact diagonalization or configuration interaction approach [411–414], Monte Carlo methods [415, 416], density matrix renormalization group methods (DMRG) [417–420], field-theoretical approaches [421–423], and variational methods [424].

In the following, we focus on the Multi-Layer Multi-Configuration Time-Dependent Hartree method for atomic mixtures (ML-MCTDHX), which is a variational approach capable of treating both the ground state and the dynamics of finite size systems of bosons, fermions and atomic mixtures thereof [425–428]. This method is based on the Multi-Layer Multi-Configuration Time-Dependent Hartree method (ML-MCTDH), which was designed as a wavepacket dynamical approach to handle molecular dynamics of distinguishable particles in the context of quantum chemistry. The key idea is to rely on sequential spectral decomposition steps to efficiently capture correlations between the various degrees of freedom [429–431]. Recently, a re-interpretation of the ML-MCTDH method in the context of tree tensor networks was also proposed,

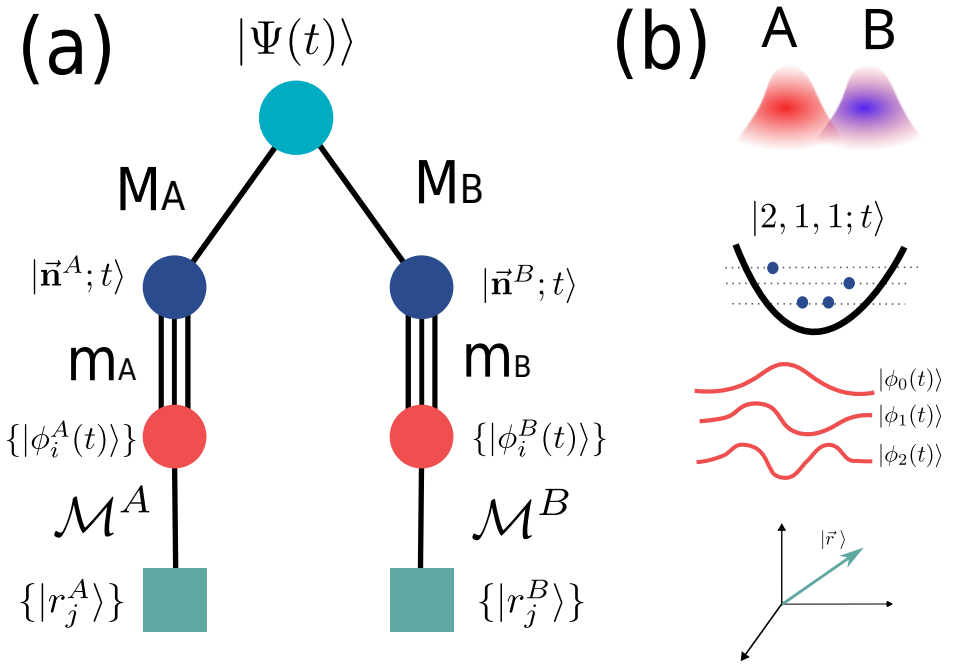

FIGURE 2.2: (a) Schematic representation of the ML-MCTDHX ansatz for a two-component bosonic mixture. (b) Visualizations of the physical context expressed at each layer of the ansatz.

highlighting how it can serve as a clear extension and generalization of matrix-product-state methods (eg. DMRG) [432–436]. To extend the methodology to indistinguishable bosons, MCTDHB was proposed [437–440]. It takes into account the exchange symmetry of the bosons, both at the level of the wavefunction Ansatz and at the level of the resulting equations of motion, and it has been successfully applied to various bosonic systems [441–446]. MCTDHB was subsequently further extended into the ML-MCTDHX, which is flexible enough to handle both bosonic and fermionic permutation symmetry as well as mixtures of arbitrary species in all spatial dimensions and internal degrees of freedom (including eg. spin components), by utilizing the multilayer scheme [447, 448]. Below, we provide further details into the ML-MCTDHX, which is used in [IE1, IE2] to address two-component mixtures, primarily consisting of two bosonic components, but also a Bose-Fermi mixture in [IE2]. It it worth noting, however, that the ML-MCTDHX has also been applied to atomic systems in harmonic traps [80, 449] and lattices [448, 450], different spatial dimensions [428], polaron dynamics [451, 452], as well as for spinor components [447, 453]. Finally, the predictions of ML-MCTDHX have been benchmarked against various approaches including for two harmonically trapped particles [454], for systems hosting impurities [455, 456], and for spin-chain settings [457].

2.3.1 Many-body Wavefunction Ansatz for Binary Mixtures

ML-MCTDHX is a variational method for solving the time-dependent many-body Schrödinger equation of atomic mixtures [425–428]. As with ML-MCTDH, the total

many-body wavefunction is sequentially expanded with respect to time-dependent and variationally optimized basis states, such that they capture the important correlation effects, while using a computationally manageable basis size. In principle, the system still resides in an infinite-dimensional Hilbert space, which - even after truncated - scales exponentially with the system size, as mentioned in Sec. 2.2.1. However, depending on the inherent properties of the system it is possible that, at each time step, there exists a basis in which the expansion coefficients of the system fall rapidly resulting in only a small number of basis states having a non-negligible occupation. It turns out that this is indeed the case for many systems of interest, and as a result, variationally optimizing the time-dependent basis states allows the ML-MCTDHX to numerically determine such a basis at each time step. Thus, ML-MCTDHX requires a reduced number of basis states compared to expansions relying on a time-independent basis. This idea can also be linked to the notion of a co-moving basis. At each timestep the system occupies a certain subspace of the total Hilbert space, hence to track its dynamics only this subspace needs to be spanned by our basis set. Assuming that this subspace is always a small enough fraction of the total Hilbert space, a dynamically optimized basis of numerically tractable size can track the dynamics of the system without losing information. Finally, the multilayer ansatz allows us to efficiently account for intra and interspecies correlations when simulating the dynamics of atomic mixtures.

Focusing on a two-component mixture, the total Hilbert space is $H^{AB} = H^A \otimes H^B$, with H^σ representing the Hilbert space in which the σ species resides. In general, the σ species can correspond to bosons, fermions, or distinguishable particles. For simplicity, we restrict this brief presentation to bosonic atoms. In order to efficiently account for the interspecies correlations, the total many-body wavefunction $|\Psi(t)\rangle$ is expressed in a truncated Schmidt decomposition [96, 99] of rank M:

$$|\Psi(t)\rangle = \sum_{k=1}^{M} \sqrt{\lambda_k(t)}\, |\Psi_k^A(t)\rangle\, |\Psi_k^B(t)\rangle\,. \tag{2.40}$$

The Schmidt weights $\lambda_k(t)$, assumed to be in decreasing order, are referred to as the natural species populations of the k-th species function $|\Psi_k^\sigma(t)\rangle$ of the σ species. Note that $\{\Psi_k^\sigma\}$ is an orthonormal set of N^σ-body wavefunction residing in H^σ and spanning a subspace within it. The system is entangled [95, 100, 458, 459] when $\lambda_k(t)$ is non-zero for more than one values of k, meaning that the many-body state cannot be expressed as a direct product of two states in H^A and H^B respectively.

In turn, each species function $|\Psi_k^\sigma(t)\rangle$ is expanded in terms of the bosonic number states $|n_1^{\sigma;k}, n_2^{\sigma;k}, ..., n_{m_\sigma}^{\sigma;k}; t\rangle \equiv |\mathbf{n}_k^\sigma\rangle$. The bosonic number states, are constructed based on allowing the particles to occupy m_k^σ time-dependent single-particle functions (SPFs) $|\phi_i^{\sigma;k}(t)\rangle$, with time-dependent weights $A_{n_k^\sigma}(t)$ and $N^\sigma = \sum_i^{m_\sigma} n_i^{\sigma;k}$ the

number of bosons in species σ. Explicitly, this expansion is given by:

$$|\Psi_k^\sigma(t)\rangle = \sum_{\mathbf{n}_k^\sigma | N^\sigma} A_{n_k^\sigma}(t) \, |\mathbf{n}_k^\sigma\rangle \, . \tag{2.41}$$

The SPFs $|\phi_i^{\sigma;k}(t)\rangle$ evolve in the single-particle Hilbert space spanned by the time-independent (primitive) basis $\{|r_j^{k;\sigma}\rangle\}_{j=1}^{\mathcal{M}}$. Namely:

$$|\phi_i^{\sigma;k}(t)\rangle = \sum_{j=1}^{\mathcal{M}} C_{i;j}^{\sigma;k} \, |r_j^{k;\sigma}\rangle \, . \tag{2.42}$$

The latter can correspond eg. to an 1D grid in real space, or in a combination of continuous and discrete variables corresponding to spatial, momentum, or spin degrees of freedom in one or more spatial dimensions. Finally, a further ML-MCTDH expansion of the SPFs can in general be employed if one needs to capture complex geometries or inter-particle interactions which strongly couple the primitive degrees of freedom. See also Fig. 2.2(a) for a schematic representation of the many-body wavefuntion ansatz, illustrated as a tree-diagram. In Fig. 2.2(b) we also include corresponding schematics at each layer, in order to highlight the physical context represented by the respective layer.

The ML-MCTDHX many-body wavefuntion ansatz is then inserted into a variational principle, such as the Lagrangian [460], McLachlan [461] or the Dirac - Frenkel [462, 463], yielding the ML-MCTDHX equations of motion [425–428]. For bosonic mixtures, these refer to a set of M^2 ordinary (linear) differential equations of motion for the Schmidt coefficients $\lambda_k(t)$, coupled to a set of $M[\binom{N_A+m_A+1}{N_A} + \binom{N_B+m_B+1}{N_B}]$ non-linear integrodifferential equations for the species functions, and $m_A + m_B$ non-linear integrodifferential equations for the SPFs.

Concluding, let us mention explicitly that in the limit $M = m_A = m_B = 1$ the ML-MCTDHX ansatz reduces to the MF one discussed in Sec. 2.2.2, and the equations of motion become the (coupled set of) Gross-Pitaevskii equation(s). Systematically increasing the parameters M, m_σ, and $\mathcal{M}$ until the observables of interest converge up to the desired numerical accuracy, allows us to determine the convergence of the ML-MCTDHX simulations. Of course, increasing the number of basis functions of the ML-MCTDHX method also increases the computational cost of the corresponding many-body simulations and at some point it becomes prohibitive. Finally, let us note that, unlike the MF approximation, the LHY theory does not emerge as a clear limit of the ML-MCTDHX ansatz. Instead, the LHY theory constitutes an intermediate model, between the single-orbital approximation of the MF ansatz and the full many-body treatment of the ML-MCTDHX. Namely, the LHY theory captures the energy of the underlying many-body state, as well as the corresponding single-particle density of each species, but only up to the accuracy of the second order perturbative treatment.

Chapter 3

Outline of Scientific contributions

Self-bound quantum droplets [113, 139–142] are correlated quantum many-body (MB) phases of matter [29], manifesting the existence of quantum correlations in macroscopic mixtures, represented to first order by the Lee-Huang-Yang (LHY) correction term [163]. Interestingly, the impact of quantum correlations in quantum droplets is evident already at single-particle observables, such as the energy or the particle density. Moreover, in three dimensions (3D), quantum correlations stabilize the system against collapse stemming from mean-field (MF) effects [139–142].

These correlated macroscopic structures have been realized [173–175, 183] in contact interacting bosonic mixtures in three-dimensions, as well as in dipolar gases [113, 114, 119, 166, 167] and mixtures thereof [140, 141], indicating the ubiquitous nature of the main phenomenology. Focusing on short-range interactions, several experiments have addressed droplet dynamical formation [183, 464], the droplet to a gaseous BEC crossover [174, 465, 466] and their collisional properties [177], with their self-evaporation and three-body recombination [173–175, 183] constituting the main experimental challenges. These challenges are significantly suppressed in one dimension (1D), where the droplet lifetime is expected to be prolonged [181, 182] and correlation effects are usually enhanced [162, 176, 178–180, 184, 189, 190, 467].

In the following outlined works, we aim to provide further insights on the correlation properties of 1D bosonic mixtures. We begin by investigating the ground state and dynamical properties of a harmonically trapped two-component bosonic mixture [IE1, IE2], utilizing the *ab-initio* many-body ML-MCTDHX method, which is able to capture LHY and beyond-LHY correlations present in the system. Hence, we aim to benchmark and validate the perturbative predictions of the LHY theory, while also being able to characterize higher-order observables such as the entanglement content between the two-components and the two-body correlations within the same component. Moreover, we are able to further our investigations to regimes outside the formal assumptions of the LHY theory, namely in terms of the external confinement, the interatomic interaction strengths, and the number of atoms in each component. Surprisingly, the persistence of the LHY phenomenology was verified

even in regimes where formally it would be expected to fail, while however, significant quantitative deviations remain evident.

Armed with these observations and the intuition developed through this *ab-initio* numerical treatment, we revisited the LHY theory in 1D [IE3]. The original derivation [162], motivated by the idea of utilizing quantum fluctuations to stabilize the mixture against MF collapse in 3D, focused explicitly in the attractive edge of the MF regime. However, we found that such an assumption is unnecessary in 1D and quantum droplets were shown persist throughout the MF stability regime. Indeed, since in 1D bosonic systems the contribution of quantum correlations is attractive, self-bound droplets can emerge in free space for any interaction strength within the MF stability regime. This is in sharp contrast to the 3D case, where the contribution of quantum correlations is repulsive, thus quantum droplets emerge only past the attractive stability threshold [139]. Moreover, we provided a derivation of the LHY energy and the resulting eGPEs, valid throughout the MF stability regime, for two-, three-, and four-component mixtures. The latter was shown to be the highest number of components for which an analytical derivation is possible in the general case. Finally, the three-component case was studied in more detail [IE4], focusing in the case of particle imbalanced droplets and investigating the resulting ground state configurations and the supported elementary excitations.

3.1 *Ab-Initio* Many-Body One-Dimensional Binary Quantum Droplets in a Harmonic Trap

3.1.1 Correlated Dynamics of Quantum Droplets in a One-Dimensional Harmonic Trap

As mentioned, the lifetime of quantum droplets is expected to be increased in 1D [181, 182] and especially in heteronuclear mixtures [175], where correlation effects should also be more pronounced owing to the mixed character of the system. In [IE1] we contributed one of the early explorations in the impact of of correlations in heteronuclear mixtures and the resulting droplet configurations. In particular, due to the lack of a corresponding closed form eGPEs the heteronuclear setting had not been extensively studied [176–178, 184]. Moreover, few works had addressed homonuclear mixtures with non-perturbative approaches to unveil beyond-LHY physics in free space [184–186] and later in lattice settings [192, 468]. A non-perturbative investigation of 1D harmonically trapped droplets was presented, addressing the impact of correlations in stationary and out-of-equilibrium droplet configurations, in the realistic scenario where trap effects are not neglected [173–175, 183]. For the non-perturbative treatment, we relied on the multi-layer multi-configuration time-dependent Hartree method for atomic mixtures (ML-MCTDHX) [425–427], while comparing our results with the common MF approach [25], as well as with the predictions of the eGPEs [162].

First, we showcased that signatures of the characteristic FT density profile of quantum droplets are observed in symmetric homonuclear mixtures for weak attraction or higher atom numbers. This effect is not present in the predictions of the eGPE [184, 469]. Moreover, for larger attraction the many-body configuration transitions from a FT to a Gaussian-shaped density profile, as in the case of free space [184, 186]. Finally, similar structures were observed also for interaction or mass imbalanced bosonic mixtures. Namely, the more strongly repulsive or the heavier component also exhibits FT signatures for reduced intercomponent attraction, while the two-components are spatially mixed. In all cases, the correlation pattern of droplets reveals an anti-bunching behavior reducing the probability of simultaneously finding two bosons of the same species at the same spatial location. Instead, bosons belonging in different components are weakly spatially correlated. We interpret this correlation pattern to be an important higher-order observable characterizing the droplet configurations, which is also found to persist in free-space [184] and in lattice settings [468].

Subsequently, a quench of the trap frequency was employed to probe the breathing dynamics of the droplet. Sufficiently large quench amplitudes cause higher-lying motional excitation modes to build-upon the homonuclear droplet bulk, while simultaneously part of the density tails becomes expelled. This process is reminiscent of the self-evaporation mechanism appearing in 3D [183, 464]. This self-evaporation mechanism, is absent in 1D free-space [179, 184], illustrating that the interplay with the external confinement can crucially effect the dynamical response of quantum droplets. The onset of this unstable dynamics was found to be accompanied by an increase in intercomponent entanglement and the emergence of long-range correlations in the two-body intracomponent density. Moreover, we provided analytical estimations within the LHY theory [180], along with numerical estimations, for the resulting breathing frequency. The breathing frequency appears to approach the ideal gas limit for large attraction, while it features a decreasing tendency as the droplet transitions towards the FT regime, similarly to its behavior in free space [184–186]. Turning our attention to the dynamics of heteronuclear mixtures, we found that a species selective quench can lead to a pronounced correlation driven dephasing. The mechanism behind this dephasing appears to be the competition between the bound nature of the system, which favors the two components oscillating in-phase, and the different trapping frequencies applied to each component, which seeds differing breathing frequencies for each component.

Finally, the harmonic confinement permitted us to also excite the dipole mode of droplets, which is absent in free space. Indeed, sudden displacements of the trap position leads to coherent oscillations of the center of mass of the droplet configuration, which were found to be insensitive to the interaction strengths. In addition, we employed a species selective quench protocol, where either only the harmonic trap

applied to one of the components was shifted or both harmonic traps were simultaneously shifted in opposite directions. For weak attractions these quenches give rise to irregular dipole patterns characterized by intercomponent collisions, leading to energy transfer between the components. Conversely, strongly attractive droplets preferentially maximized their overlap even at the cost of residing further than the minimum of their respective external potentials.

3.1.2 Particle Imbalanced One-Dimensional Quantum Droplets

Within the framework of the LHY theory [139], the particle density of two - component droplet configurations is described by a coupled set of eGPEs. Imposing a fixed density ratio condition, which is determined by the ratio of the intracomponent interaction strengths, the genuinely two-component system can be further reduced to an effective single-component one [139, 162]. Moreover, this ratio condition corresponds to the optimal stability regime for quantum droplets in 3D [178, 183]. As such, the majority of studies on quantum droplet studies tend to focus in this regime. Our previous theoretical investigation [IE1] inadvertently explored deviations from this regime, in 1D, by employing mass or interaction inter-component imbalance, without explicitly fixing the density ratio. A similar approach was taken also to address genuinely two-component droplet configurations in free-space [184]. Meanwhile, in experimental works, such a precise control of the particle ratio is challenging, hence the effects of deviations from this optimal condition are naturally probed [175, 183]. Overall, these studies provided evidence that quantum droplets can also remain stable when this fixed density ratio condition is weakly violated. From the theoretical side, this was studied explicitly for mass balanced configurations within the LHY theory in 3D [194–196]. However, these works also showed, that 3D droplet configurations indeed, become unstable when this fixed density ratio condition is significantly violated. In 1D, particle imbalanced configurations were addressed for strongly interacting bosonic mixtures in a lattice geometry [193] focusing on many-body bound state formation and within LHY theory in a ring geometry [190] addressing rotational properties.

In [IE2] we considered a harmonically trapped two-component bosonic mixture, featuring weak short-range interactions. We focused primarily on large particle differences and we addressed the complex interplay between particle, interaction and mass imbalance on the droplet formation. We use the terms majority component for the component, which consists of a larger number of particles, and minority component for the other less populated component. Our approach allows us to follow a multi-pronged approach to explore the particle imbalanced setting both from the macroscopic and the few-body limit. Namely, to address the former we construct an effective analytical model at the limit of large particle imbalance based on the LHY theory. Meanwhile, we treat the case were the minority component is reduced to the

few-body limit using the ML-MCTDHX [50, 425–427, 470] method, which accounts also for beyond LHY effects.

In particular, we derived an effective reduced set of equations in free-space based on the full system of eGPEs [162, 189]. We use this model to obtain analytical insights into the possibility of droplet states emerging and on the crucial role of the particle imbalance and the interaction strengths on the resulting configurations. For instance, our model predicts that in the limit of large particle imbalance the system approximately decouples into a configuration consisting of a quantum droplet for the majority component and a localized bright-soliton structure for the minority one. Moreover, our effective model suggests that deviations from the decoupled limit are driven primarily by the intracomponent repulsion between the minority atoms. These results were also verified by *ab-initio* ML-MCTDHX simulations, while also allowing us to explore the impact of increasing interaction strengths as well as addressing more massive impurities. In both cases this increase results in enhanced spatial modulations of the density profile of the majority component at the overlap region with the minority component, while the former maintains signatures of a FT droplet profile. Interestingly, the phenomenology derived for macroscopic configurations is found to persist for the most part, even when the minority component is occupied by as few as two or four atoms. Finally, we considered the case of few fermionic minority atoms immersed in the bosonic majority component. In this case, the phenomenology described above vanishes resulting in configurations with delocalized fermionic density overlapping with the majority bosonic component, which no longer features FT signatures. This result offers additional support for the crucial role of the bosonic quantum fluctuations also within the minority component, in the development of the above described droplet phenomenology.

Our results highlight the surprising effectiveness of the LHY-theory in capturing the genuinely many-body behavior of binary bosonic mixtures even far from its formal validity region. Moreover, our findings illustrate the ability of the LHY-theory to adequately capture the behavior of the system even when the minority component is pushed to the few-body limit. In this limit the minority component operates essentially as few interacting impurities emersed in the bosonic bath of the majority component. Thus, the persistence of LHY-based phenomenology indicates a strong connection between quantum droplets and the physics of weakly coupled impurities (e.g. polarons and especially bi-, tri-polarons, etc.).

3.2 Lee-Huang-Yang Theory of Multi-component Bosonic Mixtures in One Dimension

As mentioned, quantum droplets have significantly distinct features in 1D, as compared to 3D and also 2D, which crucially affects their phenomenology. In particular,

quantum fluctuations as captured by the LHY correction exhibits a strong dependence on the dimensionality of the system [182, 471, 472]. This is in sharp contrast to the simpler MF approach, which only differs in the kinetic term regardless of the dimensionality or more generally the external geometry [25, 26]. Namely, the LHY term is attractive [162] in 1D, while it is repulsive in 3D [139], which crucially changes the droplet parametric region and its resulting phenomenology. One crucial difference between the 3D and 1D settings, already evident at the MF level, is that the 3D bosonic gas experiences collapse in the regime where the average interaction becomes attractive (eg. $g_{AB} + \sqrt{g_A g_B} < 0$ for binary mixtures), meaning that the energy minimum of the system diverges to $-\infty$. In contrast, the 1D system can support localized bright-soliton solutions in the attractive regime [83, 85, 94]. Let us note however, that although collapse does not explicitly occur in the 1D system, upon increasing attraction the bright-soliton solutions become progressively more localized. For a realistic quasi-1D system, the system is well described by the 1D approximation as long as the length scale of the gas in the strongly confined (transverse) directions is much smaller than the length scales in the weakly confined (longitudinal) direction. Hence, as the 1D attraction increases in the quasi-1D system, the width of the configuration will eventually become comparable to the transverse length scale, thus exposing the genuinely 3D nature of the system and rendering the 1D description invalid. Note however, that this 1D "collapse" does not coincide with the explicit 3D collapse, since due to the confinement induced Feshbach resonance the strongly attractive quasi-1D regime corresponds to the weakly repulsive 3D regime ($a_{3D} \approx a_{\perp}$) [390].

The repulsive contribution of the LHY correction in the 3D bosonic mixture places the droplet parametric region in the regime of overall attractive average interaction, where the system collapses within the MF approximation. In this case, the repulsive LHY term competes with the overall attraction resulting in the liquid-like self-bound quantum droplet configurations, while arresting the MF collapse. It's worth mentioning, however, that in this attractive regime the LHY energy term becomes complex with the real part being positive. This imaginary energy component suggests that the standard LHY theory is not formally valid in this regime, and a different approach should be taken for a fully consistent description of this case. Nevertheless, the standard approach [26, 139, 168, 198] is to simply fix the LHY energy to its value at the attractive stability edge and assume that it is a good approximation also in the vicinity of the edge. Alternatively, some works simply neglect the imaginary part and consider the energy correction term to have the value of the real part of the LHY energy [175, 197]. Indeed, this approach has proven extremely effective, leading to the experimental observation of quantum droplets as predicted by the LHY theory in both contact interacting [173–175, 183], and in dipolar gases [113, 114, 119, 166, 167]. The latter are owed to a somewhat different mechanism. However, the repulsive energy contribution of the LHY term remains a crucial factor. Finally, let us note that the LHY correction is present also in 3D atomic gases within the MF stability

regime where the overall interaction is repulsive [25, 26, 203]. However, since it only contributes an additional perturbatively small repulsive correction, it only provides a small quantitative correction without significantly altering the phenomenology. There are two main reasons for this. Firstly, the opposite signs of the MF and LHY terms directly result in the existence of an energy minimum at finite density, which gives the resulting structures their liquid-like and self-bound character. Secondly, at the edge of the attractive MF stability regime, the average MF interaction, as defined above, becomes zero. Hence, in the vicinity of this edge, the average MF interaction can be also considered to be perturbatively small and comparable to the LHY contribution, thus enhancing impact of the LHY correction. One exception, where the LHY correction can qualitatively impact the repulsive regimes is the possibility of sustaining bubble configurations close to the repulsive edge of the MF stability, although, further study is required at this regime [203].

Early studies on 1D quantum droplets [162, 180, 185, 186] were motivated by their 3D counterparts and hence also focused on the attractive edge of the stability region and on the corresponding approximation of the LHY energy. In [IE3] we focus explicitly on the 1D system and we revisit the derivation of the LHY energy, with the aim of clarifying the required assumptions and emphasize the unique droplet phenomenology available in the 1D system. Concretely, the 1D geometry i) does not feature MF collapse in the standard 3D sense, ii) hosts stable bright-soliton configurations [83, 85, 94] at the overall attractive regime iii) hosts a droplet regime (once beyond MF corrections are taken into account) which coincides with the MF stability regime. Moreover, within the MF perspective, multi-component mixtures undergo phase separation at the repulsive edge of the MF stability regime (eg. $g_{AB} > \sqrt{g_A g_B}$ for binary mixtures). As we will discuss below, we find that once extended to be valid throughout the MF stability regime, the LHY terms leads to an early onset of phase separation, which occurs also within the MF stability regime for genuinely multi-component settings. Interestingly, these differences suggest that 1D platforms could host more stable, controllable and enriched quantum droplet phases throughout the MF stability regime and not just at the attractive edge, especially in multicomponent settings [IE2, 190, 193, 194, 196, 197]. Hence, in [IE3] we provide a more general framework which accurately captures the LHY correction across the MF stability region for both homonuclear and heteronuclear mixtures in 1D free-space. Moreover, we extend the LHY framework to three- and four-component mixtures in 1D, while again ensuring it is valid throughout the MF stability regime, with the aim of unveiling novel self-bound structures. Previous efforts related to three-component 1D droplets considered a single impurity in the third component [199, 200, 202, 473] or assumed only MF coupling between the droplet and the impurities [474, 475].

In particular, we employed the perturbative Bogoliubov approach (see also Sec. 2.2.3) to derive the LHY energy and the corresponding extended Gross-Pitaevskii equatios for two-, three- and four-component 1D bosonic mixtures. Whenever possible, we

provided exact closed form formulas for the LHY energy and for the resulting nonlinear terms of the eGPEs. The original treatment for two-component settings [162], naturally emerges as a limiting case, when the interaction strengths are fixed at the attractive threshold of the MF stability regime. As mentioned, our approach remains valid throughout the 1D MF stability regime, encompassing both attractive and repulsive interspecies interactions. For symmetric two-component mixtures, our approach provides quantitative corrections to the predictions of the approximate one, which generally underestimates (overestimates) the droplet width (density maximum). Significant qualitative differences emerge when considering weakly coupled or repulsively coupled genuinely two-component mixtures. Namely, weakly coupled configurations become mixed, while in the approximate framework they always tend to maximize their overlap. Moreover, in the repulsive side of the MF stability regime we found an early onset of phase-separation for both homonuclear and heteronuclear mixtures. This is absent within the approximate framework, where again droplets prefer to maximize their overlap. The reason for these deviations is that the approximate framework consistently overestimates the impact of the LHY energy, which we find takes its minimum (negative) value at the MF stability thresholds (both the attractive and the repulsive one).

Next, we focused on higher-component mixtures where we provided exact closed form expressions for the LHY energies and the respective eGPEs of a three-component mixture with either three or two identical components. Note that the calculation for the general three-component was also provided and it can be solved numerically, inspite of the lack of a closed form expression. For the symmetric three-component 1D mixture, quantum droplet configurations are supported throughout the MF stability regime similar to the two-component case. For the case of two identical components, we found that intriguing mixed configurations emerge upon tuning the interspecies coupling. Such configurations will be further studied in [IE4]. In general the three-component droplet setting introduced in [IE3] offers a broad range of possibilities for future investigations in stable mixed droplet phases, which are absent in lower-component settings. Additionally, we derived a closed form expression for the LHY energy and interaction terms for the fully symmetric four-component mixture, which is the highest-component mixture for which the Bogoliubov modes may be determined analytically in the general case. Again the symmetric four-component mixture supports droplet configurations throughout the MF stability regime. Finally, we note that throughout [IE3] we attempted to present the derivations in a detailed and structured manner, in the interest of providing a useful entry point for researchers interested in the rapidly expanding field of quantum droplets.

3.3 Three-Component Particle Imbalanced One - dimensional Quantum Droplets

As mentioned already, recent studies have addressed two-component droplet systems, where one component is occupied by a reduced number of particles compared to the majority component both in 3D [194–196] and in 1D [IE2, 191, 193, 476]. These studies have, first of all, demonstrated the enhanced persistence of droplet configurations in 1D, as compared to the 3D case. In the latter case, more stable droplet configurations emerge when a fixed density ratio between the two-components, determined by their interaction, is strictly imposed [139, 178, 183]. In addition, they have unveiled several intriguing mixed configurations which exhibit unique droplet phenomenology both within the LHY theory framework [191, 476] and by employing *ab-initio* approaches [IE2, 193]. Moreover, these works hint at an interesting link between the physics of quantum droplets and that of interacting ("dressed") impurities or polarons.

The two-component setting, however, faces some challenges, stemming from the large differences in the length scales exhibited by the two-components in the 1D particle imbalanced regime. In the works mentioned above this limitation was counterbalanced by including external geometries, namely a ring [476], a harmonic trap [IE2, 191], or an optical lattice [193]. However, the LHY theory is not formally valid in the presence of external confinement, which significantly impedes the interpretation of the observed phenomenology.

In [IE4] we focused on 1D three-component bosonic mixtures with contact interactions in free space, by employing the LHY framework derived in [IE3]. Let us note that a similar framework has been derived for the 3D case as well [197, 198]. In this context, one of the three components is considered to be the minority component hosting a significantly smaller number of particles. In contrast to the two-component case, the three-component mixture allows for the two majority components to form a significantly more strongly self-bound droplet. As such, it results in higher particle densities and hence in smaller length scales for the droplet bath, which is coupled to the third, minority, component. Thus we can overcome the challenges mentioned above, without relying in an external confinement and we are able to study the particle-imbalanced droplet setting within a fully consistent LHY framework.

By tuning the intercomponent coupling strength or the ratio of the numbers of atoms, the system transitions between regimes where either the majority or the minority components exhibit a higher degree of localization. An intermediate regime, where all components are in configurations with comparable spatial extents and unity normalized densities, is also identified. Monitoring the chemical potentials of the system throughout these transitions, we are able to characterize both strongly and weakly self-bound configurations emerging in the ground state of three-component

particle-imbalanced droplets. Depending on the interplay between the particle number and the strength of the intercomponent interaction between the minority component and the majority ones, both strongly and weakly self-bound configurations can occur in either the minority localization regime or in the intermediate regime of similar localization-degree for all components. These transitions were realized by employing a newton method with analytically derived phase conditions. Furthermore, we derived and solved the Bogoliubov-de-Gennes (BdG) equations for the 1D three-component mixture to obtain the spectrum of low-amplitude excitations emerging on top of the ground-state density across the aforementioned transitions, and to further characterize the system. Let us note, that this measure is directly accessible in relevant experiments in 1D. The different localization regimes were found to exhibit also clearly distinguishable spectra regarding the low-amplitude excitations they support. In particular, when all three components feature a similar degree of localization, their excitations spectrum exhibits pairs of low-amplitude excitation modes, while this degeneracy is lifted as the minority component localizes further. This transition is also characterized by most of the paired modes crossing above the particle-emission threshold, before the non-degenerate ones cross the particle-emission threshold from above, and becoming available to the system. Moreover, the regime where the majority components exhibit larger widths was found to possess a rather rich low-amplitude excitation spectrum, suggesting that it has the potential of hosting a variety of intriguing dynamical regimes.

Finally, similar to the process curried out in [IE2], we derived a sequence of effective models based on the assumption that the third component hosts a much smaller number of particles than the two majority components. Meanwhile, all three components are assumed to be occupied by a macroscopic number of particles, such that the LHY approach remains formally valid. First, the fully decoupled limit was derived, where the majority components form a two-component droplet unperturbed by the presence of the minority component, while the minority component experiences an effective potential created by the droplet bath. Unlike the MF picture [474] however, within the LHY theory, quantum fluctuations play an important role in this model, affecting the system at the intra-component and at the inter-component level. Namely, at the intracomponent level, both the minority component and the majority components experience their respective LHY corrections, appearing as an additional non-linear term in the eGPEs. Moreover, at the inter-component level, the effective potential created by the droplet bath, which the minority component experiences, is modified by the presence of quantum fluctuations. In this regime, the ground state of the majority components has the analytical droplet solution [139, 162]. Meanwhile, the ground state of the minority component can be approximated with a Thomas-Fermi profile, modified by the influence of quantum fluctuations compared to the usual MF Thomas-Fermi limit [25]. This simple model was found to be reasonably accurate for weak inter-component coupling, allowing us to obtain useful analytical insights regarding the beyond MF effects in the behavior of

the particle-imbalanced three-component mixture in 1D. Finally, we can further improve our model by re-introducing the direct intra-component coupling terms in our model, thus including also the back-action of the minority component to the droplet bath. The predictions of this model where found to be in very good agreement with the results obtained from the full numerical treatment of the exact three-component eGPES, for both weak and larger values of the inter-component coupling strength.

Chapter 4

Scientific Contributions

4.1 Correlated Dynamics of Collective Droplet Excitations in a One - Dimensional Harmonic Trap

PHYSICAL REVIEW A **107**, 023320 (2023)

Correlated dynamics of collective droplet excitations in a one-dimensional harmonic trap

I. A. Englezos [1,*] S. I. Mistakidis [2,3] and P. Schmelcher [1,4]

[1] *Center for Optical Quantum Technologies, Department of Physics, University of Hamburg, Luruper Chaussee 149, 22761 Hamburg, Germany*

[2] *ITAMP, Center for Astrophysics | Harvard & Smithsonian, Cambridge, Massachusetts 02138, USA*

[3] *Department of Physics, Harvard University, Cambridge, Massachusetts 02138, USA*

[4] *The Hamburg Centre for Ultrafast Imaging, University of Hamburg, Luruper Chaussee 149, 22761 Hamburg, Germany*

(Received 12 June 2022; accepted 18 January 2023; published 23 February 2023)

We address the existence and dynamics of one-dimensional harmonically confined quantum droplets appearing in two-component mixtures by deploying a nonperturbative approach. We find that, in symmetric homonuclear settings, beyond-Lee-Huang-Yang correlations result in flat-top droplet configurations for either decreasing intercomponent attraction or larger atom number. Asymmetric mixtures feature spatial mixing among the involved components with the more strongly interacting or heavier one exhibiting flat-top structures. Applying quenches on the harmonic trap we trigger the lowest-lying collective droplet excitations. The interaction-dependent breathing frequency, being slightly reduced in the presence of correlations, shows a decreasing trend for stronger attractions. Semianalytical predictions are also obtained within the Lee-Huang-Yang framework. For relatively large quench amplitudes the droplet progressively delocalizes and higher-lying motional excitations develop in its core. Simultaneously, enhanced intercomponent entanglement and long-range two-body intracomponent correlations arise. In sharp contrast, the dipole motion remains robust irrespective of the system parameters. Species-selective quenches lead to a correlation-induced dephasing of the droplet or to irregular dipole patterns due to intercomponent collisions.

DOI: 10.1103/PhysRevA.107.023320

I. INTRODUCTION

Ultracold atoms constitute versatile platforms for probing correlated quantum many-body (MB) phases of matter [1] such as self-bound quantum droplets [2–6]. The latter manifest the existence of quantum correlations in macroscopic mixtures, represented to first order by the Lee-Huang-Yang (LHY) correction term [7], stabilizing the system against collapse due to mean-field (MF) effects [2,4–6]. Importantly, these self-bound states have been realized in both homonuclear [8–10] and heteronuclear [11] short-range interacting bosonic mixtures in three dimensions as well as in single component [3,12,13] and binary dipolar gases [14,15] and mixtures thereof [4,5]. Focusing on short-range interacting droplets, several experiments have addressed their dynamical formation [10,16], the droplet to a gaseous BEC crossover [9,17,18] and their collisional properties [19] with their self-evaporation and three-body recombination being central issues [8–11].

On the theoretical side, droplets have been found to emerge also in Bose-Fermi mixtures with [20] and without spin-orbit coupling [21,22], as well as in Bose-Bose mixtures in the presence of three-body interactions [23,24]. Moreover, collective excitations [25] and the properties of topological excitations [26–30], e.g., vortices [26] embedded in a droplet background have been investigated to a certain extent. Additionally, bosonic droplets can be accommodated in optical lattices in both one [31,32] and two dimensions [33,34] as well as in semidiscrete settings [35,36]. Their excitation spectrum was studied especially in one dimension [37–41] and in the crossover from three dimensions to one dimension [42]. Droplets spatial configurations acquire a flat-top (FT) profile for larger atom number [2], while associated thermal instabilities leading to their self-evaporation have also been reported [43–47].

The lifetime of droplets is expected to be prolonged in one dimension [48,49] and in the case of heteronuclear mixtures, due to their lower density [11]. In spite of this advantage, heteronuclear mixtures, where correlation effects should be enhanced due to the mixed character of the ensuing droplet, have not been extensively studied thus far [50–52]. This is in part due to the complicated form of the corresponding extended Gross-Pitaevskii equation (eGPE) [19,50]. It is a partial aim of our study to explore the role of correlations in harmonically trapped heteronuclear mixtures and the associated droplet configurations. In one dimension, droplets have been primarily described within the eGPE framework [37–39,41,53],with notable exceptions where nonperturbative approaches were utilized to unveil beyond-LHY physics in free space [52,54,55] and in lattice settings [31,32]. Interestingly, however, the formation of one-dimensional (1D) harmonically trapped droplets remains largely unexplored [52,56,57]. Within the eGPE framework [52,56], FT

*ilias.englezos@physnet.uni-hamburg.de

droplet structures were shown to be suppressed, while it was argued that they can exist using temporally varying interactions [57].

In this sense, it is highly desirable to inspect the interplay of correlations for both stationary droplet entities as well as in their dynamics when trap effects, being commonly unavoidable in experiments [8–11], are not omitted. The conditions under which FT configurations occur in an external harmonic trap and importantly whether the presence of beyond-LHY correlations favors their formation remain unclear [52]. Moreover, droplet collective excitations, being crucial for understanding, e.g., their ability to support nonlinear excitations [30], can be triggered owing to the tunability of the external confinement, without exciting higher order correlations as is the case, e.g., for interaction quenches [52]. While the behavior of the droplet breathing frequency in one dimension has been studied to some extent [37,52], the dynamical response of the system and the build-up of intercomponent correlations still remain elusive especially when species-selective quenches are applied. In the present work, we study the ground state and collective dynamics of 1D harmonically trapped droplet structures in both homonuclear and heteronuclear mixtures which experience repulsive (attractive) intra- (inter-)component interactions. For addressing correlation effects on the formation of harmonically trapped droplets beyond the LHY approximation we rely on the nonperturbative multilayer multiconfiguration time-dependent Hartree method for atomic mixtures (ML-MCTDHX) [58–60]. Additionally, in order to explicate the role of correlations at different levels we compare our results with the common MF treatment [61] as well as the predictions of the eGPE [53].

We showcase that FT signatures stemming from beyond-LHY correlations are present in symmetric homonuclear mixtures for either decreasing attraction or an increasing atom number, in contrast to the predictions of the eGPE [52,56]. Otherwise, a larger attraction leads to an alteration of the droplet configuration from a FT to a Gaussian-shaped one as in free space [52,55]. Another central result of our findings is that similar structures occur also for interaction (mass) imbalanced bosonic mixtures, whose 1D eGPE is not known, where the more strongly repulsive (heavier) component features FT signatures for reduced intercomponent attraction and the setting is spatially mixed. In all cases, the droplets show an antibunching (bunching) behavior at the same (different) locations.

The breathing dynamics of the droplet is initiated through quenching the trap frequency. Interestingly, using relatively large quench amplitudes higher-lying motional excitations build-upon the droplet core and simultaneously density portions are expelled, a process that is reminiscent of the self-evaporation mechanism in three dimensions [10,16]. This self-evaporation mechanism, however, has not been previously reported in 1D settings [38,52], exposing the crucial effect of the external confinement on the dynamical response of quantum droplets. We show herein that this overall unstable dynamics is accompanied by enhanced intercomponent entanglement and the development of long-range two-body intracomponent spatial correlations. Analytical predictions for the breathing frequency are provided at relevant limits by extending the variational approximation within the LHY theory introduced in Ref. [37], while numerical estimations show that it tends to the ideal gas case for strong attractions and it is reduced towards the FT regime in accordance with Refs. [52,54,55]. Another important result is the development of a pronounced correlation driven dephasing in the dynamics of heteronuclear mixtures, where the relevant eGPE equation is not available. This dephasing is owed to the tendency of the individual components to oscillate in phase (with a phase difference) for strong (weak) attractions. In contrast to free space, here the confinement allows to also excite the droplet dipole motion, via a sudden displacement of the trap position, which is found to be insensitive to interactions. Moreover, utilizing relevant species-selective quenches for weak attractions gives rise to irregular dipole patterns as a result of intercomponent collisions and consequent energy transfer, while at strong attractions the droplets prefer to maximize their overlap.

This work is organized as follows. In Sec. II we introduce the bosonic mixture under investigation and briefly discuss the established eGPE theory and the nonperturbative ML-MCTDHX approach used for the description of quantum droplets. Section III elaborates on the static properties of harmonically confined droplets, with an emphasis on their correlation aspects. The nonequilibrium droplet dynamics upon considering quenches of the trap is subsequently examined focusing on their collective excitations and in particular their breathing mode (Sec. IV) and dipole motion (Sec. V). We conclude offering also perspectives for future work in Sec. VI. The Appendix provides the ingredients of the variational approximation and the time-dependent Gaussian ansatz employed for a complementary interpretation of the droplet properties.

II. ATTRACTIVELY INTERACTING MIXTURE AND THEORY MODELS

A. Many-body two-component bosonic system

We employ a particle-balanced bosonic mixture with $N_A = N_B = N$ atoms confined in a weak 1D harmonic trap. To address confined droplet structures in both homonuclear and heteronuclear mixtures we shall consider mass ratios $m_A/m_B = 1$ and $m_B/m_A \approx 2.1$ respectively. Such two-component systems can be experimentally emulated using two hyperfine states of ^{39}K [8–10] or in the heteronuclear case a mixture composed of ^{42}K and ^{87}Rb [11]. Our setting focuses in the ultracold temperature limit where s-wave scattering dominates [62]. In this sense, interparticle interactions correspond to contact potentials characterized by effective intra- (g_A, g_B) and intercomponent (g_{AB}) coupling strengths. They can be tuned either through the three-dimensional (3D) s-wave scattering lengths using Feshbach resonances [63,64] or via the transversal confinement with confinement induced resonances [62]. The MB Hamiltonian reads

$$H = \sum_{\sigma=A,B}\sum_{i=1}^{N_\sigma}\left[-\frac{\hbar^2}{2m_\sigma}\left(\frac{\partial^2}{\partial x_i^{\sigma\,2}}\right) + \frac{1}{2}m\omega^2\left(x_i^\sigma\right)^2\right] + \sum_{\sigma=A,B} g_\sigma \sum_{i<j}^{N_\sigma}\delta\left(x_i^\sigma - x_j^\sigma\right) + g_{AB}\sum_{i=1}^{N_A}\sum_{j=1}^{N_B}\delta\left(x_i^A - x_j^B\right). \tag{1}$$

The frequency of the longitudinal (ω_x) over the transverse ($\omega_\perp$) trapping frequencies is fixed to $\omega = \omega_x/\omega_\perp = 0.01$. Similar values are commonly employed experimentally to realize 1D settings [65]. In the following, we rescale the Hamiltonian in terms of $\hbar\omega_\perp$. This means that the length, time, and interaction strengths are expressed with respect to $\sqrt{\hbar/(m\omega_\perp)}$, $1/\omega_\perp$, and $\sqrt{\hbar^3\omega_\perp/m}$, respectively.

B. Droplet region and the extended Gross-Pitaevskii equation

Within the local density approximation and under the impact of the first-order quantum correction term (LHY contribution), Bogoliubov theory leads to the so-called eGPE framework [2,53]. It has been demonstrated that the eGPE, in the absence of confinement ($\omega = 0$) and in the thermodynamic limit, describes the formation of quantum droplets [53]. Considering the average repulsion $g = \sqrt{g_A g_B}$, the droplet interval is quantified by the measure $\delta g = g + g_{AB}$ with $0 < \delta g \ll g$ [53], which implies interspecies attraction $g_{\rm AB} < 0$. For a symmetric mixture, i.e., $m_A = m_B \equiv m$, $N_A = N_B \equiv N$, and $g_A = g_B \equiv g$, the genuine two-component system is described by a reduced single-component eGPE equation which in the presence of a sufficiently weak ($\omega \ll 1$) harmonic trap reads

$$i\hbar\frac{\partial\Psi(x,t)}{\partial t} = -\frac{\hbar^2}{2m}\frac{\partial^2\Psi(x,t)}{\partial x^2} + \delta g|\Psi(x,t)|^2\Psi(x,t) - \frac{\sqrt{2m}}{\pi\hbar}g^{\frac{3}{2}}|\Psi(x,t)|\Psi(x,t) + \frac{1}{2}m\omega^2x^2\Psi(x,t). \tag{2}$$

Within the interaction regime $0 < \delta g \leqslant g$ a structure reminiscent of a liquid puddle appears being characterized by a FT density profile, which saturates at $n_0 = 8mg^3/(9\pi^2\hbar^2\delta g^2)$ [53]. However, an increasing attraction such that $0 < \delta g \ll g$ results in a transition behavior towards more localized solutions having a Gaussian shape. In both cases, these self-bound localized structures emerge due to the competition between the overall quadratic MF repulsion and the linear LHY attraction and thus constitute a beyond MF effect. Moreover, in the case that the interspecies MF attraction balances exactly the respective intraspecies repulsion, namely, $\delta g = 0$, the eGPE equation depends purely on the quantum fluctuation LHY term and the so-called LHY fluid arises [66]. Finally, turning to $\delta g < 0$ the eGPE approach admits various soliton-type solutions, including "bubble" or "W-shaped" configurations under suitable conditions; see for details Refs. [41,67,68].

The inclusion of a harmonic trap ($\omega \neq 0$) leads to localized Gaussian-shaped (soliton-type) configurations in the MF realm, independently of the value of the interspecies interaction g_{AB} [61]. The corresponding density distributions exhibit a larger width for decreasing $|g_{AB}|$ [61,69]. Hence, as we shall demonstrate below, the more pronounced BMF effect that is expected in the presence of confinement is the existence of a FT density profile restricted around the trap center, where trap effects are diminished.

Concluding, the eGPE (2) was derived in the absence of confinement ($\omega = 0$), and it is valid for macroscopic systems close to the MF balance point $\delta g \approx 0$ [53]. However, it has been demonstrated that its predictions can be in good qualitative agreement with nonperturbative methods even for finite values of δg and N, i.e., for mesoscopic systems [52,54,55]. The inclusion of a harmonic trap is expected to affect the Bogoliubov modes and therefore the form of the LHY term [49]. Nevertheless, throughout this work, we employ the eGPE framework since it provides an adequate phenomenological description of quantum droplets and in order to exemplify when effects beyond the standard LHY theory become important.

C. Many-body wave function approach

To expose the impact of beyond LHY correlation effects on the ground state and quench dynamics of quantum droplets we shall utilize the *ab initio* ML-MCTDHX method [58–60]. It enables us to numerically solve the time-dependent MB Schrödinger equation of the mixture and specifically its multilayer structure of the total MB wave function is tailored to account for both intra- and intercomponent correlations. Comprehensive discussions on the ingredients, successful applicability and benchmarking of this approach to various multicomponent settings such as impurity setups, cavities and spinor systems and reductions to other approaches can be found in the recent reviews [70,71].

Particularly, to address the intercomponent correlations of the bosonic mixture, the MB wave function is written as a truncated Schmidt decomposition [72] based on D different species functions, $|\Psi_k^\sigma(t)\rangle$, for each component $\sigma = A, B$. Accordingly

$$|\Psi(t)\rangle = \sum_{k=1}^{D}\sqrt{\lambda_k(t)}\big|\Psi_k^A(t)\big\rangle\big|\Psi_k^B(t)\big\rangle. \tag{3}$$

The time-dependent Schmidt weights $\sqrt{\lambda_k(t)}$ characterize the degree of intercomponent correlations (or entanglement) of the system, since if only $\lambda_1(t) = 1$ is nonzero and $\lambda_{k>1}(t) = 0$, then the MB ansatz is a product (nonentangled) state. Conversely, the wave function is in a superposition and the system is referred to as entangled [70,72].

Subsequently, intracomponent correlations are incorporated, by expanding each species function as a linear superposition of time-dependent number states $|\mathbf{n_k}^\sigma\rangle$ with time-dependent expansion coefficients $A^\sigma_{n_k}(t)$. The number states $|\mathbf{n}_k^\sigma\rangle$ refer to the full set of permanent states defined by d_σ time-dependent variationally optimized single-particle functions (SPF's) or orbitals $|\Phi_i^\sigma\rangle$ with occupation numbers $\mathbf{n} = (n_1, \ldots, n_{d_\sigma})$. Moreover, the d_σ time-dependent SPFs evolve in the single-particle Hilbert space spanned by the time-independent basis $\{|r_j^k\rangle\}_{j=1}^{\mathcal{M}}$. The latter, in our case, is taken to be an $\mathcal{M}$-dimensional discrete variable representation with $\mathcal{M} = 1000$ grid points. The equations of motion for the coefficients of the ML-MCTDHX wave function ansatz describing the MB Hamiltonian of Eq. (1) are found, e.g., using the Dirac-Frenkel variational principle [60,73], $\langle\delta\Psi|(i\hbar\partial_t - \hat{H})|\Psi\rangle = 0$.

Summarizing, a major asset of the above outlined approach is the expansion of the MB wave function in terms of time-dependent and variationally optimized basis sets. In this sense, the relevant Hilbert space is efficiently spanned employing a computationally feasible basis size as compared to other approaches such as exact diagonalization using a

time-independent basis. Naturally, as in every *ab initio* method, the superposition of multiple orbitals restricts its applicability to mesoscopic systems when the degree of correlations is enhanced. For instance, in the current attractively interacting mixture where intercomponent correlations become appreciable the truncated Hilbert space is characterized by the orbital configuration space $C = (D; d_A; d_B) = (10, 4, 4)$ for $N_A = N_B = N = 20$ and $C = (10, 6, 6)$ for $N_A = N_B = N = 5$. As a consequence, the number of the respective equations of motion that are numerically solved is tractable. Notice that due to the variational character of the method, its convergence has been carefully checked, namely, the used observables remain unchanged within a desired accuracy upon increasing the basis size.

The ML-MCTDHX wave function ansatz naturally reduces to the usual MF one [61], where all correlation are absent, when only a single Schmidt coefficient and SPF for each species are used ($D = d_A = d_B = 1$). In this case, the corresponding wave function takes a simple product form, and considering a variational principle yields the widely used coupled set of Gross-Pitaevskii equations for the bosonic mixture [61,69]; namely,

$$i\hbar\frac{\partial\Phi^\sigma(x,t)}{\partial t} = -\frac{\hbar^2}{2m}\frac{\partial^2\Phi^\sigma(x,t)}{\partial x^2} + \frac{m\omega^2x^2}{2}\Phi^\sigma(x,t) + g_\sigma|\Phi^\sigma(x,t)|^2\Phi^\sigma(x,t) + g_{\sigma\sigma'}|\Phi^{\sigma'}(x,t)|^2\Phi^\sigma(x,t). \quad (4)$$

By comparing the MF predictions to the MB ones, we are able to infer the impact of interparticle correlations on the formation and dynamics of confined quantum droplets.

III. GROUND STATE DROPLETS

We begin by studying the formation of 1D harmonically trapped quantum droplets appearing in two-component short-range interacting bosonic mixtures. Our analysis is mainly based on the above-discussed MB ML-MCTDHX approach which allows us to systematically account for beyond MF corrections. To expose the latter we also occasionally compare with the predictions of the eGPE treatment and the common MF method.

A. Symmetric bosonic mixtures

Initially, we consider a fully symmetric homonuclear mixture characterized by $N_A = N_B \equiv N$, $m_A = m_B \equiv m$, $g_A = g_B \equiv g = 0.1$ while the interspecies attraction $g_{AB} < 0$ is tuned. Recall that in this case the two components behave equivalently [2,37,70], since they also experience the same external trap and thus the mixture reduces to a single-component system. The respective one-body density[1] $\rho(x)$, which is throughout normalized to unity, is depicted in Fig. 1(a). Apparently, there is a transition from the Gaussian density

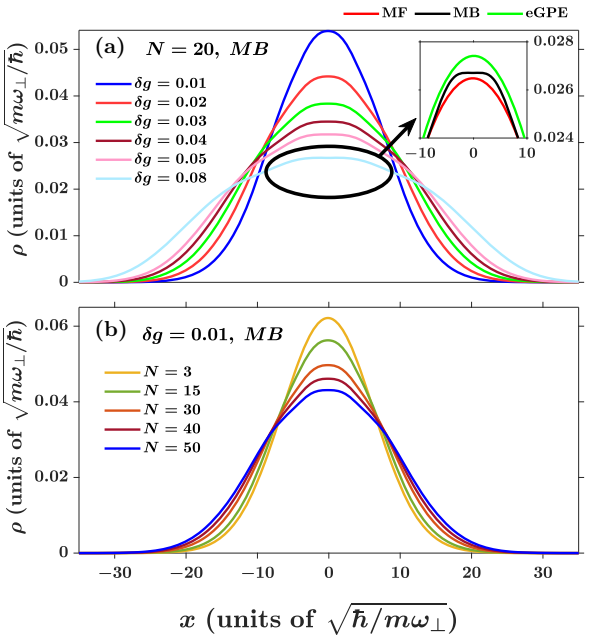

FIG. 1. Ground state droplet densities of a symmetric mixture in a harmonic trap as obtained in the MB approach. The cases of (a) different δg and fixed $N_A = N_B = N = 20$ and (b) varying atom number N for constant interaction $\delta g = 0.01$ are presented. A transition from a Gaussian-type distribution to a FT one for increasing either δg or N occurs. In (b) a FT profile appears for $N = 50$. Inset of (a): Density around the trap center within the MF, MB and the eGPE approach for $\delta g = 0.08$. Notice that only the MB calculation captures the FT profile.

profile (see, e.g., $\delta g = 0.01$) to a more delocalized FT one (e.g., for $\delta g = 0.08$) around the trap center for increasing $\delta g = g + g_{AB}$. The FT structure appears only for the MB case, and it is an effect of residual beyond LHY correlations since it does not appear in the eGPE case; see the inset of Fig. 1(a). However, it should be mentioned that the above-described delocalization trend of the density for larger δg is also captured within the eGPE (not shown), and it can be explained by the scaling of the healing length $\xi \propto \delta g/g^{3/2}$ [38]. Accordingly, also the MF fails to capture this FT structure showing a relatively more delocalized density distribution.

Naturally, in our trapped system the FT features are not as prominent as in free space. Quantitatively, if the system resides in its ground state with density close to its saturation value in free space, i.e., $|\Psi(x,t)|^2 \approx n_0 = 8g^3/(9\pi^2\delta g^2)$, then it is described to a good approximation by the static eGPE in the Thomas-Fermi limit, namely, $\delta g n_0 - \frac{\sqrt{2}}{\pi\hbar}g^{\frac{3}{2}}\sqrt{n_0} + \frac{1}{2}\omega^2x^2 = 0$. The effect of the harmonic trap then becomes comparable to that of the MF and LYH terms for $x \approx \sqrt{8g^3/(9\pi^2\delta g)}\omega^{-1} \lessapprox 10$, for the parameter values considered here, which gives an estimation for the size of the observed FT profiles. This suggests that the FT profile is not expected to grow significantly in size even for very large particle numbers. Of course, a systematic study of the first- (LHY) and potentially higher-order perturbative corrections in

[1]In the case of the symmetric mixture the observables associated with the two components are the same. For instance, the densities $\rho_A(x) = \rho_B(x) \equiv \rho(x)$ as well as the reduced density matrices [Eq. (5)] $\rho^{(2)}_{AA}(x_1, x_2) = \rho^{(2)}_{BB}(x_1, x_2) \equiv \rho^{(2)}(x_1, x_2)$.

the presence of the trap would be required to fully characterize the FT configurations, a study that lies beyond the scope of this work.

A similar structural deformation from a Gaussian to a FT configuration can be realized for a fixed interspecies attraction, e.g., $\delta g = 0.01$ and by varying the atom number as illustrated in Fig. 1(b). This behavior can be understood in terms of the eGPE predictions in free space. Particularly, it has been shown [53] that in the absence of a trap, the droplet exhibits a FT profile when its particle density saturates towards $n_0 = 8g^3/(9\pi^2\delta g^2) \approx 0.9$ for $g = 0.1$ and $\delta g = 0.01$. In our case where $\omega \neq 0$ we can assume that the mixture resides within the spatial region $|x| < 2a_{\rm osc} = 20$. As such, its peak density is of the order of $N/4a_{\rm osc}$ with $a_{\rm osc} = 1/\omega$. Then the above-mentioned free space saturation density is reached as long as $N_s/4a_{\rm osc} \approx n_0$, which corresponds to a critical atom number $N_s \approx 36$ for saturation in the trap. This prediction is found to be consistent with our MB calculations [Fig. 1(b)], where the FT profile emerges only for $N > 40$. Note, however, that this argument does not apply for larger values of δg. As an example, for $g = 0.1$ and $\delta g = 0.08$, the saturation density in free space is $n_0 \approx 0.014$ and the corresponding critical particle number for saturation in the trap is $N_s \approx 0.5$. The latter implies that a FT should occur for any atom number, which is of course not confirmed within our simulations (not shown). Let us mention that in the absence of an external trap it was argued, by employing a quantum Monte Carlo approach, that for larger values of δg droplet formation is inhibited due to the generation of dimers that appear due to beyond-LHY correlations [54,74]. This can be understood from the fact that the droplet saturation density $n_0 = 8g^3/(9\pi^2\delta g^2)$ lies below the dimer threshold $2n_0/g \leqslant 1$ for sufficiently large $\delta g \approx g$. Evidently, in our setup, the harmonic trap prevents the mixture from reaching such low densities and, e.g., in the case of $N = 20$, $g = 0.1$, and $\delta g = 0.08$ a liquid-like state with saturation density $n_{tr}(\delta g = 0.08) = N\rho_{\rm max}(\delta g = 0.08) = 0.5342$, where $\rho_{\rm max}$ denotes the droplet peak density, is established as observed in Fig. 1(a).

Overall, we can conclude that in our setting the interaction region where FT structures appear (for fixed particle number) is shifted to larger values of δg when compared to their free space counterparts. Moreover, the Lieb-Liniger parameter [70,75] $\gamma = mg/(\hbar^2 n_{\rm max})$ takes the value $\gamma = 0.19$ [$\gamma = 0.047$] for the parameters where FT structures occur in the case of $N = 20$ and $\delta g = 0.08$ [$N = 50$ and $\delta g = 0.01$]. Notice that the eGPE framework is expected to be valid for $\gamma \ll 1$ [38], and indeed it provides a somewhat adequate description for the $N = 50$ case, while it fails in the case of $N = 20$ as discussed above. Therefore, the increased localization and hence peak density caused by the presence of the trap, shifts the validity region of the eGPE further towards macroscopic weakly interacting systems, i.e., $\delta g \ll g$ and $N \gg 1$.

B. Asymmetric two-component settings

We address now droplet configurations arising in asymmetric bosonic mixtures. First, for a homonuclear mixture, corresponding, e.g., to two hyperfine states of ^{39}K, e.g., $|1,-1\rangle$ and $|1,0\rangle$ as in the experiments of Refs. [8–10]; here $g_B = 2g_A = 0.1$ while $m_A = m_B \equiv m$ and $N_A = N_B = N = 20$.

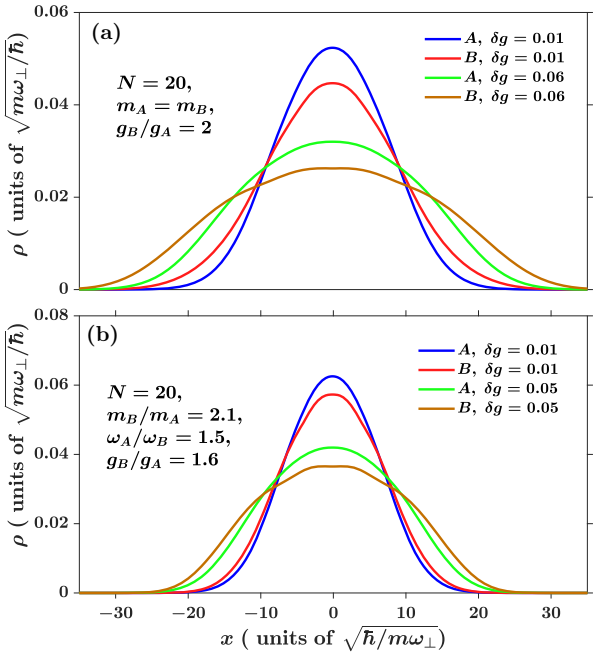

FIG. 2. Density profiles of harmonically confined droplets within the MB approach for varying δg in (a) an interaction-imbalanced ($g_B = 2g_A = 0.1$) and (b) a mass-imbalanced ($m_B = 2.1m_A$) bosonic mixture. A tendency towards a FT droplet building upon the B component being either (a) more strongly interacting or (b) heavier takes place for larger δg. Intercomponent spatial mixing is also enhanced for increasing δg. In both cases $N_A = N_B = N = 20$, while in the mass-imbalance setting $g_B = 1.6g_A = 0.08$.

Tuning the interspecies coupling, only the ground state density of the more strongly interacting component B exhibits a transition from a Gaussian profile ($\delta g = 0.01$) to one featuring a FT signature ($\delta g = 0.06$) [Fig. 2(a)]. Instead, the more weakly interacting component A features a significantly more localized Gaussian profile for all attractions. This is attributed to the implicit violation of the particle number condition $N_A/N_B = \sqrt{g_B/g_A}$ [2,53]. We aim to address this intriguing question in more detail in a future work. Last, since $g_A \neq g_B$, the SU(2) symmetry of the mixture is broken and thus the components are not equivalent [10]. As a result intercomponent spatial mixing is induced independently of δg and becomes more prominent for larger δg.

Similarly, the components are distinguishable and spatially mixed for heteronuclear (i.e., mass-imbalanced) settings [Fig. 2(b)]. To support this argument we employ a mixture of $N = 20$ in a species-selective harmonic trap with $\omega_A = 1.5\omega_B = 0.015$, a mass ratio $m_B/m_A = 2.1$, and intraspecies interactions $g_A = 0.05$ and $g_B = 0.08$ inspired by the experiment of Ref. [11] where the isotopes ^{41}K and ^{87}Rb have been exploited. Apparently, an intercomponent spatial mixing trend between the components occurs. This is a result of the mass imbalance which counteracts the interaction imbalance as well as the weaker confinement of the heavier species. The two latter contribute towards a larger width of the heavier component density distribution. We note that this effect will

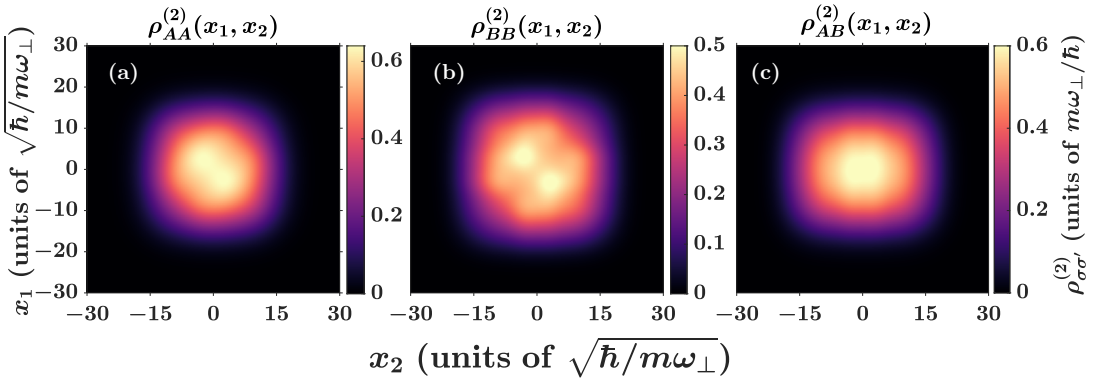

FIG. 3. Two-body reduced intracomponent density for species (a) A and (b) B as well as (c) the respective intercomponent density in the ground state of the mass and interaction-imbalanced mixture with $m_B = 2.1m_A$, $g_B = 1.6g_A = 0.08$, $\delta g = 0.05$ and $N_A = N_B = N = 20$. An intraspecies antibunching behavior at the center of the droplet occurs [see the diagonal of $\rho^{(2)}_{AA}(x_1,x_2)$, $\rho^{(2)}_{BB}(x_1,x_2)$], which is more prominent for the more strongly interacting B component. Intercomponent mixing is identified in $\rho^{(2)}_{AB}(x_1,x_2)$.

have a significant impact on the dipole dynamics of mass-imbalanced mixtures, as we shall argue below in Sec. V.

C. Two-body droplet configurations

To further probe the superposition nature of the droplet MB state we examine the respective two-body reduced densities

$$\rho^{(2)}_{\sigma\sigma'}(x_1,x_2) = \langle\Psi|\hat{\Psi}^\dagger_\sigma(x_1)\hat{\Psi}^\dagger_{\sigma'}(x_2)\hat{\Psi}_\sigma(x_1)\hat{\Psi}_{\sigma'}(x_2)|\Psi\rangle, \quad (5)$$

where $\hat{\Psi}_\sigma(x_i)$ denotes the bosonic field operator annihilating a σ-species particle at position x_i. $\rho^{(2)}_{\sigma\sigma'}(x_1,x_2)$ refers to the probability of simultaneously measuring one boson of species σ at position x_1 and a boson of species σ' located at x_2 [76,77].

Focusing on the case of a mass-imbalanced mixture, we observe that each species features a tendency towards an anti-correlated behavior; see Figs. 3(a) and 3(b). This is evident by the suppressed amplitude of the diagonal of the intraspecies two-body densities which implies a reduced probability of two σ-species atoms to reside at the same position. However, it is more likely two atoms of the same component to be symmetrically placed close to $x = 0$, as it can be seen from the two-body density humps appearing in $\rho^{(2)}_{\sigma\sigma}(0.5 < x_1 < 6, -6 < x_2 < -0.5)$. Such two-body patterns occur also in the the absence of a trap [52]. Naturally, the anticorrelation is more pronounced for the heavier component which is the more strongly interacting one. In contrast, intercomponent two-body correlations take place among the species especially at the trap center where the FT profile forms [Fig. 3(c)]. The above discussed two-body correlation patterns are found to be robust for the different systems considered herein (not shown) and become enhanced for stronger repulsions or increasing particle numbers. It should also be noted that we do not observe a sharp increase of interspecies correlations for increasing δg. Such an enhancement would be associated with the generation of dimers predicted in free space due to beyond-LHY correlations [54,74]. However, as we argued in Sec. III A the presence of the harmonic confinement suppresses dimer formation.

IV. COLLECTIVE EXCITATIONS OF DROPLETS

Having determined the ground state of harmonically confined droplets, let us now investigate the impact of correlations during their nonequilibrium dynamics. The presence of the external harmonic trap enables us to seed dynamical scenarios that have not been addressed previously. Specifically, in order to trigger the time evolution of quantum droplets, a quench of either the frequency (Secs. IV A and IV E) or the position (Sec. V) of the external trap is applied. These protocols naturally excite the breathing and dipole motion of the quantum droplet respectively. Moreover, by employing species-selective quenches we are able to break the SU(2) symmetry of the symmetric mixture and consequently monitor the emergent droplet interspecies collisions. Notice that performing these trap quenches, while keeping the interactions intact, provides the possibility to study the build-up of correlations both at the FT and the Gaussian-type phase independently. Concluding, the dynamics of the above-mentioned low-lying collective modes are monitored in heteronuclear mixtures (Secs. IV E and V), which are found to feature enhancement of correlations and intercomponent mixing.

A. Homonuclear mixtures: Breathing dynamics

To excite the lowest-lying breathing mode of the droplet, building upon the homonuclear mixture, a quench of the trap frequency is performed from an initial $\omega^{\rm i}$ to a final value $\omega^{\rm f}$. The bosonic setting consists of $N_A = N_B = N = 20$ atoms with $g_A = g_B = g = 0.1$ and different intercomponent attractions $g_{AB} < 0$. Since we aim to also reveal the interplay between the quench amplitude and the droplet excitation dynamics two different postquench frequencies are employed, namely, $\omega^{\rm f} = 4\omega^{\rm i} = 0.04$ and $\omega^{\rm f} = 2\omega^{\rm i} = 0.02$.

To track the dynamics of the ensuing breathing motion of the droplet cloud we initially invoke its one-body density. The time evolution of this observable for a weakly attractive mixture with $\delta g = 0.08$ and a postquench frequency $\omega^{\rm f} = 4\omega^{\rm i} = 0.04$ is presented in Figs. 4(a) and 4(b) within the MB and the eGPE approach respectively. Overall, a periodic

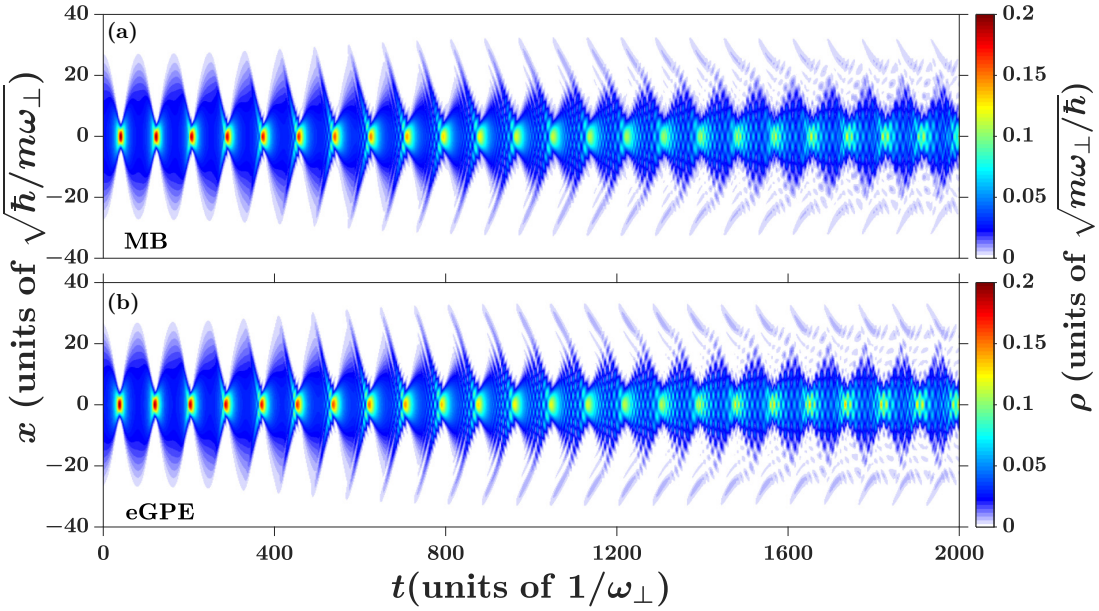

FIG. 4. Density evolution of a weakly attractive, symmetric mixture upon considering a sudden increase of the trap frequency, namely, $\omega^{\mathrm{f}} = 4\omega^{\mathrm{i}} = 0.04$ within (a) the ML-MCTDHX and (b) the perturbative eGPE approach. The droplet undergoes a breathing motion, while higher-lying motional excitations arise in the droplet for long evolution times ($t > 1000$). Apparently the eGPE prediction slightly overestimates the delocalization of the droplet density profile and the peak density of the localized excitations around the trap center at long evolution times. The bosonic mixture contains $N_A = N_B = N = 20$ atoms with $g_A = g_B = 0.1$ and $\delta g = 0.08$.

expansion and contraction of the droplet is observed within both methods for timescales $t < 500$ followed by a progressive delocalization of the density profile. Later, for $t > 800$, prominent spatial undulations arise in the droplet density especially around the trap center manifesting its excited nature; see also selective density snapshots in Fig. 5(a). They initially appear as relatively small density humps around $t = 830$ [solid red line in Fig. 5(a)] and eventually dominate the droplet profile rendering the FT background no longer visible; see, e.g., the dashed green line in Fig. 5(a).

It is also worth mentioning that even during the contraction process there are delocalized density tails; see, e.g., $|x| \approx 20$ of the dotted blue line at $t = 1845$ in Fig. 5(a). These motional excitations can be understood in terms of the MB wave function superposition and in particular stem from the non-negligible occupation of higher-lying natural orbitals being the eigenstates of the one-body reduced density matrix. To support this argument the densities of the first four orbitals, $|\Phi_i(x)|^2$ where $i = 1, \ldots, 4$, are also provided for the same time instants in Figs. 5(b)–5(d). As expected, higher-order orbitals exhibit a hierarchy in terms of their nodal structure accompanied by an enhanced spatial delocalization. Hence, the existence of higher-lying orbitals is responsible for both the delocalization and the excitation of the droplet.

Notably, the eGPE provides a somewhat accurate description of the observed MB dynamics, as it captures both the delocalization trend and the spatial undulations appearing in the time-evolved one-body density; see Fig. 4. However, it should be emphasized that the delocalized density tails are slightly more pronounced within the eGPE treatment indicating a tendency towards a slightly less stable droplet state as compared to the MB approach. A closer inspection of Figs. 4(a) and 4(b) for $t > 1600$ and $|x| > 20$ or of the corresponding variances (not shown) indicates an increased delocalization in the eGPE compared to the MB approach of the order of ∼4% of the initial droplet width. Also, the spatial undulations predicted by the eGPE are characterized by more prominent density peaks and thus a higher degree of localization; see Figs. 4(a) and 4(b). These differences may be interpreted at the microscopic level in terms of the superposition of the orbitals shown in Figs. 5(b)–5(d). The fact that beyond-LHY correlations are not substantial during the evolution is partly attributed to the quench protocol related to the single-particle potential.

The above-described dynamical phenomena appear in experimentally accessible evolution times, e.g., for customarily used 1D trap frequencies $\omega_x = 2\pi \times 1.5$ Hz and $\omega_\perp = 2\pi \times 300$ Hz [65,78,79] the excitations become evident after $t \approx 265$ ms and the delocalization around $t \approx 530$ ms. While exact estimations of the lifetimes of 1D quantum droplets remain still elusive, experimental observations in higher dimensions typically report lifetimes of the order of 10 ms for homonuclear mixtures [10] and significantly higher ones for heteronuclear systems, i.e., ∼120 ms [11]. Importantly, three-body losses which lead to droplet decay, are commonly reduced by one order of magnitude in 1D settings [80], and they have been recently argued to become negligible in the droplet regime [44,49], resulting in even longer droplet lifetimes. These substantially improved lifetimes constitute a major benefit for studying 1D systems and especially

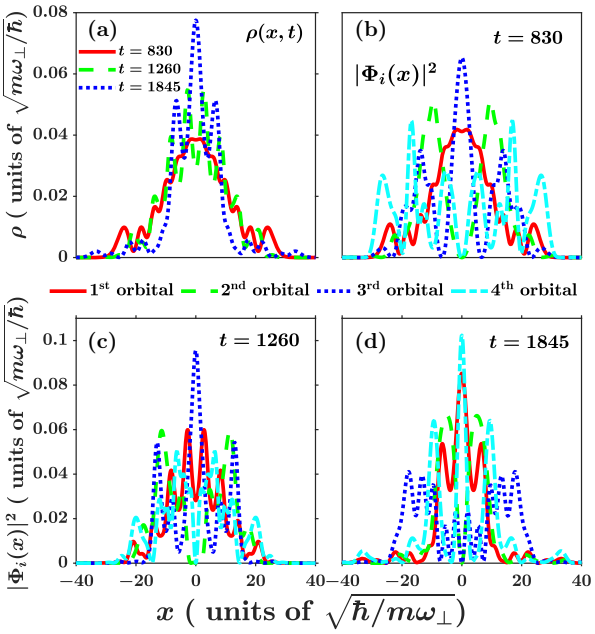

FIG. 5. Density profiles of (a) the symmetric homonuclear droplet and (b)–(d) the respective orbitals $|\Phi_i(x)|^2$ with $i = 1, \ldots, 4$ (see legend) at different evolution times. Namely, at (b) $t = 830$, (c) $t = 1260$, and (d) $t = 1845$. Evidently, higher-lying orbitals support the spatial delocalization and excitation patterns of the density, while the lowest orbital has the dominant contribution to the density. The breathing dynamics of the symmetric mixture, characterized by $g_A = g_B = 0.1$, $N_A = N_B = N = 20$, is triggered by a frequency quench where $\omega^{\mathrm{f}} = 4\omega^{\mathrm{i}} = 0.04$.

heteronuclear droplets and suggest that the long-time dynamics presented herein, might be experimentally accessible.

The aforementioned delocalization behavior suggests a dissociation tendency of the droplet, resembling the well-known self-evaporation mechanism observed in 3D experiments [2,8,9]. This dynamical response has not yet been reported in 1D free space [38,52], and it is thus inherently related to the presence of the trap. On the other hand, the robustness of the excitation patterns in the central droplet region for long evolution times supports the assumption that the FT configuration can maintain nonlinear structures, e.g., solitons, a study that will be interesting to be pursued in the future.

B. Correlation and entanglement dynamics

A feature that is inherently related with the droplet formation is their correlated character [31,52,54], while the fate of dynamical droplet correlations remains largely unexplored. Specifically, in our setting we aim to reveal the correlation patterns that correspond to the above-mentioned droplet excitation processes. Below, we infer the build-up of intraspecies two-body correlations during the breathing evolution of the droplet in a spatially resolved manner by investigating the so-called two-body coherence function [76,77]:

$$G^{(2)}_{\sigma\sigma}(x_1, x_2, t) = \frac{\rho^{(2)}_{\sigma\sigma}(x_1, x_2, t)}{\rho_\sigma(x_1, t)\rho_\sigma(x_2, t)}. \tag{6}$$

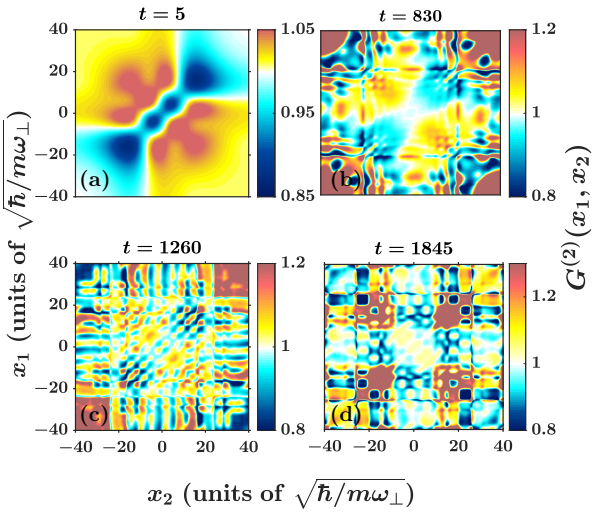

FIG. 6. (a)–(d) Profiles of the two-body coherence $G^2(x_1, x_2)$ in the breathing dynamics of the symmetric mixture with $g_A = g_B = 0.1$, $N_A = N_B = N = 20$ at distinct time instants (see legend) after a quench to $\omega^{\mathrm{f}} = 4\omega^{\mathrm{i}} = 0.04$. Suppression of two-body correlations in the bulk $[G^2(x_1, x_2 = x_1)]$ occurs for long evolution times while a correlated behavior is evident for bosons located at different edges of the droplet $[G^2(x_1, x_2 = -x_1)]$.

The two-body reduced density matrix $\rho^{(2)}_{\sigma\sigma}(x_1, x_2, t)$ is defined in Eq. (5). Naturally, in the symmetric mixture case $G^{(2)}_{AA}(x_1, x_2) = G^{(2)}_{BB}(x_1, x_2) = G^{(2)}(x_1, x_2)$. Apparently, a two-body correlated (anticorrelated) behavior occurs for $G^{(2)}(x_1, x_2, t) > 1$ ($G^{(2)}(x_1, x_2, t) < 1$), while the case of $G^{(2)}(x_1, x_2, t) = 1$ is said to be two-body uncorrelated.

Snapshots of $G^{(2)}(x_1, x_2, t)$ are illustrated in Figs. 6(a)–6(d). At the initial stages of the dynamics [Fig. 6(a)] the droplet maintains the two-body anticorrelated behavior of its ground state (see Sec. III) for two bosons at the same location [i.e., $G^{(2)}(x_1, x_2 = x_1, t) < 1$] while two atoms placed symmetrically with respect to the FT exhibit a correlated tendency, namely $G^{(2)}(x_1, x_2 = -x_1, t) > 1$. For longer evolution times where the density delocalization is observed [Fig. 4(a)], a suppression of two-body correlations takes place at the central bulk region since $G^{(2)}(x_1, x_2 = x_1, t) \approx 1$; see Figs. 6(b)–6(d). However, the delocalized density tails [see, e.g., $\rho(|x| > 20, t > 1000)$ in Fig. 4(a)] develop a noticeable two-body correlated behavior among each other as can be deduced, e.g., from the antidiagonal of $G^{(2)}(x_1, x_2 = -x_1, t) > 1$ depicted in Fig. 6(d) (e.g., at $x_1 = -x_2 \approx 20$).

Regarding the impact of intercomponent correlations (entanglement) on the breathing dynamics of quantum droplets we analyze the corresponding von Neumann entropy [72]

$$S_{\mathrm{VN}}(t) = -\sum_{k=1}^{D} \lambda_k(t) \ln[\lambda_k(t)]. \tag{7}$$

In this expression, $\lambda_k(t)$ refer to the Schmidt coefficients of the MB wave function ansatz (3) which are essentially the eigenvalues of the species reduced density matrix [72]. This entropic measure captures the degree of intercomponent

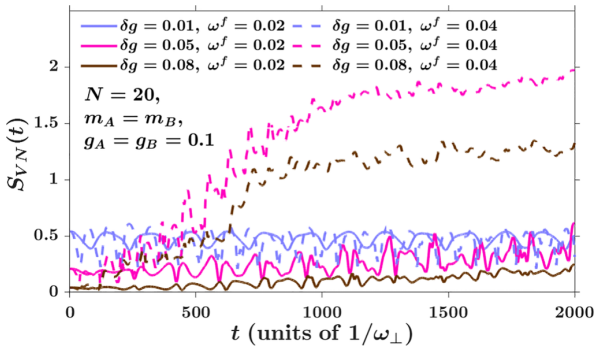

FIG. 7. Time evolution of the von Neumann entropy in the course of the droplet breathing motion induced by various quenches of the trap frequency at distinct interspecies couplings (see legend). The symmetric bosonic mixture with $N_A = N_B = N = 20$ experiences $g_A = g_B = 0.1$ (see legend). The finite entropy evinces the presence of intercomponent entanglement, while its sharp increase for sufficiently large δg and ω^f signals the prominent excitation dynamics of the droplet.

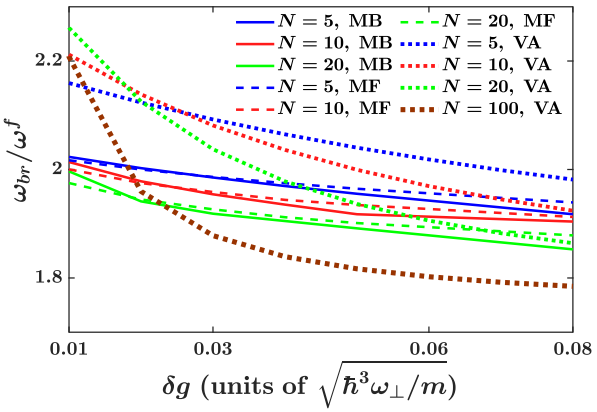

FIG. 8. Breathing mode frequency ($\omega_{\rm br}/\omega^{\rm f}$) of the symmetric mixture with $g_A = g_B = 0.1$ in units of the postquench trap frequency for varying interspecies attraction and atom number (see legend). The predictions of $\omega_{\rm br}/\omega^{\rm f}$ are given within the MB approach (solid lines), the MF (dashed lines) and variational (dotted lines) approximation. A monotonic decreasing behavior of $\omega_{\rm br}/\omega^{\rm f}$ is observed for increasing either δg or $N_A = N_B = N$. The breathing frequency is (slightly) smaller in the MB approach as compared to the MF and the variational approximation.

entanglement, namely, a nonentangled state corresponds to $\lambda_1(t) = 1$ and $\lambda_{k\neq 1}(t) = 0$ leading to $S_{\rm VN}(t) = 0$. We note that the entanglement is crucial for quantum droplets since the widely used MGP approach primarily takes into account the effects stemming from intraspecies quantum fluctuations. Instead the interspecies coupling processes should be generally introduced perturbatively in terms of $\delta g/g$ as it has been argued in Refs. [2,41,54,74,81].

The harmonically confined droplets discussed herein, offer a promising setting for exploring beyond-LHY effects in the course of the time evolution. Indeed, the dynamics is induced by applying a quench on the trap frequency while keeping fixed the interaction parameters (g_A, g_B and g_{AB}). This allows us to study the build-up of intercomponent correlations both in the Gaussian and the FT regimes which occur at strong and weak attractions respectively.

For postquench amplitudes $\omega^{\rm f} = 2\omega^{\rm i} = 0.02$ we observe that $S_{\rm VN}(t)$ fluctuates around a mean value determined by the strength of g_{AB}; see Fig. 7. Generically, the degree of entanglement is larger for stronger attractions. This behavior is related to the fact that the breathing motion of the droplet is nearly stable, exhibiting regular periodic expansion and contraction for this quench amplitude independently of δg and excitations do not appear, e.g., on the one-body density level (not shown). Turning to the case of larger quench amplitudes, i.e., $\omega^{\rm f} = 4\omega^{\rm i} = 0.04$, the entanglement dynamics of the droplet is more involved; namely, for Gaussian-shaped droplets ($\delta g = 0.01$) the entropy oscillates around $S_{\rm VN}(t) \approx 0.5$. In this regime again the droplet can not sustain excitations due to its narrow width. Remarkably, within the FT regime ($\delta g = 0.08$) $S_{\rm VN}(t)$ features initially a moderately increasing tendency and thereafter exhibits a strong increase when localized excitations arise in the droplet core as presented in Fig. 4(a), e.g., for $|x| < 20$ and $t > 700$. Subsequently, the delocalization of the droplet edges as seen in Fig. 4(a), e.g., for $|x| > 20$ and $t > 1200$ is related to a saturation trend of $S_{\rm VN}(t)$ e.g., towards $S_{\rm VN}(t) \approx 1.25$ for $\delta g = 0.08$. Therefore, the appearance of higher-lying motional excitations at the droplet center is accompanied by a noticeable increase of interspecies correlations which then approach a plateau behavior as long as the droplet delocalizes.

C. Droplet breathing mode frequency

Next, we employ the position variance of the bosonic cloud

$$\left\langle X_\sigma^2(t)\right\rangle = \langle\Psi(t)|\hat{x}_\sigma^2|\Psi(t)\rangle - \langle\Psi(t)|\hat{x}_\sigma|\Psi(t)\rangle^2, \qquad (8)$$

where $\hat{x}_\sigma$ denotes the σ-species position operator and $\langle\Psi(t)|\hat{x}_\sigma|\Psi(t)\rangle = 0$ due to the preserved "parity" symmetry. This experimentally accessible measure via time-of-flight imaging [82,83], captures the breathing motion of the cloud and its spectrum contains the respective breathing mode frequency, $\omega_{\rm br}$. The latter is provided in Fig. 8, upon considering a quench with $\omega^{\rm f} = 4\omega^{\rm i} = 0.04$, as a function of δg for various particle numbers composing the droplet and within different approaches. These approaches refer to the full MB treatment including the correlations of the mixture, the MF approximation where correlations are neglected and a variational approximation (VA) within the LHY theory. The latter was also exploited in Ref. [37] to estimate $\omega_{\rm br}$ of 1D droplets in the absence of an external trap. It is based on a time-dependent Gaussian ansatz (see details in the Appendix) providing an approximate analytical solution of the eGPE (2) by utilizing a Gaussian wave function with variationally optimal width. This explicit time dependence of this ansatz can provide semianalytical insights into the dynamical droplet properties, e.g., the breathing frequency (see the discussion below).

Focusing on the outcome of the MB and the MF approaches it is found that overall $\omega_{\rm br}$ is close to the prediction in the ideal gas limit, i.e., $\omega_{\rm br} \approx 2\omega^{\rm f}$, for strong interspecies attraction (or otherwise small δg), while it shows a weakly

decreasing tendency towards the decoupled scenario corresponding to increasing δg. This behavior of $\omega_{\rm br}$ in terms of δg holds also independently of N, but $\omega_{\rm br}$ also decreases for a larger atom number since for an increasing N the effective MF interactions ($\propto \delta g N$) are enhanced. Thus, deviations from the noninteracting limit become more prominent. This reduced trend of $\omega_{\rm br}$ for smaller g_{AB} has also been reported in free space using a quantum Monte Carlo method [55]. Moreover, by closely inspecting $\omega_{\rm br}$ it can be deduced that within the MF approximation it is smaller for stronger attractions and larger in the reverse case as compared to the MB result. Interestingly, the crossing point with respect to δg between the two predictions shifts towards the MF balance point ($\delta g = 0$) for larger N. This is due to the fact that the contribution of the LHY term to the breathing frequency is positive for $\delta g \approx 0$ and negative when $\delta g \neq 0$, as we shall explicate below using the VA method; see in particular Eq. (10). Additionally, the deviations of the MB and the MF results become more pronounced in the few-body limit, e.g., $N = 5$, due to the involvement of higher-order correlations.

Turning to the VA method we observe that it fails to capture $\omega_{\rm br}$, especially for few-body systems (e.g., $N = 5$). Still, it improves significantly for increasing N, and it approaches more closely the MB prediction as compared to the MF approximation at the FT regime, e.g., around $\delta g = 0.08$ for $N = 20$. We remark that this agreement between the VA and the MB cases solely occurs for the breathing frequency, while the density profile is not appropriately captured by the VA (not shown). However, the VA approximation completely overestimates $\omega_{\rm br}$ for stronger attractions such as $\delta g = 0.01$. In particular, for large $N \gg 1$ and stronger attractions such that $\delta g \approx 0$ (LHY fluid) it can be proven, following the minimization of the underlying effective potential [see Eq. (A4)], that the breathing frequency scales as

$$\omega_{\rm br}^{\rm VA} \propto N^{2/3}. \tag{9}$$

Hence, within the VA a diverging breathing frequency at the limit of the LHY fluid for increasing particle numbers is encountered.

On the other hand, for finite values of δg and ω the scaling of the optimal width of the Gaussian wave function is dominated by the average MF repulsion, with the LHY term providing only a higher-order correction leading to a stronger localization, namely, $W \approx (\frac{\delta g N}{m\omega^2\sqrt{2\pi}})^{1/3} - \frac{8^{1/4}}{3\pi\hbar\omega}\sqrt{(g^3/\delta g)}$. In this case within VA the breathing frequency reads

$$\omega_{\rm br}^{\rm VA} \approx \sqrt{3}\omega - O[g^{3/4}(\delta g N)^{-1/6}], \tag{10}$$

where the correction term originates from the LHY contribution. It is also worth mentioning that, in the thermodynamic limit $N \to \infty$, where the above-discussed results become exact, the VA prediction reduces to the one of the usual Gross-Pitaevskii equation [84]. Indeed, for $N \to \infty$ we obtain a breathing frequency $\omega_{\rm br}^{\rm VA} \approx \sqrt{3}\omega$, which is nearly reached, e.g., for $N = 100$ as shown by the dotted brown line in Fig. 8.

D. Dynamics of interaction-imbalanced mixtures

In an attempt to generalize the persistence of the droplet excitation processes in the course of its breathing motion we also investigate interaction-imbalanced homonuclear mixtures with $g_B = 2g_A = 0.1$, $g_{\rm AB} < 0$, $m_A = m_B \equiv m$ and $N_A = N_B = N = 20$, for its ground state characteristics. Generically imbalanced mixtures are, among others, particularly prone to experience higher-order correlation phenomena, due to the different degrees of miscibility that may emerge. These systems are far less explored, and they are described by a set of coupled eGP equations as has been reported, e.g., in Refs. [41,52] instead of the simple reduced single-component eGPE (2). In order to seed the breathing motion of the mixture we perform a quench of the trap frequency towards $\omega^{\rm f} = 4\omega^{\rm i} = 0.04$ and track the dynamics through the σ-species variance $\langle X_\sigma^2(t)\rangle$ [Eq. (8)] shown in Fig. 9(a). For stronger attractions ($\delta g = 0.01$), both $\langle X_A^2(t)\rangle$ and $\langle X_B^2(t)\rangle$ undergo almost constant amplitude oscillations being in phase among each other; see in particular the dashed lines in Fig. 9(a). The minor deviations between the oscillation amplitude of

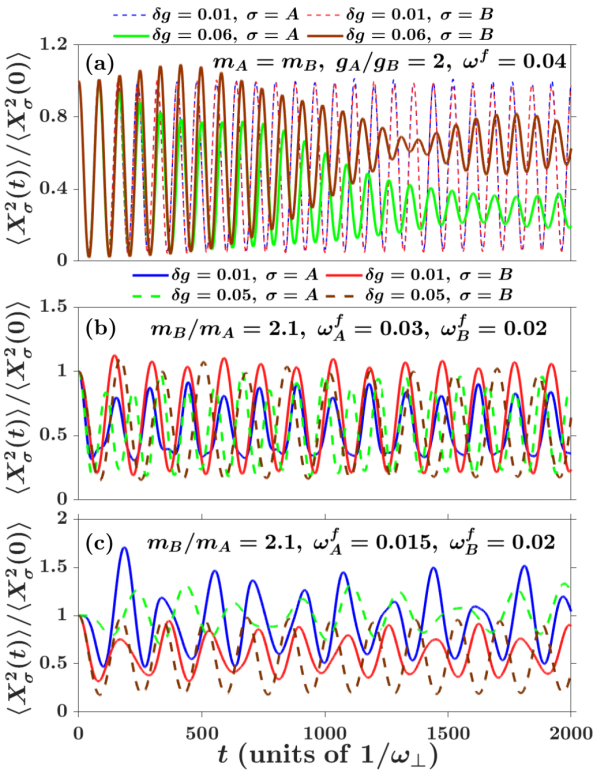

FIG. 9. Time evolution of the position variance of droplets within the MB method. (a) The case of a trap quenched ($\omega^{\rm f} = 4\omega^{\rm i} = 0.04$) homonuclear mixture, characterized by $g_B = 2g_A = 0.1$, $N = 20$, for varying interspecies attractions (see legend) is depicted. The collapse and revival pattern observed in the weakly attractive mixture constitutes an imprint of the droplet excitations during its breathing motion. (b), (c) Same as (a) but for a heteronuclear mixture with $m_B = 2.1m_A$, $g_B = 1.6g_A = 0.08$, and $N = 20$, following (b) a sudden increase of the trap frequency according to $\omega^f = 2\omega^i$ and (c) a species-selective quench where $\omega_{\rm B}^{\rm f} = 2\omega_{\rm B}^{\rm i} = 0.02$ and $\omega_{\rm A}^{\rm f} = \omega_{\rm A}^{\rm i} = 0.015$. The dynamics change from being out of phase to phase locked among the two components for increasing attraction.

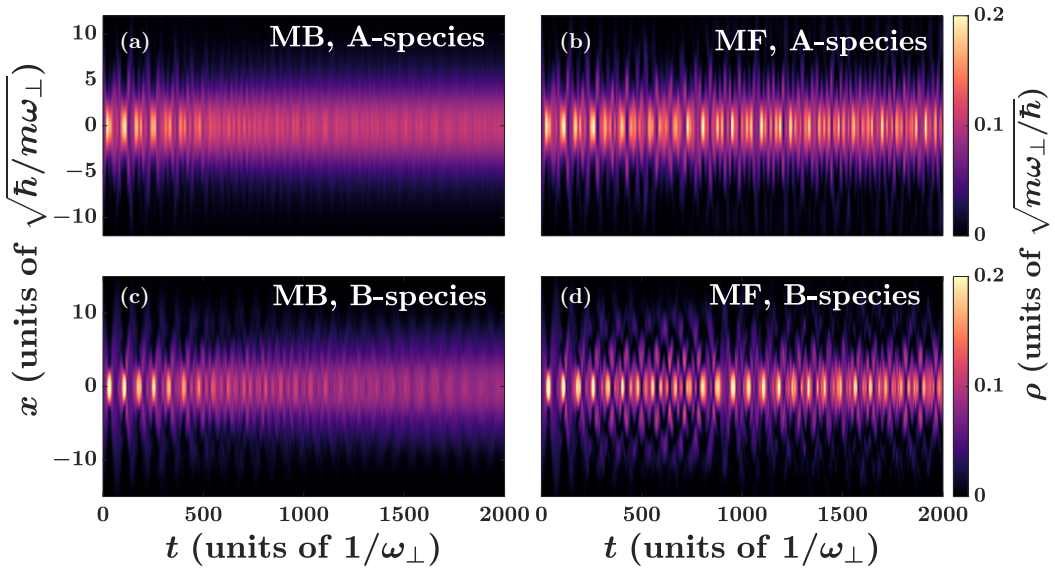

FIG. 10. Density evolution of the σ component (see legends) of a heteronuclear mass-imbalanced mixture with $m_B = 2.1m_A$, $g_B = 1.6g_A = 0.08$, $N_A = N_B = N = 20$ and strong intercomponent attraction $\delta g = 0.01$. The dynamics induced by quenching the trap frequency, $\omega_\sigma^{\rm f} = 4\omega_\sigma^{\rm i}$, is monitored within (a), (c) the MB and (b), (d) MF approaches. Evidently, the build-up of correlations leads to a dephasing of the breathing mode amplitude at long evolution times.

$\langle X_A^2(t)\rangle$ and $\langle X_B^2(t)\rangle$ in the long time dynamics ($t > 1300$) evinces the suppressed degree of intercomponent mixing in this interaction regime which is caused by the strong attractive coupling. Notably, the persistence of the amplitude of the position variances implies that excitations do not form in this two-component droplet scenario.

However, for weaker interspecies attractions ($\delta g = 0.06$) the ensuing motion of the two components is drastically altered. Specifically, the components expand and contract in a periodic manner initially ($0 < t < 150$) with almost the same amplitude. The latter progressively differentiates between $\langle X_A^2(t)\rangle$ and $\langle X_B^2(t)\rangle$, while afterwards a pronounced damping (i.e., reduction of the oscillation amplitude) is evident followed by a revival pattern at least for the more strongly repulsively interacting B component which exhibits a FT profile; see the solid lines in Fig. 9(a). This distinct behavior of $\langle X_A^2(t)\rangle$ and $\langle X_B^2(t)\rangle$ along with their damping is an imprint of the excitations building upon each component in the course of its breathing motion. In particular, the density of the B component experiences similar structural deformations in this case ($\delta g = 0.06$) with the interaction balanced mixture depicted in Fig. 4(a). Instead, the A component having a Gaussian-shaped ground state density profile features a significantly lower degree of spatial delocalization.

E. Heteronuclear mixtures: Breathing dynamics

Next, we examine the main features of the breathing dynamics of mass-imbalanced heteronuclear bosonic mixtures, e.g., consisting of ^{41}K and ^{87}Rb isotopes that have been experimentally realized [11]. In this sense, we consider a mass-imbalanced mixture $m_B = 2.1m_A$, with fixed intraspecies repulsions $g_B = 1.6g_A = 0.08$, particle numbers $N_A = N_B = N = 20$, and varying interspecies attraction $g_{AB} < 0$; see also Sec. III B for the ground state properties of this system. In order to study the response of this setting, a sudden change of the original trap frequencies $\omega_{\rm A}^{\rm i} = 1.5\omega_{\rm B}^{\rm i} = 0.015$ is applied and the breathing motion of each cloud is initiated. Below, our investigations are restricted within the ML-MCTDHX framework and the common MF treatment. We remark that the respective eGPE for mass-imbalanced mixtures in three dimensions was used in Refs. [11,51] but with the LHY contribution possessing a somewhat complicated form. To the best of our knowledge, the exact form of the 1D, mass-imbalanced eGPE has not yet been reported.

We first excite the breathing mode of the system, by suddenly doubling the harmonic trap frequencies for each species, i.e., $\omega_\sigma^{\rm f} = 2\omega_\sigma^{\rm i}$. Monitoring the time evolution of the σ-species position variance [Eq. (8)] it becomes apparent that each component expands and contracts [Fig. 9(b)] but importantly the response of $\langle X_\sigma^2(t)\rangle$ depends strongly on g_{AB}. Specifically, for weak attractions, e.g., $\delta g = 0.05$ the widths $\langle X_\sigma^2(t)\rangle$ feature a phase difference and distinct frequencies ($\omega_{\rm br}^{\rm A} \approx 1.3\omega_{\rm br}^{\rm B}$) during the dynamics. Notice that this breathing frequency ratio is slightly smaller than that of the respective traps, namely $\omega^{\rm A} \approx 1.5\omega^{\rm B}$. This reduced frequency ratio evinces that the heavier component B possesses a higher breathing frequency compared to the mass-balanced case; see also the stable breathing mode of the strongly attractive interaction-imbalanced mixture depicted in Fig. 9(a). Furthermore, the oscillation amplitude of the heavier species is nearly constant, in contrast to the one of the lighter component which becomes significantly suppressed when it oscillates out

of phase with the heavier species. On the other hand, for stronger attractions $\delta g = 0.01$, the heavier component "effectively" traps the lighter one, and they oscillate in phase with $\omega_{\rm br} \approx 2\omega_B^{\rm f}$.

To further exploit the asymmetries of our system, we apply a species-selective quench on the harmonic trap of the heavier species, i.e., $\omega_{\rm B}^{\rm f} = 2\omega_{\rm B}^{\rm i}$ whilst $\omega_{\rm A}^{\rm f} = \omega_{\rm A}^{\rm i}$ [Fig. 9(c)]. A close inspection of $\langle X_\sigma^2(t)\rangle$ for stronger attractions such as $\delta g = 0.01$, reveals that the heavy component imparts at the initial stages of the dynamics ($t < 100$) part of its energy to the lighter species which is subsequently set to breathing motion. The two components oscillate almost in phase but with distinct amplitudes among each other and also varying in the course of the evolution. We remark that this response is in sharp contrast to the high degree of delocalization that species-selective quenches excite on mass-balanced mixtures (not shown). Turning to weaker attractions ($\delta g = 0.05$), we observe a somewhat delayed energy transfer towards the lighter species. The latter consequently undergoes breathing dynamics characterized by two dominant breathing frequencies while exhibiting a phase difference with the heavier species as shown by the dashed lines in Fig. 9(c). $\langle X_A^2(t)\rangle$ exhibits distorted oscillations leading to a slightly larger frequency $\omega_A^{\rm br}$ at long evolution times ($t > 1500$), than at the initial stages of the dynamics ($t < 500$). As a consequence, at long evolution times ($t > 1500$) there is a breathing frequency ratio $\omega_B^{\rm br}/\omega_A^{\rm br} \approx 1.23$ between the two components. This ratio is slightly smaller than that of their respective postquench traps, i.e., $\omega_B^{\rm f}/\omega_A^{\rm f} \approx 1.33$, similar to the breathing evolution of the mass-imbalanced setting discussed above [Fig. 9(b)]. It is worth to be mentioned that small deviations between the MB and the MF predictions are again evident in the respective one-body density evolution, especially for smaller particle numbers, e.g., $N = 5$, which manifests that few-body effects come into play (not shown).

Performing a more intense quench characterized by $\omega_\sigma^{\rm f} = 4\omega_\sigma^{\rm i}$, we observe a prominent beyond MF effect for the strongly attractive ($\delta g = 0.01$) mass-imbalanced droplet configurations (Fig. 10). At short timescales ($0 < t < 400$) they exhibit a breathing motion [Figs. 10(a) and 10(c)] whose amplitude afterwards decays (Fig. 11) as a result of a dephasing mechanism due to the build-up of both intra- and intercomponent correlations, with the former being enhanced for the heavier species. This dephasing is established faster in the lighter component (Fig. 11). Evidently, this response is not captured by the MF approximation, where each component performs a breathing motion of nonnegligible amplitude (Fig. 11) throughout the time evolution accompanied by density delocalization during the expansion of the clouds; see Figs. 10(b) and 10(d). We also note in passing that motional excitations do not emerge in the course of the evolution which suggests that the observed response corresponds to a collective mechanism of the mixture.

The dephasing effect is attributed to the competition between the tendency of the two components to oscillate in phase in the strongly attractive case and the pronounced difference of their postquench confinement frequency. In this case, the heavier species B cannot instantly trap the rapidly oscillating lighter species A, as in the case of the less intense quench presented in Fig. 9(b). Instead, significant intercomponent collisions occur initially ($t < 500$) rendering the breathing modes of both components highly distorted, as can also be seen from the position variance of the mixture (Fig. 11). Subsequently, the heavier species B imposes its oscillation frequency on the lighter one, while the respective amplitudes of both species reduce significantly. However, species A maintains also a significant admixture of its initial frequency along with the one of species B resulting in a prominent dephasing behavior of $\langle X_A^2(t)\rangle$; see, e.g., Fig. 11 in the interval $t = [500–900]$. The above description also applies in the MF case [Figs. 10(c) and 10(d)]; see the agreement with the MB results in the variance for $t < 200$ in Fig. 11. However, in the absence of correlations, the heavier component B is not able to impose its oscillation frequency to the lighter one (Fig. 11). Rather, intercomponent collisions dominate throughout the time evolution, leading to irregular breathing dynamics and a high degree of spatial delocalization; see, e.g., $t \approx 500$ and $t \approx 1600$ in Figs. 10(c) and 10(d). This discrepancy, among the MF and MB predictions, could be interpreted as a manifestation of the self-bound nature of quantum droplets. Indeed, we overall observe an enhanced stability in the dynamics of heteronuclear mixtures, which is in accordance with the recent experimental observations in three dimensions [11].

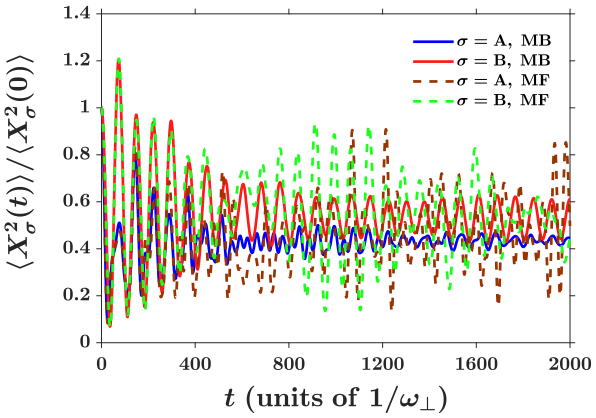

FIG. 11. Time evolution of the σ-species position variance of a mass-imbalanced heteronuclear mixture characterized by $m_B = 2.1m_A$, $g_B = 1.6g_A = 0.08$, $N_A = N_B = N = 20$, and strong intercomponent attraction $\delta g = 0.01$. The dynamics induced by a quench where $\omega_\sigma^{\rm f} = 4\omega_\sigma^{\rm i}$ is monitored within the MB (solid lines) and MF (dashed lines) approach. A correlation-induced dephasing behavior is observed in the MB case in sharp contrast to the MF dynamics where an irregular breathing motion persists.

V. DIPOLE DROPLET DYNAMICS

The presence of the external trap allows us to excite the dipole motion of the droplet by quenching the position of the trap center according to the protocol $V(x) \to V(x + \delta x_\sigma)$. The ensuing dynamics can be monitored through the σ-species one-body densities and the average position of the center of mass $\langle X_\sigma(t)\rangle = \langle \Psi(t)|\hat{x}_\sigma|\Psi(t)\rangle$ whose spectrum provides the dipole mode frequency. The properties of this collective droplet mode have not been previously addressed in detail,

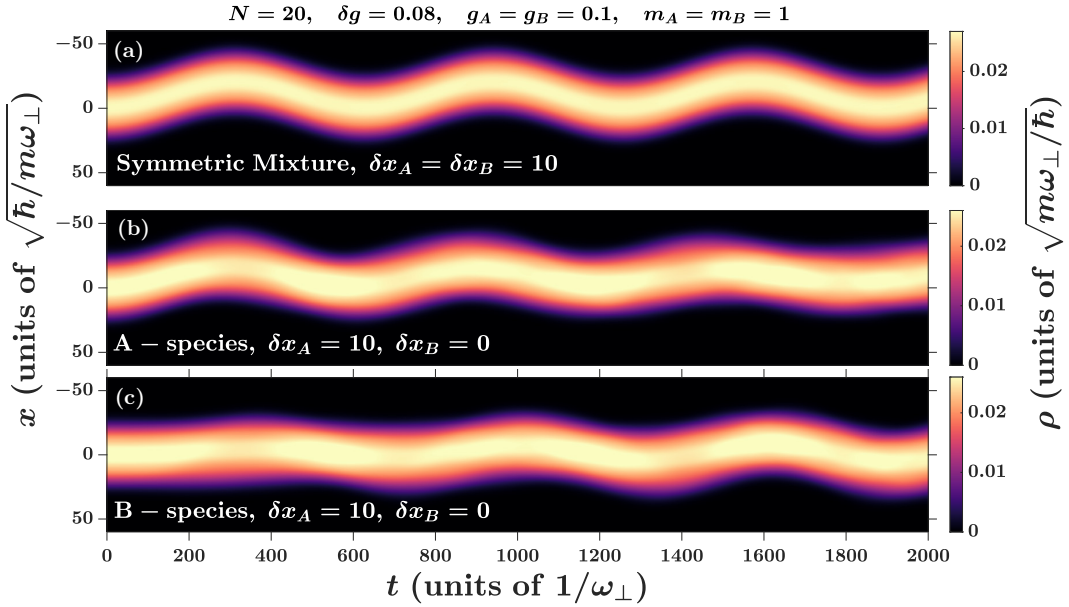

FIG. 12. One-body density evolution of a droplet building upon a weakly attractive symmetric mixture with $N_A = N_B = N = 20$, $g_A = g_B = 0.1$, and $\delta g = 0.08$ after an abrupt displacement of the trap center by δx_σ. (a) The displacement is performed in both components, where $\delta x_A = \delta x_B = 10$, resulting in a stable dipole motion having a frequency equal to the one of the trap. (b), (c) A species-selective quench with $\delta x_A = 10$ and $\delta x_B = 0$ leads to an energy transfer from species A to B and consequent out-of-phase dipole oscillations of the individual components. All results were obtained within the MB approach.

since these self-bound structures have been predominantly studied in flat geometries, where the translational invariance of the system leads to a vanishing dipole mode [38].

We first consider a FT droplet building upon a symmetric mixture characterized by $N_A = N_B = N = 20$, $g_A = g_B \equiv g = 0.1$, $\delta g = 0.08$, and $m_A = m_B$, while being subjected to a sudden displacement of the trap position, i.e., $\delta x_A = \delta x_B = 10$, of both species. The emergent dipole motion of this self-bound configuration corresponding to a collective oscillation of the droplet cloud around $x = -10$ with a frequency equal to the trap one is showcased in Fig. 12(a). We have verified that it is perfectly stable for long evolution times and independent of the interparticle interactions [see the dashed lines in Fig. 13(a)]. The interaction-independent character of the droplet dipole mode persists for different atom numbers, as well as for interaction-imbalanced mixtures irrespectively of the FT or Gaussian-shape of the homonuclear droplet. This behavior can be readily inferred from the insensitivity of the $\langle X_\sigma(t)\rangle$ for various system parameters depicted in Fig. 13(a). The only impact of the value of the involved interaction strengths on the dipole motion is on the constant spatial width of the oscillating droplet, which is determined by the respective ground state configuration (Figs. 1 and 2). As we shall explicate below this stable dipole response is a characteristic of homonuclear droplets after symmetrically quenching both components. The above-described insensitivity of the dipole mode takes equally place also within the different approaches, i.e., the MF and the eGPE (not shown), by means that its frequency and oscillation amplitude remain the same but the width of the droplet changes among the distinct frameworks, a result that can be traced back to the impact of correlations on the droplet initial width.

To exploit the inherent two-component nature of the symmetric droplet we perform a species-selective quench on the trap position. Namely, we shift the trap of species A by $\delta x_A = 10$ while keeping the trap of species B intact ($\delta x_B = 0$). Within the FT regime ($\delta g = 0.08$), the quenched species A is set to dipole motion while slowly transferring energy to component B, due to the finite interspecies coupling [70,85,86], and thus inducing to it a small amplitude dipole motion; see Figs. 12(b), 12(c) and Fig. 13(b). Subsequently, component B is further perturbed due to its collisions with component A; see, e.g., Fig. 13(b) at $t \approx 500$. As such, both components exhibit an oscillatory motion around the center of their respective trap, i.e., $x_A = -10$ and $x_B = 0$. Their oscillations are characterized by a temporally varying amplitude and a phase difference stemming from their periodic collisions and the initial slow energy transfer respectively. For instance, the oscillation amplitude of species A reduces from $\Delta X_A^{\max}(t \approx 297) \approx 8.6$ to $\Delta X_A^{\max}(t = 1789) \approx 4.9$, while the respective amplitude of species B increases from $\Delta X_B^{\max}(t = 400) \approx 3.9$ to $\Delta X_B^{\max}(t = 1916) \approx 6.7$ as can seen in Fig. 13(b). This change of amplitudes further indicates the nonnegligible energy transfer from the quenched component A to the externally unperturbed component B. An interesting perspective from the above-described process would be to study under which conditions a periodic energy exchange among the components takes place. In contrast, for stronger attractions, e.g., $\delta g = 0.01$ the quenched component A induces a dipole motion to component B almost instantly as shown in Fig. 13(b). Af-

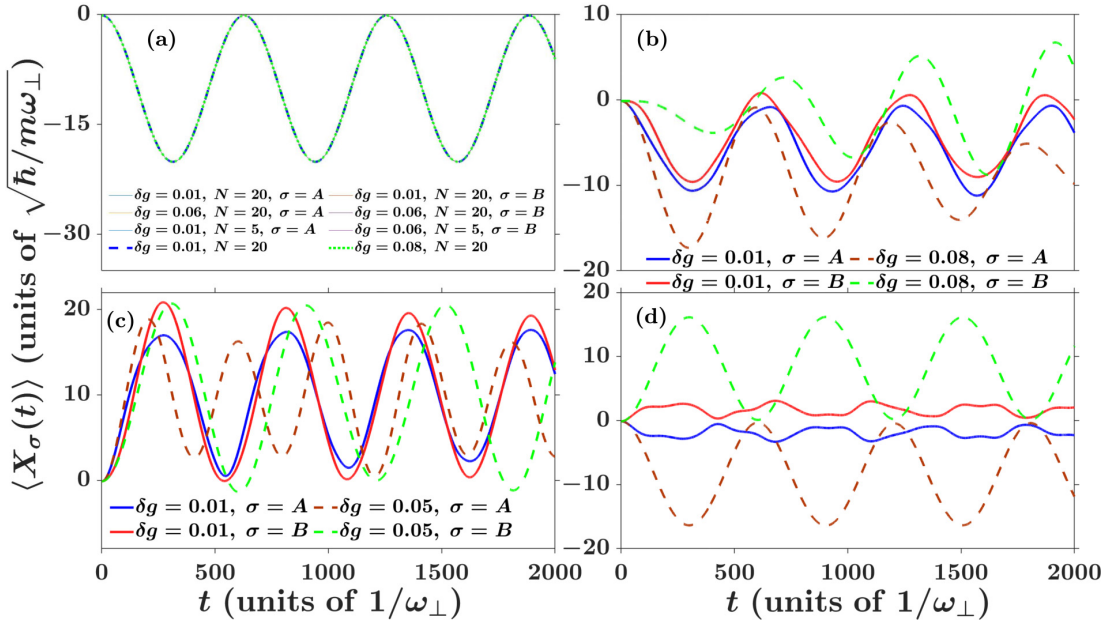

FIG. 13. Dynamics of the spatially averaged position of the σ-species center of mass $\langle X_\sigma(t)\rangle$ following a sudden displacement of the trap center by an amount δx_σ within the MB approach. (a) The case of homonuclear interaction-imbalanced $g_B = 2g_A = 0.1$ (solid lines) and balanced with $g_B = g_A = 0.1$ (dashed lines) bosonic mixtures subjected to quenches with $\delta x_A = \delta x_B = 10$ for different interactions and atom numbers (see legends) is depicted. The emergent dipole motion is independent of the system parameters. Species-selective quenches with (b) $\delta x_A = 10$, $\delta x_B = 0$ and (d) $\delta x_A = -\delta x_B = 10$ in a symmetric mixture characterized by $g_A = g_B = 0.1$, $N_A = N_B = N = 20$. (c) Dipole motion induced by $\delta x_A = \delta x_B = -10$ in a mass-imbalanced heteronuclear mixture where $m_B = 2.1m_A$, $g_B = 1.6g_A = 0.08$, and $N_A = N_B = N = 20$. Apparently, following either species-selective quenches or using mass-imbalanced mixtures gives rise to a more complex dipole dynamics, with a strong dependence on δg.

terwards, both components perform a nearly in-phase dipole motion centered towards the midpoint of their respective trap origins (i.e., $x = -5$) and having an amplitude which is half of the symmetric dipole mode [Fig. 13(a)]. The small asymmetries appearing in the amplitude of each component motion are attributed to their mutual interactions.

Next, we explore the impact of intercomponent mass imbalance on the droplet dipole mode which is induced by a common displacement of the σ-species trap center, i.e., $\delta x_A = \delta x_B = -10$. Indeed, the dipole dynamics of the heteronuclear mixture ($m_B = 2.1m_A$, $g_B = 1.6g_A = 0.08$, and $N_A = N_B = N = 20$) is interaction-dependent [see Fig. 13(c)] in sharp contrast to homonuclear settings [Fig. 13(a)]. In particular, similarly to the breathing mode response analyzed in Sec. IV E for mass-imbalanced systems, a stronger interspecies attraction (e.g., here $\delta g = 0.01$) enforces the two components to oscillate with the same dipole frequency as shown in Fig. 13(c). Conversely, weaker attractions such as $\delta g = 0.05$ lead to distinct dipole motions among the two components characterized by frequencies slightly higher than the ones of their respective traps. Moreover, the presence of the heavier B species causes the lighter one (A) to exhibit an enhanced or reduced oscillation amplitude when it evolves in-phase or with π-phase difference with respect to B [Fig. 13(c)]. Additionally, the dipole mode frequency of the heavier component, B, reduces with decreasing attraction, namely, $\omega_B^{\rm dip}(\delta g = 0.05) \approx 0.9\omega_B^{\rm dip}(\delta g = 0.01)$.[2] This is to be opposed with the dipole motion of homonuclear mixtures [Fig. 13(a)], which is independent of the interspecies attraction.

Concluding, a counterdisplacement of the component trap centers, i.e., $\delta x_A = -\delta x_B = 10$ is applied on the symmetric mixture aiming to induce intercomponent collisions; see Fig. 13(d). Close to the decoupling limit, e.g., $\delta g = 0.08$, the droplets undergo stable in time and nearly independent dipole oscillations, with opposite phase, whose amplitudes are reduced by approximately 15% as compared to the common dipole motion of the symmetric case depicted in Fig. 12(a) and Fig. 13(a). Importantly, within this weakly attractive regime the droplets feature elastic intercomponent collisions around $x = 0$ in a periodic manner as can be deduced by their constant oscillation amplitude. It is also worth mentioning that in spite of the smooth center-of-mass droplet oscillations, the respective densities do not remain unaffected in the course of the evolution. Instead, they develop enhanced density peaks at their collision events which become suppressed at maximum separation. Moreover, the droplets maintain their FT profile

[2]Note that a similar comparison for the lighter component A is not possible since it adopts the dipole frequency of the heavier species in the more strongly attractive case ($\delta g = 0.01$), as we discussed above [Fig. 13(c)].

at maximum separation while exhibiting a flattened "wavefront" close to their oscillation centers (not shown). Turning to strong attractions, e.g., $\delta g = 0.01$, the droplets remain tightly self-bound at the origin. However, certain density portions are emitted from the droplet edges and reattach to it periodically. This results in the fluctuations captured by the mean position of the cloud [Fig. 13(d)].

VI. SUMMARY AND OUTLOOK

We have studied the ground state properties and quench dynamics of 1D harmonically confined droplet configurations appearing in both homonuclear (interaction balanced or imbalanced) and heteronuclear (mass-imbalanced) bosonic mixtures. To appreciate the role of beyond-LHY correlations different theoretical approaches are employed and compared, namely the *ab initio* ML-MCTDHX approach the so-called eGPE as well as the standard MF approximation.

Regarding the ground state of the trapped interaction balanced mixtures we identify a transition from Gaussian shaped to FT droplets due to beyond-LHY correlations for either weak attractions or larger atom numbers. This result is in contrast to the predictions of both the MF and the eGPE frameworks, with the former recovering FT droplet structures when tending to the homogeneous limit as discussed in Ref. [56]. For interaction or mass-imbalanced mixtures it is shown that the involved components become spatially mixed. In the case of interaction-imbalanced systems the strongly repulsive component experiences FT signatures for reduced intercomponent attraction, while the remaining one has a Gaussian profile. A similar behavior occurs for mass-imbalanced mixtures where the heavier component exhibits FT structures for weaker attractions. Furthermore, a robust antibunching behavior is identified at the same location of the droplet, while two bosons are correlated when placed at opposite sides of the droplet.

Following, a quench of the trap frequency seeds the droplet breathing dynamics. For homonuclear mixtures we explicate that in addition to the expected contraction and expansion each cloud also experiences a complex excitation process in the long-time evolution. Specifically, a progressive spatial delocalization of the droplet takes place accompanied by the build-up of motional excitations around its core along with the simultaneous expulsion of density portions. These excitation mechanisms originate from the participation of higher-lying orbitals of the MB wave function and are associated with the development of enhanced intercomponent entanglement and long-range two-body correlations. The breathing frequency of the droplet is close to the ideal gas prediction for stronger attractions, while it shows a reduction for weaker ones where the FT is attained. Our results are corroborated through analytical estimations of the breathing frequency in the large atom limit by invoking a variational time-dependent Gaussian ansatz. In heteronuclear mixtures the components undergo an in-phase breathing at strong attractions, while experiencing a phase difference towards the decoupling limit. Interestingly, a pronounced dephasing develops for sufficiently strong quench amplitudes emanating from the competition between the tendency to phase-lock and the difference of the species trap frequencies. Instead, in the absence of correlations solely intercomponent collisions dominate the dynamics.

The droplet dipole motion is triggered by a sudden displacement of the trap's position which turns out to be remarkably stable and insensitive to parametric variations of the homonuclear mixture. However, the individual components of heteronuclear mixtures feature phase-locked dipole motions for strong interspecies attraction, otherwise they exhibit a phase difference. Furthermore, irregular dipole patterns occur due to component collisions and intercomponent energy transfer, when considering species-selective quenches of the trap position. Concluding, after a counter displacement of each component trap center the droplets experience elastic collisions for weak attractions while they remain to a large extent bound for stronger ones.

Our findings pave the way for various interesting future research directions. A fruitful prospect is to utilize beyond-LHY correlations to reveal droplet mixed states in species-selective traps and study their dynamical response following time-dependent rampings of the intercomponent attraction across the identified phases. Also, an explicit derivation of the LHY or higher-order contributions in the presence of external confinement would be at least theoretically desirable. Furthermore, the investigation of self-bound state formation in the crossover from highly particle imbalanced to balanced settings is another interesting perspective. Certainly, the interplay of beyond-LHY correlations and entanglement for the droplet formation in three-component mixtures [87,88] is another promising route to follow.

ACKNOWLEDGMENTS

This work (P.S. and I.A.E.) has been funded by the Deutsche Forschungsgemeinschaft (DFG, German Research Foundation), SFB 925, Project No. 170620586. S.I.M. acknowledges support from the National Science Foundation through a grant for ITAMP at Harvard University. This research was supported in part by the National Science Foundation under Grant No. NSF PHY-1748958.

APPENDIX: VARIATIONAL ANSATZ FOR CONFINED DROPLETS

To provide further insights into the stationary and dynamical properties of quantum droplets in the main text we have employed, besides the MB ML-MCTDHX and the eGPE approaches, also a so-called variational approximation (VA) [84]. It relies on the eGPE framework and utilizes a time-dependent Gaussian ansatz. This method was recently employed to solve the reduced single-component eGPE in free space [37], while relevant generalizations have also been reported for dipolar settings [13]. Particularly, it was argued that it fails to capture the ground state one-body density of the system, especially close to the FT regime. However, it can provide adequate estimates regarding the frequency of the droplet collective excitations. Here we seek to apply this method to confined droplets, where it is anticipated that the density of the system can be better approximated by a Gaussian profile, due to the presence of the harmonic trap.

To construct this VA scheme we initially define the Lagrangian density of the eGPE (2)

$$\mathcal{L} = \frac{i\hbar}{2}(\Psi\Psi_t^* - \Psi^*\Psi_t) + \frac{\hbar^2}{2m}|\Psi_x|^2 + \frac{\delta g}{2}|\Psi|^4 - \frac{2\sqrt{2m}}{3\pi\hbar}g^{\frac{3}{2}}|\Psi|^3 + \frac{1}{2}m\omega^2x^2|\Psi|^2. \tag{A1}$$

The subscripts x, t refer to the space and time derivatives respectively. Then, a Gaussian ansatz characterized by time-dependent amplitude $[A(t)]$, width $[W(t)]$, and phases $[\phi(t), b(t)]$ is introduced:

$$\Psi(x,t) = A(t)\exp\left[i\phi(t) + ib(t)x^2 - \frac{x^2}{2W(t)^2}\right]. \tag{A2}$$

It is normalized to the particle number, namely, $N = A(t)^2W(t)\sqrt{\pi}$.

Substituting this wave function ansatz into the Lagrangian density of Eq. (A1) and integrating over the entire space $[-\infty, \infty]$, we arrive at the effective Lagrangian per particle

$$\frac{L_{\rm VA}}{N} = \hbar\dot{\phi} + \left[\hbar\dot{b} + \frac{2\hbar^2}{m}\left(b^2 + \frac{1}{4W^4}\right) + \frac{m\omega^2}{2}\right]\frac{W^2}{2} + \frac{N\delta g}{2\sqrt{2\pi}W} - \frac{\sqrt{2mg^3}}{3^{\frac{3}{2}}\pi^{\frac{5}{4}}\hbar}\sqrt{\frac{N}{W}}. \tag{A3}$$

The corresponding Euler-Lagrange equations of motion in terms of ϕ, W and b reduce to a classical equation of motion for the width, namely, $m\ddot{W} = -\frac{dU_{\rm eff}}{dW}$. Hence, in the framework of the VA method the stationary optimal Gaussian solution corresponds to the minimum of the effective potential

$$U_{\rm eff}(W) = \frac{m\omega^2}{2}W^2 + \frac{\hbar^2}{2mW^2} + \frac{N\delta g}{\sqrt{2\pi}W} - 2\frac{\sqrt{2mg^3}}{\pi^{\frac{5}{4}}\hbar}\sqrt{\frac{N}{W}}. \tag{A4}$$

Having determined the optimal width ($W_{\rm min}$) of our Gaussian ground state ansatz, the energy per particle of the system is given by $E = U_{\rm eff}(W_{\rm min}/2)$ and the frequency of the breathing mode is the lowest eigenvalue of the Hessian matrix

$$\left[\omega_{\rm br}^{\rm VA}\right]^2 = \frac{1}{m}\frac{d^2U_{\rm eff}}{dW^2}\bigg|_{W_{min}}. \tag{A5}$$

As discussed in the main text, this approximation can adequately describe the breathing frequency of quantum droplets especially in the vicinity of the FT regime. However, it fails to capture the underlying density profiles in most of the cases. Interestingly, the obtained analytical predictions, in the large particle number limit, provide invaluable insights on the scaling of the droplet breathing frequency in terms of the system parameters and importantly on the LHY contribution.

[1] I. Bloch, J. Dalibard, and S. Nascimbène, Nat. Phys. **8**, 267 (2012).
[2] D. S. Petrov, Phys. Rev. Lett. **115**, 155302 (2015).
[3] I. Ferrier-Barbut, H. Kadau, M. Schmitt, M. Wenzel, and T. Pfau, Phys. Rev. Lett. **116**, 215301 (2016).
[4] F. Böttcher, J.-N. Schmidt, J. Hertkorn, K. S. H. Ng, S. D. Graham, M. Guo, T. Langen, and T. Pfau, Rep. Prog. Phys. **84**, 012403 (2021).
[5] Z.-H. Luo, W. Pang, B. Liu, Y.-Y. Li, and B. A. Malomed, Front. Phys. **16**, 32201 (2021).
[6] B. A. Malomed, Front. Phys. **16**, 22504 (2021).
[7] T. D. Lee, K. Huang, and C. N. Yang, Phys. Rev. **106**, 1135 (1957).
[8] C. R. Cabrera, L. Tanzi, J. Sanz, B. Naylor, P. Thomas, P. Cheiney, and L. Tarruell, Science **359**, 301 (2018).
[9] P. Cheiney, C. R. Cabrera, J. Sanz, B. Naylor, L. Tanzi, and L. Tarruell, Phys. Rev. Lett. **120**, 135301 (2018).
[10] G. Semeghini, G. Ferioli, L. Masi, C. Mazzinghi, L. Wolswijk, F. Minardi, M. Modugno, G. Modugno, M. Inguscio, and M. Fattori, Phys. Rev. Lett. **120**, 235301 (2018).
[11] C. D'Errico, A. Burchianti, M. Prevedelli, L. Salasnich, F. Ancilotto, M. Modugno, F. Minardi, and C. Fort, Phys. Rev. Res. **1**, 033155 (2019).
[12] F. Böttcher, J.-N. Schmidt, M. Wenzel, J. Hertkorn, M. Guo, T. Langen, and T. Pfau, Phys. Rev. X **9**, 011051 (2019).
[13] L. Chomaz, I. Ferrier-Barbut, F. Ferlaino, B. Laburthe-Tolra, B. L. Lev, and T. Pfau, Rep. Prog. Phys. **86**, 026401 (2023).
[14] R. N. Bisset, L. A. Peña Ardila, and L. Santos, Phys. Rev. Lett. **126**, 025301 (2021).
[15] J. C. Smith, D. Baillie, and P. B. Blakie, Phys. Rev. Lett. **126**, 025302 (2021).
[16] G. Ferioli, G. Semeghini, S. Terradas-Briansó, L. Masi, M. Fattori, and M. Modugno, Phys. Rev. Res. **2**, 013269 (2020).
[17] A. Cappellaro, T. Macrì, and L. Salasnich, Phys. Rev. A **97**, 053623 (2018).
[18] X. Cui and Y. Ma, Phys. Rev. Res. **3**, L012027 (2021).
[19] G. Ferioli, G. Semeghini, L. Masi, G. Giusti, G. Modugno, M. Inguscio, A. Gallemí, A. Recati, and M. Fattori, Phys. Rev. Lett. **122**, 090401 (2019).
[20] X. Cui, Phys. Rev. A **98**, 023630 (2018).
[21] D. Rakshit, T. Karpiuk, M. Brewczyk, and M. Gajda, SciPost Phys. **6**, 079 (2019).
[22] J.-B. Wang, J.-S. Pan, X. Cui, and W. Yi, Chin. Phys. Lett. **37**, 076701 (2020).
[23] Y. Sekino and Y. Nishida, Phys. Rev. A **97**, 011602(R) (2018).
[24] I. Morera, B. Juliá-Díaz, and M. Valiente, arXiv:2103.16499.
[25] P. Stürmer, M. N. Tengstrand, R. Sachdeva, and S. M. Reimann, Phys. Rev. A **103**, 053302 (2021).
[26] Y. V. Kartashov, B. A. Malomed, L. Tarruell, and L. Torner, Phys. Rev. A **98**, 013612 (2018).
[27] Y. Li, Z. Chen, Z. Luo, C. Huang, H. Tan, W. Pang, and B. A. Malomed, Phys. Rev. A **98**, 063602 (2018).
[28] M. N. Tengstrand, P. Stürmer, E. O. Karabulut, and S. M. Reimann, Phys. Rev. Lett. **123**, 160405 (2019).
[29] Z. Lin, X. Xu, Z. Chen, Z. Yan, Z. Mai, and B. Liu, Commun. Nonlinear Sci. Numer. Simul. **93**, 105536 (2021).
[30] P. Examilioti and G. M. Kavoulakis, J. Phys. B: At. Mol. Opt. Phys. **53**, 175301 (2020).
[31] I. Morera, G. E. Astrakharchik, A. Polls, and B. Juliá-Díaz, Phys. Rev. Res. **2**, 022008(R) (2020).
[32] I. Morera, G. E. Astrakharchik, A. Polls, and B. Juliá-Díaz, Phys. Rev. Lett. **126**, 023001 (2021).

[33] Y.-Y. Zheng, S.-T. Chen, Z.-P. Huang, S.-X. Dai, B. Liu, Y.-Y. Li, and S.-R. Wang, Front. Phys. **16**, 22501 (2021).
[34] Y. Machida, I. Danshita, D. Yamamoto, and K. Kasamatsu, Phys. Rev. A **105**, L031301 (2022).
[35] B. Liu, H.-F. Zhang, R.-X. Zhong, X.-L. Zhang, X.-Z. Qin, C. Huang, Y.-Y. Li, and B. A. Malomed, Phys. Rev. A **99**, 053602 (2019).
[36] X. Zhang, X. Xu, Y. Zheng, Z. Chen, B. Liu, C. Huang, B. A. Malomed, and Y. Li, Phys. Rev. Lett. **123**, 133901 (2019).
[37] G. E. Astrakharchik and B. A. Malomed, Phys. Rev. A **98**, 013631 (2018).
[38] M. Tylutki, G. E. Astrakharchik, B. A. Malomed, and D. S. Petrov, Phys. Rev. A **101**, 051601(R) (2020).
[39] S. R. Otajonov, E. N. Tsoy, and F. K. Abdullaev, Phys. Lett. A **383**, 125980 (2019).
[40] M. N. Tengstrand and S. M. Reimann, Phys. Rev. A **105**, 033319 (2022).
[41] T. Mithun, A. Maluckov, K. Kasamatsu, B. A. Malomed, and A. Khare, Symmetry **12**, 174 (2020).
[42] P. Zin, M. Pylak, T. Wasak, M. Gajda, and Z. Idziaszek, Phys. Rev. A **98**, 051603(R) (2018).
[43] J. Wang, H. Hu, and X.-J. Liu, New J. Phys. **22**, 103044 (2020).
[44] G. De Rosi, G. E. Astrakharchik, and P. Massignan, Phys. Rev. A **103**, 043316 (2021).
[45] N. Guebli and A. Boudjemâa, Phys. Rev. A **104**, 023310 (2021).
[46] A. Boudjemâa, Sci. Rep. **11**, 21765 (2021).
[47] T. Mithun, S. I. Mistakidis, P. Schmelcher, and P. G. Kevrekidis, Phys. Rev. A **104**, 033316 (2021).
[48] G. E. Astrakharchik and S. Giorgini, J. Phys. B: At. Mol. Opt. Phys. **39**, S1 (2006).
[49] L. Lavoine and T. Bourdel, Phys. Rev. A **103**, 033312 (2021).
[50] C. Fort and M. Modugno, Appl. Sci. **11**, 866 (2021).
[51] F. Ancilotto, M. Barranco, M. Guilleumas, and M. Pi, Phys. Rev. A **98**, 053623 (2018).
[52] S. I. Mistakidis, T. Mithun, P. G. Kevrekidis, H. R. Sadeghpour, and P. Schmelcher, Phys. Rev. Res. **3**, 043128 (2021).
[53] D. S. Petrov and G. E. Astrakharchik, Phys. Rev. Lett. **117**, 100401 (2016).
[54] L. Parisi, G. E. Astrakharchik, and S. Giorgini, Phys. Rev. Lett. **122**, 105302 (2019).
[55] L. Parisi and S. Giorgini, Phys. Rev. A **102**, 023318 (2020).
[56] A. Debnath, A. Khan, and S. Basu, Phys. Lett. A **439**, 128137 (2022).
[57] M. R. Pathak and A. Nath, Sci. Rep. **12**, 6904 (2022).
[58] S. Krönke, L. Cao, O. Vendrell, and P. Schmelcher, New J. Phys. **15**, 063018 (2013).
[59] L. Cao, S. Krönke, O. Vendrell, and P. Schmelcher, J. Chem. Phys. **139**, 134103 (2013).
[60] L. Cao, V. Bolsinger, S. I. Mistakidis, G. M. Koutentakis, S. Krönke, J. M. Schurer, and P. Schmelcher, J. Chem. Phys. **147**, 044106 (2017).
[61] C. J. Pethick and H. Smith, *Bose–Einstein Condensation in Dilute Gases*, 2nd ed. (Cambridge University Press, Cambridge, 2008).
[62] M. Olshanii, Phys. Rev. Lett. **81**, 938 (1998).
[63] C. Chin, R. Grimm, P. Julienne, and E. Tiesinga, Rev. Mod. Phys. **82**, 1225 (2010).
[64] T. Köhler, K. Góral, and P. S. Julienne, Rev. Mod. Phys. **78**, 1311 (2006).
[65] A. Görlitz, J. M. Vogels, A. E. Leanhardt, C. Raman, T. L. Gustavson, J. R. Abo-Shaeer, A. P. Chikkatur, S. Gupta, S. Inouye, T. Rosenband, and W. Ketterle, Phys. Rev. Lett. **87**, 130402 (2001).
[66] T. G. Skov, M. G. Skou, N. B. Jørgensen, and J. J. Arlt, Phys. Rev. Lett. **126**, 230404 (2021).
[67] I. V. Barashenkov and E. Y. Panova, Physica D: Nonlin. Phenom. **69**, 114 (1993).
[68] H. Triki, A. Biswas, S. P. Moshokoa, and M. Belic, Optik **128**, 63 (2017).
[69] L. Pitaevskii and S. Stringari, *Bose–Einstein Condensation and Superfluidity* (Oxford University Press, Oxford, 2016).
[70] S. I. Mistakidis, A. G. Volosniev, R. E. Barfknecht, T. Fogarty, T. Busch, A. Foerster, P. Schmelcher, and N. Zinner, arXiv:2202.11071.
[71] A. U. J. Lode, C. Lévêque, L. B. Madsen, A. I. Streltsov, and O. E. Alon, Rev. Mod. Phys. **92**, 011001 (2020).
[72] R. Horodecki, P. Horodecki, M. Horodecki, and K. Horodecki, Rev. Mod. Phys. **81**, 865 (2009).
[73] J. Frenkel, *Wave Mechanics; Elementary Theory* (Clarendon Press, Oxford, 1932).
[74] H. Hu, J. Wang, and X.-J. Liu, Phys. Rev. A **102**, 043301 (2020).
[75] T. Giamarchi, *Quantum Physics in One Dimension* (Clarendon Press, Oxford, 2003).
[76] K. Sakmann, A. I. Streltsov, O. E. Alon, and L. S. Cederbaum, Phys. Rev. A **78**, 023615 (2008).
[77] M. Naraschewski and R. J. Glauber, Phys. Rev. A **59**, 4595 (1999).
[78] G. C. Katsimiga, S. I. Mistakidis, T. M. Bersano, M. K. H. Ome, S. M. Mossman, K. Mukherjee, P. Schmelcher, P. Engels, and P. G. Kevrekidis, Phys. Rev. A **102**, 023301 (2020).
[79] T. M. Bersano, V. Gokhroo, M. A. Khamehchi, J. D'Ambroise, D. J. Frantzeskakis, P. Engels, and P. G. Kevrekidis, Phys. Rev. Lett. **120**, 063202 (2018).
[80] B. Laburthe Tolra, K. M. O'Hara, J. H. Huckans, W. D. Phillips, S. L. Rolston, and J. V. Porto, Phys. Rev. Lett. **92**, 190401 (2004).
[81] H. Hu and X.-J. Liu, Phys. Rev. Lett. **125**, 195302 (2020).
[82] J. P. Ronzheimer, M. Schreiber, S. Braun, S. S. Hodgman, S. Langer, I. P. McCulloch, F. Heidrich-Meisner, I. Bloch, and U. Schneider, Phys. Rev. Lett. **110**, 205301 (2013).
[83] T. Fukuhara, A. Kantian, M. Endres, M. Cheneau, P. Schauß, S. Hild, D. Bellem, U. Schollwöck, T. Giamarchi, C. Gross, and I. Bloch, Nat. Phys. **9**, 235 (2013).
[84] L. Salasnich, Int. J. Mod. Phys. B **14**, 1 (2000).
[85] S. I. Mistakidis, G. M. Koutentakis, F. Grusdt, H. R. Sadeghpour, and P. Schmelcher, New J. Phys. **23**, 043051 (2021).
[86] S. I. Mistakidis, G. C. Katsimiga, G. M. Koutentakis, T. Busch, and P. Schmelcher, Phys. Rev. Res. **2**, 033380 (2020).
[87] Y. Ma, C. Peng, and X. Cui, Phys. Rev. Lett. **127**, 043002 (2021).
[88] K. Keiler, S. I. Mistakidis, and P. Schmelcher, Phys. Rev. A **104**, L031301 (2021).

4.2 Particle Imbalanced Weakly Interacting Quantum Droplets in One-Dimension

PHYSICAL REVIEW A **110**, 023324 (2024)

Particle-imbalanced weakly interacting quantum droplets in one dimension

I. A. Englezos [1], P. Schmelcher,[1,2] and S. I. Mistakidis [3,4,5]

[1]*Center for Optical Quantum Technologies, Department of Physics, University of Hamburg, Luruper Chaussee 149, 22761 Hamburg, Germany*

[2]*The Hamburg Centre for Ultrafast Imaging, University of Hamburg, Luruper Chaussee 149, 22761 Hamburg, Germany*

[3]*ITAMP, Center for Astrophysics | Harvard and Smithsonian, Cambridge, Massachusetts 02138, USA*

[4]*Department of Physics, Harvard University, Cambridge, Massachusetts 02138, USA*

[5]*Department of Physics, Missouri University of Science and Technology, Rolla, Missouri 65409, USA*

(Received 21 December 2023; revised 23 July 2024; accepted 29 July 2024; published 22 August 2024)

We explore the formation of one-dimensional two-component quantum droplets with intercomponent particle imbalance using an *ab initio* many-body method. It is shown that for moderate particle imbalance each component maintains its droplet flat-top or Gaussian-type character depending on the intercomponent attraction. Importantly, large particle imbalance leads to a flat-top shape of the majority component with the minority exhibiting spatially localized configurations. The latter imprint modulations on the majority component which become more pronounced for increasing interspecies attraction. The same holds for larger mass or increasing repulsion of the minority species. Such structural transitions are also evident in the underlying two-body correlation functions. To interpret the origin and characteristics of these droplet states we derive an effective model based on the established Lee-Huang-Yang theory providing adequate qualitative analytical predictions even away from its expected parametric region of validity. In contrast, the droplet character is found to vanish in the presence of fermionic minority atoms. Our results pave the way for unveiling complex droplet phases of matter.

DOI: 10.1103/PhysRevA.110.023324

I. INTRODUCTION

Correlated quantum many-body states can be nowadays designed and experimentally prepared within ultracold atom platforms [1]. Prototypical examples are self-bound quantum droplets [2–6] and quasiparticles such as polarons [7,8]. The experimental observation of Bose [9–13] and Fermi polarons [14–16] verified the crucial role of correlations in these settings. In turn, significant theoretical attention [17,18] has been devoted towards the study of correlation effects in the stationary [19–23] and the far less explored nonequilibrium dynamics [24–27] of polarons.

Higher-order correlations are similarly integral in the formation of quantum droplets. The latter can appear in short-range interacting bosonic mixtures [28–30] but also in single-component [3,31,32] and mixtures [33,34] of dipolar gases. Droplet states manifest when quantum fluctuations, commonly accounted for by the Lee-Huang-Yang (LHY) correction term [35], stabilize the gas against collapse originating from mean-field interaction effects [2,4–6]. Interestingly, other theory proposals for droplets suggest their occurrence in the presence of three-body interactions [36,37] but also in Bose-Fermi mixtures with [38] and without spin-orbit coupling [39,40]. Quantum droplets exhibit features of a dilute liquidlike state [2], manifesting, for example, in the development of a flat-top (FT) profile in their spatial density configuration. In three dimensions, the quantum liquid character of droplets can be unveiled in terms of their surface tension [2,41] and incompressibility [42]. However, the study of three-dimensional (3D) droplets is hindered by their characteristic self-evaporation process [2,43]. The latter is absent in one-dimensional (1D) systems [44], which emerge as ideal settings for studying long-lived (due to lower densities) and stable quantum droplets, where correlation effects are naturally enhanced.

The majority of the quantum droplet investigations focused on imposing the fixed density ratio condition between the two components determined by their intracomponent interaction strengths. In this regime, droplets are expected to be more stable and in fact the two-component setting is reduced to an effective single-component one [2,45]. Recently, some attention has been placed on exploring the genuine two-component nature of the system by employing either mass imbalance or different intracomponent interactions [30,46,47]. These studies indicated that quantum droplets can also remain stable when the fixed density ratio is violated. This has been further explored in three dimensions [48–50] within the context of the LHY theory. Similar conclusions were drawn in 1D systems of strongly interacting lattice trapped particle-imbalanced bosonic mixtures using the density-matrix renormalization-group method [51] and in a ring geometry focusing on the rotational properties of droplets within LHY theory [52]. Therefore, the stability region of droplets has been extended to a wider range of density ratios relying on small intercomponent particle imbalances. However, considering larger particle imbalances shares the premise of constructing effective methods, through which analytical predictions can be made, but also enhances interparticle correlations (beyond LHY) since one of the components can be even reduced to a few-body sample. Note, also, that the works mentioned above [49–52]

explored the scenario of mass balanced mixtures featuring equal intraspecies interactions, leaving the number of particles per component as the only source of intercomponent imbalance.

For these reasons, we focus on two-component short-range weakly interacting bosonic mixtures in one dimension aiming to understand the interplay of particle, intracomponent interaction, and mass imbalance on the droplet formation. In this context, one component (majority) consists of a significantly larger number of atoms than the second (minority). We derive an effective model based on the coupled system of extended-Gross-Pitaevskii equations (eGPEs) [2,53] which allows for analytical insights into the two-component droplet formation. For instance, it predicts a decoupling of the two-component system into a quantum droplet for the majority component and a localized bright-soliton structure for the minority one in the case of extreme atom imbalance. The results obtained from this effective theory are verified utilizing the *ab initio* multilayer multiconfiguration time-dependent Hartree method for atomic mixtures (ML-MCTDHX) [54–58]. Furthermore, the impact of increasing the involved interaction strengths or the mass of the minority atoms is revealed. It predominantly results in spatial modulations of the majority component which maintains a FT droplet profile. Next, it is shown that the droplet character of the majority bosonic subsystem vanishes in the presence of fermionic minority atoms, which in turn delocalize and spread over the former. Our results illustrate the surprising effectiveness of the LHY theory in capturing droplet formation even far from its expected validity region.

This paper is structured in the following way. In Sec. II, we describe the two-component attractively interacting bosonic mixture supporting droplet solutions. Section III briefly introduces the underlying LHY theory as well as the nonperturbative ML-MCTDHX approach deployed for the investigation of quantum droplets. Section IV is devoted to the derivation and solution of the effective eGPEs in the limit of large intercomponent particle imbalance. It is used, later on, as an interpretation tool for the two-component droplet configurations. The phenomenology provided by the eGPEs is confirmed by comparing to the predictions of the *ab initio* ML-MCTDHX method in both the one- (Sec. V) and two-particle (Sec. VI) level. Droplet structures appearing in heteronuclear (Bose-Bose or Bose-Fermi) mixtures are briefly addressed in Sec. VII. Conclusions and possible future research directions are offered in Sec. VIII. In Appendix A, we compare the droplet density profiles extracted from the many-body method, the complete system of eGPEs, and the effective model. For completeness, the predictions of the effective model and the eGPE approaches in the absence of an external trap are exemplarily compared in Appendix B.

II. PARTICLE-IMBALANCED BOSONIC MIXTURE

We employ a highly particle-imbalanced bosonic mixture containing $N_A < N_B$ atoms of mass m_σ ($\sigma = A, B$) and being confined in a weak 1D harmonic trap. Such a setting can be readily prepared via the technique of radio-frequency spectroscopy utilizing a two-photon Raman transition, where a portion of the atoms initial prepared in a single hyperfine state (e.g., $|F = 1, m_F = -1\rangle$ of ^{39}K) is transferred to another hyperfine state (e.g., $|F = 1, m_F = 0\rangle$ of ^{39}K). Consequently, the percentage of atoms in each state can be controlled through the amplitude and Rabi frequency of the applied pulse [28,29,45,59]. The mixture is at cold temperatures where *s*-wave scattering is the predominant scattering process [60] and thus interactions are modeled by contact potentials. The interparticle interactions are characterized by effective repulsive intra- ($g_A > 0$, $g_B > 0$) and attractive intercomponent ($g_{AB} < 0$) coupling strengths. These coefficients can be experimentally tuned through Feshbach resonances [61,62] via an external homogeneous magnetic field or confinement induced resonances [60] by means of manipulating the transversal trapping frequency.

The resulting many-body Hamiltonian has the form

$$H = \sum_{\sigma=A,B}\sum_{i=1}^{N_\sigma}\left[-\frac{\hbar^2}{2m_\sigma}\left(\frac{\partial^2}{\partial x_i^{\sigma\,2}}\right) + \frac{1}{2}m\omega^2\left(x_i^\sigma\right)^2\right] + \sum_{\sigma=A,B} g_\sigma \sum_{i<j}^{N_\sigma}\delta\left(x_i^\sigma - x_j^\sigma\right) + g_{AB}\sum_{i=1}^{N_A}\sum_{j=1}^{N_B}\delta\left(x_i^A - x_j^B\right). \tag{1}$$

In order to ensure the 1D nature of the ensuing dynamics we consider a fixed and adequately large aspect ratio between the longitudinal (ω_x) and the transverse ($\omega_\perp$) trapping frequencies. Specifically, $\omega = \omega_x/\omega_\perp = 0.01$ which is typical in 1D experiments [63,64]. Moreover, the chemical potential (μ) of the total system should be smaller than the transverse trap energy-level spacing, i.e., $\mu < \hbar\omega_\perp$. The above conditions prevent excitations along the transverse directions [63,65]. Finally, for computational convenience we rescale the above Hamiltonian with respect to $\hbar\omega_\perp$. Hence, the length, time, and interaction strengths are given in units of $a_\perp = \sqrt{\hbar/(m\omega_\perp)}$, $1/\omega_\perp$, and $\sqrt{\hbar^3\omega_\perp/m}$ respectively.

III. MANY-BODY DESCRIPTION

A. Extended Gross-Pitaevskii equations

Two-component, homonuclear ($m_A = m_B \equiv m$), 1D quantum droplets in the presence of the first-order quantum correction (LHY contribution) are described, in the weakly interacting regime, by the following coupled eGPEs [53,66]:

$$i\hbar\frac{\partial\Psi_A(x,t)}{\partial t} = \Bigg[-\frac{\hbar^2}{2m}\frac{\partial^2}{\partial x^2} + G_A|\Psi_A|^2 - (1-G)g|\Psi_B|^2 + V(x) - \frac{g_A\sqrt{m}}{\pi\hbar}\sqrt{g_A|\Psi_A|^2 + g_B|\Psi_B|^2}\Bigg]\Psi_A(x,t), \tag{2a}$$

$$i\hbar\frac{\partial\Psi_B(x,t)}{\partial t} = \Bigg[-\frac{\hbar^2}{2m}\frac{\partial^2}{\partial x^2} + G_B|\Psi_B|^2 - (1-G)g|\Psi_A|^2 + V(x) - \frac{g_B\sqrt{m}}{\pi\hbar}\sqrt{g_A|\Psi_A|^2 + g_B|\Psi_B|^2}\Bigg]\Psi_B(x,t). \tag{2b}$$

In these expressions, $G_A = g_A + Gg_B$, $G_B = g_B + Gg_A$, and $G = 2g\delta g/(g_A + g_B)^2$. The average mean-field repulsion is $g = \sqrt{g_A g_B}$, and the distance from the mean-field balance point is given by $\delta g = g + g_{\rm AB}$. Also, $V(x)$ represents the external trapping potential which we consider herein to be a harmonic trap as in the many-body Hamiltonian of Eq. (1). For our simulations, we use the normalization condition $\int |\Psi_\sigma|^2 dx = N_\sigma$, where $\Psi_\sigma(x,t)$ represents the 1D wave function of the $\sigma = A, B$ component and $n_\sigma = |\Psi_\sigma|^2$ is the respective density normalized to the atom number. Notice that for a balanced mixture, i.e., $|\Psi_A|^2\sqrt{g_B} = |\Psi_B|^2\sqrt{g_A}$, it is known that the two-component system is reduced to an effective single-component one [53], where both components behave identically. In this case, a transition of the droplet density from a Gaussian to a FT configuration takes place for either increasing particle number ($N = N_A + N_B$) or decreasing intercomponent attraction ($|g_{\rm AB}|$) with $0 < -g_{\rm AB} < g$ [53]. Interestingly, due to the droplet incompressibility, the emergent FT structures exhibit a saturation peak density at $n_0 = 8g/(9\pi^2\delta g^2)$ [53]. However, it is not *a priori* expected that these droplet properties are retained in the particle-imbalanced two-component setting. This is one of the questions that we address below.

It is also important at this point to explicate the validity of the eGPEs (2). This framework in principle holds for macroscopic systems, in free space and close to the mean-field balance point $\delta g \approx 0$ [53]. However, several works relying on nonperturbative methods have demonstrated that the eGPEs can provide accurate predictions, at least on the qualitative level, even for mesoscopic systems and for nonvanishing δg [46,67,68] but also in the presence of a shallow ($\omega_x \ll \omega_\perp$) external trap [47]. Therefore, the eGPE framework has been shown to provide an accurate phenomenological description of quantum droplets, even for certain systems which it is not designed for. Throughout this paper we study the crossover from particle-balanced droplet configurations to strong intercomponent imbalance where the minority component tends to the impurity limit. As such, we explore parametric regimes lying far outside the expected validity region of the eGPEs framework. We showcase, however, by comparing with *ab initio* calculations, that the eGPEs provide surprisingly valuable insights on the rich phenomenology exhibited close to the impurity limit ($N_A \ll N_B$).

B. Many-body variational approach

As discussed above, in order to judge the parametric regions of validity of the eGPEs for mesoscopic mixtures but also identify the impact of beyond LHY correlations on the formation of particle-imbalanced droplets we independently rely on the *ab initio* ML-MCTDHX method [54–56]. Within this approach the full many-body wave function is expressed in a multilayer structure. The latter utilizes a variationally optimized time-dependent basis set in order to numerically solve the corresponding many-body Schrödinger equation [57,58]. Accordingly, the relevant Hilbert space is spanned efficiently and interparticle correlations are captured.

The intercomponent correlations (entanglement) of the bosonic mixture are taken into account through a truncated Schmidt decomposition [69]. This way, D different orthonormal species functions, $|\Psi_k^\sigma(t)\rangle$, are used for each component $\sigma = A, B$ and the many-body wave function reads

$$|\Psi(t)\rangle = \sum_{k=1}^{D} \sqrt{\lambda_k(t)}\,\big|\Psi_k^A(t)\big\rangle\big|\Psi_k^B(t)\big\rangle. \tag{3}$$

Here, the eigenvalues of the species reduced density matrix [56,70] are the time-dependent Schmidt weights $\sqrt{\lambda_k(t)}$ which determine the degree of intercomponent correlations. Namely, if at least two distinct λ_k's are finite the many-body wave function is in a superposition and the system may be considered entangled [57,69]. However, in the case of $\lambda_1(t) = 1$ and $\lambda_{k>1}(t) = 0$, the many-body ansatz is simply a product (nonentangled) state.

As a next step, intracomponent correlations are included by expanding each species function in terms of a linear superposition of time-dependent number states $|\mathbf{n}_\mathbf{k}^\sigma\rangle$:

$$\big|\Psi_k^\sigma(t)\big\rangle = \sum_{\mathbf{n}_\mathbf{k}^\sigma|N_k} A_{n_k}^\sigma(t)\,\big|\mathbf{n}_k^\sigma\big\rangle, \tag{4}$$

with time-dependent expansion coefficients $A_{n_k}^\sigma(t)$. These number states $|\mathbf{n}_k^\sigma\rangle$ correspond to the full set of permanents constructed by d_σ time-dependent variationally optimized single-particle functions $|\Phi_i^\sigma\rangle$ with occupation numbers $\mathbf{n} = (n_1, \ldots, n_{d_\sigma})$. In turn, the d_σ time-dependent single-particle functions evolve in the single-particle Hilbert space spanned by the time-independent (primitive) basis $\{|r_j^k\rangle\}_{j=1}^{\mathcal{M}}$. In this paper, the latter refers to a $\mathcal{M}$-dimensional discrete variable representation with $\mathcal{M} = 1000$ grid points. Finally, the resulting equations of motion for the coefficients of the ML-MCTDHX wave-function ansatz describing the many-body Hamiltonian of Eq. (1) are found, for instance, by using the Dirac-Frenkel variational principle [56,71], $\langle\delta\Psi|(i\hbar\partial_t - \hat{H})|\Psi\rangle = 0$.

Concluding, we note in passing that the ML-MCTDHX wave-function ansatz easily reduces to the usual mean-field one that neglects all correlations [72], $|\Psi_{\rm MF}(t)\rangle = \prod_{i=1}^{N_A}|\Phi_i^A(t)\rangle\prod_{i=1}^{N_B}|\Phi_i^B(t)\rangle$, by using $D = d_A = d_B = 1$. Then the variational principle recovers the well-known coupled set of Gross-Pitaevskii equations for the bosonic mixture [65,72]. However, the eGPEs (2) take into account correlations in a perturbative manner and thus do not follow directly from the ML-MCTDHX ansatz. The latter incorporates beyond LHY correlations and therefore allows one to determine whether the eGPE description is sufficient to capture the participating correlation effects, to a good approximation, or if higher-order ones become significant.

IV. EFFECTIVE DESCRIPTION IN THE LARGE PARTICLE IMBALANCE LIMIT

We consider a two-component mixture in free space [$V(x) = 0$], with attractive intercomponent interactions, featuring extreme particle imbalance between the two macroscopically occupied components, i.e., $N_B \gg N_A \gg 1$. In this case, we may keep in the eGPE description [Eq. (2)] only terms scaling at least as $\sqrt{N_B}$ ($\sqrt{N_A}$) in the majority (minority) component equation but ignore contributions $O(N_A/N_B)$ and $O(N_A)$, respectively (see also the discussion below). Then,

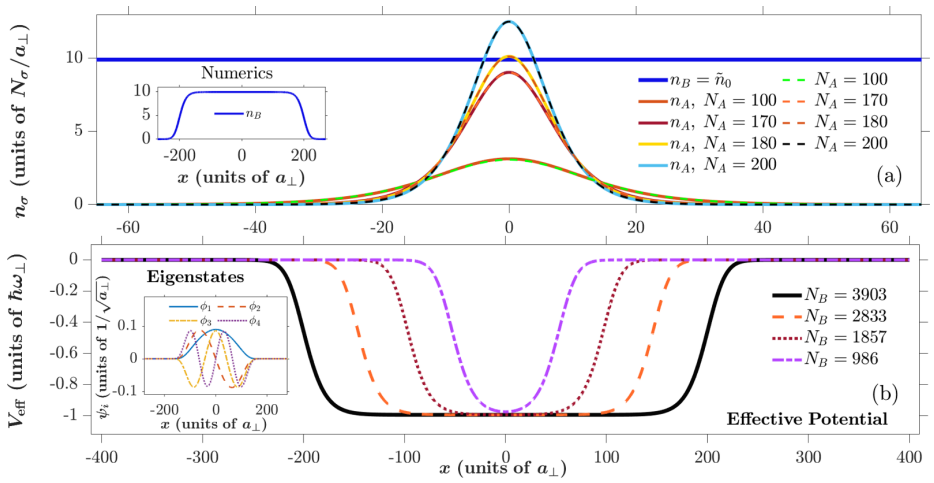

FIG. 1. (a) Density profiles for fixed $N_B = 3903$, $g_B = 0.05$, $g_A = 0.049$, and $g_{AB} = -0.149$ obtained from the analytical (8) and the numerical solutions of the reduced eGPEs (5) for various particle numbers in the minority component (see legend). The minority component densities among the two approaches are in near perfect agreement. The inset of panel (a) depicts the droplet density of the majority component as predicted by Eq. (7). Upon increasing the particle number of the minority component N_A, its density maximum becomes comparable to the droplet saturation density, in spite of the large particle difference, for all values of N_B which result in a FT configuration (see main text). (b) The effective potential experienced by the minority component for different N_B. The inset of panel (b) illustrates the first four eigenstates of the effective potential of Eq. (6) for $N_B = 3903$ (see legend).

assuming $\sqrt{N_B} \gg N_A$, the genuine two-component system of eGPEs (2a) and (2b) reduces to

$$i\hbar\frac{\partial\Psi_A}{\partial t} = \left[-\frac{\hbar^2}{2m}\frac{\partial^2}{\partial x^2} + V_{\rm eff}(|\Psi_B|) + G_A|\Psi_A|^2\right]\Psi_A, \tag{5a}$$

$$i\hbar\frac{\partial\Psi_B}{\partial t} = \left[-\frac{\hbar^2}{2m}\frac{\partial^2}{\partial x^2} + G_B|\Psi_B|^2 - \frac{g_B\sqrt{mg_B}}{\pi\hbar}|\Psi_B|\right]\Psi_B. \tag{5b}$$

Apparently, in this limit, the minority component experiences an effective potential created by the majority species of the form

$$V_{\rm eff}(|\Psi_B|) = -(1-G)g|\Psi_B|^2 - \frac{g_A\sqrt{mg_B}}{\pi\hbar}|\Psi_B|. \tag{6}$$

It turns out that the majority component decouples from the minority and obeys a reduced single-component eGPE [53]. The latter contains modified effective nonlinear interaction parameters determined by the presence of the minority component, i.e., $\tilde{\delta}g = G_B$ and $\tilde{g} = g_B/2^{1/3}$. This indicates that the presence of the minority component induces a global effect on the majority one, i.e., extending beyond their overlap region. In this sense, the creation and structural configurations of dropletlike states in the majority component depend strongly on the characteristics of the minority one. According to the above, it is possible to control the saturation density and hence the overall behavior of the majority species, via tuning the interaction strengths associated with the minority component (g_A, g_{AB}), and therefore also G_B.

The majority component equation (5b) has the well-known 1D droplet solution [53,66] (setting $\hbar = m = 1$)

$$\Psi_B(x,t) = \frac{\sqrt{\tilde{n}_0}(\tilde{\mu}/\tilde{\mu}_0)e^{-i\tilde{\mu}t}}{1+\sqrt{1-\tilde{\mu}/\tilde{\mu}_0}\cosh\sqrt{-2m\tilde{\mu}}x}, \tag{7}$$

where $\tilde{\mu}_0 = -\tilde{\delta}g\tilde{n}_0/2$ represents the minimum value of the chemical potential $\tilde{\mu}$ above which droplet solutions exist [44,53]. For sufficiently large particle number, Eq. (7) predicts a self-bound droplet with FT density profile at the droplet saturation density $\tilde{n}_0 = 8\tilde{g}^3/(9\pi^2\tilde{\delta}g^2)$. The latter uniform solution ($\Psi_B = \tilde{n}_0$) is shown in Fig. 1(a) with the thick blue line, while the finite FT droplet configuration as captured by Eq. (7) is depicted in the inset of Fig. 1(a). Using the droplet solution of Eq. (7) we provide characteristic examples of the effective potential, $V_{\rm eff}(|\Psi_B|)$, experienced by the minority component for various atom numbers (N_B) in the majority component [see Fig. 1(b)]. For completeness, we remark that the exact particle number of the majority component—$N_B = 2\sqrt{\tilde{n}_0/\tilde{\delta}g}[\ln(1+\sqrt{\tilde{\mu}/\tilde{\mu}_0})/\sqrt{1-\tilde{\mu}/\tilde{\mu}_0} - \sqrt{\tilde{\mu}/\tilde{\mu}_0}]$—which is obtained by fixing the chemical potential $\tilde{\mu}$ [53], does not significantly affect the qualitative behavior of the minority subsystem illustrated in Fig. 1, as long as we remain in the FT regime.

As expected, $V_{\rm eff}(|\Psi_B|)$ exhibits an inverse droplet profile being reminiscent of a square well with a pronounced flat potential minimum at large majority atom numbers, N_B, and transits towards a bell shaped inverted profile for decreasing N_B. The first four eigenstates of $V_{\rm eff}(|\Psi_B|)$, obtained numerically via diagonalization, when the droplet solution is deep in the FT regime ($N_B = 3903$) are provided in the inset of Fig. 1(b). Evidently, they are reminiscent of the eigenstates of a square well, featuring sinusoidal profiles, with a hierarchy in terms of their nodes for higher-lying ones, inside the FT region and rapidly decaying at the tails of the droplet. Importantly, as we explicate below, the spatial localization of the minority component does not mainly originate from the presence of this effective potential. It is primarily a result of the induced self-attraction of the minority atoms

mediated by the majority component [see in particular the $\sim G_A$ nonlinear term in the effective Eq. (5a)]. As such, the spatial width of the minority component (Ψ_A) is significantly smaller than the characteristic length scale of the effective potential [$V_{\rm eff}(|\Psi_B|)$]. Interestingly, the aforementioned induced self-attraction is inherently related to the presence of the LHY contribution and it would be otherwise absent.

Since we consider $N_B \gg N_A \gg 1$, i.e., operate close to the thermodynamic limit, it is natural to assume that the majority component is deep in the FT regime. Accordingly, its density profile acquires the constant saturation value $|\Psi_B(x)|^2 \approx \tilde{n}_0$ away from the edges of the atomic cloud, and hence also in the comparatively much smaller spatial overlap region with the minority component. The latter then may be well approximated by a bright soliton solution of the form $\Psi_A(x) \approx A\mathrm{sech}(\lambda x)e^{-i\mu_A t}$ where μ_A is the chemical potential of the minority species. By substituting this solution into Eq. (5a) and assuming a uniform density distribution for the majority component, i.e., $|\Psi_B(x)|^2 \approx \tilde{n}_0$, we find

$$\lambda^2 = -2m\left[(1-G)g\tilde{n}_0 + \frac{g_A\sqrt{mg_B}}{\pi}\sqrt{\tilde{n}_0} + \mu_A\right],$$
$$|A|^2 = \frac{-\lambda^2}{m(g_A + Gg_B)}. \tag{8}$$

Notice that even the constant [when assuming $|\Psi_B(x)|^2 \approx \tilde{n}_0$] energy shift provided by the effective potential of Eq. (6) plays an important role in determining the soliton solution. This solution, $\Psi_A(x)$, determined through Eq. (8) predicts that the minority component becomes gradually more localized in space and features an increased amplitude for larger N_A and fixed interaction coefficients as shown by the solid lines in Fig. 1(a). Hence, in spite of the pronounced intercomponent particle imbalance, there is a critical minority atom number at which $|A|^2 \approx \tilde{n}_0$. In this limit, the assumption of decoupled components ceases to be valid [see, e.g., the light-blue or yellow lines depicted in Fig. 1(a)]. Namely, using the normalization condition $\int |\Psi_A|^2 dx = N_A$ together with Eq. (8) we find the critical chemical potential $\mu_A^{\rm crit} = V_{\rm eff}(\sqrt{\tilde{n}_0}) + G_A\tilde{n}_0/2$ and critical number of particles in the minority component $N_A^{\rm crit} = \sqrt{-\frac{4\tilde{n}_0}{G_A m}}$, e.g., $N_A^{\rm crit} \approx 174$ for the parameter values used in Fig. 1. Note also that $N_A^{\rm crit}$ is independent of N_B. Beyond this point (i.e., for $N_A > N_A^{\rm crit}$) the majority component is expected to exhibit density modulations, on top of the FT, which are located at the overlap region with the minority component. To confirm the validity of the analytical soliton solution for the minority component in the case of a highly particle-imbalanced system we provide the ground-state densities of the minority species [Eq. (8); see dashed lines of Fig. 1(a)], obtained from the simulation of the reduced single-component Eq. (5a) assuming the FT solution of Eq. (7) for the majority component [see inset of Fig. 1(a)]. A comparison of the wave forms depicted in Fig. 1(a) reveals an almost perfect agreement between the two approaches (see also Appendices A and B for comparisons of the effective model with the full set of eGPEs).

To shed light on these density undulations of the majority component, we deploy the next-order correction to the one used for obtaining the reduced Eqs. (5a) and (5b). It stems from the nonvanishing intercomponent particle number ratio $N_A/N_B \neq 0$. This next-order correction, scaling as $N_A/\sqrt{N_B}$, originates from the LHY term and it is given by $-g_{A[B]}\frac{g_A|\Psi_A|^2}{2\sqrt{g_B|\Psi_B|}}\Psi_{A[B]}$ for each component respectively. Evidently, this term manifests a direct coupling among the components and it is responsible for the aforementioned density modulations on the FT profile of the majority component. These modulations are predominantly enhanced for increasing either N_A or g_A. The same holds for larger g_B or smaller N_B but in a "slower" manner since the underlying scaling is of square-root type.

For completeness, we note that the next higher-order correction term (scaling as N_A) to the majority species Eq. (5b) stems from the direct coupling to the minority component, i.e., $-(1-G)g|\Psi_A|^2\Psi_B$, and it apparently also directly depends on g_A and N_A. This term also depends on the interspecies interaction g_{AB}, and increasing g_{AB} for fixed g_A indeed results in enhanced modulations of the density of the majority component. However, as we shall explicate below, the impact of g_{AB} appears to be less prominent as compared to the effect following an increase of g_A. Hence, g_A is the most important interaction parameter for probing deviations with respect to the intercomponent decoupled limit characterized by Eqs. (5a) and (5b). Finally, it should be emphasized that the effective description of Eqs. (5a) and (5b) should not be considered as an exact quantitative model especially so for finite systems and far from the overlap region between the components. It is, however, a rather qualitative model in the thermodynamic limit, predicting that the majority species can maintain its finite droplet character while highlighting the main sources of deviations from a FT droplet profile through the higher-order perturbative corrections. The usefulness of this model is further exposed below, where we explore imbalanced droplet configurations with the *ab initio* many-body ML-MCTDHX method in the presence of a weak harmonic trap. It is showcased that the insights of the effective model aid in the interpretation of the obtained many-body configurations.

V. MANY-BODY GROUND STATE

Naturally, the striking two-component droplet behavior predicted within the effective eGPE framework [Eqs. (5a) and (5b)] needs to be verified by explicit many-body calculations especially so away from the thermodynamic limit. Moreover, it is worth mentioning that we operate in a regime, where the condition $n_A/n_B \approx \sqrt{g_B/g_A}$ is violated, and thus it lays outside the commonly considered parameter region of symmetric droplets [48–51].

For this reason, we employ the *ab initio* ML-MCTDHX method [46,47,56] which allows one to quantify the many-body properties of the system; see also Appendix A for a comparison with the full eGPE [Eq. (2)] predictions. To render this setup numerically tractable with an *ab initio* method, we constrain the size of the majority component to mesoscopic [here $N_B = 40$ presented in Fig. 2 and $N_B = 20$ (not shown for brevity)]. Also, a weak harmonic trap, which is an experimentally common situation [63], characterized by $\omega = 0.01$ is applied. Both of these restrictions result in droplet configurations having comparatively smaller FT density

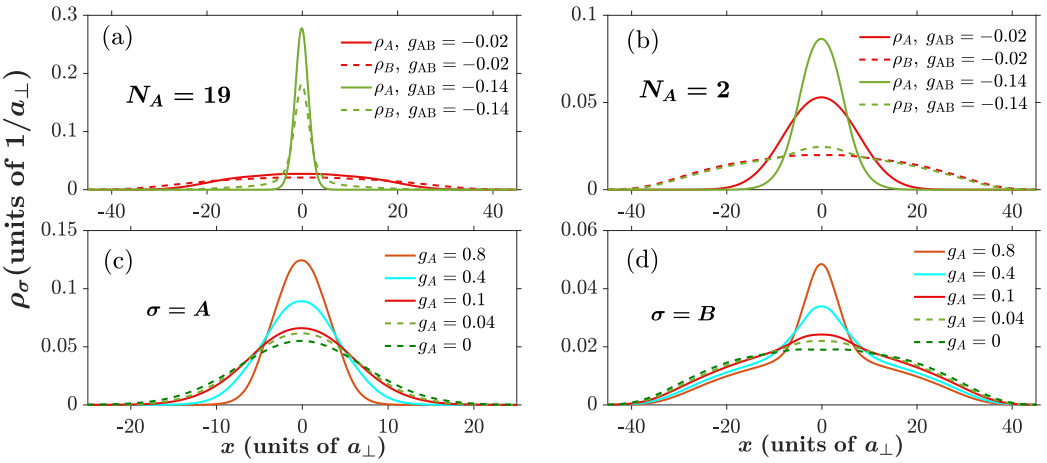

FIG. 2. Density profiles of the two-component bosonic droplet many-body ground-state configurations for different intercomponent attractions g_{AB} (see legends) and (a) $N_A = 19$ or (b) $N_A = 2$. (c), (d) Ground-state densities of the (c) minority and (d) majority component for $N_A = 4$ and $\delta g = 0.01$, while tuning the intracomponent repulsion of the minority species g_A (see legends). For sufficiently small ratios N_A/N_B the majority component maintains its droplet configuration, while modulations upon the FT profile arise with increasing intercomponent attraction or intracomponent repulsion of the minority species. In all cases, the remaining system parameters $N_B = 40$ and $g_A = g_B = 0.1$ are kept fixed (unless stated otherwise), while a shallow harmonic trap, $\omega = 0.01$, is used.

signatures (from their free-space counterparts) located around the trap center as it was demonstrated, for instance, in Refs. [47,68]. However, as we shall explicate below, a close inspection of the corresponding density profiles $\rho_\sigma(x) = \langle\Psi|\hat{\Psi}^\dagger_\sigma(x)\hat{\Psi}_\sigma(x)|\Psi\rangle$ (normalized to unity), as well as the intracomponent two-body correlation functions (see Sec. VI), allows us to identify the dropletlike character (being either FT or Gaussian shaped) of the majority component in the resulting many-body configurations. Also, we remark that all configurations to be presented below possess an energy per particle that is below the first trapped state, i.e., $E_{\rm MB}/(N_A + N_B) < \hbar\omega/2$, thus further confirming the bound-state character of the ensuing many-body state.

First, we assume small particle imbalance, i.e., $N_B = 40$ and $N_A = 19$, and study the underlying ground-state configurations for different intercomponent attractions g_{AB} [see Fig. 2(a)]. It becomes evident that due to the increasing attraction the component densities deform from spatially extended FT droplet structures to highly localized, soliton-type, profiles [see, e.g., the green solid and dashed lines in Fig. 2(a)]. The aforementioned transition behavior is also known to occur in the case of particle-balanced mixtures and will eventually lead the system to collapse[1] for sufficiently strong intercomponent attraction [46,53,72]. Nevertheless, the densities of both components closely follow each other with the majority species showing presignatures of extended tails that become pronounced for larger particle number ratios as we showcase below. In three dimensions it has been recently shown [48–50] that in the case of moderate particle imbalance, such as the one portrayed in Fig. 2(a), the ground state of the system is characterized by either a bound imbalanced droplet or droplet-gas coexistence for varying particle number ratios. The existence of such ground-state configurations can be related to the well-known particle emission (or self-evaporation) mechanism of 3D droplets. This mechanism dictates that a fully bound droplet is not always the lowest-energy configuration of the attractive 3D mixture [2] and dynamically it can expedite the decay of droplet states [45]. This instability mechanism, however, is absent in one dimension [53,73] at least within the weakly interaction regime. Hence, we observe the majority component maintaining its droplet character for all particle imbalances and as we shall argue later on also in terms of their two-body correlation patterns (see Sec. VI).

In sharp contrast, we observe that upon further decreasing the atom number in the minority subsystem (e.g., $N_B = 40$, $N_A = 2$), the majority component largely retains its FT droplet configuration which is distorted only within the spatial overlap region of the components, as long as $g_{AB} \neq 0$ [see Fig. 2(b)]. On the other hand, the density of the minority component exhibits a soliton-type structure, exhibiting increased spatial localization for larger attractions. This behavior reaffirms the predictions of the reduced system of the eGPEs [Eqs. (5a) and (5b) in Sec. IV] indicating that sufficiently large particle imbalance, i.e., $N_B/N_A \gg 1$, prevents or at least delays the 1D collapse taking place for increasing attraction. This is a quite interesting mechanism that should be also testified in the quasi-1D system and it is thus a fruitful perspective for future investigations. Additionally, the majority component retains its FT droplet configuration (for large particle numbers $N_B \gg 1$), while the minority species develops a solitonic profile as dictated by Eq. (5).

As a next step, we focus on the above-discussed large particle-imbalanced system and explore its dependence on the minority species repulsion, g_A. Notice that previous

[1]By collapse in one dimension we refer here to the increasing spatial localization, until the width of the density in the elongated direction becomes comparable to the transverse length scale, $a_\perp$. In this latter regime the assumption of the 1D setting is invalidated [72].

works considering particle-imbalanced droplets mainly assumed $g_A = g_B$ [49–52]. Hence, the understanding of the interplay between different sources of intercomponent imbalance is far from complete. Here, we address the impact of interaction imbalance, while in Sec. VII we discuss the effect of intercomponent mass imbalance in particle-imbalanced droplets.

Recall that in Sec. IV we argued that the correction to the majority species equation, originating from the LHY term, is $-\sqrt{g_B}g_A\frac{|\Psi_A|^2}{2|\Psi_B|}\Psi_B$ and it enforces coupling among the components. This implies that the spatial undulations of the majority component in its overlap region with the minority one strongly depend on g_A. Figures 2(c) and 2(d) present the density configurations of both the minority and the majority components respectively for various g_A values. The minority component has a Gaussian density configuration [Fig. 2(c)] becoming gradually more localized and tending towards a solitonic structure for increasing repulsion [74,75]. Simultaneously, the majority component shows a modulated FT droplet structure for all values of g_A and features more prominent modulations in the vicinity of the minority species for larger g_A [Fig. 2(d)]. Surprisingly, this behavior for increasing g_A is in qualitative agreement with the predictions of the reduced eGPE model in the limit of large particle imbalance, despite the fact that the present setting lies outside the validity region of the eGPEs (5a) and (5b). Notice also that the density modulations of the majority component on top of its FT profile essentially vanish for $g_A = 0$. In particular, for $g_A = 0$ and $N_A = 4$ [see the dashed-green lines in Figs. 2(c) and 2(d)], the majority component features a clear FT density profile with no visible modulation even within the overlap region. This is in accordance with the decoupled scenario described by Eq. (5) and presented in Fig. 1(a). Moreover, we observe that tuning the intraspecies interaction strength g_A (for fixed δg) has a more significant impact on the density profile of the majority component, as compared to adjusting the interspecies attraction g_{AB} (for fixed g_A). This becomes evident by the relatively enhanced density modulations of the majority shown in Figs. 2(c) and 2(d) when contrasted to the ones in Fig. 2(b). It is also consistent with the conclusions of the effective model, since both the correction originating from the LHY term (i.e., $-\sqrt{g_B}g_A\frac{|\Psi_A|^2}{2|\Psi_B|}\Psi_B$) and the one stemming from the direct coupling to the minority species, i.e., $-(1-G)g|\Psi_A|^2\Psi_B$, explicitly depend on g_A. They also vanish for $g_A = 0$, while g_{AB} enters explicitly only on the latter. In particular, the prefactor of the latter, i.e., $-(1-G)g$, is reduced by a factor of 2 upon tuning the interspecies interaction strength from $g_{AB} = -0.02$ to -0.14 (for fixed g_A), while the former scales linearly with g_A.

It is worth noting here that the opposite limit of strong intra- and intercomponent interactions (such that δg is relatively small) and moderate particle imbalance was recently studied in Ref. [51] utilizing an optical lattice. Under these conditions, the system was found to feature imbalanced droplets at the overlap region between the two components, while excess particles remained in a gas or a super-Tonks-Girardeau gas phase [51]. Similarly, a droplet-gas coexistence was identified for a sufficiently strongly interacting mixture in a rotating ring geometry, within the LHY approximation [52]. This behavior in the overlap region appears to be already consistent with our effective model analysis. Apparently, for strong interactions the coupling terms discussed above dominate (instead of providing perturbative corrections as in the limit of weak interactions considered here). Hence, we expect the droplet or gas character of the mixture to be primarily characterized by the behavior at the overlap region between the two components [51,52]. However, we note that in this limit of strong interactions the perturbative LHY theory does not apply and droplet formation is interpreted in terms of the formation of dimers [67,76] and larger polymers [77–79]. As such, both the stationary and the excitation properties of weakly and strongly interacting droplets are expected to be different and are not directly comparable with each other. A systematic study focused on the crossover between the two regimes would be intriguing. However, this exploration would require elaborated many-body methods that can successfully operate in the crossover region. Such a task lies beyond the scope of the current paper.

VI. TWO-BODY DROPLET CONFIGURATIONS

To further probe the superposition nature of the two-component droplet many-body states we examine the intracomponent two-body coherence functions $C_{\sigma\sigma}(x_1, x_2) = \rho^{(2)}_{\sigma\sigma}(x_1, x_2)/[\rho_\sigma(x_1)\rho_\sigma(x_2)]$ [57,70]. They are defined in terms of the respective intracomponent two-body reduced densities:

$$\rho^{(2)}_{\sigma\sigma}(x_1, x_2) = \langle\Psi|\hat{\Psi}^\dagger_\sigma(x_1)\hat{\Psi}^\dagger_\sigma(x_2)\hat{\Psi}_\sigma(x_1)\hat{\Psi}_\sigma(x_2)|\Psi\rangle, \quad (9)$$

where $\hat{\Psi}_\sigma(x_i)$ [$\hat{\Psi}^\dagger_\sigma(x_i)$] refers to the bosonic field operator annihilating [creating] a σ-species atom at position x_i. $\rho^{(2)}_{\sigma\sigma'}(x_1, x_2)$ is the probability of simultaneously detecting a σ-species boson located at x_1 and another one at x_2 [80,81]. In this sense, two σ-species bosons show a bunching [antibunching] behavior if $C_{\sigma\sigma}(x_1, x_2; t) > 1$ [$C_{\sigma\sigma}(x_1, x_2; t) < 1$], and they are two-body uncorrelated for $C_{\sigma\sigma}(x_1, x_2; t) = 1$.

The two-body correlation function, in the case of large particle imbalance, i.e., $N_A/N_B = 1/20$, is provided in Fig. 3 both for the majority and the minority components at two different intercomponent attractions. These are chosen such that the majority component has a FT shape and the minority exhibits a Gaussian profile. For weak attractions ($g_{AB} = -0.02$) the components are almost decoupled, while for stronger ones ($g_{AB} = -0.142$) they are coupled and therefore the density of the majority is modulated within their overlap region. It can be seen that for increasing attraction the minority species features a transition from a two-body anticorrelated behavior (at the same position $x_1 = x_2$) indicative of quantum droplets [46,47,68] to a correlated pattern characteristic of solitonlike structures [82–85] [compare in particular the main diagonal in Figs. 3(a) and 3(c)]. This observation is further supported by the off-diagonal correlation behavior where for $g_{AB} = -0.02$ ($g_{AB} = -0.142$) two minority species atoms show an antibunching (bunching) tendency. This modified two-body correlation behavior is suggestive of a transition from a bright-droplet [44,86] to a bright-soliton [72,75] character for the minority component, as it is also indicated by Eq. (8) of our effective model. Elaborating further on the presence and properties of this transition is an intriguing prospect for future

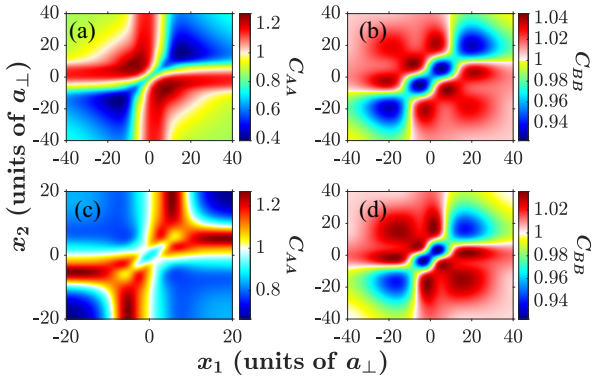

FIG. 3. Two-body coherence function of (a), (c) the minority component A and (b), (d) the majority component B for (a), (b) weak ($g_{AB} = -0.02$) and (c), (d) strong ($g_{AB} = -0.142$) attraction. The remaining parameters are $g_A = g_B = 0.1$, $N_A = 2$, and $N_B = 40$. The minority component exhibits a transition from dropletlike to solitonlike correlation patterns. Surprisingly, the majority component maintains its droplet character in all cases.

investigations. In contrast to the above, the majority component experiences an antibunching at the same location in both cases [see the diagonal in Figs. 3(b) and 3(d)], while two bosons placed symmetrically with respect to the FT are bunched. This correlation pattern further confirms our argument regarding the persistence of the underlying droplet character of these structures for large particle number ratios.

In contrast to the above behavior, for moderate particle number ratio, e.g., $N_A/N_B \approx 1/2$, both components undergo a progressive transition towards a localized solitonic structure characterized by a correlated behavior upon increasing attraction (not shown). This is in agreement with the expectation that for systems close to particle balance, sufficiently strong intercomponent attraction gradually favors the collapse of the system [53,65,72].

VII. IMBALANCED DROPLETS IN HETERONUCLEAR MIXTURES

Having described the peculiar ground-state droplet many-body configurations appearing in homonuclear particle-imbalanced bosonic mixtures we next move to the investigation of heteronuclear (either bosonic or Bose-Fermi) ones. Specifically, we consider the same bosonic majority component as above but minority atoms composed of either a different bosonic element or fermionic isotope. Admittedly, the experimental preparation of such settings is more involved compared to the homonuclear mixtures. However, heteronuclear settings, e.g., of ^{41}K, or ^{23}Na and ^{87}Rb isotopes have been experimentally realized [30,87] and importantly they offer the premise to unveil valuable insights on mechanisms that are absent in their single-component counterparts such as intercomponent mixing, rich many-body phases, and excitation processes [46,47]. Below, we solely rely on many-body ML-MCTDHX simulations since the eGPEs for heteronuclear 1D mixtures have not yet been constructed; rather they are known in three dimensions [30,41].

The case of $N_A = 2$ heavy bosons immersed in a majority species of light $N_B = 40$ bosons is presented in Figs. 4(a) and 4(b) for various mass ratios ($r_m = m_A/m_B = 1/2,\ 10$) and intercomponent attractions ($g_{AB} = -0.02,\ -0.14$). As expected, due to their larger mass, the minority atoms experience gradually enhanced spatial localization for increasing mass ratio m_A/m_B and fixed g_{AB} or larger attraction (g_{AB}) and constant m_A/m_B [see Fig. 4(a)]. As a consequence, the majority component shows progressively more pronounced spatial undulations in the vicinity of the minority species for either increasing mass ratio m_A/m_B or attraction g_{AB}. Accordingly, the width of the majority cloud slightly shrinks but it overall remains approximately the same. In that light we can deduce that light minority species atoms coupled to the majority component through weak attraction offer better candidates to access the decoupled regime [see Eqs. (5a) and (5b) in Sec. IV and Fig. 2(b)]. Recall, however, that in the presence of mass imbalance Eqs. (2a) and (2b) are not valid. Interestingly, the phenomenology obtained for the mass-balanced and intercomponent particle-imbalanced settings holds also for heteronuclear bosonic setups.

Next, we briefly address Bose-Fermi droplet settings where fermionic minority atoms, e.g., $N_A = 3$ and 5, are embedded within a majority species containing $N_B = 30$ bosons [see Figs. 4(c) and 4(d)]. Our analysis relies on the many-body ML-MCTDHX approach [72,88,89], in which the number states used for the expansion of the wave function given by Eq. (4) become Slater determinants of the d_σ time-dependent variationally optimized single-particle functions (see also Sec. III B). As can be readily seen from Figs. 4(c) and 4(d), the shape of the Bose-Fermi mixture is strikingly different compared to the Bose-Bose one. Namely, the fermionic component tends to be equally or more delocalized than the bosonic majority species which is attributed to the Pauli exclusion principle. Also, as expected, for increasing intercomponent attraction both components become more localized. The energy per particle of the mixture is above the lowest trap state. Clearly, the effective model presented in Sec. IV was derived for a weakly interacting bosonic mixture and thus it is not applicable for the Bose-Fermi setting.

It has been argued that, at least for 3D systems [38–40], a highly imbalanced Bose-Fermi mixture, with the bosonic component being the majority one, could accommodate droplet structures. In Ref. [39], for example, it was explicated that a mixture of potassium $^{41}\mathrm{K} - ^{40}\mathrm{K}$ with densities $n_B \approx 10 n_F$ (where $n_{B,[F]}$ is the bosonic [fermionic] density, normalized to the particle number in the respective component) and interaction strength ratio $|g_{BF}|/g_B \gtrapprox 0.25$ would result in a stable Bose-Fermi droplet in 3D free space. We study the possibility of Bose-Fermi droplet formation in one dimension. Our results indicate that the relevant parameter region for the realization of Bose-Fermi droplets is significantly shifted in the 1D case as compared to the 3D one [38–40]. This could provide an interesting pathway for realizing 1D quantum Bose-Fermi droplets, since their 3D counterparts require large attractions and bosonic densities but also suffer from significant three-body recombination rates [38–40]. The latter, being already suppressed in one dimension, could potentially be further reduced if, as hinted by our results, 1D Bose-Fermi droplets prove to form in a parameter region

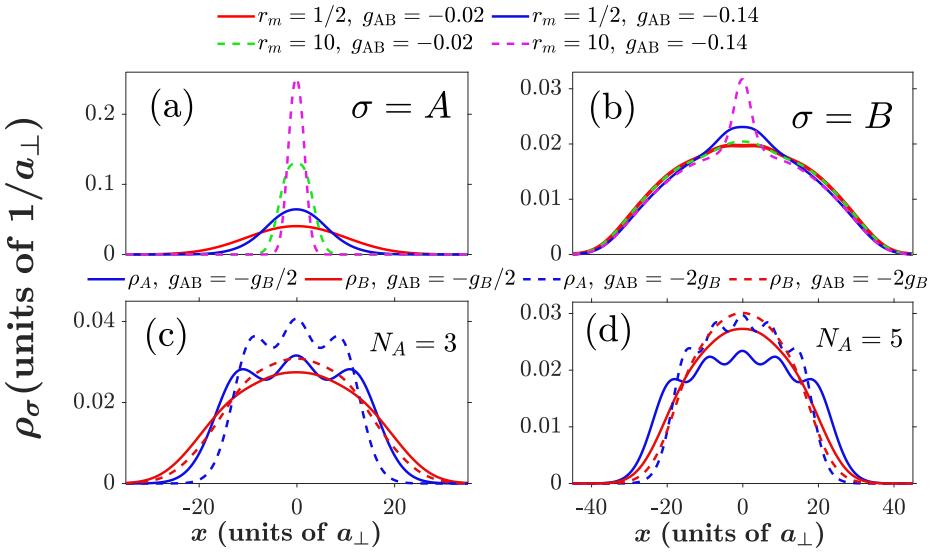

FIG. 4. Ground-state droplet densities in heteronuclear Bose-Bose and Bose-Fermi mixtures within the many-body approach. (a), (b) Profiles of (a) $N_A = 2$ bosons and (b) a majority species with $N_B = 40$ bosons for $g_A = g_B = 0.1$ and varying mass ratio $r_m = m_A/m_B$ and intercomponent attraction g_{AB} (see legend). (c), (d) Density configurations of (c) $N_A = 3$ and (d) $N_A = 5$ fermionic atoms within a majority species of $N_B = 40$ bosons featuring $g_B = 0.05$ for different intercomponent attractions g_{AB} (see legend). Evidently, heavier minority bosons act against the FT droplet profile of the majority component, whereas droplet formation is suppressed in the presence of fermionic minority atoms.

with lesser three-body losses. Such a systematic study of 1D Bose-Fermi droplets is beyond the scope of our current paper, however it would be intriguing to be pursued in the future.

We note in passing that in order to judge the degree of correlations in the Bose-Fermi mixture we have also inspected the underlying orbital populations (not shown). It turns out that there is an increasing occupation of higher-lying species functions for larger attractions, while the bosons mainly reside in the first orbital. This indicates an increase of the intercomponent entanglement, accompanied by minor intracomponent correlations for the bosonic species. Hence, we find the opposite microscopic behavior for the Bose-Fermi mixture as compared to the Bose-Bose one, where the dropletlike states are characterized by significant intracomponent (anti)correlations and relatively small intercomponent ones [46,47,67,68]. This is consistent with the absence of the signatures of the LHY phenomenology discussed above (see Sec. IV) on the densities of the Bose-Fermi mixture in Figs. 4(c) and 4(d), since the LHY theory primarily accounts for the impact of intracomponent correlations in the form of phonons [65,67,72,76].

VIII. SUMMARY AND PERSPECTIVES

We have studied the formation of two-component bosonic droplet configurations with contact (intra-) intercomponent (repulsion) attraction in the limit of large particle imbalance among the components. It is argued that the majority component can be arranged in a FT droplet shape exhibiting tunable in amplitude and spatial extent localized modulations in the vicinity of the minority atoms. These modulations become more pronounced for either increasing intercomponent attraction or intracomponent repulsion of the minority component as well as for larger mass of the latter. The intracomponent repulsion of the minority subsystem appears to have the stronger impact on the aforementioned undulations of the majority component. For instance, they vanish in the limit of noninteracting minority species. This qualitative behavior is analytically predicted via a reduction of the established eGPEs in the limit of large particle imbalance to a single-component effective model. It is further verified using many-body *ab initio* simulations within the ML-MCTDHX method.

This many-body method enabled us to also address droplet formation in heteronuclear mixtures, where the corresponding 1D eGPEs are not available. Specifically, for Bose-Bose settings it is found that heavier atoms in minority species enhance the localized undulations imprinted on the density of the majority species. Turning to Bose-Fermi systems we show that the FT signatures on the bosonic majority species vanish in the presence of fermions in the other component. This behavior supports the droplet suppression in Bose-Fermi mixtures.

Based on our results there is a multitude of future research directions that can be pursued. A straightforward extension is to study the dynamical response of the identified droplet structures utilizing, for instance, quenches across the different phases in order to analyze the emergent pattern formation [90]. Moreover, characterizing the droplet structures in the dimensional crossover and hence also exploring the parametric regions of validity of the 1D eGPE description is highly desirable for both experiment and theory within [91–93] and especially beyond the symmetric droplet settings. The

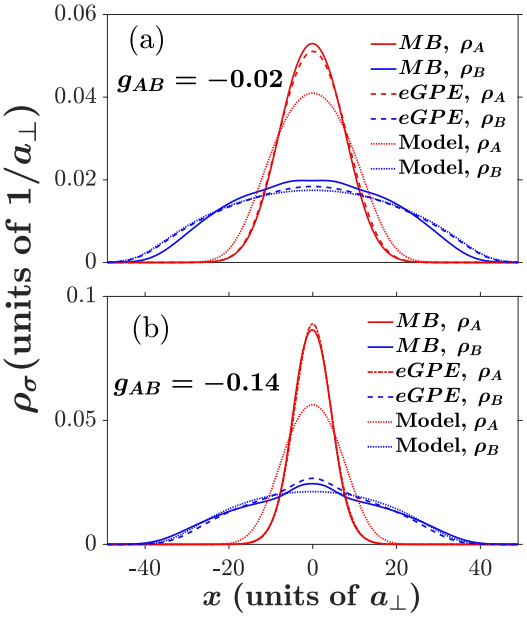

FIG. 5. Ground-state droplet density profiles in homonuclear Bose-Bose harmonically confined ($\omega = 0.01$) mixtures within the many-body (MB), the eGPE, and the effective model approaches (see legends). The mixture contains $N_A = 4$ and $N_B = 40$ bosons and features intercomponent attraction of strength (a) $g_{AB} = -0.02$ and (b) $g_{AB} = -0.14$. In all cases the intracomponent repulsion is fixed to $g_A = g_B = 0.1$. The eGPE and the effective model predictions are in qualitative agreement with the many-body results. Within the first two approaches a relatively smoother density profile occurs for the majority component but the FT behavior is absent. Also, the spatial undulations of the majority density at the overlap region with the minority component are absent within the effective model

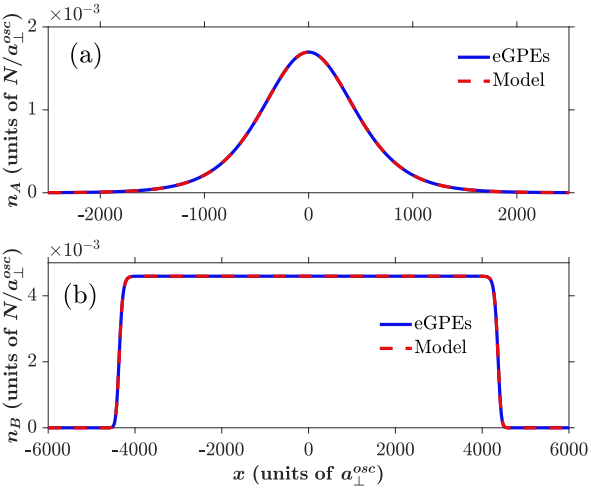

FIG. 6. Ground-state droplet density profiles of the (a) minority and (b) majority components within the eGPEs and the effective model approaches, in free space (see legends). The mixture is characterized by $N_A = 2$ and $N_B = 40$ bosons, while the intercomponent (intracomponent) attraction (repulsion) is $g_{AB} = -0.054$ ($g_A = 0.01$, $g_B = 0.1$). The predictions of the two methods are in near perfect agreement for the selected parameters lying in the validity region of the effective model.

stability analysis of the two-component droplet configurations as it was done for the symmetric setting [86] is another fruitful prospect, while considering spin-orbit coupling would introduce additional unstable modes [94]. The characterization of such phases for strong interactions lying essentially beyond the validity of the eGPE would require one to employ sophisticated many-body methods, such as the ML-MCTDHX used herein or exact diagonalization [95], for capturing the underlying excitation spectrum and impact of thermal effects.

ACKNOWLEDGMENTS

This work (P.S. and I.A.E.) has been funded by the Deutsche Forschungsgemeinschaft (SFB 925 Project No. 170620586. S.I.M. acknowledges support from the NSF through a grant for ITAMP at Harvard University.

APPENDIX A: COMPARISON BETWEEN THE MANY-BODY AND THE EGPE PREDICTIONS ON THE DENSITY PROFILES

It is instructive to provide some additional insights on the ability of the LHY theory to capture the highly imbalanced two-component states discussed in the main text. For this reason, we present a brief comparison on the single-particle density level obtained with the eGPEs, the effective model of Eqs. (5a) and (5b), and the *ab initio* ML-MCTDHX method.

Paradigmatic ground-state density profiles of the two component bosonic mixture with equal intraspecies repulsion ($g_A = g_B = 0.1$) and $N_B = 40$ ($N_A = 4$) bosons in the majority (minority) component are illustrated in Fig. 5 for different interspecies attractions. The ground states are obtained numerically through the imaginary-time propagation method applied either to the full system eGPEs [Eqs. (2a) and (2b)] or reduced eGPEs [Eqs. (5a) and (5b)] and the many-body ML-MCTDHX approach (see also Sec. III B). The chosen parameter values are such that a variation of the interspecies attraction from weak [Fig. 5(a)] to stronger values [Fig. 5(b)] takes place in the case of $N_A = 4$ similarly to the results shown in the main text [see also Fig. 2(b)]. A careful comparison between the predictions of the many-body and the full set of eGPEs reveals an adequate qualitative agreement of the resulting one-body spatial configurations of each component. Specifically, within the eGPE framework a slightly less (more) localized density profile for the majority component is obtained in the case of weak (stronger) attraction, as can be readily seen from Fig. 5(a) [Fig. 5(b)]. Similarly, the effective model of the reduced eGPEs [Eqs. (5a) and (5b)] leads to significantly (slightly) less localized structures for the minority (majority) component when compared to the predictions of the other methods. Also, as expected, no modulations of the majority density profile appear in the intercomponent overlap region, since the two components are assumed to be decoupled in the context of the effective model.

Furthermore, it is apparent that the density structures within the full system of eGPEs and the effective model are

consistently smoother when compared to the corresponding many-body outcome, while the FT signatures present in the first two approaches are absent. This behavior is consistent with earlier predictions focusing on the symmetric mixture or equivalently single droplet case [47,57,68] and attributing the emergent deviations to residual beyond-LHY correlations. Finally, it should be emphasized that despite the satisfactory agreement among the two approaches observed on the single-particle density level, the many-body method allows to calculate higher-order observables such as correlation functions which are inaccessible with the eGPEs. At the level of these observables larger deviations are naturally expected especially in the course of the evolution.

APPENDIX B: EFFECTIVE MODEL VS EGPE DENSITIES IN FREE SPACE

As mentioned in the main text, the effective model of Eqs. (5a) and (5b) is not expected to be in general quantitatively exact. Hence, it is primarily used for qualitative predictions and to assist with the interpretation of the results obtained via the *ab initio* ML-MCTDHX method. However, there exist certain cases where the predictions of the effective model are in fairly good agreement with those of the full set of eGPEs [Eqs. (2a) and (2b)].

One such case is depicted in Fig. 6 for a bosonic mixture with $N_A = 2$ and $N_B = 40$ short-range interacting bosons featuring effective coupling strengths $g_{AB} = -0.054$, $g_A = 0.01$, and $g_B = 0.1$. The two methods are in near perfect qualitative agreement for the selected parameters, which are taken such that the validity assumptions of the effective model are ensured. Namely, we have chosen $N_A \ll \sqrt{N_B}$ and $g_A \ll g_B$ (see the discussion in Sec. IV). This condition enforces the minority density component to be significantly more localized than the one of the majority component. This is indeed the case as also predicted by the numerical simulations of the eGPEs presented in Figs. 6(a) and 6(b); see in particular the different scales along the x axis. For completeness, we mention that the full set of eGPEs [Eqs. (2a) and (2b)] was solved numerically via imaginary-time propagation, using the fourth-order Runge-Kutta method and employing the solutions of the effective model [Eqs. (5a) and (5b)] as an initial ansatz. Naturally, when the above conditions are not fulfilled and hence the effective model is not *a priori* valid, significant deviations between the two approaches occur (not shown for brevity).

[1] I. Bloch, J. Dalibard, and S. Nascimbène, Nat. Phys. **8**, 267 (2012).
[2] D. S. Petrov, Phys. Rev. Lett. **115**, 155302 (2015).
[3] I. Ferrier-Barbut, H. Kadau, M. Schmitt, M. Wenzel, and T. Pfau, Phys. Rev. Lett. **116**, 215301 (2016).
[4] F. Böttcher, J.-N. Schmidt, J. Hertkorn, K. S. H. Ng, S. D. Graham, M. Guo, T. Langen, and T. Pfau, Rep. Prog. Phys. **84**, 012403 (2021).
[5] Z.-H. Luo, W. Pang, B. Liu, Y.-Y. Li, and B. A. Malomed, Front. Phys. **16**, 32201 (2021).
[6] B. A. Malomed, Front. Phys. **16**, 22504 (2021).
[7] P. Massignan, M. Zaccanti, and G. M. Bruun, Rep. Prog. Phys. **77**, 034401 (2014).
[8] R. Schmidt, M. Knap, D. A. Ivanov, J.-S. You, M. Cetina, and E. Demler, Rep. Prog. Phys. **81**, 024401 (2018).
[9] T. Fukuhara, A. Kantian, M. Endres, M. Cheneau, P. Schauß, S. Hild, D. Bellem, U. Schollwöck, T. Giamarchi, C. Gross, I. Bloch, and S. Kuhr, Nat. Phys. **9**, 235 (2013).
[10] J. Catani, G. Barontini, G. Lamporesi, F. Rabatti, G. Thalhammer, F. Minardi, S. Stringari, and M. Inguscio, Phys. Rev. Lett. **103**, 140401 (2009).
[11] N. B. Jørgensen, L. Wacker, K. T. Skalmstang, M. M. Parish, J. Levinsen, R. S. Christensen, G. M. Bruun, and J. J. Arlt, Phys. Rev. Lett. **117**, 055302 (2016).
[12] M.-G. Hu, M. J. Van de Graaff, D. Kedar, J. P. Corson, E. A. Cornell, and D. S. Jin, Phys. Rev. Lett. **117**, 055301 (2016).
[13] Z. Z. Yan, Y. Ni, C. Robens, and M. W. Zwierlein, Science **368**, 190 (2020).
[14] C. Kohstall, M. Zaccanti, M. Jag, A. Trenkwalder, P. Massignan, G. M. Bruun, F. Schreck, and R. Grimm, Nature (London) **485**, 615 (2012).
[15] F. Scazza, G. Valtolina, P. Massignan, A. Recati, A. Amico, A. Burchianti, C. Fort, M. Inguscio, M. Zaccanti, and G. Roati, Phys. Rev. Lett. **118**, 083602 (2017).
[16] M. Koschorreck, D. Pertot, E. Vogt, B. Fröhlich, M. Feld, and M. Köhl, Nature (London) **485**, 619 (2012).
[17] F. Grusdt and E. Demler, in *Proceedings of the International School of Physics "E. Fermi", Course*, Vol. 191, edited by M. Inguscio, W. Ketterle, S. Stringari, and G. Roati (IOS Press, 2016), pp. 235–411.
[18] S. P. Rath and R. Schmidt, Phys. Rev. A **88**, 053632 (2013).
[19] M. Bruderer, A. Klein, S. R. Clark, and D. Jaksch, Phys. Rev. A **76**, 011605(R) (2007).
[20] A. S. Dehkharghani, A. G. Volosniev, and N. T. Zinner, Phys. Rev. Lett. **121**, 080405 (2018).
[21] L. A. Peña Ardila and S. Giorgini, Phys. Rev. A **92**, 033612 (2015).
[22] F. Grusdt, R. Schmidt, Y. E. Shchadilova, and E. Demler, Phys. Rev. A **96**, 013607 (2017).
[23] T. Ichmoukhamedov and J. Tempere, Phys. Rev. A **100**, 043605 (2019).
[24] A. G. Volosniev, H.-W. Hammer, and N. T. Zinner, Phys. Rev. A **92**, 023623 (2015).
[25] S. I. Mistakidis, G. C. Katsimiga, G. M. Koutentakis, T. Busch, and P. Schmelcher, Phys. Rev. Lett. **122**, 183001 (2019).
[26] S. I. Mistakidis, A. G. Volosniev, N. T. Zinner, and P. Schmelcher, Phys. Rev. A **100**, 013619 (2019).
[27] F. Grusdt, K. Seetharam, Y. Shchadilova, and E. Demler, Phys. Rev. A **97**, 033612 (2018).
[28] C. R. Cabrera, L. Tanzi, J. Sanz, B. Naylor, P. Thomas, P. Cheiney, and L. Tarruell, Science **359**, 301 (2018).

[29] P. Cheiney, C. R. Cabrera, J. Sanz, B. Naylor, L. Tanzi, and L. Tarruell, Phys. Rev. Lett. **120**, 135301 (2018).

[30] C. D'Errico, A. Burchianti, M. Prevedelli, L. Salasnich, F. Ancilotto, M. Modugno, F. Minardi, and C. Fort, Phys. Rev. Res. **1**, 033155 (2019).

[31] F. Böttcher, J.-N. Schmidt, M. Wenzel, J. Hertkorn, M. Guo, T. Langen, and T. Pfau, Phys. Rev. X **9**, 011051 (2019).

[32] L. Chomaz, I. Ferrier-Barbut, F. Ferlaino, B. Laburthe-Tolra, B. L. Lev, and T. Pfau, Rep. Prog. Phys. **86**, 026401 (2022).

[33] R. N. Bisset, L. A. Peña Ardila, and L. Santos, Phys. Rev. Lett. **126**, 025301 (2021).

[34] J. C. Smith, D. Baillie, and P. B. Blakie, Phys. Rev. Lett. **126**, 025302 (2021).

[35] T. D. Lee, K. Huang, and C. N. Yang, Phys. Rev. **106**, 1135 (1957).

[36] Y. Sekino and Y. Nishida, Phys. Rev. A **97**, 011602(R) (2018).

[37] I. Morera, B. Juliá-Díaz, and M. Valiente, Phys. Rev. Res. **4**, L042024 (2022).

[38] X. Cui, Phys. Rev. A **98**, 023630 (2018).

[39] D. Rakshit, T. Karpiuk, M. Brewczyk, and M. Gajda, SciPost Phys. **6**, 079 (2019).

[40] J.-B. Wang, J.-S. Pan, X. Cui, and W. Yi, Chin. Phys. Lett. **37**, 076701 (2020).

[41] F. Ancilotto, M. Barranco, M. Guilleumas, and M. Pi, Phys. Rev. A **98**, 053623 (2018).

[42] G. Ferioli, G. Semeghini, L. Masi, G. Giusti, G. Modugno, M. Inguscio, A. Gallemí, A. Recati, and M. Fattori, Phys. Rev. Lett. **122**, 090401 (2019).

[43] C. Fort and M. Modugno, Appl. Sci. **11**, 866 (2021).

[44] G. E. Astrakharchik and B. A. Malomed, Phys. Rev. A **98**, 013631 (2018).

[45] G. Semeghini, G. Ferioli, L. Masi, C. Mazzinghi, L. Wolswijk, F. Minardi, M. Modugno, G. Modugno, M. Inguscio, and M. Fattori, Phys. Rev. Lett. **120**, 235301 (2018).

[46] S. I. Mistakidis, T. Mithun, P. G. Kevrekidis, H. R. Sadeghpour, and P. Schmelcher, Phys. Rev. Res. **3**, 043128 (2021).

[47] I. A. Englezos, S. I. Mistakidis, and P. Schmelcher, Phys. Rev. A **107**, 023320 (2023).

[48] L. He, H. Li, W. Yi, and Z.-Q. Yu, Phys. Rev. Lett. **130**, 193001 (2023).

[49] T. A. Flynn, L. Parisi, T. P. Billam, and N. G. Parker, Phys. Rev. Res. **5**, 033167 (2023).

[50] T. A. Flynn, N. A. Keepfer, N. G. Parker, and T. P. Billam, Phys. Rev. Res. **6**, 013209 (2024).

[51] J. Vallès-Muns, I. Morera, G. E. Astrakharchik, and B. Juliá-Díaz, SciPost Phys. **16**, 074 (2024).

[52] M. N. Tengstrand and S. M. Reimann, Phys. Rev. A **105**, 033319 (2022).

[53] D. S. Petrov and G. E. Astrakharchik, Phys. Rev. Lett. **117**, 100401 (2016).

[54] S. Krönke, L. Cao, O. Vendrell, and P. Schmelcher, New J. Phys. **15**, 063018 (2013).

[55] L. Cao, S. Krönke, O. Vendrell, and P. Schmelcher, J. Chem. Phys. **139**, 134103 (2013).

[56] L. Cao, V. Bolsinger, S. I. Mistakidis, G. M. Koutentakis, S. Krönke, J. M. Schurer, and P. Schmelcher, J. Chem. Phys. **147**, 044106 (2017).

[57] S. I. Mistakidis, A. G. Volosniev, R. E. Barfknecht, T. Fogarty, T. Busch, A. Foerster, P. Schmelcher, and N. T. Zinner, Phys. Rep. **1042**, 1 (2023).

[58] A. U. J. Lode, C. Lévêque, L. B. Madsen, A. I. Streltsov, and O. E. Alon, Rev. Mod. Phys. **92**, 011001 (2020).

[59] B. Bakkali-Hassani, C. Maury, Y.-Q. Zou, E. Le Cerf, R. Saint-Jalm, P. C. M. Castilho, S. Nascimbene, J. Dalibard, and J. Beugnon, Phys. Rev. Lett. **127**, 023603 (2021).

[60] M. Olshanii, Phys. Rev. Lett. **81**, 938 (1998).

[61] C. Chin, R. Grimm, P. Julienne, and E. Tiesinga, Rev. Mod. Phys. **82**, 1225 (2010).

[62] T. Köhler, K. Góral, and P. S. Julienne, Rev. Mod. Phys. **78**, 1311 (2006).

[63] A. Görlitz, J. M. Vogels, A. E. Leanhardt, C. Raman, T. L. Gustavson, J. R. Abo-Shaeer, A. P. Chikkatur, S. Gupta, S. Inouye, T. Rosenband, and W. Ketterle, Phys. Rev. Lett. **87**, 130402 (2001).

[64] A. Romero-Ros, G. C. Katsimiga, S. I. Mistakidis, S. Mossman, G. Biondini, P. Schmelcher, P. Engels, and P. G. Kevrekidis, Phys. Rev. Lett. **132**, 033402 (2024).

[65] L. Pitaevskii and S. Stringari, *Bose-Einstein Condensation and Superfluidity* (Oxford University, New York, 2016).

[66] T. Mithun, A. Maluckov, K. Kasamatsu, B. A. Malomed, and A. Khare, Symmetry **12**, 174 (2020).

[67] L. Parisi, G. E. Astrakharchik, and S. Giorgini, Phys. Rev. Lett. **122**, 105302 (2019).

[68] L. Parisi and S. Giorgini, Phys. Rev. A **102**, 023318 (2020).

[69] R. Horodecki, P. Horodecki, M. Horodecki, and K. Horodecki, Rev. Mod. Phys. **81**, 865 (2009).

[70] S. I. Mistakidis, G. C. Katsimiga, P. G. Kevrekidis, and P. Schmelcher, New J. Phys. **20**, 043052 (2018).

[71] J. Frenkel, *Wave Mechanics: Elementary Theory* (Clarendon, Oxford, 1934).

[72] C. J. Pethick and H. Smith, *Bose-Einstein Condensation in Dilute Gases*, 2nd ed. (Cambridge University, New York, 2008).

[73] M. Tylutki, G. E. Astrakharchik, B. A. Malomed, and D. S. Petrov, Phys. Rev. A **101**, 051601(R) (2020).

[74] V. M. Pérez-García and J. B. Beitia, Phys. Rev. A **72**, 033620 (2005).

[75] F. K. Abdullaev and J. Garnier, Bright solitons in Bose-Einstein condensates: Theory, in *Emergent Nonlinear Phenomena in Bose-Einstein Condensates: Theory and Experiment*, edited by P. G. Kevrekidis, D. J. Frantzeskakis, and R. Carretero-González (Springer-Verlag, Berlin, 2008), pp. 25–43.

[76] H. Hu, J. Wang, and X.-J. Liu, Phys. Rev. A **102**, 043301 (2020).

[77] A. Bulgac, Phys. Rev. Lett. **89**, 050402 (2002).

[78] A. Pricoupenko and D. S. Petrov, Phys. Rev. A **97**, 063616 (2018).

[79] I. Morera, G. E. Astrakharchik, A. Polls, and B. Juliá-Díaz, Phys. Rev. Lett. **126**, 023001 (2021).

[80] K. Sakmann, A. I. Streltsov, O. E. Alon, and L. S. Cederbaum, Phys. Rev. A **78**, 023615 (2008).

[81] M. Naraschewski and R. J. Glauber, Phys. Rev. A **59**, 4595 (1999).

[82] R. V. Mishmash and L. D. Carr, Phys. Rev. Lett. **103**, 140403 (2009).

[83] S. Krönke and P. Schmelcher, Phys. Rev. A **91**, 053614 (2015).

[84] S. Krönke and P. Schmelcher, Phys. Rev. A **92**, 023631 (2015).

[85] G. C. Katsimiga, S. I. Mistakidis, G. M. Koutentakis, P. G. Kevrekidis, and P. Schmelcher, New J. Phys. **19**, 123012 (2017).

[86] G. C. Katsimiga, S. I. Mistakidis, G. N. Koutsokostas, D. J. Frantzeskakis, R. Carretero-González, and P. G. Kevrekidis, Phys. Rev. A **107**, 063308 (2023).
[87] Z. Guo, F. Jia, L. Li, Y. Ma, J. M. Hutson, X. Cui, and D. Wang, Phys. Rev. Res. **3**, 033247 (2021).
[88] S. I. Mistakidis, L. Hilbig, and P. Schmelcher, Phys. Rev. A **100**, 023620 (2019).
[89] T. Karpiuk, K. Brewczyk, S. Ospelkaus-Schwarzer, K. Bongs, M. Gajda, and K. Rzażewski, Phys. Rev. Lett. **93**, 100401 (2004).
[90] F. Ancilotto, M. Barranco, and M. Pi, Phys. Rev. A **107**, 063312 (2023).
[91] P. Zin, M. Pylak, T. Wasak, M. Gajda, and Z. Idziaszek, Phys. Rev. A **98**, 051603(R) (2018).
[92] T. Ilg, J. Kumlin, L. Santos, D. S. Petrov, and H. P. Büchler, Phys. Rev. A **98**, 051604(R) (2018).
[93] L. Lavoine and T. Bourdel, Phys. Rev. A **103**, 033312 (2021).
[94] S. Gangwar, R. Ravisankar, S. I. Mistakidis, P. Muruganandam, and P. K. Mishra, Phys. Rev. A **109**, 013321 (2024).
[95] L. Chergui, J. Bengtsson, J. Bjerlin, P. Stürmer, G. M. Kavoulakis, and S. M. Reimann, Phys. Rev. A **108**, 023313 (2023).

4.3 Multicomponent One-Dimensional Quantum Droplets Across The Mean-Field Stability Regime

SciPost Phys. 19, 133 (2025)

Multicomponent one-dimensional quantum droplets across the mean-field stability regime

I. A. Englezos[1⋆], P. Schmelcher[1,2] and S. I. Mistakidis[3]

1 Center for Optical Quantum Technologies, Department of Physics, University of Hamburg, Luruper Chaussee 149, 22761 Hamburg Germany
2 The Hamburg Centre for Ultrafast Imaging, University of Hamburg, Luruper Chaussee 149, 22761 Hamburg, Germany
3 Department of Physics and LAMOR, Missouri University of Science and Technology, Rolla, MO 65409, USA

⋆ ilias.englezos@uni-hamburg.de

Abstract

The Lee-Huang-Yang (LHY) energy correction at the edge of the mean-field stability regime is known to give rise to beyond mean-field structures in a wide variety of systems. In this work, we analytically derive the LHY energy for two-, three- and four-component one-dimensional bosonic short-range interacting mixtures across the mean-field stability regime. For varying intercomponent attraction in the two-component setting, quantitative deviations from the original LHY treatment emerge being imprinted in the droplet saturation density and width. On the other hand, for repulsive interactions an unseen early onset of phase-separation occurs for both homonuclear and heteronuclear mixtures. Closed LHY expressions for the fully-symmetric three- and four-component mixtures, as well as for mixtures comprised of two identical components coupled to a third independent component are provided and found to host a plethora of mixed droplet states. Our results are expected to inspire future investigations in multicomponent systems for unveiling exotic self-bound states of matter and unravel their nonequilibrium quantum dynamics.

Received 2025-03-18
Accepted 2025-10-21
Published 2025-11-24
doi:10.21468/SciPostPhys.19.5.133

Contents

SciPost SciPost Phys. 19, 133 (2025)

1 Introduction

Since the first experimental realization of the Bose-Einstein condensate [1–3], outstanding progress has been sealed in terms of realizing, monitoring and controlling multicomponent atomic gases [4–6]. This is largely owed to exploiting Feshbach resonances [7] and trapping techniques [8, 9] to manipulate the interatomic interaction strength or range and the external confinement landscape respectively. Starting from single-component bosonic gases, a multitude of correlated phases beyond the weakly interacting mean-field (MF) limit were observed, such as the (Super-) Tonks-Girardeau states for strong (attractions [10, 11]) repulsions [12–15]. Turning to bosonic mixtures arguably enriched correlated phases, already for weak interactions, occur due to the competition between the intra- and inter-species interactions. This has lead, for instance, to phase separation [16–18], when the interspecies repulsion surpasses the average intraspecies one, bubble phases at the immiscibility threshold [19], or the recently realized quantum droplets [20–23] when the interspecies attraction slightly overcomes the intraspecies repulsions.

The emergence of the self-bound liquid-type configurations known as quantum droplets in contact interacting three-dimensional (3D) bosonic mixtures [24, 25], as well as in dipolar gases [26, 27], is a manifestation of the impact of quantum fluctuations. These may be captured by the Lee-Huang-Yang (LHY) energy [20, 28], representing the first-order correction to the Bogoliubov MF theory, which arrests the expected collapse of the ensuing attractive system at the edge of the MF stability regime [5]. Several properties of these intriguing many-body bound states of matter have already been explored. These refer, exemplarily, to their spectrum [29, 30], collective excitations [20, 29, 31], collisions [31, 32] and coexistence with nonlinear soliton [33, 34] and vortex [35–38] states, within the context of the LHY theory [21, 22, 39], see also Refs. [40–43] for the exposition of beyond-LHY effects by deploying *ab-initio* methods. Experimentally, quantum droplets have been observed in 3D in both homonuclear [24, 25, 44] and heteronuclear [45–47] mixtures. One of the main challenges faced by these experimental efforts stems from the relatively short droplet lifetimes caused (primarily) by three-body recombination [48]. These lifetimes are increased in relevant 1D settings [49, 50] due to lower densities but also in heteronuclear mixtures [45].

A particularly interesting property is the dependence of the LHY term on the dimensionality [50–52], in contrast to MF interactions [6]. In 1D that we focus herein, the LHY term is attractive [53] instead of being repulsive as in 3D, significantly changing the droplet parametric region and its phenomenology. Concretely, the 1D geometry causes the droplet parametric

SciPost SciPost Phys. 19, 133 (2025)

regions to i) not feature collapse, ii) host stable bright-soliton solutions [54–56] and iii) coincide with the respective MF stability regimes. Hence, 1D platforms share the premise of hosting, comparatively easier to control, enriched droplet phases even more in the genuine two- [57–61] and three-component [62] settings. Additionally, quantum droplets and more generally the impact of quantum fluctuations in 1D can be studied throughout the MF stability regime. However, the majority of the current investigations have been motivated by the correspondence to the 3D case, and thus solely focused on the attractive threshold of the MF stability regime. Hence, a general framework being able to describe droplets across the MF stability region but also heteronuclear mixtures in 1D is still lacking. Moreover, extraction and investigation of the LHY energy in higher-component setups is an open question. Indeed, previous studies on three-component mixtures in 1D have been focused on the case of a single-impurity in the third component [63–65] or a MF density coupling between the droplet and the impurities [66, 67]. Instead, appropriate inclusion of the LHY term among all components may be able to unveil unseen self-bound structures.

To address the above-discussed open problems, we derive the LHY energy (in a closed form whenever possible) and associated extended Gross-Pitaevskii equations (eGPEs) for two-, three- and four-component 1D bosonic mixtures based on the perturbative Bogoliubov treatment. Previous treatments restricted to two-component settings [53], can be obtained as a limiting case of our framework and are restricted to the 3D wave collapse threshold. In contrast to those, which (for convenience) we dub herein as "original", our exact approach remains valid throughout the 1D MF stability regime. Namely, it encompasses both attractive and repulsive interspecies interactions and interestingly it is able to tackle homonuclear as well as heteronuclear two-component settings. Direct comparisons of our approach to the approximate one in the attractive intercomponent interaction regime reveals quantitative deviations. These are imprinted as a reduced droplet saturation density and increased width in the exact case. Turning to the repulsive side, our results predict an early onset of phase-separation for both homonuclear and heteronuclear mixtures which is absent within the approximate framework.

Next, we provide exact closed form expressions for the LHY energies and ensuing eGPEs of a three-component mixture with either three or two identical components. It is explicated that such settings offer a broad range of possibilities for creating mixed droplet phases that are absent in lower-component setups. Additionally, a closed form LHY expression is extracted for the fully symmetric four-component mixture, constituting the higher-component mixture for which the Bogoliubov modes may be derived analytically in the general case. We present the derivations in a detailed and structured manner aiming to provide a useful resource for researchers entering the rapidly expanding field of quantum droplets and in general attractively interacting bosonic setups.

This work is structured as follows. In Section 2, we introduce the general multicomponent bosonic mixture featuring short-range contact interactions, the Bogoliubov transformation, and the original approximate two-component LHY theory being valid at the edge of the MF stability regime. Section 3 is devoted to the derivation and solution of the exact eGPEs for the genuine two-component mixture across the entire MF stability regime. This treatment is generalized to the three-component (Sec. 4) and the four-component (Sec. 5) bosonic mixture. Concluding remarks and perspectives for future investigations are offered in Sec. 6. In Appendix A, we provide further details regarding the three-component mixture stability conditions. Appendix B discusses the existence of asymmetric (domain-wall like) droplet distributions in the phase-separated regime.

SciPost SciPost Phys. 19, 133 (2025)

2 Basic settings and background

2.1 Multicomponent bosonic droplet setting

We consider a multicomponent bosonic mixture consisting of N_σ atoms of mass m_σ (where $\sigma = A, B, C, D, \ldots$) residing in 1D free space and featuring periodic boundary conditions. Notice, however, that our results (to be presented below) persist also in the case of a box potential provided that its length is sufficiently large and does not impact the edges of the discussed self-bound droplet configurations. The mixture is assumed to be close to zero temperature, where s-wave scattering dominates [68]. Hence, interparticle interactions are represented by contact potentials. Their effective coupling strengths are intracomponent repulsive (i.e. $g_{\sigma\sigma} \equiv g_\sigma > 0$) and intercomponent attractive ($g_{\sigma\sigma'} < 0$) or repulsive ($g_{\sigma\sigma'} > 0$). In a corresponding experiment, they can be adjusted either via Fano-Feshbach resonances [69, 70] through the 3D scattering length or through confinement induced resonances [68] by modifying the transverse trap frequency, $\omega_\perp$. This is significantly tight such that transverse excitations are prohibited and the atomic motion is restricted across the elongated x-direction as in corresponding 1D experiments [71].

The many-body Hamiltonian in second quantized form reads

$$H = \int dx \left(\sum_\sigma \left(\Psi_\sigma^\dagger \hat{h}_\sigma \Psi_\sigma + \frac{g_\sigma}{2} \Psi_\sigma^\dagger \Psi_\sigma^\dagger \Psi_\sigma \Psi_\sigma + \sum_{\sigma' > \sigma} \frac{g_{\sigma\sigma'}}{2} \Psi_\sigma^\dagger \Psi_{\sigma'}^\dagger \Psi_\sigma \Psi_{\sigma'} \right) \right), \tag{1}$$

where $\hat{h}_\sigma = -\frac{\hbar^2}{2m_\sigma} \left(\frac{\partial^2}{\partial {x_\sigma}^2} \right)$ is the underlying single-particle hamiltonian and $\Psi_\sigma(x)$ refers to the field operator annihilating a σ species boson at position x. In what follows, for computational convenience, we rescale the above Hamiltonian with respect to the energy scale set by $m_A g_A^2/\hbar^2$. Hence, the length, time, and interaction strengths are given in units of $\hbar^2/(m_A g_A)$, $\hbar^3/(m_A g_A^2)$, and g_A respectively.

2.2 Bogoliubov transformation

For an arbitrary set of n bosonic operators $A^\dagger = (\hat{\alpha}_1^\dagger, \hat{\alpha}_2^\dagger, \ldots, \hat{\alpha}_n^\dagger, \hat{\alpha}_1, \hat{\alpha}_2, \ldots, \hat{\alpha}_n)$ the general Bogoliubov transformation is defined by $A = UB$. Here, $B^\dagger = (\hat{\beta}_1^\dagger, \hat{\beta}_2^\dagger, \ldots, \hat{\beta}_n^\dagger, \hat{\beta}_1, \hat{\beta}_2, \ldots, \hat{\beta}_n)$ are the Bogoliubov operators and $U = \begin{pmatrix} M & N \\ N^* & M^* \end{pmatrix}$ is the Bogoliubov transformation matrix, where M, N are $n \times n$ matrices [72]. Demanding that both A and B satisfy bosonic commutation relations translates to $\mathcal{M}_b = [A, A^\dagger] = [B, B^\dagger] = \begin{pmatrix} I_n & 0 \\ 0 & -I_n \end{pmatrix}$, with I_n denoting the n-dimensional identity matrix. As such, utilizing the arbitrary Bogoliubov transformation yields

$$\mathcal{M}_b = U \mathcal{M}_b U^\dagger . \tag{2}$$

Thus, demanding that Eq. (2) holds is equivalent to imposing that the Bogoliubov transformation preserves the commutation relations of the set of bosonic operators. However, in this case, it is not required to explicitly derive the constraints on the elements of the transformation matrix U, as done in the usual textbook derivation [5, 6].

Another useful property of the Bogoliubov transformation is that it can be used to diagonalize a bilinear (in terms of the arbitrary set of bosonic operators A) operator, such as $\hat{H} = A^\dagger H A$. Here, $\hat{H}$ is an one-body operator (expressed in second quantized form) with respect to $\hat{a}_i$, $\hat{a}_i^\dagger$ and H is its corresponding matrix representation. Accordingly, it holds that $\hat{H} = A^\dagger H A = B^\dagger U^\dagger H U B = B^\dagger \mathcal{M}_b U^{-1} \mathcal{M}_b H U B$. Then, by requiring that the Bogoliubov trans-

SciPost Phys. 19, 133 (2025)

formation[1] diagonalizes $\hat{H}$ in terms of the bilinear form with respect to B or equivalently diagonalizes the matrix $\mathcal{H}_M = \mathcal{M}_b H$, as $U^{-1}\mathcal{H}_M U = D$, where D is a diagonal matrix, we obtain the eigenvalues of $\mathcal{H}_M$ through the characteristic equation

$$\det(\mathcal{M}_b H - \lambda I_{2n}) = 0\,. \tag{3}$$

This leads to $\mathcal{M}_b D = \mathrm{diag}(\lambda_1,\ldots,\lambda_n,-\lambda_{n+1},\ldots,-\lambda_{2n})$ and therefore the operator $\hat{H}$ takes the form

$$\hat{H} = B^\dagger \mathcal{M}_b D B = \sum_{i=1}^{n}\left(\lambda_i \hat{\beta}_i^\dagger \hat{\beta}_i - \lambda_{n+i}\hat{\beta}_i\hat{\beta}_i^\dagger\right) = \sum_{i=1}^{n}(\lambda_i - \lambda_{n+i})\hat{\beta}_i^\dagger\hat{\beta}_i - \sum_{i=1}^{n}\lambda_{n+i}\,. \tag{4}$$

In the last step, we have used that $[\beta_i, \beta_i^\dagger] = 1$. In this sense, $h_0 = -\sum_{i=1}^{n}\lambda_{n+i}$ is the eigenvalue of $\hat{H}$ corresponding to the quasi-particle vacuum in terms of the bosonic quasi-particle operators $(\beta_i,\ \beta_i^\dagger)$, while $h_i = \lambda_i - \lambda_{n+i}$ are the eigenvalues corresponding to the quasi-particle excitations.

2.3 Original two-component LHY treatment

For a two-component, homonuclear ($m_A = m_B \equiv m$), 1D mixture the MF stability regime is given by the condition $g_{AB}^2 \leq g_A g_B$ [5]. In the attractive limit where $g_{AB} = -\sqrt{g_A g_B}$ holds, taking into account the first-order (LHY) quantum correction it was shown [53] to result in the following coupled set of "approximate" eGPEs describing two-component 1D quantum droplets

$$i\hbar\frac{\partial\Psi_\sigma}{\partial t} = \left(-\frac{\hbar^2}{2m}\frac{\partial^2}{\partial x_\sigma^2} + g_\sigma|\Psi_\sigma|^2 + g_{AB}\left|\Psi_{\sigma'\neq\sigma}\right|^2 - \frac{g_\sigma\sqrt{m}}{\pi\hbar}\sqrt{g_A|\Psi_A|^2 + g_B|\Psi_B|^2}\right)\Psi_\sigma\,. \tag{5}$$

In these equations, the first terms represent the usual mean-field Gross-Pitaevskii equations (GPEs) and the last term provides the LHY correction. In the symmetric system, where the intracomponent interactions $g_\sigma \equiv g$ and the species densities $n_\sigma \equiv n$, with $N_\sigma = \int n_\sigma dx = \int |\Psi_\sigma|^2 dx$ the components behave equivalently. Accordingly, it has been demonstrated [21, 23] that these eGPEs predict a transition of the droplet density from a Gaussian to a flat-top (FT) configuration upon either increasing the particle number (N) or decreasing the intercomponent attraction ($|g_{AB}|$) with $0 < -g_{AB} < g$ [53]. The emergent FT structures feature a saturated peak density at [53] $n_0 = \frac{8mg^3}{9\hbar^2\pi^2(g+g_{AB})^2}$, with energy density $\mathcal{E}_0(n=n_0) = -(g+g_{AB})n_0^2$, chemical potential $\mu_0 = \frac{\partial\mathcal{E}_0}{\partial n}(n=n_0) = -(g+g_{AB})n_0$, and healing length $\xi_0 = \sqrt{-\frac{\hbar^2}{2m\mu_0}} = \sqrt{\frac{\hbar^2}{2m(g+g_{AB})n_0}}$.

It is imperative to clarify that the extraction of Eq. (5) is based on the assumption that we are operating at the interaction boundary $g_{AB} = -\sqrt{g_A g_B}$. This is indeed well motivated by the respective 3D setting in which the LHY contribution is repulsive and provides stabilization outside the MF stability regime where droplets emerge [20]. However, in 1D systems the LHY correction turns out to be attractive [23, 53], and therefore the droplet configurations are hosted within the MF stability regime. Hence, as we will explicate in detail below, no assumptions (beyond the usual ones deployed for a dilute and weakly interacting gas) are needed, and we can analytically extract eGPEs which are valid throughout the MF stability regime and not only in the boundary as was currently known. This is one of the main results of our work which presents the generalized two-component eGPEs and exposes deviations from the predictions of the "original" ones described by Eq. (5).

[1] The Bogoliubov transformation matrix U is not unique. Thus, additional constraints can be imposed by exploiting the remaining (i.e. not the ones required to preserve the bosonic symmetry) degrees-of-freedom.

SciPost SciPost Phys. 19, 133 (2025)

3 Two-component mixture

The Hamiltonian density for a short-range (contact) interacting two-component bosonic mixture in a box of length L, can be easily deduced from the general multicomponent Hamiltonian given by Eq. (1) with $\sigma = A,B$ and $\sigma' = A,B \neq \sigma$. A corresponding experimentally relevant system of choice here could be, for instance, two different hyperfine states of ^{39}K as in the 3D case [24]. Next, we express the field operators in the plane-wave basis as $\hat{\Psi}_A(x) = \frac{1}{\sqrt{L}}\hat{a}_0 + \sum_{k\neq 0}\frac{e^{ikx}}{\sqrt{L}}\hat{a}_k$ and $\hat{\Psi}_B(x) = \frac{1}{\sqrt{L}}\hat{b}_0 + \sum_{k\neq 0}\frac{e^{ikx}}{\sqrt{L}}\hat{b}_k$, where we have implicitly assumed periodic boundary conditions. Substitution of these operators into the aforementioned two-component Hamiltonian and integration over the box length, leads to the Hamiltonian

$$\begin{aligned}\hat{\mathcal{H}} = &\frac{g_A}{2L}\hat{a}_0^\dagger\hat{a}_0^\dagger\hat{a}_0\hat{a}_0 + \frac{g_B}{2L}\hat{b}_0^\dagger\hat{b}_0^\dagger\hat{b}_0\hat{b}_0 + \frac{g_{AB}}{L}\hat{a}_0^\dagger\hat{b}_0^\dagger\hat{a}_0\hat{b}_0 + \frac{\hbar^2}{2m_A}\sum_{k\neq 0}k^2\hat{a}_k^\dagger\hat{a}_k + \frac{\hbar^2}{2m_B}\sum_{k\neq 0}k^2\hat{b}_k^\dagger\hat{b}_k \\ &+ \frac{g_A}{2L}\sum_{k\neq 0}\left[\hat{a}_0^\dagger\hat{a}_0^\dagger\hat{a}_k\hat{a}_{-k} + \hat{a}_0\hat{a}_0\hat{a}_k^\dagger\hat{a}_{-k}^\dagger + 4\hat{a}_0^\dagger\hat{a}_0\hat{a}_k^\dagger\hat{a}_k\right] \\ &+ \frac{g_B}{2L}\sum_{k\neq 0}\left[\hat{b}_0^\dagger\hat{b}_0^\dagger\hat{b}_k\hat{b}_{-k} + \hat{b}_0\hat{b}_0\hat{b}_k^\dagger\hat{b}_{-k}^\dagger + 4\hat{b}_0^\dagger\hat{b}_0\hat{b}_k^\dagger\hat{b}_k\right] \\ &+ \frac{g_{AB}}{L}\sum_{k\neq 0}\left[\hat{a}_0^\dagger\hat{b}_0^\dagger\hat{a}_k\hat{b}_{-k} + \hat{a}_0^\dagger\hat{a}_0\hat{b}_k^\dagger\hat{b}_k + \hat{a}_0^\dagger\hat{b}_0\hat{b}_k^\dagger\hat{a}_k + \hat{b}_0^\dagger\hat{a}_0\hat{a}_k^\dagger\hat{b}_k + \hat{b}_0^\dagger\hat{b}_0\hat{a}_k^\dagger\hat{a}_k + \hat{a}_0\hat{b}_0\hat{a}_k^\dagger\hat{b}_{-k}^\dagger\right] \\ &+ \mathcal{O}(\hat{a}_k^3)\,.\end{aligned} \tag{6}$$

Here, terms higher than bilinear in the bosonic operators $\hat{a}_k$, $\hat{b}_k$ are neglected. From this expression, it is possible to readily retrieve the zeroth order (MF) approximation by setting $\hat{a}_0 = \sqrt{N_A}$, $\hat{b}_0 = \sqrt{N_B}$ and neglecting all other terms with $(\hat{a}_{k\neq 0}, \hat{b}_{k\neq 0})$. Such a process results in the known MF energy density of the two-component setting

$$\mathcal{E}_{\rm MF} = \frac{E_{\rm MF}}{L} = \frac{1}{2}g_A n_A^2 + \frac{1}{2}g_B n_B^2 + g_{AB}n_A n_B\,. \tag{7}$$

To obtain the first-order correction to the MF energy, one needs to account for the depletion of the condensate due to quantum fluctuations. This is achieved by expressing the particle number operators as $N_A = \hat{a}_0^\dagger\hat{a}_0 + \sum_{k\neq 0}\hat{a}_k^\dagger\hat{a}_k$ and $N_B = \hat{b}_0^\dagger\hat{b}_0 + \sum_{k\neq 0}\hat{b}_k^\dagger\hat{b}_k$. Inserting those into the Hamiltonian of Eq. (6) and defining the set of operators $\Phi^\dagger = (\hat{a}_k^\dagger, \hat{b}_k^\dagger, \hat{a}_{-k}, \hat{b}_{-k})$, we arrive at the bilinear Hamiltonian

$$\hat{H} = \sum_{k>0}\Phi^\dagger H\Phi + \frac{g_A N_A^2}{2L} + \frac{g_B N_B^2}{2L} + \frac{g_{AB}N_B N_A}{L} - \sum_{k>0}\left(\frac{\hbar^2k^2}{2m_A} + \frac{\hbar^2k^2}{2m_B} + g_A n_A + g_B n_B\right). \tag{8}$$

The operators, Φ, satisfy the bosonic commutation relations, i.e. $\mathcal{M}_b = [\Phi, \Phi^\dagger] = \begin{pmatrix} I_2 & 0 \\ 0 & -I_2 \end{pmatrix}$, where I_2 is the 2×2 identity matrix. Also, the Hamiltonian matrix

$$H = \begin{pmatrix} h_A(k) & h_{AB} & g_A n_A & h_{AB} \\ h_{AB} & h_B(k) & h_{AB} & g_B n_B \\ g_A n_A & h_{AB} & h_A(k) & h_{AB} \\ h_{AB} & g_B n_B & h_{AB} & h_B(k) \end{pmatrix}, \tag{9}$$

where $h_\sigma(k) = \frac{\hbar^2k^2}{2m_\sigma} + g_\sigma n_\sigma$ and $h_{AB} = g_{AB}\sqrt{n_A n_B}$. Note that the sums in Eq. (8) are now over positive momenta only. As argued in Sec. 2.2, we can diagonalize the Hamiltonian of Eq. (8) in terms of an appropriate Bogoliubov transformation, by solving the

SciPost SciPost Phys. 19, 133 (2025)

characteristic equation (Eq. (3)) $\det(\mathcal{M}_b H - \omega_k I_4) = 0$ which in this case takes the form $\omega^4 + \beta\omega^2 + \gamma = 0$. The parameters are $\beta = -\epsilon_A^2(k) - \epsilon_B^2(k)$ and $\gamma = \epsilon_A^2(k)\epsilon_B^2(k) - g_{AB}^2 n_A n_B \frac{\hbar^4 k^4}{m_A m_B}$, with $\epsilon_\sigma(k) = \sqrt{\frac{\hbar^4 k^4}{4m_\sigma^2} + \frac{\hbar^2 k^2}{m_\sigma} g_\sigma n_\sigma}$ representing the corresponding single-component Bogoliubov dispersion relations [6]. The solutions of the characteristic polynomial equation yield the underlying dispersion relation for the two-component system in the presence of the first-order quantum correction

$$\omega_\pm^2 = \frac{\epsilon_A^2 + \epsilon_B^2 \pm \sqrt{(\epsilon_A^2 - \epsilon_B^2)^2 + 4g_{AB}^2 n_A n_B \frac{\hbar^4 k^4}{m_A m_B}}}{2}. \tag{10}$$

Finally, utilizing the diagonal form of a bilinear operator within the Bogoliubov transformation prescribed by Eq. (4) and collecting the constant terms in Eq. (8), we find the respective ground state energy

$$E_0 = \frac{g_A N_A^2}{2L} + \frac{g_B N_B^2}{2L} + \frac{g_{AB} N_B N_A}{L} + \sum_{k>0} \left(\omega_+ + \omega_- - \frac{\hbar^2 k^2}{2m_A} - \frac{\hbar^2 k^2}{2m_B} - g_A n_A - g_B n_B \right). \tag{11}$$

Apparently, the first terms in Eq. (11) correspond to the standard MF intra- and inter-component interaction energies respectively, while the sum is the first-order LHY quantum correction for the two-component mixture. To calculate the LHY contribution, we substitute the sum in Eq. (11) with an integral over k according to $\sum_{k>0} \to (L/2\pi) \int_0^{+\infty} dk$. We note in passing that in the 3D case, additional terms ($\propto + \frac{m g_{\sigma\sigma'} n_\sigma}{\hbar^2 k^2}$) enter the corresponding sum over k, while the latter has to be substituted with the corresponding 3D integral [6].

3.1 Exact closed form solution for the homonuclear mixture

As already discussed above, unlike the 3D case (see Ref. [20]), in 1D it is not necessary to impose the approximation $g_{AB}^2 \approx g_A g_B$ (which leads to Eq. (5)) in the dispersion relation of Eq. (10). In particular, it is possible to calculate exactly the ground state energy for a homonuclear ($m_A = m_B \equiv m$) mixture. Indeed, setting $p := \frac{4(g_{AB}^2 - g_A g_B) n_A n_B}{(g_A n_A + g_B n_B)^2}$, and by employing the change of variables $\hbar k = \sqrt{m(g_A n_A + g_B n_B)}\, y$ to calculate the integral in Eq. (11), the ground state energy density becomes

$$\mathcal{E} = \frac{E_0}{L} = \mathcal{E}_{\mathrm{MF}} + \underbrace{\frac{\sqrt{m}(g_A n_A + g_B n_B)^{\frac{3}{2}}}{2\hbar\pi} \mathcal{I}(p)}_{\mathcal{E}_{\mathrm{LHY}}}, \tag{12}$$

where the function of the beyond MF energy contribution

$$\mathcal{I}(p) = -\frac{\sqrt{2}}{3} \left((1 - \sqrt{p+1})^{\frac{3}{2}} + (1 + \sqrt{p+1})^{\frac{3}{2}} \right). \tag{13}$$

Importantly, the generalized two-component energy density described by Eq. (12) *is valid for any interaction strength and particle number* for which the MF treatment is valid. Moreover, the LHY energy is real-valued and negative, as long as $-1 \leq p \leq 0$, i.e. $|g_{AB}| \leq \sqrt{g_A g_B}$, so that $p \leq 0$ (while $p \geq -1$ is trivially satisfied). Notice that this interaction interval corresponds to the *entire MF stability region*, ranging from the usual droplet threshold ($-g_{AB} \approx \sqrt{g_A g_B}$) all the way to the standard miscibility threshold ($g_{AB} \approx \sqrt{g_A g_B}$) [16, 23]. It is also worth mentioning explicitly that, in the limit of $p = 0$, we obtain $\mathcal{I}(p = 0) = -4/3$, i.e. *we recover the original droplet energy* which results in Eq. (5). Moreover, at the edge of the MF stability regime where

SciPost SciPost Phys. 19, 133 (2025)

$g_{AB}^2 \approx g_A g_B$, it holds that $|p| \ll 1$, leading to $I(p) \approx -\frac{4}{3} - \frac{p}{2}$. Finally, in the opposite limit of an uncoupled mixture ($g_{AB} = 0$) we find $I(p=-1) = -2\sqrt{2}/3$. Hence, in this case the LHY term is reduced by a factor of $\sqrt{2}$. A similar expression was recently derived in the context of a mobile impurity immersed in a droplet host [66].

Having determined the ground state energy of the two-component bosonic mixture in the presence of the LHY correction, we can subsequently derive the exact eGPEs. This is done by evaluating the Euler-Lagrange equations with respect to n_σ yielding:

$$i\hbar\frac{\partial\Psi_\sigma}{\partial t} = \left(-\frac{\hbar^2}{2m}\frac{\partial^2}{\partial x^2} + \frac{\partial\mathcal{E}}{\partial n_\sigma}\right)\Psi_\sigma = \left(-\frac{\hbar^2}{2m}\frac{\partial^2}{\partial x^2} + g_\sigma|\Psi_\sigma|^2 + g_{AB}\left|\Psi_{\sigma'\neq\sigma}\right|^2 + \frac{\partial\mathcal{E}_{\mathrm{LHY}}}{\partial n_\sigma}\right)\Psi_\sigma\,. \quad (14)$$

In general, the full eGPEs have a quite complicated form, since

$$\frac{\partial\mathcal{E}_{\mathrm{LHY}}}{\partial n_\sigma} = \frac{3g_\sigma\sqrt{m(g_A n_A + g_B n_B)}}{4\hbar\pi}\mathcal{I}(p) + \frac{\sqrt{m(g_A n_A + g_B n_B)^3}}{2\hbar\pi}\frac{\partial\mathcal{I}}{\partial p}\frac{\partial p}{\partial n_\sigma}\,, \quad (15)$$

where

$$\frac{\partial\mathcal{I}}{\partial p} = \frac{\sqrt{2}(\sqrt{1-\sqrt{p+1}} - \sqrt{1+\sqrt{p+1}})}{4\sqrt{p+1}}\,, \quad (16a)$$

$$\frac{\partial p}{\partial n_\sigma} = \frac{4n_{\sigma\prime}(g_A g_B - g_{AB}^2)(g_\sigma n_\sigma - g_{\sigma\prime} n_{\sigma\prime})}{(g_A n_A + g_B n_B)^3}\,, \quad (16b)$$

with $\sigma \neq \sigma\prime$. Notably, the form and subsequent impact of the LHY correction away from the droplet limit ($-g_{AB} \approx \sqrt{g_A g_B}$) and even for repulsive intercomponent interactions (where e.g. bubble configurations have been predicted [19]) is largely unknown. Considering stronger intercomponent interactions outside the MF stability, i.e. $|g_{AB}| > \sqrt{g_A g_B}$ where $p > 0$, results in a complex LHY correction. A common practice in the literature is to simply neglect the imaginary part of $\mathcal{E}$ [20, 62], assuming that it is sufficiently small and hence the growth rate of the resulting instability is slower than e.g. the decay due to three-body recombination. Examining the validity of this treatment by comparing its predictions e.g. with MF computations, *ab-initio* calculations [40–43] or experimental data would be a particularly interesting direction for future studies, especially in 1D. This is because, aside from being more amenable to *ab-initio* calculations, 1D systems do not experience MF collapse in this limit, unlike their 3D counterparts where stable solutions exist only in the presence of the LHY term [20].

An insightful application of our generalized framework is to consider the limiting case of a fully balanced mixture characterized by $g_A = g_B \equiv g$ and $n_A = n_B \equiv n$, and therefore $p = (\frac{g_{AB}}{g})^2 - 1$. Accordingly, the second term in Eq. (15) vanishes and the LHY term becomes $\sim (g^3 n)^{1/2} I(p)$. Thus, in this case, the exact LHY term has the same density dependence as in the "approximate" eGPEs [53] given by Eq. (5), but they are quantitatively different since the exact LHY term depends also on g_{AB}. Using the exact energy of the full two-component system given by Eq. (12), we find the minimum of the energy per particle for the aforementioned balanced mixture to occur at the saturation density

$$n_s = \frac{m g^3 I^2(p)}{2\hbar^2\pi^2(g+g_{AB})^2} = \frac{2mg^3\left[1 + 3(g_{AB}/g)^2 + (1-(g_{AB}/g)^2)^{3/2}\right]}{9\hbar^2\pi^2(g+g_{AB})^2}\,. \quad (17)$$

Here, the energy density $\mathcal{E}(n=n_s) = \frac{-m^2 g^6 I^4(p)}{8\hbar^4\pi^4(g+g_{AB})^3} = -(g+g_{AB})n_s^2$, the chemical potential $\mu_s = \frac{-mg^3 I^2(p)}{2\hbar^2\pi^2(g+g_{AB})} = -(g+g_{AB})n_s$, and the healing length $\xi_s = \sqrt{-\frac{\hbar^2}{2m\mu_s}} = \sqrt{\frac{\hbar^2}{2m(g+g_{AB})n_s}}$.

SciPost Phys. 19, 133 (2025)

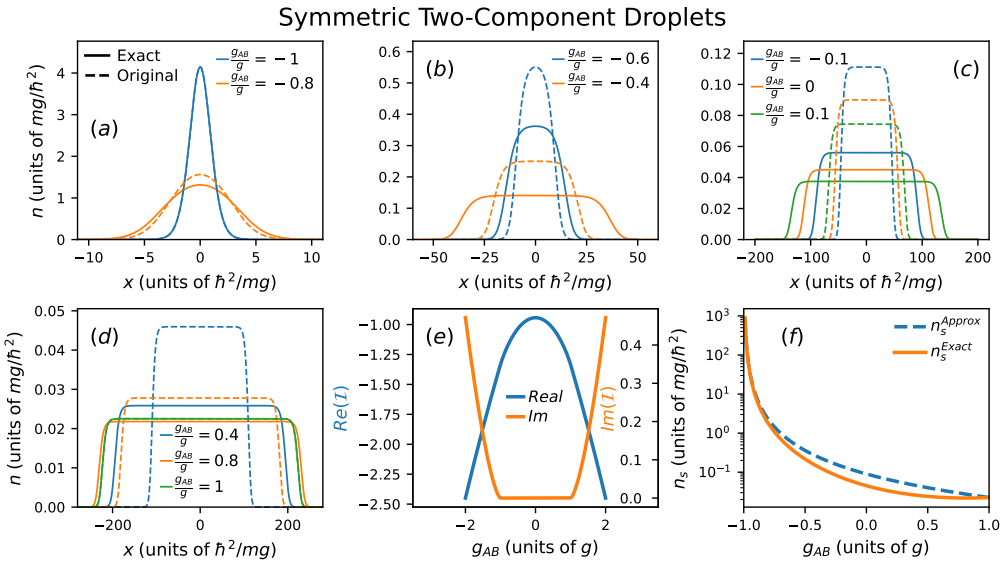

Figure 1: Ground state droplet densities for a symmetric mixture featuring $N_A = N_B = N = 10$, $g_A = g_B = g$, and varying intercomponent interactions g_{AB} (see legends). A plethora of different cases are shown ranging from (a) strong and (b) weak attractions, to (c) weak (nearly suppressed) couplings all the way towards (d) repulsive intercomponent interactions. In all cases, the ground state density obtained within the original given by Eq. (5) (dashed lines) and the exact (solid lines) eGPEs (14) are depicted. Evidently, the original eGPEs consistently predict significantly more localized configurations when $|g_{AB}| \neq g$, while in some cases (e.g. $g_{AB} = -0.6g$) it even fails to adequately capture the droplet's FT density profile. Note that the dashed blue and green lines in panels (a) and (d) respectively are hardly visible since they coincide with the solid ones. (e) Dependence of the real and imaginary parts (see legend) of the LHY energy coefficient ($I(p)$) in Eq. (13) on the interspecies interaction strength. (f) The droplet saturation density in both the exact and original approaches (see legend) with respect to g_{AB}.

Apparently, these exact results exhibit quantitative differences from the predictions of the original LHY approach described by Eq. (5). This can be readily deduced, for instance, by comparing them with the approximate saturation density (n_0) as well as the chemical potential and healing length discussed in Sec. 2.3 for the balanced mixture. Note that the chemical potentials and energies for all 1D droplet configurations discussed throughout this work, are negative. This supports their self-bound nature in the entire MF stability regime.

To further elucidate the deviations between the original (Eq. (5)) and the exact (Eq. (14)) eGPEs predictions we numerically compute, via imaginary time-propagation, the corresponding ground state droplet densities for the symmetric mixture with $g_A = g_B \equiv g$ and $N_A = N_B \equiv N = 10$. Since, the exact eGPEs (Eq. (14)) are valid throughout the MF stability regime, we present results for the standard droplet regime $g_{AB} < 0$ [Fig. 1(a), (b)], but also for the nearly intercomponent decoupled ($g_{AB} \approx 0$) system [Fig. 1(c)] and even for repulsive interactions within the miscible regime quantified by $0 < g_{AB} \leq g$ [Fig. 1(d)]. The underlying LHY energy, $\mathcal{E}(n = n_s) = -(g + g_{AB})n_s^2$, attains its maximum (or minimum absolute) value for the decoupled system, whilst it decreases when g_{AB} is nonzero. Interestingly, it acquires a relatively small imaginary component for $|g_{AB}| > g$ as shown in Fig. 1(e).

SciPost Phys. 19, 133 (2025)

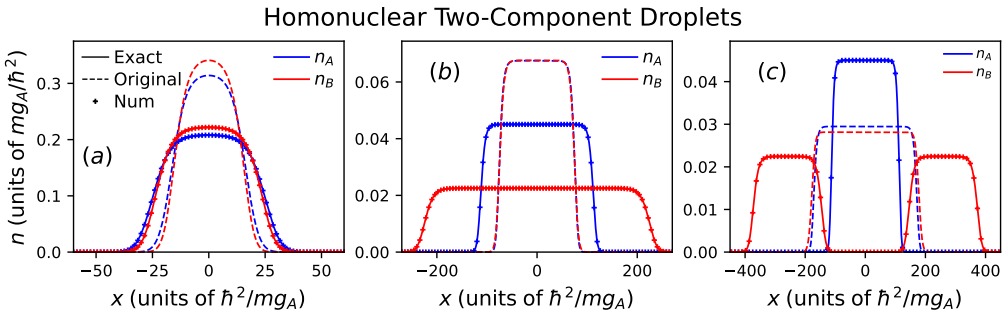

Figure 2: Ground state density configurations of a homonuclear two-component mixture for fixed $N_A = N_B \equiv N = 10$, $m_A = m_B \equiv m$, and $g_B = 0.5g_A$. Different intercomponent coupling strengths are considered ranging from (a) attractive $g_{AB} = -0.4g_A$, to (b) decoupled $g_{AB} = 0$, and (c) repulsive $g_{AB} = 0.4g_A$ cases. The outcome of the exact [Eq. (14)] and the original [Eq. (5)] eGPEs is illustrated as well as the one stemming from numerical integration of the sum of the LHY energy [Eq. (11)]. As for the balanced mixture, see Fig. 1, the original eGPEs overestimate the peak density of the droplets and underestimate their width. Interestingly, as long as the intercomponent interaction becomes repulsive [panel (c)], an early onset of the miscible-to-immiscible transition, coexisting with droplet configurations, appears to take place, and being solely captured by the exact eGPEs.

A close inspection of Fig. 1 reveals that the original eGPEs (Eq. (5)) are only accurate when $|g_{AB}| = g$. In contrast, deviating from this condition they significantly overestimate the droplet's saturation density and localization in all other interaction regimes, see Fig. 1(a)-(d). In particular, the difference in the saturation density among the two approaches becomes larger for intermediate intercomponent couplings lying in the interval $-g < g_{AB} < g$ as illustrated in Fig. 1(f). Even more, for $g_{AB} = -0.6$ the original eGPEs predict a Gaussian profile for the ground state density and they fail to capture the FT density profile of the droplet as predicted by the exact eGPEs, see Fig. 1(b). Additionally, as mentioned before, it is clear that the droplet solution exists throughout the MF stability regime within both approaches, exhibiting FT configurations (for sufficiently large particle number) irrespectively of the intercomponent interaction, g_{AB}, value [Fig. 1(a)-(d)]. Specifically, the droplet becomes progressively more delocalized and its saturation density decreases as g_{AB} varies from $g_{AB} = -g$ to $g_{AB} = g$. Namely, the droplet saturation density (width) reduces (increases) sharply between the two limits, reaching a minimum value of $n_s(g_{AB} = g) = \frac{2mg}{9\hbar^2\pi^2} \approx 0.0225$ for the parameter values considered here, see also Fig. 1(f). As such, it could be that in practice, after a certain value of g_{AB} the droplet would be dilute and extended enough appearing to have effectively disperse thus rendering challenging its experimental resolution by the corresponding imaging apparatus.

As a next step, we turn our attention to an intracomponent interaction imbalanced homonuclear ($m_A = m_B \equiv m$) mixture, with $g_A \neq g_B$ and fixed $g_B = 0.5g_A$, as well as $N_A = N_B \equiv N = 10$. The corresponding two-component droplet configurations within the exact [Eq. (14)] and original [Eq. (5)] eGPEs, but also the solutions obtained by calculating the LHY energy through direct numerical integration of the sum in Eq. (11) are visualized in Fig. 2 upon different variations of the g_{AB} attraction.[2] For clarity, the ensuing solutions are marked by "Exact", "Original", and "Num" respectively. In general, it appears that as long as

[2] We remark that a larger g_B repulsion results in more localized structures in both components, without any qualitative differences from the configurations depicted in Fig. 2 (not shown).

SciPost SciPost Phys. 19, 133 (2025)

the intercomponent coupling is attractive (i.e. $g_{AB} < 0$) the two components prefer to maximize their spatial overlap [30, 61], while exhibiting similar density profiles as can be seen in Fig. 2(a). Moreover, tuning g_{AB} towards weaker attractions, both components become less localized, until a transition from a Gaussian-type to a FT density profile takes place, compare in particular Fig. 2(a) and (b). Once more, as in the fully symmetric mixture, the original eGPEs predict appreciably more localized droplet densities alongside a higher FT value.

Additionally, approaching the weakly coupled intercomponent regime ($g_{AB} \approx 0$) the individual component droplet separation becomes more prominent, with the more strongly repulsive component exhibiting a more localized density profile and a higher saturation density [Fig. 2(b)]. Strikingly, this effect is absent within the original eGPEs, predicting instead a largely overlapping behavior for all intercomponent interactions shown in Fig. 2. Turning to repulsive intercomponent couplings, e.g. $g_{AB} = 0.4g_A$, we observe a phase separation of the droplet density between the two components, even though we are still operating well within the MF stability regime, see Fig. 2(c). A behavior that is completely absent within the original eGPEs. This phase separation can be understood from energetic arguments. Indeed, by ignoring the spatial overlap between the two components, it is possible to approximate the system shown in Fig. 2(c) by three distinct single-component droplets. Estimating their energy, in the homogeneous FT case, through minimization of the energy per particle (see also Eq. (12)) for each component in the absence of the other, results in $E_\sigma^{1\text{comp}} = -\frac{8m_\sigma^3 g_\sigma^3}{81\hbar^4\pi^4} L_\sigma$. Here, L_σ designates the spatial extent of each individual droplet. With this approximation (setting L_σ as the full-width-at-half-maximum for each structure) we find the total energy $E = E_A^{1\text{comp}} + 2E_B^{1\text{comp}} \approx -0.2832$ which is in excellent agreement with the numerically obtained energy $E = -0.2816$. The relatively small deviations stem from the (positive) contributions of the finite overlap and the kinetic terms. In particular, we can approximate the kinetic energy of each droplet as $K.E._\sigma = \int \frac{\hbar^2}{2m_\sigma} |\frac{\partial \Psi_\sigma}{\partial x}|^2 dx \approx 2\frac{\hbar^2}{2m_\sigma} |\frac{\sqrt{n_{s_\sigma}}}{\xi_\sigma}|^2 \xi_\sigma = \frac{8m_\sigma g_\sigma^2}{27\hbar^2\pi^2} = \frac{2g_\sigma}{3\pi} n_s$, where ξ_σ is the healing length of the droplet and the factor of two stems from the two edges of the droplet. Interestingly, this suggests that the kinetic energy of the droplet scales as $\propto m_\sigma g_\sigma^2$ explaining why the more weakly interacting (and as we shall see below the lighter component) splits preferentially in the phase separated configurations, in order to reduce the systems kinetic energy. Clearly, an overlapping arrangement, with component B in a single FT configuration centered at $x = 0$ and length $L_B' \approx 2L_B$ would be associated with higher energy due to the repulsive intercomponent coupling. The energy contribution of the latter is $E_{AB} \approx g_{AB} n_A n_B L_{overlap}$, and it would be of order $\sim +0.1$ assuming similar saturation densities to those in Fig. 2(c) and $L_{overlap} \approx L_A \leq L_B'$. Hence, this hypothetical overlapping configuration would have a total energy of order $E' \approx E_A^{1\text{comp}} + E_B^{1\text{comp}}(L_\sigma = L_B') + E_{AB} = E + E_{AB} \sim -0.18$, which is significantly larger that the phase separated configuration.

Note that throughout this work, we focus on parity symmetric[3] density configurations, an assumption that pertains only to phase-separated structures. The droplet equations, however, support also parity asymmetric (or domain-wall like) configurations which, in the case of phase-separation, possess slightly lower energies (typically of the order of 0.3%) than the parity symmetric splited configurations e.g. depicted in Fig. 2(c). Such parity asymmetric distributions while existing within the classical field approximation are not, in general, permitted within a many-body wavefunction perspective which in the absence of an explicitly symmetry breaking contribution in the Hamiltonian should retain the symmetry. In this context, the lowest energy parity symmetric configurations correspond to a good approximation to the reduced one-body density of the underlying atomic gas in the ground state, see also Appendix B for further details and the respective asymmetric density distributions. It is important

[3] Due to translation invariance, parity symmetry is defined with respect to the arbitrary center-of-mass of the mixture, here set to $x = 0$.

SciPost SciPost Phys. 19, 133 (2025)

to emphasize that these asymmetric single domain-wall like configurations are intriguing on their own right and deserve further investigation, while they are promising for being exploited for unprecedented nucleation of topological excitations and hydrodynamic instabilities in the droplet realm. Finally, it is worth noting that in the presence of e.g. an external harmonic confinement, the components phase-separate at the standard miscibility threshold [23, 73].

3.2 Heteronuclear two-component mixtures

Besides homonuclear mixtures, droplets can also be hosted in genuinely heteronuclear settings consisting of two different isotopes. Such systems have already been experimentally investigated in 3D deploying the isotopes ^{87}Rb and ^{41}K [45, 74] or ^{87}Rb and ^{23}Na [75] but also in 1D with the former composition [47]. It is a known fact that the ensuing 3D eGPEs are far more complicated compared to the homonuclear ones due to the arguably complex form of the LHY contribution. However, thus far, in 1D (to the best of our knowledge) the extraction of the respective eGPEs remains elusive. Below, we elaborate on their construction and provide corresponding numerical results based on this framework.

Specifically, in the most general case of a heteronuclear mixture ($m_A \neq m_B$) the integral encompassing the LHY contribution represented by Eq. (11) cannot be calculated in a closed analytical form. An interesting limit arises for $\frac{g_B n_B}{g_A n_A} = \frac{m_B}{m_A}$ and $g_{AB} \approx 0$. Recall that the first of these conditions when $m_A = m_B$ reduces to the usual density fixing relation where the two-component eGPE framework reduces to a single-component one [20, 53]. Retaining both (interaction) conditions, the LHY energy can be calculated analytically acquiring the closed form

$$\mathcal{E}_{LHY} = \frac{E_{LHY}}{L} = -\frac{m_A^2 + m_B^2}{2\hbar\pi}\Big(\frac{g_A n_A}{m_A} + \frac{g_B n_B}{m_B}\Big)^{\frac{3}{2}}. \tag{18}$$

However, this scenario is somewhat specialized. It requires the presence of appreciable experimental tunability in terms of Feshbach resonances that is not yet reached for these recently realized systems. As such, in what follows, we focus on general heteronuclear setups that do not satisfy the above-discussed conditions.

More concretely, we first and foremost numerically calculate the LHY energy density given by Eq. (11) and hence $\frac{\partial \mathcal{E}_{LHY}}{\partial n_\sigma}$ to be incorporated in the corresponding eGPEs featuring intercomponent mass imbalance, $m_A \neq m_B$. For the sake of comparison, we will also contrast the above-discussed ground state droplet densities with the ones obtained from either the original (Eq. (5)) or exact (Eq. (14)) eGPEs (exact only in the mass-balanced case, $m_A = m_B \equiv m$), by directly substituting the different masses of each component in the respective equation such that we can "artificially" emulate the heteronuclear setting. We mainly focus on moderate mass-imbalances with $m_B = 2m_A$ to unveil the basic droplet structures and afterwards comment on the impact of increasing imbalance.

For sufficiently strong intercomponent attraction, see Fig. 3(a), namely within the Gaussian droplet regime, the exact homonuclear eGPEs prediction is in excellent agreement with the fully general numerical approach. Deviations among the two approaches arise and progressively increase for decreasing intercomponent attraction, where the system transitions towards the FT region, see Fig. 3(b) where $g_{AB} = -0.4g_A$. In both cases intercomponent mixing is minor, i.e. the droplet profiles are close to one another, and becomes gradually more pronounced as we move to the noninteracting limit presented in Fig. 3(c) where the droplets maintain their FT structure. In contrast, for repulsive g_{AB}, the heteronuclear system prefers to phase separate into a central droplet occupied by the heavier component, while the lighter species fragments into two FT droplets on either side [Fig. 3(d)]. This preference of the lighter component to allocate into two different fragments is attributed to its reduced kinetic energy $\sim m_\sigma g_\sigma^2$ as compared to the corresponding one of the heavier component (see also the discussion at the

SciPost Phys. 19, 133 (2025)

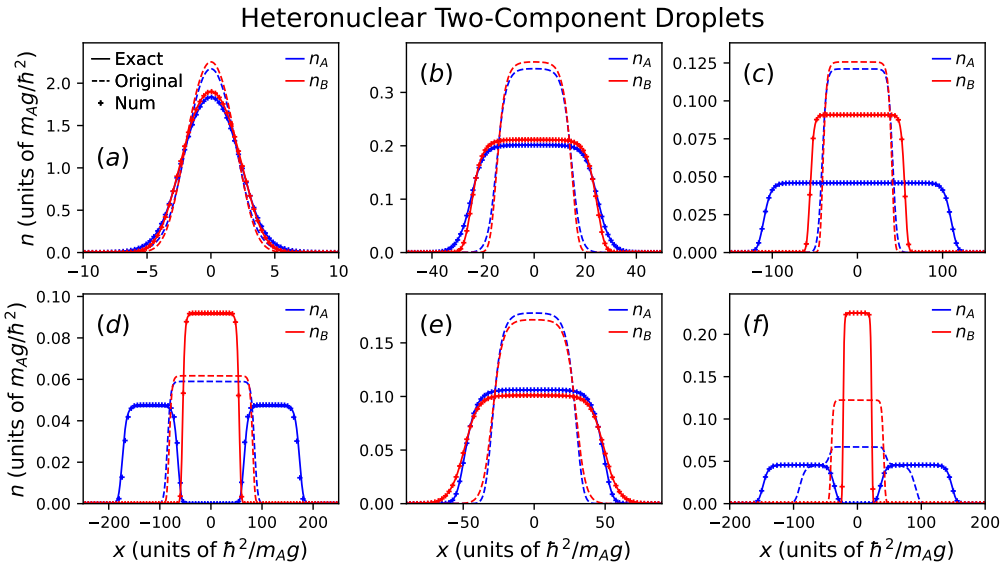

Figure 3: Ground state phases of heteronuclear droplet densities for (a)-(d) $m_B = 2m_A$, (e) $m_B = 0.5m_A$, and (f) $m_B = 5m_A$, whilst $N_A = N_B \equiv N = 10$, $g_A = g_B \equiv g$. The results are obtained within the original mass-balanced eGPEs [Eq. (5)] marked by "Original", the exact mass-balanced eGPEs given by Eq. (14) and indicated as "Exact", and the full numerically calculated heteronuclear eGPEs designated by "Num". In the first two cases, the mass of each component is plugged in the corresponding equation. The heteronuclear systems feature attractive (a) $g_{AB} = -0.8g$, and (b), (e) $g_{AB} = -0.4g$, (c) decoupled, $g_{AB} = 0$, and (d), (f) repulsive $g_{AB} = 0.4g$ intercomponent couplings. Interestingly, there is an excellent agreement between the ground state droplet densities predicted by the mass-balanced exact eGPEs [Eq. (14)] and the fully general numerical approach. Minor deviations are observed for small mass differences and repulsive interactions which are, for instance, hardly visible in panel (d). Conversely, the original eGPEs [Eq. (5)] exhibit significant quantitative disagreement.

end of Sec. 3.1). In this case we observe a relatively small disagreement (hardly visible) with the fully general numerical approach, primarily at the edges of the droplet. As in the case of homonuclear mixtures we enforce parity symmetry, while asymmetric configurations are addressed in Appendix B.

On the other hand, the original eGPEs [Eq. (5)] completely miss this phase-separation behavior, predicting miscible droplets in the repulsive limit, while overestimating (underestimating) as before the droplet peak (width). For completeness, note that by employing a lighter species for component B (e.g. $m_B = 0.5m_A$) results in the same to the above-discussed phenomenology with the droplet configurations reversed while occupying overall larger length scales, compare for instance Fig. 3(b) and (e) with $m_B = 2m_A$ and $m_B = 0.5m_A$ respectively. In general, we find that both the exact (for $m_A = m_B \equiv m$) eGPEs [Eq. (14)] and the full numerical treatment of the heteronuclear mixture do not unveil fundamentally altered droplet configurations with respect to the mass-imbalance. As an example, for $m_B = 0.2m_A$, $0.5m_A$, $2m_A$, or $5m_A$ variations mainly the droplet localization is affected (not shown for brevity). Instead, the original eGPEs [Eq. (5)] exhibit high sensitivity to the mass ratio predicting significantly different behavior, see for instance Fig. 3(d), (f) with $m_B = 0.5m_A$ and $m_B = 5m_A$ where structural deformations are at play.

SciPost SciPost Phys. 19, 133 (2025)

Concluding our investigation on the characterization of 1D two-component droplet setups, it is worth mentioning explicitly that neglecting the LHY correction and hence reducing our description to the standard GPEs the system displays the properties of a uniform gas. This in part stems from the absence of wave collapse in 1D. Indeed, all the droplet structures that we revealed as well as the ones to be discussed in the following Sections are inherently owed to beyond MF effects. This means that they represent a direct manifestation of the involvement of quantum fluctuations as accounted for by the perturbative LHY correction.

4 Three-component mixture

Here, we extend our considerations on the construction of the relevant eGPEs to three-component 1D droplet settings. For their realization, three different states of ^{39}K could be potentially employed. The understanding and properties of such states are largely unexplored in all spatial dimensions [62, 63, 65, 67], while their 1D description through eGPEs taking the appropriate LHY correction is, to the best of our knowledge, missing. Following the standard assumptions, we only consider two-body contact interparticle interactions and restrict the Hamiltonian to include up to bilinear combinations of operators. It is then straightforward to obtain the Hamiltonian for the three-component mixture, by employing the corresponding field operators ($\hat{\Psi}_A(x)$, $\hat{\Psi}_B(x)$, $\hat{\Psi}_C(x)$) as was done in Eq. (6). Along these lines, the three-component Hamiltonian is readily found to be (see also Ref. [62] for the 3D case)

$$\begin{aligned}\hat{\mathcal{H}} = &\frac{g_A N_A^2}{2L} + \frac{g_B N_B^2}{2L} + \frac{g_C N_C^2}{2L} + \frac{g_{AB} N_A N_B}{L} + \frac{g_{AC} N_A N_C}{L} + \frac{g_{BC} N_B N_C}{L} \\ &+ \sum_{k\neq 0}\Big[\Big(\frac{\hbar^2 k^2}{2m_A} + g_A n_A\Big)\hat{a}_k^\dagger \hat{a}_k + \Big(\frac{\hbar^2 k^2}{2m_B} + g_B n_B\Big)\hat{b}_k^\dagger \hat{b}_k + \Big(\frac{\hbar^2 k^2}{2m_C} + g_C n_C\Big)\hat{c}_k^\dagger \hat{c}_k\Big] \\ &+ \frac{1}{2}\sum_{k\neq 0}\Big[g_A n_A\big(\hat{a}_k \hat{a}_{-k} + \hat{a}_k^\dagger \hat{a}_{-k}^\dagger\big) + g_B n_B\big(\hat{b}_k \hat{b}_{-k} + \hat{b}_k^\dagger \hat{b}_{-k}^\dagger\big) + g_C n_C\big(\hat{c}_k \hat{c}_{-k} + \hat{c}_k^\dagger \hat{c}_{-k}^\dagger\big)\Big] \\ &+ g_{AB}\sqrt{n_A n_B}\sum_{k\neq 0}\big(\hat{a}_k \hat{b}_{-k} + \hat{a}_k^\dagger \hat{b}_{-k}^\dagger + \hat{a}_k \hat{b}_k^\dagger + \hat{a}_k^\dagger \hat{b}_k\big) \\ &+ g_{AC}\sqrt{n_A n_C}\sum_{k\neq 0}\big(\hat{a}_k \hat{c}_{-k} + \hat{a}_k^\dagger \hat{c}_{-k}^\dagger + \hat{a}_k \hat{c}_k^\dagger + \hat{a}_k^\dagger \hat{c}_k\big) \\ &+ g_{BC}\sqrt{n_B n_C}\sum_{k\neq 0}\big(\hat{b}_k \hat{c}_{-k} + \hat{b}_k^\dagger \hat{c}_{-k}^\dagger + \hat{b}_k \hat{c}_k^\dagger + \hat{b}_k^\dagger \hat{c}_k\big) + \mathcal{O}(\hat{a}_k^3)\,.\end{aligned} \tag{19}$$

Next, by defining the set of operators $\Phi^\dagger = (\hat{a}_k^\dagger, \hat{b}_k^\dagger, \hat{c}_k^\dagger, \hat{a}_{-k}, \hat{b}_{-k}, \hat{c}_{-k})$, which satisfy the bosonic commutation condition $\mathcal{M}_b = [\Phi, \Phi^\dagger] = \begin{pmatrix} I_3 & 0 \\ 0 & -I_3 \end{pmatrix}$, where I_3 is the 3×3 identity matrix, we can express the Hamiltonian of Eq. (19) in the following bilinear form

$$\begin{aligned}\hat{H} = &\sum_{k>0}\Phi^\dagger H \Phi + \frac{g_A N_A^2}{2L} + \frac{g_B N_B^2}{2L} + \frac{g_C N_C^2}{2L} + \frac{g_{AB} N_A N_B}{L} + \frac{g_{AC} N_A N_C}{L} + \frac{g_{BC} N_B N_C}{L} \\ &- \sum_{k>0}\sum_{\sigma}\Big(\frac{\hbar^2 k^2}{2m_\sigma} + g_\sigma n_\sigma\Big)\,.\end{aligned} \tag{20}$$

The respective Hamiltonian matrix (H), due to its involved form is provided in Appendix A. As it was shown in Sec. 2.2, this Hamiltonian can be diagonalized by solving its characteristic

SciPost Phys. 19, 133 (2025)

equation (see also Eq. (3)) $\det(\mathcal{M}_b H - \omega_k I_6) = 0$, which yields the characteristic polynomial

$$\begin{aligned}\omega^6 - (\epsilon_A^2+\epsilon_B^2+\epsilon_C^2)\omega^4 + \big[\epsilon_A^2\epsilon_B^2+\epsilon_A^2\epsilon_C^2+\epsilon_B^2\epsilon_C^2 - 4(J_{AB}+J_{AC}+J_{BC})\big]\omega^2 \\ + \big[-\epsilon_A^2\epsilon_B^2\epsilon_C^2 + 4(J_{AB}\epsilon_C^2 + J_{AC}\epsilon_B^2 + J_{BC}\epsilon_A^2) - 16\,\mathrm{sgn}(g_{AB}g_{AC}g_{BC})\sqrt{|J_{AB}J_{AC}J_{BC}|}\big] = 0\,.\end{aligned} \tag{21}$$

As expected, it contains the single-component Bogoliubov energies $\epsilon_\sigma^2 = (\frac{\hbar^2k^2}{2m_\sigma})^2 + \frac{\hbar^2k^2}{m_\sigma} g_{\sigma\sigma} n_\sigma$ and $J_{\sigma\sigma'} = \frac{\hbar^2k^2}{2m_\sigma}\frac{\hbar^2k^2}{2m'_\sigma} g^2_{\sigma\sigma'} n_\sigma n_{\sigma'}$ which represents the interspecies coupling contribution.

The roots $(\omega_1^2,\ \omega_2^2,\ \omega_3^2)$ of the characteristic polynomial can be calculated analytically, albeit they have a rather involved form in the general case. Accordingly, the ground state energy becomes

$$\begin{aligned}E_0 = \frac{g_A N_A^2}{2L} + \frac{g_B N_B^2}{2L} + \frac{g_C N_C^2}{2L} + \frac{g_{AB} N_A N_B}{L} + \frac{g_{AC} N_A N_C}{L} + \frac{g_{BC} N_B N_C}{L} \\ + \sum_{k>0}\Big(\omega_1+\omega_2+\omega_3 - \frac{\hbar^2k^2}{2m_A} - \frac{\hbar^2k^2}{2m_B} - \frac{\hbar^2k^2}{2m_C} - g_A n_A - g_B n_B - g_C n_C\Big).\end{aligned} \tag{22}$$

Apparently, already at the MF level, the system is characterized by 12 independent variables spanning the parameter space $(g_{\sigma\sigma'},\, n_\sigma,\, m_\sigma)$. This renders rather challenging the systematic exploration of ensuing phases and development of a unified understanding in the general case. Hence, it is more convenient and instructive (at least for the purpose of this work) to address only certain characteristic cases, both from the MF and even more so from the LHY perspective.

4.1 Fully symmetric mixture

The simplest reduction of the three-component system corresponds to that of a fully symmetric mixture, which can be retrieved by requiring $m_\sigma = m$, $g_{\sigma\sigma} = g$, $g_{\sigma\sigma'} = G$, and $n_\sigma = n$ for every $\sigma \neq \sigma'$. It is important to first examine this reduction since, despite its simplicity, it offers a useful benchmark with the respective single-component droplet system [31, 53], while deviating from it allows to build-up a systematic understanding of the more complex three-component setting. Employing the above-mentioned assumptions from Eq. (22) we can readily obtain the underlying ground state energy density

$$\begin{aligned}\mathcal{E} = \frac{E_0}{L} &= \frac{3gn^2}{2} + 3Gn^2 + \frac{1}{L}\sum_{k>0}\Big(\omega_1+\omega_2+\omega_3 - \frac{3\hbar^2k^2}{2m} - 3gn\Big) \\ &= 3(\frac{g}{2}+G)n^2 \underbrace{- \frac{2(mg^3n^3)^{\frac{1}{2}}}{3\hbar\pi}\Big[(1+\frac{2G}{g})^{\frac{3}{2}} + 2(1-\frac{G}{g})^{\frac{3}{2}}\Big]}_{\mathcal{E}_{\mathrm{LHY}}^{\mathrm{3comp}}},\end{aligned} \tag{23}$$

where $\omega_1 = \omega_2 = \sqrt{\epsilon^2 - 2J}$ and $\omega_3 = \sqrt{\epsilon^2 + 4J}$[4] with Bogoliubov energies $\epsilon^2 = (\frac{\hbar^2k^2}{2m})^2 + \frac{\hbar^2k^2}{m} gn$ and interspecies coupling contribution $J = \frac{\hbar^2k^2}{2m} Gn$. Finally, for convenience we define the dimensionless density independent parameter

$$F(G/g) = \mathcal{E}_{\mathrm{LHY}}^{\mathrm{3comp}} / \sqrt{mg^3n^3\hbar^{-2}} = -\frac{2}{3\pi}\Big[(1+2G/g)^{3/2} + 2(1-G/g)^{3/2}\Big] < 0\,.$$

Note that as long as $-g/2 \leq G \leq g$ (which corresponds to the MF stability regime as discussed in Appendix A) the eigenvalues ω_i are real. Also, in line with the two-component case, the

[4] These are the solutions of the reduced characteristic polynomial equation

$$\omega^6 - 3\epsilon^2\omega^4 + (3\epsilon^4 - 12J^2)\omega^2 + (-\epsilon^6 + 12\epsilon^2J^2 - 16J^3) = 0\,.$$

SciPost Phys. 19, 133 (2025)

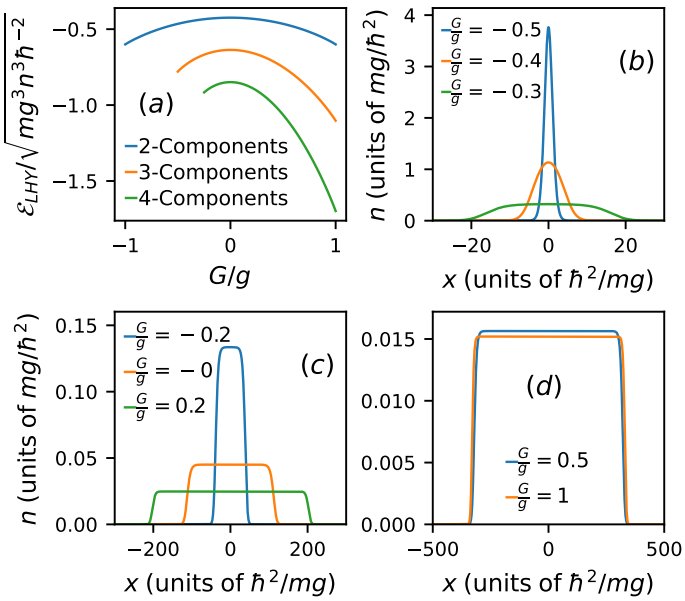

Figure 4: (a) The behavior of the LHY energy for the symmetric mixture stemming from a reduction of the genuine two-, three- and four-component settings as a function of the intercomponent interaction G. (b)-(d) Ground state densities of a fully symmetric three-component mixture with $N = 10$ for varying interaction G (see legends). A transition from a Gaussian to a FT profile with increasingly larger spatial extent, upon reducing the attraction [panels (b), (c)] or increasing repulsion [panels (c), (d)] is evident.

symmetric three-component mixture reduces to an effectively single-component one. This effectively single-component system, however, depends on two interaction parameters, namely g and G. It is inherently different from the corresponding single field reduction stemming from the two-component setup exclusively due to the respective LHY corrections (see the discussion below).

The LHY energy of this reduced system, again remains $\sim n^{3/2}$ throughout the MF stability regime $G \in [-g/2, g]$. Moreover, the density independent proportionality factor ranges from $F(G/g) = -\sqrt{6}/\pi$ for $G = -g/2$, to $F(G/g) = -2\sqrt{3}/\pi$ for $G = g$, while it takes its maximum $F(G/g) = -2/\pi$ value at $G = 0$, as shown in Fig. 4(a). Interestingly, the strength of quantum fluctuations appears to be larger close to the immiscibility threshold $G = g$ as compared to the one close to the droplet regime $G = -g/2$, as evidenced by the more strongly attractive LHY energy (see e.g. Fig. 4(a) and Eq. (23)). This is in contrast to the two-component mixture where quantum fluctuations contribute equally at the two limits, see in particular Fig. 1(e) and Eq. (13). We attribute this behavior of the three-component system to the aforementioned "asymmetric" MF stability regime (see also Appendix A for a more elaborated discussion on its asymmetric nature).

On the other hand, the MF interaction term vanishes at the droplet threshold $G \approx -g/2$, while it takes its maximum value at the immiscibility threshold $g = G$. Hence, it is not *a-priori* obvious how important the role of the LHY correction becomes at each limit (e.g. from Eq. (23)) and one has to solve the corresponding eGPE, as we shall do below. Finally, it is interesting to note that in the fully symmetric case the corresponding LHY energy of the original three-component mixture is always smaller than the one of the reduced two-component

SciPost Phys. 19, 133 (2025)

system, namely it holds that $\left|\mathcal{E}_{\rm LHY}^{\rm 3comp}\right| \geq \frac{3}{2}\left|\mathcal{E}_{\rm LHY}^{\rm 2comp}\right|$ with the equality being valid for $G = 0$. As such, it appears that the effect of quantum fluctuations is enhanced in the case of a three-component mixture, even beyond the additive effect owing to the additional component, due to the interspecies coupling. Instead, for the MF energy it holds that $\mathcal{E}_{\rm MF}^{\rm 3comp}/3 = \mathcal{E}_{\rm MF}^{\rm 2comp}/2$, i.e. the ratio of the MF energy divided by the number of components remains constant for any number of components in the symmetric case.

To obtain the effective single-component eGPE equation emanating from the fully symmetric three-component mixture we evaluate the Euler-Lagrange equations (from Eq. (23)) with respect to n. This standard procedure leads to the symmetric eGPE:

$$3i\hbar\frac{\partial\Psi}{\partial t} = -3\frac{\hbar^2}{2m}\frac{\partial^2\Psi}{\partial x^2} + 3(g+2G)|\Psi|^2\Psi + F(G/g)\frac{3\sqrt{mg^3}}{2\hbar}|\Psi|\Psi\,. \tag{24}$$

Similarly to the case of a symmetric two-component mixture, this symmetric eGPE accepts a droplet solution with saturation density $n_s = F^2(G/g)\frac{mg^3}{9\hbar^2(2G+g)^2}$, energy density $\mathcal{E}^{3comp}(n=n_s) = -\frac{3}{2}(g+2G)n_s^2$, chemical potential $\mu_s = -\frac{3}{2}(g+2G)n_s$, and healing length $\xi = \sqrt{-\frac{3\hbar^2}{2m\mu_s}} = \sqrt{\frac{9\hbar^4(g+2G)}{m^2g^3F^2(G/g)}} = \sqrt{\frac{\hbar^2}{m(g+2G)n_s}}$. Again, in accordance with the two-component symmetric mixture, the ground state density of the symmetric three-component system transits from a Gaussian-type profile (for $G \approx -1/2g$) to a FT one for decreasing intercomponent attraction as captured by the G coefficient. This behavior is explicitly illustrated in Fig. 4(b) for a fixed atom number.[5] Additionally, the ground state density maintains its FT character throughout the repulsive interaction regime, $G > 0$, see Fig. 4(c) and (d). The saturation density [width] decreases [increases] by over an order of magnitude as $G \approx g$, eventually acquiring the minimum saturation density $n_s(G=g) = \frac{4mg}{27\pi^2\hbar^2} \approx 0.015$ deep in the repulsive interaction regime as can be seen in Fig. 4(d).

4.2 Two identical components

As it was argued above, already in the limiting case of a fully symmetric three-component mixture evident differences arise (concerning, for instance, the droplet saturation density, and the LHY correction) when compared to the corresponding reduced two-component system. However, by construction three-component mixtures offer additional possibilities for intercomponent asymmetry, that could lead to intriguing phenomena and phases that can not be captured within the two-component setting. A step forward to delve more into the three-component properties is to consider a system where two of the components are identical (i.e. symmetric), while the third one is different. To be concrete, this situation is described by $m_A = m_B \equiv m$, $g_A = g_B \equiv g$, and $g_{AC} = g_{BC} \equiv G_C$, while g_{AB} and g_C are unrestricted parameters, see also Ref. [62] for the 3D case.

In this scenario, it can be found that the MF stability requires the following conditions to be fulfilled: i) $g, g_C > 0$, ii) $gg_C > G_C^2$, and $g > |g_{AB}|$ as well as iii) $G_C^2 < \frac{g_C}{2}(g+g_{AB})$, see also Appendix A for further details. We remark that the same conditions hold for the respective 3D system as reported in Ref. [62], which is to be expected because the homogeneous MF energy is independent of the dimensionality. It is also important to emphasize that the last (iii) condition is more restrictive than the second (ii) one since $g_C(g+g_{AB})/2 \leq gg_C$ if $|g_{AB}| < g$. As a consequence, it is possible for each pair of subsystems to be stable, while the overall system is outside the MF stability region, a behavior that equally holds in 3D [62]. For simplicity, here, we focus on interaction intervals where each subsystem and the overall mixture reside within the MF stability region.

[5] Similarly, for fixed interactions the FT transition occurs for increasing particle number (e.g. at $N \geq 30$ for $G = -0.4g$).

SciPost SciPost Phys. 19, 133 (2025)

Further assuming that $m_C = m$ (for convenience), we find that the LHY energy density for the general three-component system in Eq. (22) takes the form

$$\mathcal{E}_{\rm LHY} = -\frac{\sqrt{2m}}{6\hbar\pi}\Big((2(g-g_{AB})n)^{\frac{3}{2}} + (W+Q)^{\frac{3}{2}} + (W-Q)^{\frac{3}{2}}\Big), \tag{25}$$

with the parameters

$$Q = \Big((g+g_{AB})^2 n^2 - 2(g+g_{AB})g_C n n_C + 8G_C^2 n n_C + g_C^2 n_C^2\Big)^{\frac{1}{2}}, \tag{26a}$$

$$W = gn + g_{AB}n + g_C n_C\,. \tag{26b}$$

The LHY energy density is real and negative as long as $g > |g_{AB}|$ and $W - Q > 0 \longrightarrow 2G_C^2 < g_C(g+g_{AB})$, which is exactly the MF stability regime, while it becomes complex otherwise. Moreover, by removing the third component namely setting $G_C = g_C = n_C = 0$, it holds that $Q = W = (g+g_{AB})n$ and the LHY energy density becomes $\mathcal{E}_{\rm LHY} = \frac{-2\sqrt{m}(gn)^{3/2}}{3\hbar\pi}[(1-g_{AB}/g)^{3/2} + (1+g_{AB}/g)^{3/2}]$. This is exactly the LHY energy density of the symmetric two-component mixture in the MF stability regime (see Eq. (12) for $g_A = g_B \equiv g$ and $n_A = n_B \equiv n$).

As in Sec. 3.1, we can derive the LHY terms of the effective two-component eGPEs describing the system by calculating their partial derivatives

$$\frac{\partial \mathcal{E}_{\rm LHY}}{\partial n} = -\frac{\sqrt{2m}}{4\pi h}\Big(\Big(g+g_{AB}+\frac{Z}{Q}\Big)\sqrt{W-Q} + \Big(g+g_{AB}-\frac{Z}{Q}\Big)\sqrt{W+Q} + 2\sqrt{2}(g-g_{AB})^{\frac{3}{2}}\sqrt{n}\Big), \tag{27a}$$

$$\frac{\partial \mathcal{E}_{\rm LHY}}{\partial n_C} = -\frac{\sqrt{2m}}{4\pi h}\Big(\Big(g_C+\frac{P}{Q}\Big)\sqrt{W-Q} + \Big(g_C-\frac{P}{Q}\Big)\sqrt{W+Q}\Big), \tag{27b}$$

where

$$Z = -\frac{1}{2}\frac{\partial Q^2}{\partial n} = -g^2 n - 2g g_{AB} n + g g_C n_C - g_{AB}^2 n + g_{AB} g_C n_C - 4G_C^2 n_C\,, \tag{28a}$$

$$P = -\frac{1}{2}\frac{\partial Q^2}{\partial n_C} = g g_C n + g_{AB} g_C n - 4G_C^2 n - g_C^2 n_C\,. \tag{28b}$$

These LHY terms are incorporated in the corresponding eGPEs, which by additionally requiring $\Psi_A = \Psi_B \equiv \Psi$, read

$$2i\hbar\frac{\partial \Psi}{\partial t} = -\frac{\hbar^2}{m}\frac{\partial^2 \Psi}{\partial x^2} + \Big(2(g+g_{AB})|\Psi|^2 + 2G_C|\Psi_C|^2 + \frac{\partial \mathcal{E}_{\rm LHY}}{\partial n}\Big)\Psi\,, \tag{29a}$$

$$i\hbar\frac{\partial \Psi_C}{\partial t} = -\frac{\hbar^2}{2m}\frac{\partial^2 \Psi_C}{\partial x^2} + \Big(g_C|\Psi_C|^2 + 2G_C|\Psi|^2 + \frac{\partial \mathcal{E}_{\rm LHY}}{\partial n_C}\Big)\Psi_C\,. \tag{29b}$$

A few characteristic examples of the resulting ground state droplet configurations are presented in Fig. 5, with fixed $g_C = g$, and $g_{AB} = -0.5g$. Specifically, the case of $G_C = -0.5g$ refers to the respective LHY-fluid limit (attained in general here for $G_C = -g/2$ due to MF stability requirements) of the fully symmetric mixture where MF interactions cancel out. Here, the individual components become identical and possess a Gaussian type distribution, see Fig. 5(a). As we decrease the intercomponent attraction, the system transitions to a mixed state where the symmetric components (A, B) exhibit a FT configuration and the third one (C) becomes significantly distorted and delocalizes. Particularly, there is a FT droplet segment lying within the symmetric components and the remaining atoms of the third component reside outside this region in a self-bound state as shown in Fig. 5(b), (c). However, by switching-off the intercomponent interactions among the symmetric components and the third one, i.e. reaching the decoupling limit with $G_C = 0$, the subsystems feature two independent droplet structures [Fig. 5(d)].

SciPost Phys. 19, 133 (2025)

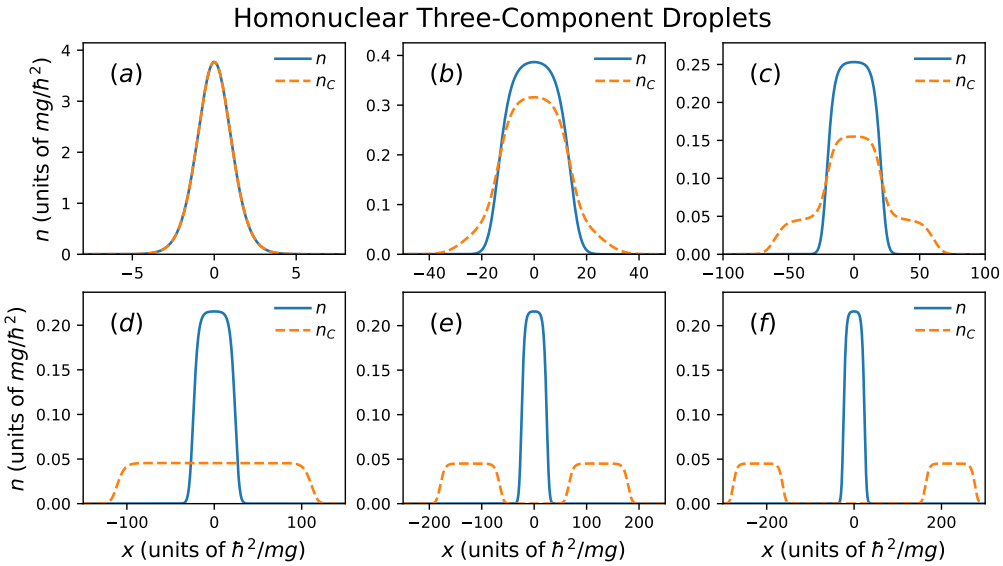

Figure 5: Droplet density configurations arising in a homonuclear three-component mixture for varying interspecies couplings $g_{AC} = g_{BC} \equiv G_C$. The latter range from the attractive (a) $G_C = -0.5g$, (b) $G_C = -0.2g$, (c) $G_C = -0.1g$, to (d) the decoupled $G_C = 0$, and (e) the repulsive $G_C = 0.1g$, (f) $G_C = 0.4g$ interaction regimes, thus covering the available parametric space. As it can be seen, mixed phases exhibiting a structurally deformed third component having both a droplet core and self-bound atoms at the tails [panel (c)] for weak intercomponent attractions or a configuration of two fully distinct droplets [panel (d)] in the decoupled regime occur. Also, an early onset of the miscible-to-immiscible transition, coexisting with droplet configurations, similarly to the two-component mixture takes place for repulsive intercomponent couplings. In all cases, the remaining system parameters are held fixed and in particular correspond to $N_A = N_B = N_C = 10$, $m_A = m_B = m_C \equiv m$, $g_A = g_B = g_C \equiv g$, and $g_{AB} = -0.5g$.

On the other hand, turning to the repulsive side of the MF stability regime (e.g. for $G_C = 0.1g$, or $G_C = 0.4g$), it turns out that the third component progressively separates from the symmetric two-component droplet and accommodates two smaller sized droplets on either side of the symmetric two-component droplet which remains localized at the center [Fig. 5(e), (f)] (see also Appendix B for the parity asymmetric configurations). Finally, it is important to emphasize that the above-described investigation is far from being exhaustive for the three-component system. A more detailed examination of the emerging droplet states and mixed phases of matter e.g. by varying N_C, g_C, g_{AB}, and G_C across the MF stability regime is certainly an interesting direction to be pursued in future studies.

5 Four-component mixture

As can be deduced from the above analysis, in order to obtain the ground state energy of the quasi-particle vacuum one needs to diagonalize the Hamiltonian matrix which has $2 \times n$ dimensions, with n representing the number of bosonic species. Due to the symmetries of the Hamiltonian (e.g. being a real Hermitian matrix) the resulting characteristic equation is

SciPost SciPost Phys. 19, 133 (2025)

a polynomial of degree n, with respect to the eigenvalues ω^2. Therefore, the four-component mixture is the most complex system for which the characteristic equation can be analytically solved and hence extract its LHY energy. For higher-component settings the characteristic equation can only be solved numerically in the general case. As such, for completeness, we present below the LHY energy for the four-component mixture, even though such a setup would be arguably more challenging to be experimentally realized.

The process for deriving the energy of the four-component mixture is identical to the ones of the two- (Sec. 3) and three- (Sec. 4) component ones described above. For brevity, we provide directly the resulting characteristic polynomial

$$\omega^8 + \alpha\omega^6 + \beta\omega^4 + \gamma\omega^2 + \delta = 0\,, \tag{30}$$

containing the rather involved coefficients

$$\alpha = -\sum_{\sigma} \epsilon_{\sigma}^2\,, \tag{31a}$$

$$\beta = \sum_{\sigma=A}^{D}\sum_{\sigma'>\sigma}^{D}\left(\epsilon_{\sigma}^2\epsilon_{\sigma'}^2 - 4J_{\sigma\sigma'}\right), \tag{31b}$$

$$\gamma = \sum_{\sigma}^{D}\Bigg[-\epsilon_{\sigma}^2\Bigg[\sum_{\sigma'>\sigma}^{D}\sum_{\sigma''>\sigma'}^{D}\epsilon_{\sigma'}^2\epsilon_{\sigma''}^2 + 4\sum_{\sigma'\neq\sigma}^{D}\sum_{\sigma''>\sigma',\sigma''\neq\sigma}^{D} J_{\sigma'\sigma''}\Bigg] + 16\prod_{\sigma'\neq\sigma,\sigma'<\sigma''}\mathrm{sgn}\left(g_{\sigma'\sigma''}\right)\sqrt{J_{\sigma'\sigma''}}\Bigg], \tag{31c}$$

$$\delta = \prod_{\sigma}\epsilon_{\sigma}^2 - 4\sum_{\mathcal{P}}\left[\left(\epsilon_{\sigma_1}^2\epsilon_{\sigma_2}^2 - 4J_{\sigma_1\sigma_2}\right)J_{\sigma_3\sigma_4}\right] + 16\sum_{\sigma}\epsilon_{\sigma}^2\prod_{\sigma_{i,j}\neq\sigma,\sigma_i<\sigma_j}\frac{\sqrt{|J_{\sigma_i\sigma_j}|}}{\mathrm{sgn}\left(g_{\sigma_i\sigma_j}\right)} - 32\frac{\sqrt{|J_{AC}J_{AD}J_{BC}J_{BD}|}}{\mathrm{sgn}\left(g_{AC}g_{AD}g_{BC}g_{BD}\right)} - 32\frac{\sqrt{|J_{AB}J_{AD}J_{BC}J_{CD}|}}{\mathrm{sgn}\left(g_{AB}g_{AD}g_{BC}g_{CD}\right)} - 32\frac{\sqrt{|J_{AB}J_{AC}J_{BD}J_{CD}|}}{\mathrm{sgn}\left(g_{AB}g_{AC}g_{BD}g_{CD}\right)}, \tag{31d}$$

where $\epsilon_{\sigma}^2 = (\frac{\hbar^2k^2}{2m_\sigma})^2 + \frac{\hbar^2k^2}{m_\sigma}g_{\sigma\sigma}n_\sigma$ are the single component Bogoliubov energies and $J_{\sigma\sigma'} = \frac{\hbar^2k^2}{2m_\sigma}\frac{\hbar^2k^2}{2m'_\sigma}g_{\sigma\sigma'}^2 n_\sigma n_{\sigma'}$ the interspecies coupling contributions. The notation $\mathcal{P}$ in the sums refers to all possible permutations of $\sigma_1, \sigma_2, \sigma_3, \sigma_4$ such that $\sigma_1 < \sigma_2$, and $\sigma_3 < \sigma_4$ and thus index duplication is avoided.

The solutions (ω_i) of the characteristic polynomial equation can be calculated exactly and the resulting ground state energy for the four-component quasi-particle vacuum reads

$$E_0 = \sum_{\sigma}\frac{g_{\sigma\sigma}N_\sigma^2}{2L} + \frac{1}{2}\sum_{\sigma\neq\sigma'}\frac{g_{\sigma\sigma'}N_\sigma N'_\sigma}{L} + \sum_{k>0}\Bigg[\sum_{i=1}^{4}\omega_i - \sum_{\sigma}\left(\frac{\hbar^2k^2}{2m_\sigma} + g_{\sigma\sigma}n_\sigma\right)\Bigg]. \tag{32}$$

It is apparent that for this setup the parametric space as defined by the different intra- and inter-component coupling combinations, the atom number and mass of each component becomes exceedingly large. While a systematic study of this system is interesting on its own right, in what follows we restrict ourselves to the relatively simpler case of the symmetric mixture.

SciPost Phys. 19, 133 (2025)

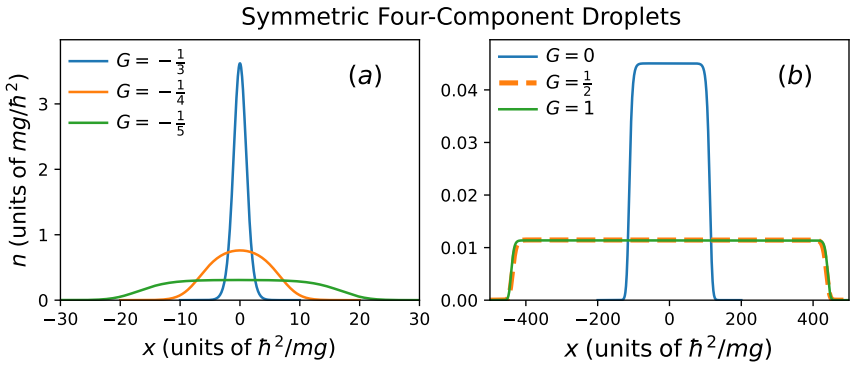

Figure 6: Ground state droplet densities within a fully symmetric four-component mixture with different intercomponent couplings G (see legend) and fixed $N = 10$. The transition from a Gaussian-like to a FT profile takes place, upon reducing attraction [panel (a)] while for increasing repulsion [panel (b)], the droplets maintain their FT structure and exhibit increasingly larger spatial widths.

5.1 Symmetric four-component mixture

Let us consider a fully symmetric four-component mixture characterized by $N_\sigma \equiv N$, $g_{\sigma\sigma} \equiv g$, and $g_{\sigma\sigma'} \equiv G_4$. Here, the MF energy (first two sums of Eq. (32)) reduces to $\mathcal{E}^{4\text{comp}}_{\text{MF}} = (2g + 6G_4)n^2$, whilst the MF stability regime is given by $-g/3 < G_4 < g$, ensuring the stability of each subsystem but also of the full four component mixture. Accordingly, the roots of the characteristic polynomial of Eq. (30) simplify to $\omega^2_{1,2,3} = \epsilon^2 - G_4\frac{\hbar^2k^2}{m}n$, and $\omega^2_4 = \epsilon^2 + 3G_4\frac{\hbar^2k^2}{m}n$ and the LHY energy density becomes

$$\mathcal{E}^{4\text{comp}}_{\text{LHY}} = -\frac{2\sqrt{mg^3n^3}}{\pi\hbar}\left(\left(1-\frac{G_4}{g}\right)^{\frac{3}{2}} + \frac{1}{3}\left(1+3\frac{G_4}{g}\right)^{\frac{3}{2}}\right). \tag{33}$$

As in the case of the symmetric two-component mixture [Sec. 3.1], the emergent droplet solution can be shown to have saturation density $n_s = \frac{mg^3}{4\pi^2\hbar^2(3G_4+g)^2}\left((1-\frac{G_4}{g})^{3/2}+\frac{1}{3}(1+3\frac{G_4}{g})^{3/2}\right)$, energy density $\mathcal{E}^{4\text{comp}}(n{=}n_s) = -2(g+3G_4)n_s^2$, chemical potential $\mu_s = -2(g+3G_4)n_s$, and healing length $\xi = \sqrt{-\frac{\hbar^2}{2m\mu_s}} = \sqrt{\frac{\hbar^2}{4m(g+3G_4)n_s}}$. Moreover, similarly to the three-component setup, the LHY energy of the fully symmetric four-component mixture is always smaller than twice the LHY energy of the corresponding symmetric two-component system, namely $\mathcal{E}^{4\text{comp}}_{\text{LHY}} \leq 2\mathcal{E}^{2\text{comp}}_{\text{LHY}}$ with the equality being valid for $G_4 = 0$. This implies the presence of enhanced quantum fluctuations in the symmetric four-component system, see also Fig. 4(a), beyond an additive contribution. On the other hand, for the MF energies it holds that $\mathcal{E}^{4\text{comp}}_{\text{MF}} = 2\mathcal{E}^{2\text{comp}}_{\text{MF}}$. Representative ground state droplet profiles of the reduced four-component setting are illustrated in Fig. 6 for different intercomponent couplings (G_4) and fixed intracomponent ones. In line with the behavior of the droplets arising in lower-component mixtures also here a deformation from a Gaussian to a FT density profile occurs for decreasing intercomponent attractions as depicted in Fig. 6(a). Finally, at the repulsive side, increasing the intercomponent interaction across the MF stability regime results in quantum droplet structures of significantly larger spatial width, as shown in Fig. 6(b).

SciPost SciPost Phys. 19, 133 (2025)

6 Conclusions and future directions

We derived, in a systematic manner, the first-order beyond mean-field LHY quantum correction and associated eGPEs for two-, three- and four-component 1D bosonic mixtures featuring short-range contact interactions. The four-component system represents the highest multicomponent setting for which the LHY energy can be analytically derived in the general case. In all cases, whenever the complexity of the system allows corresponding closed form expressions are provided. Importantly, our treatment relies only on the assumption of a dilute gas such that the perturbative Bogoliubov treatment is valid. Hence, the LHY energies and the ensuing eGPEs obtained are reliable throughout the MF stability regime, namely from the attractive to the repulsive intercomponent interaction regimes in contrast to previous treatments.

Focusing on the two-component mixture, we extracted closed form solutions for the LHY energy and constructed the corresponding exact coupled system of eGPEs for homonuclear settings but also provided numerical results for heteronuclear 1D systems. Specifically, by tuning the intercomponent interactions towards smaller attractions, we retrieve the structural deformation of the droplets from Gaussian to FT density configurations. However, it is explicated that the previously discussed original two-component LHY treatment reveals quantitative deviations as compared to our exact eGPE results and can be obtained as a limiting case from the exact expressions presented herein. These deviations are reflected by an increased saturation droplet density and decreasing width. Turning to repulsive interactions, we identify even more significant qualitative differences with the original LHY treatment, especially for heteronuclear settings featuring intercomponent mass-imbalance. In particular, self-bound structures with decreasing saturation densities are found for larger intercomponent repulsions, while an early onset of phase-separation occurs for both homonuclear and heteronuclear mixtures. The numerically computed heteronuclear droplet states are found to be in good agreement with the results of the exact eGPEs for homonuclear settings upon direct substitution of the different masses. Meanwhile, the original eGPEs fail to adequately capture the droplet densities.

Additionally, exact closed form expressions of the LHY energies and the eGPEs are discussed for three-component mixtures especially in the cases of i) a fully-symmetric system and ii) two identical components coupled to a third independent one. It is argued that the LHY energy is not additive to the number of components and it is in general larger for three-component setups as compared to two-component ones. A plethora of droplet phases exist, ranging from the underlying LHY-fluid limit, to Gaussian miscible droplet components as well as to mixed states for decreasing attraction. These mixed states refer to FT configurations for the symmetric components and a delocalized droplet distribution for the third one. The latter assembles in a FT droplet segment within the symmetric components and the remaining atoms lying beyond the intercomponent overlap region are in a self-bound state. Instead, for repulsive interactions the third component phase separates from the symmetric two-component droplet and exhibits two smaller sized droplets on either side. Finally, a closed LHY form is also provided for the fully symmetric four-component mixture. Here, the transition from Gaussian to FT droplets for decreasing attraction and afterwards to large spatial FT structures upon crossing to the repulsive intercomponent regime is observed.

There are several intriguing pathways to be followed in the future based on our work which provides the first steps towards exploring ground state multicomponent droplet configurations. A straightforward extension is to systematically study the transition towards phase-separation in heteronuclear mass-imbalanced two-component mixtures and unveil the origin of this mechanism. Similarly, the three- and four-component mixtures offer completely unexplored possibilities to create exotic droplet configurations. These include, for instance, miscible spatially deformed droplet structures, and importantly mixed droplet phases thereof as well as droplet-soliton [76] or droplet-vortex [36] coexistence. The interpolation of three-component droplet

SciPost Phys. 19, 133 (2025)

states to the few-body regime using sophisticated numerical schemes is also of particular interest [77–79]. On the other hand, dynamical crossing of these droplet phases is expected to reveal insights into their collective excitations and the spontaneous generation of nonlinear defects or delocalized structures such as shock-waves [80, 81]. Along these lines, emulating the time-of-flight measurement process of multicomponent droplet states in order to testify their self-bound nature is certainly worth pursuing. Finally, extending our treatment to 3D geometries in order to investigate the impact of the LHY term beyond the MF stability edge as well as in the presence of external potentials are very relevant open questions to address.

Acknowledgments

The authors thank P. G. Kevrekidis, G. Bougas and G.C. Katsimiga for extensive discussions on the topic of droplets.

Funding information S.I.M acknowledges support from the University of Missouri Science and Technology, Department of Physics, Startup fund.

A Details on the stability conditions of the three-component mixture

The Hamiltonian matrix for the three-component mixture used in Eq. (20) of the main text takes the form

$$H=\begin{pmatrix} \frac{\hbar^2k^2}{2m_A}+g_An_A & g_{AB}\sqrt{n_An_B} & g_{AC}\sqrt{n_An_C} & g_An_A & g_{AB}\sqrt{n_An_B} & g_{AC}\sqrt{n_An_C} \\ g_{AB}\sqrt{n_An_B} & \frac{\hbar^2k^2}{2m_B}+g_Bn_B & g_{BC}\sqrt{n_Bn_C} & g_{AB}\sqrt{n_An_B} & g_Bn_B & g_{BC}\sqrt{n_Bn_C} \\ g_{AC}\sqrt{n_An_C} & g_{BC}\sqrt{n_Bn_C} & \frac{\hbar^2k^2}{2m_C}+g_Cn_A & g_{AC}\sqrt{n_An_C} & g_{BC}\sqrt{n_Bn_C} & g_Cn_C \\ g_An_A & g_{AB}\sqrt{n_An_B} & g_{AC}\sqrt{n_An_C} & \frac{\hbar^2k^2}{2m_A}+g_An_A & g_{AB}\sqrt{n_An_B} & g_{AC}\sqrt{n_An_C} \\ g_{AB}\sqrt{n_An_B} & g_Bn_B & g_{BC}\sqrt{n_Bn_C} & g_{AB}\sqrt{n_An_B} & \frac{\hbar^2k^2}{2m_B}+g_Bn_B & g_{BC}\sqrt{n_Bn_C} \\ g_{AC}\sqrt{n_An_C} & g_{BC}\sqrt{n_Bn_C} & g_Cn_C & g_{AC}\sqrt{n_An_C} & g_{BC}\sqrt{n_Bn_C} & \frac{\hbar^2k^2}{2m_C}+g_Cn_A \end{pmatrix}.$$

Before exploring the LHY term in more detail, it is important to determine the MF stability regime. In general, the stability condition is given by demanding that the Hessian matrix (*Hess*) in terms of derivatives with respect to the densities ($Hess_{\sigma,\sigma'}=\frac{\partial^2\mathcal{E}_{\rm MF}}{\partial n_\sigma\partial n_{\sigma'}}$) has only positive eigenvalues [5]. Namely, the Hessian matrix in our case reads

$$Hess=\begin{pmatrix} g_A & g_{AB} & g_{AC} \\ g_{AB} & g_B & g_{BC} \\ g_{AC} & g_{BC} & g_C \end{pmatrix}, \tag{A.1}$$

with eigenvalues dictated by the roots of the characteristic polynomial

$$f(x)=x^3-x^2\sum_\sigma g_{\sigma\sigma}+x\sum_{\sigma<\sigma'}\Delta g_{\sigma\sigma'}+C\,. \tag{A.2}$$

In this expression, $\Delta g_{\sigma\sigma'}=g_\sigma g_{\sigma'}-g_{\sigma\sigma'}^2$ and $C=g_Ag_{BC}^2+g_Bg_{AC}^2+g_Cg_{AB}^2-g_Ag_Bg_C-2g_{AB}g_{AC}g_{BC}$. Note that the stability of the individual components requires $\Delta g_{\sigma\sigma'}>0$ (and $g_{\sigma\sigma}>0$) for all

SciPost SciPost Phys. 19, 133 (2025)

components. Then, MF stability requires

$$\begin{aligned}
&[1.] \quad g_{\sigma\sigma} > 0\,, \\
&[2.] \quad \Delta g_{\sigma\sigma'} > 0\,, \\
&[3.] \quad C < 0\,, \\
&[4.] \quad \frac{1}{3}\sum_{\sigma} g_{\sigma\sigma} - \sqrt{\Delta} > 0\,, \quad \text{where } \Delta = \sum_{\sigma} g_{\sigma\sigma}^2 + \sum_{\sigma\neq\sigma'} (g_{\sigma\sigma'}^2 - \Delta g_{\sigma\sigma'}/2)\,, \\
&[5.] \quad f\Big(\frac{\sum_\sigma g_{\sigma\sigma} - \sqrt{\Delta}}{3}\Big) \geq 0\,, \quad \text{and } f\Big(\frac{\sum_\sigma g_{\sigma\sigma} + \sqrt{\Delta}}{3}\Big) \leq 0\,.
\end{aligned} \tag{A.3}$$

In particular, the last two conditions guarantee the existence of three real solutions. However, the Hessian matrix (Eq. (A.1)) is a real and symmetric (normal) matrix, and hence it is guaranteed to be diagonalizable. As such, the characteristic polynomial (Eq. (A.2)) is already guaranteed to have three real roots by construction and we do not need to check the (rather complicated) conditions [5.] explicitly. Finally, condition [4.] is automatically satisfied as long as condition [2.] holds.

In the case of two symmetric components (i.e., $g_A = g_B = g$) coupled to the third component with the same interaction strength (namely $g_{AC} = g_{BC} = G_C$) the characteristic polynomial of the Hessian matrix becomes

$$f(x) = x^3 - x^2(2g + g_C) + x(g^2 - 2G_C^2 - 2g g_C - g_{AB}^2) + [2G_C^2 g - 2G_C^2 g_{AB} - g^2 g_C + g_{AB}^2 g_C]\,. \tag{A.4}$$

Therefore, MF stability for these three-component mixtures requires

$$\begin{aligned}
&[1.] \quad g > 0\,, \quad \text{and} \quad g_C > 0\,, \\
&[2.] \quad |g_{AB}| > g\,, \quad \text{and} \quad g g_C > G_C^2\,, \\
&[3.] \quad G_C^2 < \frac{g_C}{2}(g + g_{AB})\,.
\end{aligned} \tag{A.5}$$

For the case of the fully symmetric mixture i.e. $g_A = g_B = g_C = g$ and $g_{AB} = g_{AC} = g_{BC}$, the system is significantly simplified and the MF stability requires $-g/2 < G < g$. Evidently, the MF stability window becomes reduced compared to the respective two-component one, given by $-g < g_{AB} < g$ as discussed in Sec. 3.1, and asymmetric with respect to the sign of the inter-species interaction strength. An intuitive explanation for this phenomenology is the following. Consider a mixture consisting of $\mathcal{N}$ identical components with N particles per component, featuring intracomponent interactions $g_\sigma = g$ and intercomponent ones $g_{\sigma\sigma'} = G$, for all σ, σ'. Ignoring any complications stemming from the exchange statistics and distinguishability, a particle of species σ may scatter from $N-1$ σ-species particles with strength g and $(\mathcal{N}-1)N$ atoms of other components with strength G. Hence we expect that, on average, the intracomponent interaction strength will be suppressed by a factor of $\mathcal{N}-1$ (assuming $N \gg 1$) compared to the intercomponent one, yielding an average interaction strength $\propto (G + \frac{g}{\mathcal{N}-1})$. We anticipate the stability of this effective single-component mixture to be ensured as long as its average interaction strength is repulsive (i.e. $G \geq -\frac{g}{\mathcal{N}-1}$), since the effective single-component picture does not impose any limitations at the repulsive side. Indeed this pattern appears to hold for $\mathcal{N} = 2$, (see Sec. 3.1) $\mathcal{N} = 3$, (see Sec. 4.1) and $\mathcal{N} = 4$ (see Sec. 5.1), where the lower stability bound corresponds to $G \geq -g$, $G \geq -g/2$, and $G \geq -g/3$ respectively. On the other hand, the only upper bound imposed to the intercomponent interaction strength G, stems from the stability of its sub-systems which requires $G < g$ regardless of the number of components. This means that at the repulsive side all components will either be stable and fully overlap or all components will be mutually unstable and phase separate from all other components. A hypothetical partially phase separated configuration, with $\mathcal{M}$ overlapping components in one cluster and $\mathcal{N}-\mathcal{M}$ in the other, would feature average intra-cluster

SciPost Phys. 19, 133 (2025)

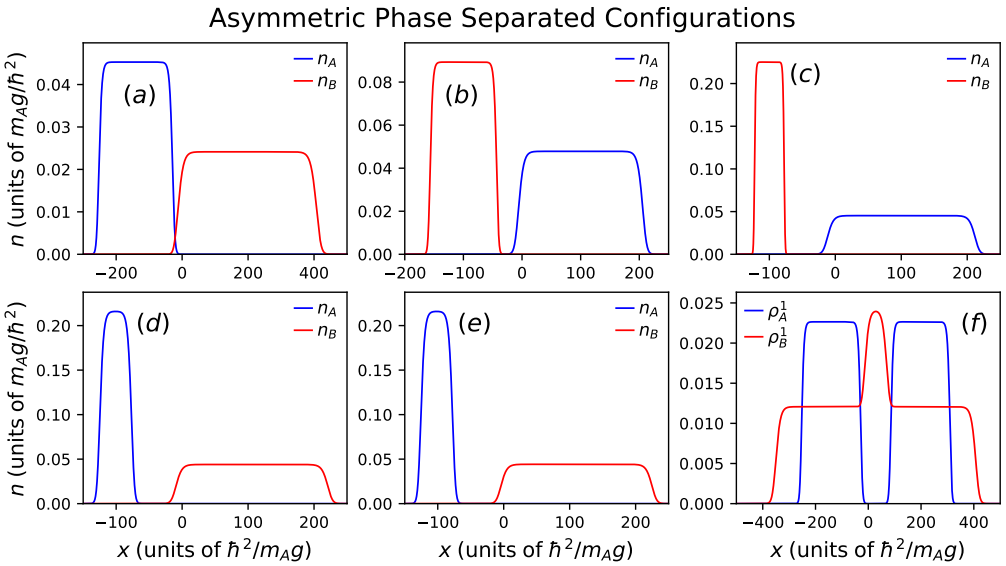

Figure 7: Parity asymmetric density configurations corresponding to (a) a homonuclear two-component mixture with interaction strengths $g_B = 0.5g_A$ and $g_{AB} = 0.4g_A$ and (b), (c) a heteronuclear mixture characterized by $g_B = g_A = g$, $g_{AB} = 0.4g$ and $m_B = 2m_A$ and $m_B = 5m_A$ respectively. (d), (e) The same as before but for a homonuclear three component mixture with two identical components featuring $g_A = g_B = g_C = g$, $g_{AB} = -0.5g$ as well as $G_C = 0.1g$ and $G_C = 0.4g$ respectively. (f) Reduced one-body density of the many-body wavefunction occupying the states corresponding to the classical-field solutions given in (a). In all cases each component contains $N_\sigma = 10$ atoms.

interaction strengths $\propto G + \frac{g}{\mathcal{M}-1}$ and $\propto G + \frac{g}{\mathcal{N}-\mathcal{M}-1}$ respectively, both of which are larger than the inter-cluster coupling strength G (considering only repulsive interactions). As such, there is no reason for the clusters to phase separate, which explains why such configurations do not seem to appear.

B Asymmetric phase-separated configurations

The eGPEs derived in the main text support also ground state solutions with spontaneously broken parity symmetry in the case of mass-, or interaction-imbalanced mixtures featuring inter-component repulsion. Namely, these solutions are present in the cases where the phase separated configurations discussed in the main text appear as illustrated in Fig. 2 (c), Fig. 3(d), (f), and Fig. 5(e), (f). In Fig. 7(a)-(e) we present the corresponding parity asymmetric solutions for all cases mentioned above. In all cases, these solutions feature slightly lower energies (e.g. the relative energy difference is $\approx 0.3\%$ [$\approx 0.25\%$] for the homonuclear [heteronuclear with $m_B = 5m_A$] two-component mixture presented in Fig. 7(a) [Fig. 7(c)]) than the parity symmetric configurations shown in the main text. However, as mentioned in the main text, we consider such asymmetric phase-separated configurations to be associated with the classical-field approximation since they are not in principle permitted under a many-body wavefunction Ansatz. As such, within the main text we present and discuss the respective parity symmetric solutions as the ground state of the system in-spite of the slightly larger energy owing to the

SciPost SciPost Phys. 19, 133 (2025)

larger kinetic energy. We have confirmed that both types of solutions (i.e., symmetric and asymmetric) are robust when exposed to small amplitude perturbations, e.g., emulated by a random noise distribution across the spatial profile of the solution, and they afterwards let to evolve at least for total evolution times $T = 10^4\,\hbar^3/(m_A g_A^2)$ that we have checked. It is also important to remark that the existence of these configurations should not be under-appreciated. They can naturally emerge in corresponding experiments e.g. even in the presence of relatively small magnetic field gradients or other symmetry breaking contributions due to un-avoidable imperfection sources. Moreover, these domain-wall like distributions are interesting on their own right e.g. for dynamical applications in order to create topological excitations or study hydrodynamic instabilities.

To clarify our argument about the many-body wavefunction structure, consider as an example the homonuclear two-component mixture. Let $\Phi_A(x)$, $\Phi_B(x)$, be the single particle wavefunctions corresponding to the densities depicted in Fig. 7(a). We note in passing that all the configurations shown in Fig. 7(a)-(e) are, of course, doubly degenerate and their parity transformed counterpart is also a solution with the same energy, due to the parity symmetry of the ensuing Hamiltonian. Hence, neglecting any higher order correlations, the simplest form of the many-body wavefuntion for our homonuclear mixture, consistent with the results from the eGPEs would be:[6]

$$|\Psi\rangle = \sqrt{\frac{N_A N_B}{2}}\Big(|\Phi_A(x)\rangle|\Phi_B(x)\rangle + |\Phi_A(-x)\rangle|\Phi_B(-x)\rangle\Big). \tag{B.1}$$

Therefore, the corresponding diagonal of the reduced single-particle density matrix (namely, $\rho^1_\sigma(x) = Tr_\sigma\langle\Psi|\Psi\rangle$) of the underlying many-body system is not the one presented in Fig. 7(a), but it has the significantly more involved spatial profile illustrated in Fig. 7(f). Obviously, this structure can be associated with a significantly higher energy (at the level of the classical-field approximation) than either the parity symmetric solution shown in Fig. 2 (c), or the parity asymmetric solution depicted in Fig. 7(a). Finally, let us mention explicitly that the parity symmetric solutions discussed throughout the text can be directly associated with the reduced single-particle density of a many-body wavefunction (at the same level of approximation) since they are not degenerate. Namely, if $\Phi^S_A(x)$, $\Phi^S_B(x)$ are the parity symmetric single particle wavefunctions corresponding to the densities illustrated in Fig. 2(c), then $|\Psi\rangle = \sqrt{N_A N_B}|\Phi^S_A(x)\rangle|\Phi^S_B(x)\rangle$ is a valid (parity symmetric) many-body wavefunction, with the diagonal of its reduced single-particle density matrix being exactly the structure shown in Fig. 2(c). Thus, the densities of the parity symmetric solutions of the eGPEs can be interpreted as the reduced single-particle densities of the ground-state many-body wavefunction of the atomic gas and their energy can be interpreted as the energy of the many-body configuration (within the accuracy of the perturbative calculation). In contrast, parity asymmetric configurations do not permit this interpretation even if they correspond to a lower energy within the classical-field approximation, although upon proper symmetrization they could correspond to a valid (in general excited) many-body configuration (as the one shown in Fig. 7(f)). Of course as mentioned already, the situation changes in the presence of external parity breaking contributions which would lift the degeneracy of the parity asymmetric configurations and void the need for the symmetrization, thus making the corresponding parity asymmetric configurations valid candidates for the ground-state of the atomic gas.

[6] In general, the mirror symmetry is around the center-of-mass of the system ($c = \frac{1}{2}(\frac{1}{N_A}\int n_A x dx + \frac{1}{N_B}\int n_B x dx) \approx 28.5$ in our case) which is arbitrary owing to the underlying translation symmetry.

SciPost Phys. 19, 133 (2025)

References

[1] M. H. Anderson, J. R. Ensher, M. R. Matthews, C. E. Wieman and E. A. Cornell, *Observation of Bose-Einstein condensation in a dilute atomic vapor*, Science **269**, 198 (1995), doi:10.1126/science.269.5221.198.

[2] K. B. Davis, M. -O. Mewes, M. R. Andrews, N. J. van Druten, D. S. Durfee, D. M. Kurn and W. Ketterle, *Bose-Einstein condensation in a gas of sodium atoms*, Phys. Rev. Lett. **75**, 3969 (1995), doi:10.1103/PhysRevLett.75.3969.

[3] C. C. Bradley, C. A. Sackett, J. J. Tollett and R. G. Hulet, *Evidence of Bose-Einstein condensation in an atomic gas with attractive interactions*, Phys. Rev. Lett. **75**, 1687 (1995), doi:10.1103/PhysRevLett.75.1687.

[4] I. Bloch, J. Dalibard and S. Nascimbène, *Quantum simulations with ultracold quantum gases*, Nat. Phys. **8**, 267 (2012), doi:10.1038/nphys2259.

[5] C. J. Pethick and H. Smith, *Bose-Einstein condensation in dilute gases*, Cambridge University Press, Cambridge, UK, ISBN 9780521846516 (2008), doi:10.1017/CBO9780511802850.

[6] L. Pitaevskii and S. Stringari, *Bose-Einstein condensation and superfluidity*, Oxford University Press, Oxford, UK, ISBN 9780198758884 (2016), doi:10.1093/acprof:oso/9780198758884.001.0001.

[7] C. Chin, R. Grimm, P. Julienne and E. Tiesinga, *Feshbach resonances in ultracold gases*, Rev. Mod. Phys. **82**, 1225 (2010), doi:10.1103/RevModPhys.82.1225 [preprint doi:10.48550/arXiv.0812.1496].

[8] H. Moritz, T. Stöferle, M. Köhl and T. Esslinger, *Exciting collective oscillations in a trapped 1D gas*, Phys. Rev. Lett. **91**, 250402 (2003), doi:10.1103/PhysRevLett.91.250402 [preprint doi:10.48550/arXiv.cond-mat/0307607].

[9] A. Görlitz et al., *Realization of Bose-Einstein condensates in lower dimensions*, Phys. Rev. Lett. **87**, 130402 (2001), doi:10.1103/PhysRevLett.87.130402 [preprint doi:10.48550/arXiv.cond-mat/0104549].

[10] G. E. Astrakharchik, J. Boronat, J. Casulleras and S. Giorgini, *Beyond the Tonks-Girardeau gas: Strongly correlated regime in quasi-one-dimensional Bose gases*, Phys. Rev. Lett. **95**, 190407 (2005), doi:10.1103/PhysRevLett.95.190407 [preprint doi:10.48550/arXiv.cond-mat/0405225].

[11] E. Haller, M. Gustavsson, M. J. Mark, J. G. Danzl, R. Hart, G. Pupillo and H.-C. Nägerl, *Realization of an excited, strongly correlated quantum gas phase*, Science **325**, 1224 (2009), doi:10.1126/science.1175850 [preprint doi:10.48550/arXiv.1006.0739].

[12] L. Tonks, *The complete equation of state of one, two and three-dimensional gases of hard elastic spheres*, Phys. Rev. **50**, 955 (1936), doi:10.1103/PhysRev.50.955.

[13] M. Girardeau, *Relationship between systems of impenetrable bosons and fermions in one dimension*, J. Math. Phys. **1**, 516 (1960), doi:10.1063/1.1703687.

[14] B. Paredes, A. Widera, V. Murg, O. Mandel, S. Fölling, I. Cirac, G. V. Shlyapnikov, T. W. Hänsch and I. Bloch, *Tonks-Girardeau gas of ultracold atoms in an optical lattice*, Nature **429**, 277 (2004), doi:10.1038/nature02530.

[15] T. Kinoshita, T. Wenger and D. S. Weiss, *Observation of a one-dimensional Tonks-Girardeau gas*, Science **305**, 1125 (2004), doi:10.1126/science.1100700.

[16] S. Tojo, Y. Taguchi, Y. Masuyama, T. Hayashi, H. Saito and T. Hirano, *Controlling phase separation of binary Bose-Einstein condensates via mixed-spin-channel Feshbach resonance*, Phys. Rev. A **82**, 033609 (2010), doi:10.1103/PhysRevA.82.033609 [preprint doi:10.48550/arXiv.1007.2690].

[17] Y. Eto, M. Takahashi, M. Kunimi, H. Saito and T. Hirano, *Nonequilibrium dynamics induced by miscible-immiscible transition in binary Bose-Einstein condensates*, New J. Phys. **18**, 073029 (2016), doi:10.1088/1367-2630/18/7/073029.

[18] S. I. Mistakidis, G. C. Katsimiga, P. G. Kevrekidis and P. Schmelcher, *Correlation effects in the quench-induced phase separation dynamics of a two species ultracold quantum gas*, New J. Phys. **20**, 043052 (2018), doi:10.1088/1367-2630/aabc6a.

[19] P. Naidon and D. S. Petrov, *Mixed bubbles in Bose-Bose mixtures*, Phys. Rev. Lett. **126**, 115301 (2021), doi:10.1103/PhysRevLett.126.115301 [preprint doi:10.48550/arXiv.2008.05870].

[20] D. S. Petrov, *Quantum mechanical stabilization of a collapsing Bose-Bose mixture*, Phys. Rev. Lett. **115**, 155302 (2015), doi:10.1103/PhysRevLett.115.155302 [preprint doi:10.48550/arXiv.1506.08419].

[21] Z.-H. Luo, W. Pang, B. Liu, Y.-Y. Li and B. A. Malomed, *A new form of liquid matter: Quantum droplets*, Front. Phys. **16**, 32201 (2020), doi:10.1007/s11467-020-1020-2.

[22] F. Böttcher, J.-N. Schmidt, J. Hertkorn, K. S. H. Ng, S. D. Graham, M. Guo, T. Langen and T. Pfau, *New states of matter with fine-tuned interactions: Quantum droplets and dipolar supersolids*, Rep. Prog. Phys. **84**, 012403 (2020), doi:10.1088/1361-6633/abc9ab.

[23] S. I. Mistakidis, A. G. Volosniev, R. E. Barfknecht, T. Fogarty, T. Busch, A. Foerster, P. Schmelcher and N. T. Zinner, *Few-body Bose gases in low dimensions – A laboratory for quantum dynamics*, Phys. Rep. **1042**, 1 (2023), doi:10.1016/j.physrep.2023.10.004 [preprint doi:10.48550/arXiv.2202.11071].

[24] C. R. Cabrera, L. Tanzi, J. Sanz, B. Naylor, P. Thomas, P. Cheiney and L. Tarruell, *Quantum liquid droplets in a mixture of Bose-Einstein condensates*, Science **359**, 301 (2018), doi:10.1126/science.aao5686 [preprint doi:10.48550/arXiv.1708.07806].

[25] G. Semeghini et al., *Self-bound quantum droplets of atomic mixtures in free space*, Phys. Rev. Lett. **120**, 235301 (2018), doi:10.1103/PhysRevLett.120.235301 [preprint doi:10.48550/arXiv.1710.10890].

[26] I. Ferrier-Barbut, H. Kadau, M. Schmitt, M. Wenzel and T. Pfau, *Observation of quantum droplets in a strongly dipolar Bose gas*, Phys. Rev. Lett. **116**, 215301 (2016), doi:10.1103/PhysRevLett.116.215301 [preprint doi:10.48550/arXiv.1601.03318].

[27] L. Chomaz, I. Ferrier-Barbut, F. Ferlaino, B. Laburthe-Tolra, B. L. Lev and T. Pfau, *Dipolar physics: A review of experiments with magnetic quantum gases*, Rep. Prog. Phys. **86**, 026401 (2022), doi:10.1088/1361-6633/aca814.

[28] T. D. Lee, K. Huang and C. N. Yang, *Eigenvalues and eigenfunctions of a Bose system of hard spheres and its low-temperature properties*, Phys. Rev. **106**, 1135 (1957), doi:10.1103/PhysRev.106.1135.

[29] M. Tylutki, G. E. Astrakharchik, B. A. Malomed and D. S. Petrov, *Collective excitations of a one-dimensional quantum droplet*, Phys. Rev. A **101**, 051601 (2020), doi:10.1103/PhysRevA.101.051601 [preprint doi:10.48550/arXiv.2003.05803].

[30] E. G. Charalampidis and S. I. Mistakidis, *Two-component droplet phases and their spectral stability in one dimension*, Phys. Rev. A **111**, 013318 (2025), doi:10.1103/PhysRevA.111.013318 [preprint doi:10.48550/arXiv.2409.19852].

[31] G. E. Astrakharchik and B. A. Malomed, *Dynamics of one-dimensional quantum droplets*, Phys. Rev. A **98**, 013631 (2018), doi:10.1103/PhysRevA.98.013631 [preprint doi:10.48550/arXiv.1803.07165].

[32] G. Ferioli, G. Semeghini, L. Masi, G. Giusti, G. Modugno, M. Inguscio, A. Gallemí, A. Recati and M. Fattori, *Collisions of self-bound quantum droplets*, Phys. Rev. Lett. **122**, 090401 (2019), doi:10.1103/PhysRevLett.122.090401 [preprint doi:10.48550/arXiv.1812.09151].

[33] G. C. Katsimiga, S. I. Mistakidis, G. N. Koutsokostas, D. J. Frantzeskakis, R. Carretero-González and P. G. Kevrekidis, *Solitary waves in a quantum droplet-bearing system*, Phys. Rev. A **107**, 063308 (2023), doi:10.1103/PhysRevA.107.063308 [preprint doi:10.48550/arXiv.2302.07767].

[34] M. Edmonds, *Dark quantum droplets and solitary waves in beyond-mean-field Bose-Einstein condensate mixtures*, Phys. Rev. Res. **5**, 023175 (2023), doi:10.1103/PhysRevResearch.5.023175 [preprint doi:10.48550/arXiv.2209.00790].

[35] Y. Li, Z. Chen, Z. Luo, C. Huang, H. Tan, W. Pang and B. A. Malomed, *Two-dimensional vortex quantum droplets*, Phys. Rev. A **98**, 063602 (2018), doi:10.1103/PhysRevA.98.063602 [preprint doi:10.48550/arXiv.1801.10274].

[36] G. Bougas, G. C. Katsimiga, P. G. Kevrekidis and S. I. Mistakidis, *Stability and dynamics of nonlinear excitations in a two-dimensional droplet-bearing environment*, Phys. Rev. A **110**, 033317 (2024), doi:10.1103/PhysRevA.110.033317 [preprint doi:10.48550/arXiv.2405.20106].

[37] M. N. Tengstrand, P. Stürmer, E. Ö. Karabulut and S. M. Reimann, *Rotating binary Bose-Einstein condensates and vortex clusters in quantum droplets*, Phys. Rev. Lett. **123**, 160405 (2019), doi:10.1103/PhysRevLett.123.160405 [preprint doi:10.48550/arXiv.1905.09738].

[38] T. A. Yoğurt, U. Tanyeri, A. Keleş and M. Ö. Oktel, *Vortex lattices in strongly confined quantum droplets*, Phys. Rev. A **108**, 033315 (2023), doi:10.1103/PhysRevA.108.033315 [preprint doi:10.48550/arXiv.2308.02704].

[39] B. A. Malomed, *The family of quantum droplets keeps expanding*, Front. Phys. **16**, 22504 (2021), doi:10.1007/s11467-020-1024-y.

[40] L. Parisi, G. E. Astrakharchik and S. Giorgini, *Liquid state of one-dimensional Bose mixtures: A quantum Monte Carlo study*, Phys. Rev. Lett. **122**, 105302 (2019), doi:10.1103/PhysRevLett.122.105302 [preprint doi:10.48550/arXiv.1810.07950].

[41] L. Parisi and S. Giorgini, *Quantum droplets in one-dimensional Bose mixtures: A quantum Monte Carlo study*, Phys. Rev. A **102**, 023318 (2020), doi:10.1103/PhysRevA.102.023318 [preprint doi:10.48550/arXiv.2003.05231].

[42] S. I. Mistakidis, T. Mithun, P. G. Kevrekidis, H. R. Sadeghpour and P. Schmelcher, *Formation and quench of homonuclear and heteronuclear quantum droplets in one dimension*, Phys. Rev. Res. **3**, 043128 (2021), doi:10.1103/PhysRevResearch.3.043128 [preprint doi:10.48550/arXiv.2108.00727].

[43] I. A. Englezos, S. I. Mistakidis and P. Schmelcher, *Correlated dynamics of collective droplet excitations in a one-dimensional harmonic trap*, Phys. Rev. A **107**, 023320 (2023), doi:10.1103/PhysRevA.107.023320 [preprint doi:10.48550/arXiv.2206.05768].

[44] P. Cheiney, C. R. Cabrera, J. Sanz, B. Naylor, L. Tanzi and L. Tarruell, *Bright soliton to quantum droplet transition in a mixture of Bose-Einstein condensates*, Phys. Rev. Lett. **120**, 135301 (2018), doi:10.1103/PhysRevLett.120.135301 [preprint doi:10.48550/arXiv.1710.11079].

[45] C. D'Errico, A. Burchianti, M. Prevedelli, L. Salasnich, F. Ancilotto, M. Modugno, F. Minardi and C. Fort, *Observation of quantum droplets in a heteronuclear bosonic mixture*, Phys. Rev. Res. **1**, 033155 (2019), doi:10.1103/PhysRevResearch.1.033155 [preprint doi:10.48550/arXiv.1908.00761].

[46] Z. Guo, F. Jia, L. Li, Y. Ma, J. M. Hutson, X. Cui and D. Wang, *Lee-Huang-Yang effects in the ultracold mixture of ^{23}Na and ^{87}Rb with attractive interspecies interactions*, Phys. Rev. Res. **3**, 033247 (2021), doi:10.1103/PhysRevResearch.3.033247 [preprint doi:10.48550/arXiv.2105.01277].

[47] L. Cavicchioli, C. Fort, F. Ancilotto, M. Modugno, F. Minardi and A. Burchianti, *Dynamical formation of multiple quantum droplets in a Bose-Bose mixture*, Phys. Rev. Lett. **134**, 093401 (2025), doi:10.1103/PhysRevLett.134.093401 [preprint doi:10.48550/arXiv.2409.16017].

[48] C. Fort and M. Modugno, *Self-evaporation dynamics of quantum droplets in a ^{41}K–^{87}Rb mixture*, Appl. Sci. **11**, 866 (2021), doi:10.3390/app11020866 [preprint doi:10.48550/arXiv.2012.10347].

[49] G. E. Astrakharchik and S. Giorgini, *Correlation functions of a Lieb-Liniger Bose gas*, J. Phys. B: At. Mol. Opt. Phys. **39**, S1 (2006), doi:10.1088/0953-4075/39/10/s01.

[50] L. Lavoine and T. Bourdel, *Beyond-mean-field crossover from one dimension to three dimensions in quantum droplets of binary mixtures*, Phys. Rev. A **103**, 033312 (2021), doi:10.1103/PhysRevA.103.033312.

[51] T. Ilg, J. Kumlin, L. Santos, D. S. Petrov and H. P. Büchler, *Dimensional crossover for the beyond-mean-field correction in Bose gases*, Phys. Rev. A **98**, 051604 (2018), doi:10.1103/PhysRevA.98.051604 [preprint doi:10.48550/arXiv.1806.01784].

[52] J. C. Pelayo, G. Bougas, T. Fogarty, T. Busch and S. I. Mistakidis, *Phases and dynamics of quantum droplets in the crossover to two-dimensions*, SciPost Phys. **18**, 129 (2025), doi:10.21468/SciPostPhys.18.4.129 [preprint doi:10.48550/arXiv.2407.16383].

[53] D. S. Petrov and G. E. Astrakharchik, *Ultradilute low-dimensional liquids*, Phys. Rev. Lett. **117**, 100401 (2016), doi:10.1103/PhysRevLett.117.100401 [preprint doi:10.48550/arXiv.1605.07585].

[54] F. K. Abdullaev and J. Garnier, *Bright solitons in Bose-Einstein condensates: Theory*, in *Emergent nonlinear phenomena in Bose-Einstein condensates*, Springer, Berlin, Heidelberg, Germany, ISBN 9783540735908 (2008), doi:10.1007/978-3-540-73591-5_2.

[55] V. M. Pérez-García and J. B. Beitia, *Symbiotic solitons in heteronuclear multicomponent Bose-Einstein condensates*, Phys. Rev. A **72**, 033620 (2005), doi:10.1103/PhysRevA.72.033620 [preprint doi:10.48550/arXiv.cond-mat/0506405].

[56] B. Malomed, L. Torner, F. Wise and D. Mihalache, *On multidimensional solitons and their legacy in contemporary Atomic, Molecular and Optical physics*, J. Phys. B: At. Mol. Opt. Phys. **49**, 170502 (2016), doi:10.1088/0953-4075/49/17/170502.

[57] M. N. Tengstrand and S. M. Reimann, *Droplet-superfluid compounds in binary bosonic mixtures*, Phys. Rev. A **105**, 033319 (2022), doi:10.1103/PhysRevA.105.033319.

[58] J. Vallès-Muns, I. Morera, G. E. Astrakharchik and B. Juliá-Díaz, *Quantum droplets with particle imbalance in one-dimensional optical lattices*, SciPost Phys. **16**, 074 (2024), doi:10.21468/SciPostPhys.16.3.074 [preprint doi:10.48550/arXiv.2306.12283].

[59] T. A. Flynn, N. A. Keepfer, N. G. Parker and T. P. Billam, *Harmonically trapped imbalanced quantum droplets*, Phys. Rev. Res. **6**, 013209 (2024), doi:10.1103/PhysRevResearch.6.013209.

[60] L. He, H. Li, W. Yi and Z.-Q. Yu, *Quantum criticality of liquid-gas transition in a binary Bose mixture*, Phys. Rev. Lett. **130**, 193001 (2023), doi:10.1103/PhysRevLett.130.193001 [preprint doi:10.48550/arXiv.2209.13559].

[61] I. A. Englezos, P. Schmelcher and S. I. Mistakidis, *Particle-imbalanced weakly interacting quantum droplets in one dimension*, Phys. Rev. A **110**, 023324 (2024), doi:10.1103/PhysRevA.110.023324 [preprint doi:10.48550/arXiv.2312.13648].

[62] Y. Ma, C. Peng and X. Cui, *Borromean droplet in three-component ultracold Bose gases*, Phys. Rev. Lett. **127**, 043002 (2021), doi:10.1103/PhysRevLett.127.043002 [preprint doi:10.48550/arXiv.2102.00674].

[63] F. K. Abdullaev and R. M. Galimzyanov, *Bosonic impurity in a one-dimensional quantum droplet in the Bose-Bose mixture*, J. Phys. B: At. Mol. Opt. Phys. **53**, 165301 (2020), doi:10.1088/1361-6455/ab9659.

[64] M. Wenzel, T. Pfau and I. Ferrier-Barbut, *A fermionic impurity in a dipolar quantum droplet*, Phys. Scr. **93**, 104004 (2018), doi:10.1088/1402-4896/aadd72.

[65] G. Bighin, A. Burchianti, F. Minardi and T. Macrì, *Impurity in a heteronuclear two-component Bose mixture*, Phys. Rev. A **106**, 023301 (2022), doi:10.1103/PhysRevA.106.023301 [preprint doi:10.48550/arXiv.2109.07451].

[66] S. Sinha, S. Biswas, L. Santos and S. Sinha, *Impurities in quasi-one-dimensional droplets of binary Bose mixtures*, Phys. Rev. A **108**, 023311 (2023), doi:10.1103/PhysRevA.108.023311 [preprint doi:10.48550/arXiv.2304.04261].

[67] J. C. Pelayo, T. Fogarty, T. Busch and S. I. Mistakidis, *Phases and dynamics of few fermionic impurities immersed in two-dimensional boson droplets*, Phys. Rev. Res. **6**, 033219 (2024), doi:10.1103/PhysRevResearch.6.033219 [preprint doi:10.48550/arXiv.2405.12466].

[68] M. Olshanii, *Atomic scattering in the presence of an external confinement and a gas of impenetrable bosons*, Phys. Rev. Lett. **81**, 938 (1998), doi:10.1103/PhysRevLett.81.938 [preprint doi:10.48550/arXiv.cond-mat/9804130].

[69] C. Chin, R. Grimm, P. Julienne and E. Tiesinga, *Feshbach resonances in ultracold gases*, Rev. Mod. Phys. **82**, 1225 (2010), doi:10.1103/RevModPhys.82.1225 [preprint doi:10.48550/arXiv.0812.1496].

[70] T. Köhler, K. Góral and P. S. Julienne, *Production of cold molecules via magnetically tunable Feshbach resonances*, Rev. Mod. Phys. **78**, 1311 (2006), doi:10.1103/RevModPhys.78.1311 [preprint doi:10.48550/arXiv.cond-mat/0601420].

[71] A. Romero-Ros, G. C. Katsimiga, S. I. Mistakidis, S. Mossman, G. Biondini, P. Schmelcher, P. Engels and P. G. Kevrekidis, *Experimental realization of the Peregrine soliton in repulsive two-component Bose-Einstein condensates*, Phys. Rev. Lett. **132**, 033402 (2024), doi:10.1103/PhysRevLett.132.033402 [preprint doi:10.48550/arXiv.2304.05951].

[72] A. G. Del Maestro and M. J. P. Gingras, *Quantum spin fluctuations in the dipolar Heisenberg-like rare earth pyrochlores*, J. Phys.: Condens. Matter **16**, 3339 (2004), doi:10.1088/0953-8984/16/20/005.

[73] P. Tommasini, E. J. V. de Passos, A. F. R. de Toledo Piza, M. S. Hussein and E. Timmermans, *Bogoliubov theory for mutually coherent condensates*, Phys. Rev. A **67**, 023606 (2003), doi:10.1103/PhysRevA.67.023606.

[74] A. Burchianti, C. D'Errico, M. Prevedelli, L. Salasnich, F. Ancilotto, M. Modugno, F. Minardi and C. Fort, *A dual-species Bose-Einstein condensate with attractive interspecies interactions*, Condens. Matter **5**, 21 (2020), doi:10.3390/condmat5010021 [preprint doi:10.48550/arXiv.2003.13362].

[75] Z. Guo, F. Jia, L. Li, Y. Ma, J. M. Hutson, X. Cui and D. Wang, *Lee-Huang-Yang effects in the ultracold mixture of ^{23}Na and ^{87}Rb with attractive interspecies interactions*, Phys. Rev. Res. **3**, 033247 (2021), doi:10.1103/PhysRevResearch.3.033247 [preprint doi:10.48550/arXiv.2105.01277].

[76] G. C. Katsimiga, S. I. Mistakidis, B. A. Malomed, D. J. Frantzeskakis, R. Carretero-Gonzalez and P. G. Kevrekidis, *Interactions and dynamics of one-dimensional droplets, bubbles and kinks*, Condens. Matter **8**, 67 (2023), doi:10.3390/condmat8030067 [preprint doi:10.48550/arXiv.2306.07055].

[77] T. D. Anh-Tai, M. A. García-March, T. Busch and T. Fogarty, *Quantum correlations and spatial localization in trapped one-dimensional ultra-cold Bose-Bose-Bose mixtures*, New J. Phys. **27**, 073201 (2025), doi:10.1088/1367-2630/ade89e.

[78] T. D. Anh-Tai, T. Fogarty, S. de María-García, T. Busch and M. A. García-March, *Engineering impurity Bell states through coupling with a quantum bath*, Phys. Rev. Res. **6**, 043042 (2024), doi:10.1103/PhysRevResearch.6.043042 [preprint doi:10.48550/arXiv.2406.06966].

[79] F. Theel, S. I. Mistakidis and P. Schmelcher, *Crossover from attractive to repulsive induced interactions and bound states of two distinguishable Bose polarons*, SciPost Phys. **16**, 023 (2024), doi:10.21468/SciPostPhys.16.1.023 [preprint doi:10.48550/arXiv.2303.04699].

[80] V. Cikojević, L. V. Markić, M. Pi, M. Barranco, F. Ancilotto and J. Boronat, *Dynamics of equilibration and collisions in ultradilute quantum droplets*, Phys. Rev. Res. **3**, 043139 (2021), doi:10.1103/PhysRevResearch.3.043139.

SciPost Phys. 19, 133 (2025)

[81] S. Chandramouli, S. I. Mistakidis, G. C. Katsimiga and P. G. Kevrekidis, *Dispersive shock waves in a one-dimensional droplet-bearing environment*, Phys. Rev. A **110**, 023304 (2024), doi:10.1103/PhysRevA.110.023304 [preprint doi:10.48550/arXiv.2404.02998].

4.4 Stability and Mixed Phases of Three-Component Droplets in One Dimension

Stability and mixed phases of three-component droplets in one dimension

I. A. Englezos,[1,*] E. G. Charalampidis,[2,†] P. Schmelcher,[1] and S. I. Mistakidis[3]

[1] *Center for Optical Quantum Technologies, Department of Physics, University of Hamburg, Luruper Chaussee 149, 22761 Hamburg Germany*

[2] *Department of Mathematics and Statistics and Computational Science Research Center, San Diego State University, San Diego, CA 92182-7720, USA*

[3] *Department of Physics, Missouri University of Science and Technology, Rolla, MO 65409, USA*

(Dated: January 9, 2026)

We explore the ground state properties and excitation spectra of one-dimensional three-component bosonic mixtures accommodating a droplet in two of the species and a third minority component. Relying on the suitable Lee-Huang-Yang framework, we reveal a plethora of distinct self-bound droplet phases and their phase transitions through variations of either the particle number of the majority components or the intercomponent coupling. The ensuing phases demonstrate that the minority component is being un-trapped, partially trapped, or fully trapped by the majority droplet species. These states are characterized by their binding energies captured by the chemical potentials and their low-amplitude excitation spectrum, including mode crossings at the particle-emission threshold. We further derive effective reduced models which are valid in the high-imbalance limit, and accurately reproduce the numerically computed ground states, while providing analytical insights into the role of quantum fluctuations. Our results map out the stability and structure of mixed droplet phases offering guidance into forthcoming experimental and theoretical studies of multicomponent quantum droplets.

I. INTRODUCTION

Quantum droplets are self-bound, ultradilute, liquid-like many-body states, whose formation entails the presence of quantum fluctuations at weakly interacting macroscopic ultracold settings [1–4]. In this context, the first order Lee-Huang-Yang (LHY) [5] quantum correction term to the mean-field (MF) energy is often sufficient to describe the emergence of droplet states [6–8]. These exotic phases-of-matter were first experimentally observed in long-range dipolar bosonic gases [1, 9–11] and soon thereafter in two-component short-range interacting bosonic mixtures [12–17]. In these latter settings, in which we also focus herein, it is important to determine the species density ratio since i) if it is fixed (and dictated by the intracomponent interaction fraction), the components behave identically, thus yielding a symmetric droplet with enhanced stability [6], while ii) if it is broken, genuine two-component droplet configurations arise [18–21].

A plethora of symmetric droplet studies in different dimensionalities have been lately exploring, among others, their ground states and spectrum [22–26] (including clusters thereof [27]), inelastic collisions [22, 28], as well as their ability to host solitons [29, 30], vortices [31–34], dispersive shock-waves [35], kinks [36–38] and rogue waves [39]. On the other hand, genuinely two-component droplets breaking the aforementioned density ratio condition, e.g. by considering particle [40], mass [15, 24] or interaction [41] imbalance between the two-components, are arguably far less investigated. Here, current results revealed mixed droplet-gas phases [18–21], the existence of excited multipole droplet states [42], and droplets of a super-Tonks gas confined in an optical lattice [43], as well as the droplet stability in a ring geometry [44] and in a harmonic trap [45], see also Refs. [40, 46, 47] elaborating on beyond LHY effects. A challenge for studying particle imbalance two-component droplets is the significantly different length scales of the involved species, which has been typically circumvented by the inclusion of external traps that is, however, formally not within the validity of the original LHY theory.

A conceivable approach to mitigate such constraints is to embed a minority species within a droplet. This would allow to indirectly limit the droplet extent via tuning the droplet-minority species attraction as it was, for instance, argued recently using attractive potential wells in a droplet [48, 49]. Additionally, important currently unresolved questions can be raised, such as i) can the third component act as a knob for the droplet structure [50]?, ii) what are the phases of the underlying three-component configurations?, and iii) are there parameter regimes where the minority species is fully or partially trapped by the droplet [51, 52]? In this vein, there are even broader implications of such a setup which also provides links with impurity physics [53–55], a topic that has been extensively addressed in the past decade with repulsive Bose gases [4, 56–58].

Motivated by these open questions, here we explore the droplet phases and their stability in a three-component bosonic mixture in one-dimension (1D). To do so, we deploy a fully self-consistent LHY framework yielding the suitable coupled extended Gross-Pitaevskii equations (eGPEs) derived for the 1D mixture in [8], see also Refs. [51, 52] for generalizations to three-dimensions. We focus on homonuclear systems where the two components

* ilias.englezos@uni-hamburg.de
† echaralampidis@sdsu.edu

are equivalent (in terms of their mass, atom number and interaction parameters) forming a strongly self-bound symmetric droplet that is coupled to a third, minority component. A key result of our work is the emergence of distinct mixed droplet phases where the minority component is un-trapped, partially trapped, or fully trapped by the symmetric droplet upon considering variations of either the intercomponent interaction strength and the particle imbalance between the droplet and the third component. These phases are characterized through their chemical potentials (being negative throughout the considered parametric variations) and low-amplitude excitation spectra. The latter are obtained via constructing a suitable Bogoliubov-de Gennes (BdG) analysis for the three-component system constituting an additional aspect of our study and complementing previous ones for symmetric [23] and two-component [45] droplets. The ensuing spectra reveal that in the transition from untrapped to fully trapped minority species, the collective mode energy branches cross the particle emission threshold from below as the intercomponent attraction increases. Additionally, other spectral fingerprints are found such as mode pairing, and avoided-crossings associated with the aforementioned transition. Finally, we derive effective reduced models in the limit of large particle imbalance. They provide analytical insights for the structure of the components and quantitatively reproduce the numerical results of the full eGPEs for weak and moderate intercomponent couplings, while deviating for strong attractions.

This work is structured as follows. In Section II, we introduce the three-component mixture under investigation governed by the suitable eGPEs, while briefly discussing the BdG framework that is leveraged to extract the low-amplitude excitation spectrum of the system. In Section III, we address the ground state configurations and excitation spectrum of both particle balanced and particle imbalanced settings for varying atom number and intercomponent coupling strengths. Section IV provides analytical insights for the interpretation of the three-component structures by constructing relevant effective reduced models based on LHY theory in the limit of large particle imbalance. We summarize and propose extensions of our results for future research in Section V. Appendix A elaborates on the derivation of the BdG equations, and Appendix B outlines the calculation of the approximate LHY energy utilized in the reduced models.

II. THREE-COMPONENT HOMONUCLEAR DROPLET SETUP

By construction, three-component mixtures due to the involved interactions and masses offer additional possibilities for intercomponent asymmetry that could lead to enriched phases-of-matter and intriguing nonequilibrium phenomena which do not exist in their two-component counterparts. However, exploring their behavior in the full parameter space containing at least twelve independent parameters (namely six interaction strengths, three masses and three atom numbers) is a formidable task. As such, it is natural to first study these systems by considering specific symmetries which reduce the number of the aforementioned free parameters. A physically motivated setting that respects this requirement is a homonuclear mixture, where $m_A = m_B = m_C \equiv m$. Additionally, it is viable to envisage that the individual components experience (almost) the same intracomponent interactions, i.e. $g_A = g_B = g_C \equiv g$, a scenario that is in principle possible using Feshbach resonances [59], and two of them accommodate the same atom number, $N_A = N_B \equiv N$. The latter can be accomplished by employing radiofrequency transitions among the involved hyperfine states. Hence, two of the components (dubbed here A and B) are equivalent and the third one (called C) is different which also implies that $g_{AC} = g_{BC} \equiv G_C$. Accordingly, the number of free parameters reduces to six (i.e. g, g_{AB}, G_C, m, N and N_C) out of which g and m are held fixed since they correspond to a specific atomic element.

These assumptions in the interaction regime of repulsive intracomponent couplings ($g > 0$) and attractive intercomponent $g_{AB} < 0$ favor the formation of a so-called symmetric droplet [6] in species A, B, while component C is independent, see also Ref. [51] for a similar 3D system. Interestingly, the aforementioned composition allows to use the third component as a knob for configuring unseen complex droplet phases-of-matter. A candidate for realizing such a system in near term experiments consists, for instance, of three ^{39}K hyperfine states two of which have already been utilized in corresponding 3D droplet experiments [12, 13]. Additionally, without loss of generality, we consider a 1D box confinement of typical length $L = 300$ (being sufficiently extended to not impact the ensuing droplet configurations) along the elongated x-direction, while the transverse ones (y, z) are assumed to be tightly confined characterized by a frequency $\omega_\perp$. This together with the requirement $|\mu + \mu_C| \ll \hbar\omega_\perp$, with μ (μ_C) representing the chemical potential of the droplet (third) component, ensure that the atoms are kinematically constrained across the x-direction. For completeness, we remark here that 1D droplet experiments are still lacking.

A. Droplet coupled to another component

Our many-body system comprises of a bosonic droplet assembled by components A, B and a third component C interacting with the symmetric two-component droplet via G_C. Recently, it was analytically demonstrated [8] that the LHY energy density of such a three-component mixture under the above-described symmetry conditions

takes the form

$$\mathcal{E}_{\rm LHY} = -\frac{\sqrt{2m}}{6\hbar\pi}\Big((2(g-g_{AB})n)^{\frac{3}{2}} + (W+Q)^{\frac{3}{2}} + (W-Q)^{\frac{3}{2}}\Big), \tag{1}$$

with the parameters

$$Q = \Big([(g+g_{AB})n - g_C n_C]^2 + 8G_C^2 n n_C\Big)^{\frac{1}{2}}, \tag{2a}$$

$$W = (g+g_{AB})n + g_C n_C. \tag{2b}$$

In these expressions, $n(x)$ and $n_C(x)$ are the densities of the two symmetric components (A, B) and of component C. The LHY energy density is real and negative admitting droplet solutions as long as $g > g_{AB}$ and $W - Q > 0 \rightarrow 2G_C^2 < g_C(g+g_{AB})$, while it becomes complex otherwise. The interaction interval $2G_C^2 < g_C(g+g_{AB})$ defines the MF stability regime of the three-component mixture as it was argued in [8]. Note also that in the absence of the third component, i.e. when $G_C = g_C = n_C = 0$, Eq. (1) reduces to the LHY energy of a symmetric droplet [7, 8].

The corresponding coupled set of 1D eGPEs describing the dynamics of the three-component droplet setting with $\psi_A = \psi_B \equiv \psi$ read [8]

$$i\hbar\frac{\partial\psi}{\partial t} = -\frac{\hbar^2}{m}\frac{\partial^2\psi}{\partial x^2} + \Big(2(g+g_{AB})|\psi|^2 + 2G_C|\psi_C|^2 + \frac{\partial\mathcal{E}_{\rm LHY}}{\partial n}\Big)\psi, \tag{3a}$$

$$i\hbar\frac{\partial\psi_C}{\partial t} = -\frac{\hbar^2}{2m}\frac{\partial^2\psi_C}{\partial x^2} + \Big(g_C|\psi_C|^2 + 2G_C|\psi|^2 + \frac{\partial\mathcal{E}_{\rm LHY}}{\partial n_C}\Big)\psi_C. \tag{3b}$$

Here, $n(x) = |\psi(x)|^2$ and $n_C(x) = |\psi_C(x)|^2$. Importantly, these eGPEs contain the LHY terms of both the symmetric droplet and the third component but also an intercomponent LHY contribution. This is in sharp contrast to previous three-component considerations where only MF couplings were taken into account between the droplet and the other component [60]. Moreover, the involved partial derivatives of the LHY energy density participating in the above equations of motion (3a)-(3b) can be readily derived from Eq. (1) and acquire the form

$$\frac{\partial\mathcal{E}_{\rm LHY}}{\partial n} = -\frac{\sqrt{2m}}{4\pi h}\Bigg(\Big(g+g_{AB}+\frac{Z}{Q}\Big)\sqrt{W-Q} + \Big(g+g_{AB}-\frac{Z}{Q}\Big)\sqrt{W+Q} + 2\sqrt{2}(g-g_{AB})^{\frac{3}{2}}\sqrt{n}\Bigg), \tag{4a}$$

$$\frac{\partial\mathcal{E}_{\rm LHY}}{\partial n_C} = -\frac{\sqrt{2m}}{4\pi h}\Bigg(\Big(g_C+\frac{P}{Q}\Big)\sqrt{W-Q} + \Big(g_C-\frac{P}{Q}\Big)\sqrt{W+Q}\Bigg), \tag{4b}$$

with

$$Z = -(g+g_{AB})^2 n + (g_C(g+g_{AB}) - 4G_C^2)n_C, \tag{5a}$$

$$P = (g_C(g+g_{AB}) - 4G_C^2)n - g_C^2 n_C. \tag{5b}$$

In what follows, the energy scale is set by $mg^2/\hbar^2$. Hence, the length, time, and interaction strengths are expressed in units of $\hbar^2/(mg)$, $\hbar^3/(mg^2)$, and g respectively.

To identify stationary droplet solutions of our three-component system, we consider the stationary version of Eqs. (3a)-(3b) that is obtained by the substitution of the (separation of variables) ansatz: $\psi_j(x,t) = \Psi_j(x)e^{-i\mu_j t}$ therein. The field $\Psi_j(x)$ is the jth steady state to be obtained, and μ_j represents its corresponding chemical potential. We note that for the two symmetric components that we will be considering below, $\mu_A = \mu_B \equiv \mu$ holds. To identify the steady states $\Psi_j(x)$ numerically, we introduce a one-dimensional computational domain $[-L, L]$ with $L = 300$ that is supplemented with homogeneous Dirichlet boundary conditions at its endpoints. The spatial derivatives that arise in the steady-state problem are replaced by a 4th-order accurate, centered finite difference formula. Then, we employ Newton's method (and variants thereof) [61] to solve the underlying coupled nonlinear system of algebraic equations.

We would like to note in passing that the present setup is defined on the free space, i.e., in the absence of external potential (unlike our recent work for a two-component system in [45]). That by itself, introduces a non-trivial kernel in the underlying Jacobian matrix that is associated with the invariances of the system. Specifically the (right) nullspace vectors therein correspond to the phase invariance and translation invariance (again, under the absence of an x-dependent potential) of the system. We restore robust convergence in Newton's method by augmenting the system through the introduction of suitable phase conditions and Lagrange multipliers that help factor out the degeneracies. For further details about this approach, we refer the reader to Ref. [62].

B. BdG Equations and Stability Matrix

To assess the stability of the computed stationary three-component droplet solutions, we deploy the BdG formalism. In particular, having at hand the stationary solutions, $\Psi(x)$, $\Psi_C(x)$, with chemical potentials μ, and μ_C respectively, obtained through the Newton's scheme, we introduce the small amplitude $\epsilon \ll 1$ perturbation Ansätze:

$$\Psi^{\rm BdG} = e^{-i\mu t}[\Psi + \epsilon(ae^{i\omega t} + b^* e^{-i\omega^* t})], \tag{6a}$$

$$\Psi_C^{\rm BdG} = e^{-i\mu_C t}[\Psi_C + \epsilon(a_C e^{i\omega t} + b_C^* e^{-i\omega^* t})], \tag{6b}$$

for the eGPEs of Eqs. (3a)-(3b). This yields the underlying linearized (i.e., of order $\mathcal{O}(\epsilon)$) system of the equations

of motion. Here, $a = a(x)$, $b = b(x)$, $a_C = a_C(x)$, $b_C = b_C(x)$ are spatially dependent complex functions composing the eigenvectors $[a(x), b(x)]^\intercal$ and $[a_C(x), b_C(x)]^\intercal$, while ω represents the eigenfrequency.

We refrain from presenting these calculations here since they are rather tedious. After separating the terms $\propto e^{i\omega t}$ and $\propto e^{-i\omega^* t}$, we arrive at a coupled system of four eigenvalue equations for the four eigenvector elements and the phase ω. Setting the vector $v = (a, b, a_C, b_C)$ it is possible to express the resulting equations in a matrix form as $\mathrm{diag}(-1, 1, -1, 1)\mathcal{A}v = \omega v$. The derivation of the elements of the 4×4 stability matrix $\mathcal{A}$ is given in Appendix A. By solving the resulting eigenvalue problem, we extract the energy spectrum containing the ensuing eigenmodes of the elementary small amplitude excitations of the stationary solutions $\Psi(x)$ and $\Psi_C(x)$. Eigenmodes associated with complex eigenvalues indicate that the obtained solution is dynamically unstable, while real eigenvalues (namely with zero imaginary part) describe stable configurations [63]. The real part of the spectrum encompasses the collective excitation branches of a given configuration.

III. MIXED DROPLET PHASES

Below, we focus on the case of a strongly attractive intercomponent interaction (i.e., close to the MF stability edge) between the two symmetric components, namely $g_{AB} = -0.96g$. This ensures that these components assemble in a tightly self-bound single-component droplet [7] in the absence of the third component. Moreover, aiming to reduce the free parameter space of our setting, we also fix throughout the particle number of the third independent component C to $N_C = 10$ and its intracomponent coupling to $g_C = g$. Under these conditions, the MF stability regime is given by $|G_C| < 0.1\sqrt{2} \approx 0.14$. Our analysis is based on the three-component droplet ground state densities to infer the emergent spatial configurations along with the underlying excitation spectrum explicating their stability and behavior of collective modes. Additionally, the chemical potential allows to deduce the bound state nature of the three-component droplet structures. We address both particle balanced and imbalanced situations between the symmetric droplet (A, B species) and the third component (C) such that we achieve partial or full trapping of the component C spatial distributions by the droplet.

Let us explicitly note here that for $G_C = 0$ (dubbed decoupled limit, see also Sec. IV) the three-component setting decouples into two independent droplet subsystems, namely components A and B constitute the first and component C the second[1]. At $G_C = 0$, the symmetric two-component droplet is characterized by saturation density $n^s = \frac{mg^3(1+3(g_{AB}/g)^2+[1-(g_{AB}/g)^2]^{3/2})}{9\hbar^2\pi^2(g+g_{AB})^2} \approx 53.3$ with saturation chemical potential $\mu^s = -n^s(g + g_{AB})/2 \approx -1.066$, while the (single-component) droplet of component C features saturation density $n_C^s = \frac{4mg_C}{9\hbar^2\pi^2} \approx 0.045$ and saturation chemical potential $\mu_C^s = -g_C n_C^s/2 \approx -0.0225$ [8].

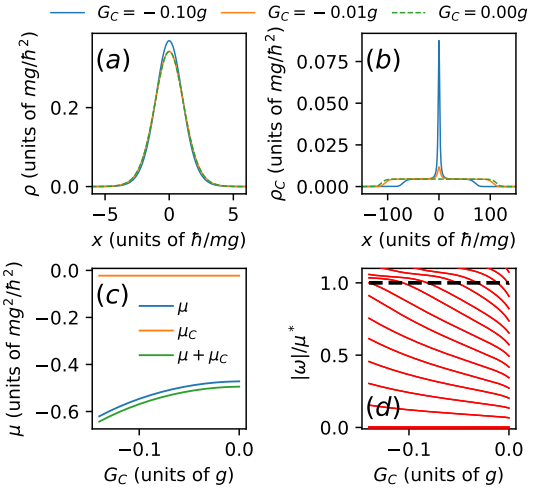

FIG. 1. Overview of particle balanced three-component droplet configurations. Ground state densities per particle of (a) the symmetric two-component droplet and (b) the third independent component C for varying intercomponent coupling G_C (see legend). The third component is either untrapped or partially trapped by the droplet for $G_C = 0$ and $G_C < 0$ respectively. (c) Chemical potentials of the symmetric droplet (μ), the C component (μ_C) and their summation $\mu + \mu_C$ as a function of G_C. It can be seen that all chemical potentials are negative implying that the ensuing configurations are strongly bound especially for larger negative G_C. (d) Elementary excitation spectrum of the particle-balanced configurations. The horizontal thick dashed line corresponds to the particle emission threshold, $\mu^* = \min(|\mu|, |\mu_C|)$. Evidently, component C remains only partially trapped by the two symmetric components for all values of G_C, with the untrapped fraction forming an extended single-component FT droplet. The particle-balanced three-component mixture consists of $N = N_C = 10$ atoms, with $g_C = g$, and $g_{AB} = -0.96g$.

A. Particle balance configurations: partial trapping of the third component

The ground-state density distributions of the symmetric droplet, $\rho(x) = |\Psi|^2/N$, consisting of two identical

[1] It can be shown that for $G_C = 0$ the minority component C satisfies the single-component droplet equation $i\hbar\frac{\partial\Psi_C}{\partial t} = \Big(-\frac{\hbar^2}{2m}\frac{\partial^2}{\partial x^2} + g_C|\Psi_C|^2 - \frac{\sqrt{mg_C^3}}{\hbar\pi}|\Psi_C|\Big)\Psi_C$.

species and the third component, $\rho_C(x) = |\Psi_C|^2/N_C$, are presented in Fig. 1(a), (b) for fixed $N = N_C = 10$ and different intercomponent interactions $G_C \leq 0$. As it can be seen, in the decoupled limit where $G_C = 0$ the droplet and species C are independent. The former assembles in a localized Gaussian-like configuration and the latter forms a flat-top (FT) structure. This situation implies that component C is un-trapped by the droplet. Turning our focus into attractive G_C, we observe that $\rho(x)$ maintains the Gaussian droplet profile regardless of the value of G_C and it exhibits a slight localization tendency for larger attractions accompanied by a small amplitude density hump at $x = 0$ (hardly visible in Fig. 1(a)). This means that the back-action of the comparatively delocalized component C to the droplet is suppressed, owing to their relatively weak coupling $|G_C| \ll |g_{AB}|$.

In sharp contrast, component C undergoes significant structural deformations upon tuning $G_C < 0$ as illustrated in Fig. 1(b). Namely, for relatively small attractive G_C, a density peak appears in $\rho_C(x)$ which simultaneously shows a localization trend. This behavior implies that a fraction of atoms from component C start to accumulate within the symmetric droplet. For stronger attractive G_C, the aforementioned density hump of $\rho_C(x)$ around $x = 0$ becomes significantly enhanced and $\rho_C(x)$ features a noticeable localization since a larger amount of C atoms are attracted and in particular trapped by the droplet. Here, it is evident that the atom fraction of species C trapped by the droplet is relatively small as can also be inferred from the somewhat small amplitude of the peak of $\rho_C(x)$ as compared to the peak of $\rho(x)$ which explains the minor impact of the former to the latter. In all cases, however, component C is only partially trapped by the symmetric droplet and the remaining atoms reside outside of it, while being distributed in a single-component FT droplet building upon $\rho_C(x)$ [Fig. 1(b)]. The FT structure has a substantially lower (higher) density (spatial extent) when compared to the droplet made by the two symmetric components and to the density peak of component C. Moreover, the FT density of component C remains constant at the single-component FT droplet density prediction [7], i.e. $\rho_C^s = n_C^s/N_C \approx 0.0045$ irrespectively of G_C, see also the discussion in Sec. IV for relevant analytical arguments of this effect.

To confirm the bound state nature of the studied configurations, we next compute the chemical potentials of the symmetric droplet μ and the third component μ_C as well as the total chemical potential $\mu_{\rm tot} = \mu + \mu_C$. These are shown in Fig. 1(c) as a function of the intercomponent coupling G_C. We note that we computed the chemical potentials by considering the total number of atoms as our principal bifurcation/continuation parameter, following our approach in Ref. [45]. We find that both $\mu < 0$ and $\mu_C < 0$ verifying that all components are self-bound even at $G_C \to 0$. Specifically, μ_C exhibits a slight decreasing trend (hardly visible in Fig. 1(c)) but overall remains nearly constant close to its saturation value $\mu_C^s = -\frac{2mg_C^2}{9\hbar^2\pi^2} \approx -0.0225$ [8]. On the other hand, μ acquires significantly more negative values compared to μ_C, which is attributed to the strong interaction ($g_{AB} = -0.96g$) between the components A and B forming a droplet even in the absence of component C. Furthermore, as expected μ experiences a noticeable decreasing trend for larger G_C attractions due to the enhanced binding with component C. Naturally, the total chemical potential, $\mu_{\rm tot} = \mu + \mu_C$, follows the same behavior with μ. The fact that $|\mu| < |\mu_{\rm tot}|$ indicates a stronger bound three-component configuration compared to the (two-component) droplet, thus manifesting the role of the third component.

Finally, we examine the excitation spectrum of the above-discussed three-component structures to understand their stability and collective mode behavior, see Fig. 1(d). As outlined in Sec. II B, the excitation spectrum is obtained using the BdG analysis, see also Appendix A for the matrix elements of the linearized equations. It turns out that the imaginary parts of the eigenvalues for all configurations studied throughout this work are zero as expected since we address ground states. Meanwhile, the real part of the spectrum is rich containing a plethora of elementary excitations that are energetically equidistant at $G_C = 0$ and their energy gap increases as the intercomponent coupling G_C becomes more attractive. The aforementioned increasing energy gap is associated with the interaction-dependent behavior of the collective modes whose branches exhibit an increasing tendency for larger attractive G_C. Interestingly, the higher-lying collective modes cross the corresponding particle emission threshold from below and hence they are lost for stronger G_C attraction. Note here that we have defined the particle emission threshold as $\mu^* = \min(|\mu|, |\mu_C|)$ which refers to the minimum excitation energy required to emit a particle from either component. This crossing entails the self-evaporation process of the three-component mixture which means that the specific collective excitation modes lying above the particle emission threshold are not sustained by the three-component droplet configuration. A similar behavior but for the collective modes of the 1D single-component droplet has been reported in [23].

Up to this point we studied the properties of three-component particle balanced mixtures, where it was shown that the third component binds to the symmetric two-component droplet and becomes partially trapped from the latter. A question that remains still open is whether the third component can be used as a knob to regulate the droplet structure and if it can be fully trapped by the symmetric droplet. In this latter case, the low density FT tails of component C may vanish or become less extended while the sharp density peaks at the center may become smoother. For these reasons, in the following, we explore the impact of particle-imbalance between the symmetric droplet and component C, where a larger atom number occupies the droplet.

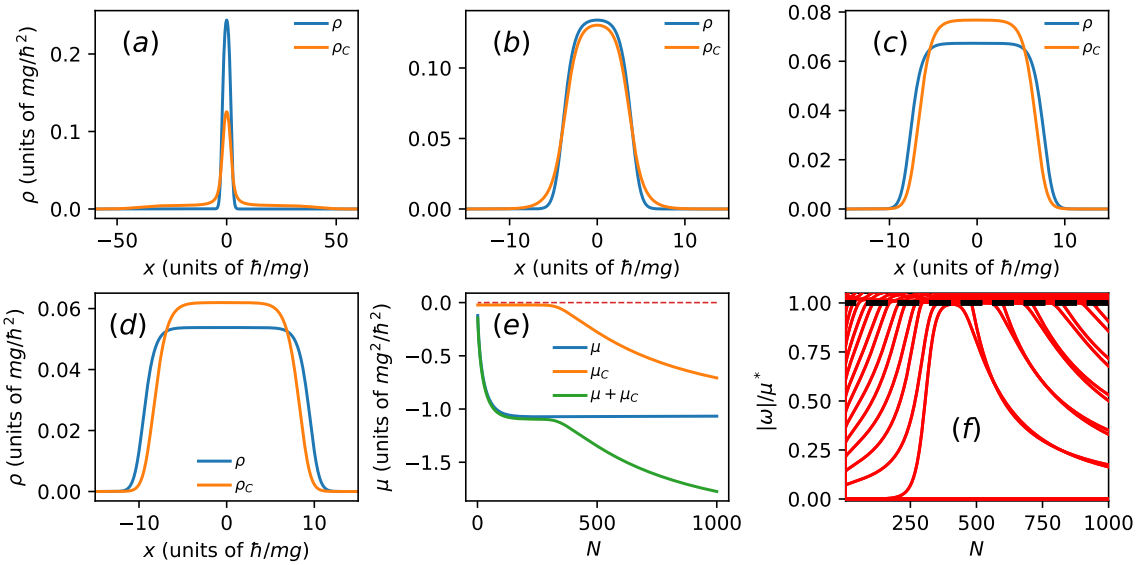

FIG. 2. Distributions of a particle imbalanced three-component mixture with $N_C = 10$ minority atoms in component C, fixed interactions $g = g_C$, $g_{AB} = -0.96g$, and $G_C = -0.01g$, and varying particle number N of the symmetric droplet. Ground-state densities of the individual components (see legends) for (a) $N = 200$, (b) $N = 400$, (c) $N = 800$ and (d) $N = 10^3$. Two distinct phases representing partial (panels (a), (b)) or full trapping (panels (c), (d)) of component C by the symmetric droplet can be discerned. (e) The total chemical potential and the ones of the symmetric droplet and component C (see legend) with respect to N. The horizontal dashed red line marks $\mu = 0$. A notable decrease of μ_C in the case of full trapping occurs. (f) Excitation spectrum of the three-component mixture for varying N. Evidently, upon increasing N the energy of the elementary excitations rises and eventually crosses the particle emission threshold (thick dashed line) as component C becomes fully trapped by the (two-component) droplet. Afterwards, further increasing N yields the particle emission threshold crossing of different excitations from above.

B. Particle imbalance: transition from partial to full trapping

It is known that a symmetric droplet in the absence of a third component (as in our case for $G_C = 0$), transitions from a Gaussian to a FT structure for increasing atom number while keeping the involved interactions fixed [22, 23]. Such a transition behavior occurs also in our setting even in the presence of intercomponent interactions ($G_C = -0.01$) between the droplet and the C component. This can be directly inferred from the blue solid lines in Fig. 2(a)-(d) representing the droplet ground state distributions for distinct particle numbers. Importantly, as the two majority components (A and B) deform toward the FT configuration, they are capable of trapping the minority component C, in-spite of the small intercomponent attraction $G_C = -0.01g$. In particular, the fraction of component C that remains untrapped by the symmetric droplet and occupies a FT single-component structure in the particle balanced case [Fig. 1(b)] becomes progressively smaller and smoother losing its FT character as N increases [Fig. 2(a), (b)], while simultaneously the droplet acquires a FT configuration. Eventually, for sufficiently large particle number the FT droplet of the majority components fully traps component C, see Fig. 2(c), (d). We have checked that this transition behavior occurs also for other G_C values, albeit shifted to larger atom numbers of the majority droplet for decreasing magnitude of G_C (i.e., smaller attractions), see also the discussion below and Fig. 3.

To further understand the aforementioned transition of the three-component mixture we inspect the dependence of the involved chemical potentials which in general take negative values throughout the considered atom number variation as shown in Fig. 2(e). Concretely, the chemical potential of the majority (two-component) droplet, μ, decreases sharply for larger particle number and subsequently saturates (for the used parameters around $N \approx 250$) close to its value $\mu^s \approx -1.066$ attained at the decoupled limit ($G_C = 0$), see also Sec. IV for further details. Beyond this point further increasing the symmetric droplet atom number N does not effect its chemical potential μ. Conversely, the chemical potential μ_C of the minority component C, is initially almost un-affected by the atom number increase of the symmetric droplet being nearly constant at its value at the decoupled limit, i.e., $\mu_C \approx \mu_C^s$. This situation takes place as long as component C remains partially trapped by the majority droplet. However, a further increase of $N > 250$ leads to pronounced and eventually ($N > 550$)

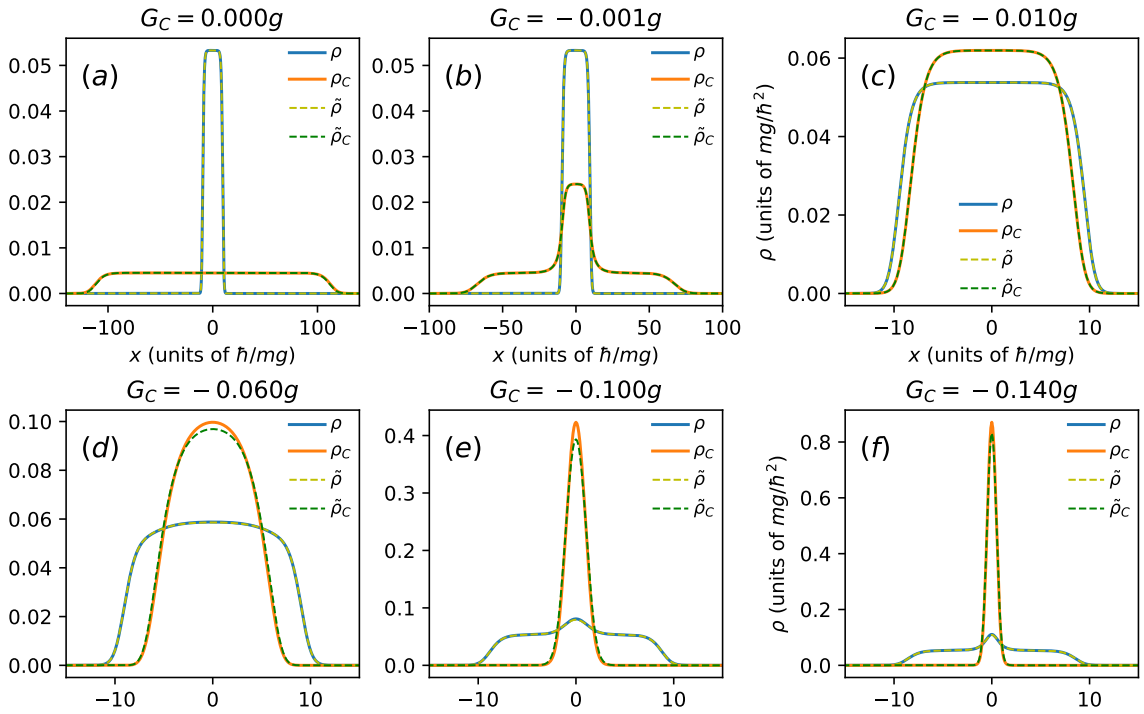

FIG. 3. Particle imbalanced ground state densities of the majority droplet with $N = 10^3$ atoms and the third component containing $N_C = 10$ particles, with $g_C = g$, $g_{AB} = -0.96g$, and different intercomponent attractions G_C (see legends). For vanishing [panel (a)] or very weak [panel (b)] intercomponent attraction G_C the majority droplet is decoupled and loosely bound respectively to the minority component C. Turning to stronger intercomponent attractions the minority component becomes fully trapped by the majority droplet [panels (c)-(f)], while relatively small undulations build progressively atop the majority droplet density in the neighborhood of component C [panels (e), (f)]. Dashed lines represent the solution of the effective model of Eq. (15) derived in Sec. IV.

to full trapping of the minority component C within the symmetric droplet and its (negative) chemical potential features a substantial decrease with N, indicating that it progressively becomes more strongly bound. This enhancement of the bound state is naturally imprinted in the total chemical potential, $\mu_{\rm tot} = \mu + \mu_C$, as can be readily seen in Fig. 2(e).

Having identified the crossover from partial to full trapping of component C by the majority droplet it is interesting to explore how this is imprinted in the underlying excitation spectrum and whether it entails modifications in the collective mode behavior. The respective numerically computed excitation spectrum in terms of the symmetric droplet atom number using the BdG analysis is illustrated in Fig. 2(f). Starting from small particle numbers N of the majority droplet comparable to the minority component C, the collective mode frequencies are well separated energetically showing an increasing trend for larger N and cross the particle emission threshold, $\mu^* = \min(|\mu|, |\mu_C|)$. This crossing takes place at different N values depending on the energy of the collective modes, namely higher-order ones typically cross μ^* at smaller N compared to energetically lower ones.

Interestingly, there is an atom number parametric window, see $N \in [380, 440]$ in Fig. 2(f), where the lowest collective mode lays very close to the particle emission threshold (here $|\omega|/\mu^* \approx 0.993$) and all energetically higher modes have crossed μ^*. This suggests that in the crossover region of component C from being partially trapped to fully trapped, the three-component mixture is in a rather delicate balance. Namely, a perturbed/excited three-component mixture does not sustain higher-lying collective modes and it rather prefers to emit particles from component C in order to enter the fully trapped regime. A further increase of the atom number (N) in the majority droplet facilitates the reappearance of excitation modes in the spectrum through crossing μ^* from above, and hence becoming again available to the three-component mixture. Importantly, the behavior of these modes is somewhat different compared to the ones that were present below the crossover region. Indeed, below the crossover region (e.g., $N < 300$) the modes are gaped (aside from their sign degeneracy), while (at least) the first few lower lying ones above this

region (e.g. $N > 500$) feature a pairing tendency becoming two-fold quasi-degenerate (on top of their trivial sign degeneracy). It is also worth mentioning that our simulations delineate that the above-discussed transition region is rather smooth and it is not easy to define a specific transition point.

Up to this point we studied the phases of the particle imbalance three-component mixture for varying atom numbers in the symmetric droplet and relatively weak intercomponent attraction (G_C) between the majority droplet and the minority species. In what follows, we examine the impact of G_C on the ensuing ground-state configurations for fixed particle imbalance set by $N = 10^3$ and $N_C = 10$, see Fig. 3. We observe that for vanishing or sufficiently small intercomponent coupling e.g., $G_C = 0$ [Fig. 3(a)] or $G_C = -0.001g$ [Fig. 3(b)], the distribution of component C is practically decoupled from the symmetric droplet being completely un-trapped and loosely trapped by the symmetric droplet respectively. Namely, if $G_C = 0$ component C configures in a FT distribution being fully decoupled from the FT configuration of the majority droplet, see also the discussion in Sec. IV. Turning to relatively small $G_C < 0$ values, the configurations of both the droplet and component C change noticeably. The symmetric droplet maintains its FT shape and its width becomes slightly smaller, while the atom cloud of component C shrinks significantly accommodating a fraction of atoms being trapped in the majority droplet and the remaining atoms residing at the delocalized density tails similarly to the particle balance case [Fig. 1(b)].

For larger attractions, such as $G_C = -0.01g$ or $G_C = -0.06g$ illustrated in Fig. 3(c), (d), the density undulations of component C disappear with the latter becoming fully trapped within the majority droplet. The density of the minority component C becomes more spatially localized transitioning from a FT for $G_C = -0.01g$ [Fig. 3(c)] to a Gaussian shape for $G_C = -0.06g$ [Fig. 3(d)). Accordingly, the majority droplet density slightly shrinks due to the increased attraction but it maintains a FT configuration enclosing the minority component. A further increase of the intercomponent attraction, e.g., to $G_C = -0.1g$ or $G_C = -0.14g$ as depicted in Fig. 3(e), (f) yields dramatic changes in the densities of both the symmetric droplet and component C. We remark that these values of G_C refer to strong attractions when compared to the MF stability edge $|G_C| \leq 0.1\sqrt{2}$. Specifically, the minority component features a substantial localization arranging in a sharply peaked soliton-like structure, while being fully trapped in the symmetric droplet which forms a comparatively spatially extended FT distribution. The latter exhibits noticeable density modulation at the vicinity of the minority cloud due to the appreciable attraction, similarly to two-component particle imbalanced droplets discussed in Ref. [40].

The degree of the bound state character of the aforementioned three-component states along with the binding of the constituting components can be estimated through the individual chemical potentials presented in Fig. 4(a) for varying G_C. As expected, the chemical potential of the majority (two-component) droplet μ is negative for every G_C since the droplet is a self-bound configuration. Interestingly, μ remains approximately constant at its saturation value $\mu^s \approx -1.066$ at the decoupled ($G_C = 0$) limit and it appears to be largely insensitive to the intercomponent coupling with the minority component C. We may attribute this insensitivity to the large particle imbalance. Recall here that in the particle balanced scenario illustrated in Fig. 1(c) the situation is reversed and μ increases with increasing G_C. On the other hand, the chemical potential of the minority component (μ_C) has a more involved behavior. Namely, at $G_C = 0$ it is slightly negative acquiring its saturation value $\mu_C^s \approx -0.0225$, and as long as $G_C \neq 0$ it monotonically decreases with decreasing G_C. This implies the formation of stronger bound configurations ~~building on top~~ of component C, while the crossing point between μ and μ_C at $G_C \approx -0.0135g$ happens when the transition from partially to fully trapped component C occurs. We remark that the total chemical potential $\mu_{\rm tot} = \mu + \mu_C$ mainly inherits the behavior of μ_C suggesting stronger binding of the three-component setting for larger attractions.

Finally, for completeness we examine the excitation spectrum of the system as a function of G_C whose real part is depicted in Fig. 4(b), (c) aiming to identify distinctive spectral signatures for the crossover from partially to fully trapped component C within the symmetric droplet. As for the configurations discussed in the previous sections the imaginary parts of the corresponding eigenvalues are zero suggesting that the underlying configurations are dynamically stable. It can be readily seen in Fig. 4(b) that the collective mode branches have a strong interaction dependence which leads to a rather complicated behavior. In particular, for strong intercomponent attraction $G_C \lessapprox -0.1g$, a sequence of avoided-crossings between consecutive modes is observed. Decreasing the intercomponent attraction toward $G_C \lessapprox -0.05g$ results in several additional modes crossing from above the particle emission threshold and featuring avoided-crossings with the pre-existent lower-lying modes along with a pairing tendency [Fig. 4(b)]. Turning to sufficiently weak attractions, such as $G_C \gtrapprox -0.02g$, energetically neighboring collective modes come very close and subsequently cross the particle emission threshold [Fig. 4(c)] with only the lower-lying one remaining below that threshold. In this regime the transition from fully to partially trapped component C by the symmetric droplet occurs.

Next, tuning $G_C \to 0$ the higher-lying modes reemerge crossing the particle emission threshold from above and appearing in gaped energy branches un-paired as component C starts to decouple from the majority (two-component) droplet [Fig. 4(c)]. Recall here that this latter behavior is consistent with the one illustrated in Fig. 2(f), where increasing the atom number while keeping fixed G_C resulted in the opposite transition as

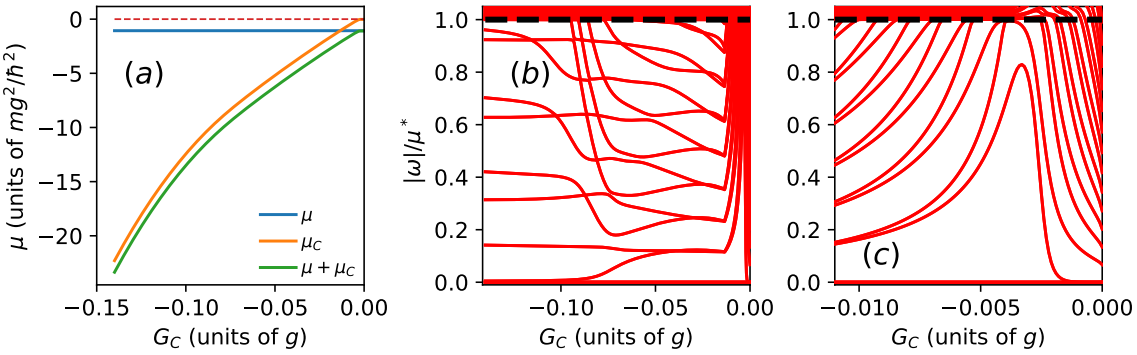

FIG. 4. (a) Chemical potentials (see legend) and (b) excitation spectrum of a particle imbalance three-component mixture as a function of the intercomponent attraction between the majority droplet with $N = 10^3$ and component C having $N_C = 10$ atoms. It is observed that upon increasing G_C, component C becomes less strongly bound as indicated by the decreasing magnitude of μ_C, while the chemical potential of the majority droplet (μ) remains largely un-affected. The horizontal red dashed line represents $\mu = 0$. In the spectrum, it is found that the collective modes show a rather complicated interaction-dependent behavior in terms of G_C [panel (b)] experiencing multiple avoided-crossings. (c) Same as (b), but restricted to weak intercomponent attractions to clearly visualize the behavior of the collective modes in this interaction regime. As in the case of varying N depicted in Fig. 2(f), the modes (except the lower-lying one) cross the particle emission threshold, $\mu^* = \min(|\mu|, |\mu_C|)$ (see dashed horizontal line), from below and afterwards they re-emerge from above. Other interaction parameters correspond to $g_C = g$, and $g_{AB} = -0.96g$.

the minority component C became trapped by the majority droplet. Summarizing, the above-discussed complicated interaction dependent behavior of the ensuing collective modes suggests that the particle imbalance three-component mixture is very promising for observing rich dynamical phenomena, e.g. upon quenching or sweeping the intercomponent coupling strength. This is certainly an intriguing direction for future studies where the nonequilbrium features imprinted on the density profiles of the individual components can be associated e.g. with the observed avoided-crossings in the spectrum.

IV. EFFECTIVE EXTENDED GROSS-PITAEVSKII EQUATION MODELS AT HIGH PARTICLE IMBALANCE

To gain further insights on the character of the three-component states discussed in the previous sections, we next develop relevant effective models based on suitable reductions of the full eGPEs (3). More concretely, we consider the case where the third component (C) is occupied by a much smaller number of atoms compared to the two symmetric components A and B forming the majority droplet, i.e. $N \gg N_C \gg 1$. Additionally, in this context, all three components remain macroscopically occupied, such that the Bogoliubov approximation remains justified. Taylor expanding with respect to N_C/N the elements in the LHY energy density described by Eq. (1) (more formally called a Puiseux expansion [64]), and keeping only terms scaling with non-negative powers of N yields the approximate expression

$$\mathcal{E}'_{\rm LHY} = \frac{-2\sqrt{mg^3}}{3\hbar\pi}\Big[(f_-^{\frac{3}{2}} + f_+^{\frac{3}{2}})n^{\frac{3}{2}} + \frac{3f_G}{4}\sqrt{f_+ n}n_C + (\frac{g_C}{g} - \frac{f_G}{2})^{\frac{3}{2}} n_C^{\frac{3}{2}} + \mathcal{O}(\frac{1}{\sqrt{N}})\Big]. \tag{7}$$

Here, the density independent parameters $f_\pm = 1 \pm g_{AB}/g$ and $f_G = 4G_C^2/(g^2 f_+)$, see also Appendix B for further details on this derivation. It is also instructive to remark that following this notation, the MF stability window translates to $0 < f_\pm < 2$ and $f_G \leq 2g_C/g$.

The scaling of the individual terms participating in the total approximate energy density, i.e.,

$$\mathcal{E}' = gn^2 + \frac{g_C}{2}n_C^2 + 2G_C n n_C + g_{AB}n^2 + \mathcal{E}'_{LHY} \tag{8}$$

and the corresponding eGPEs with the particle number is summarized in Table I for an imbalanced setting hosting $N = 10^3$ and $N_C = 10$ atoms. As can be readily seen, in all cases the dominant terms are those involving the majority components (A and B) atom number, while the ones associated with the minority component particle number are significantly smaller. Finally, the last two columns in Table I have an inverse scaling with N and they represent the first neglected terms in the expansion of the LHY energy of Eq. (7). Clearly, their contribution is indeed negligible compared e.g. to the MF terms provided in the first, second, and fifth columns of Table I. Hence, these LHY contributions can be safely omitted.

$\mathcal{E}\sim$	N^2	NN_C	$N^{\frac{3}{2}}$	$\sqrt{N}N_C$	N_C^2	$N_C^{\frac{3}{2}}$	$\frac{N_C^{\frac{5}{2}}}{N}$	$\frac{N_C}{\sqrt{N}}$
Energy	10^6	10^4	$10^{\frac{9}{2}}$	$10^{\frac{5}{2}}$	10^2	$10^{\frac{3}{2}}$	$\frac{1}{10^{\frac{1}{2}}}$	$\frac{1}{10^{\frac{1}{2}}}$
$\frac{\partial\mathcal{E}}{\partial n}\sim$	N	N_C	$N^{\frac{1}{2}}$	$\frac{N_C}{\sqrt{N}}$	0	0	$\frac{N_C^{\frac{5}{2}}}{N^2}$	$\frac{N_C}{N^{\frac{3}{2}}}$
eGPE$_{(A,B)}$	10^3	10	$10^{\frac{3}{2}}$	$\frac{1}{10^{\frac{1}{2}}}$	0	0	$\frac{1}{10^{\frac{5}{2}}}$	$\frac{1}{10^{\frac{5}{2}}}$
$\frac{\partial\mathcal{E}}{\partial n_C}\sim$	0	N	0	$\sqrt{N}$	N_C	$\sqrt{N_C}$	$\frac{N_C^{\frac{3}{2}}}{N}$	$\frac{1}{\sqrt{N}}$
eGPE$_{(C)}$	0	10^3	0	$10^{1.5}$	10	$10^{\frac{1}{2}}$	$\frac{1}{10^{\frac{3}{2}}}$	$\frac{1}{10^{\frac{3}{2}}}$

TABLE I. Scaling of the various terms appearing in the total approximate energy density [Eq. (8)] containing the LHY contribution given by Eq. (7) and the corresponding eGPEs [Eq. (3)] with respect to the atom number for a highly particle imbalanced three-component mixture containing $N = 10^3$, and $N_C = 10$. It is evident that terms encompassing the majority droplet atom number, N, have the dominant contribution.

A. Decoupled limit

As a first, somewhat crude approximation, we assume that the particle imbalance is sufficiently high such that the majority droplet component is practically unaffected by the presence of the minority species. As such, it is possible to neglect all terms in the LHY energy density of Eq. (7) that scale with N_C (and hence also intracomponent interactions of component C) and arrive in a reduced $\mathcal{E}'_{\rm red}$ out of the approximate $\mathcal{E}'$ given by Eq. (8). Following a standard variational treatment for the energy density $\mathcal{E}'_{\rm red}$ results in the approximate eGPEs

$$i\hbar\frac{\partial\Psi'}{\partial t} = -\frac{\hbar^2}{2m}\frac{\partial^2\Psi'}{\partial x^2} + \Big((g+g_{AB})\,|\Psi'|^2 - \frac{\sqrt{m}}{2\hbar\pi}(f_-^{3/2}+f_+^{3/2})g^{3/2}\,|\Psi'|\Big)\Psi', \tag{9a}$$

$$i\hbar\frac{\partial\Psi'_C}{\partial t} = \Big(-\frac{\hbar^2}{2m}\frac{\partial^2}{\partial x^2} + V_{\rm eff}(n')\Big)\Psi'_C, \tag{9b}$$

where $n'(x) = |\Psi'(x)|$ and $n'_C(x) = |\Psi'_C(x)|$. These expressions reveal that in this limit and to lowest-order, the majority droplet satisfies a single-component eGPE, while the minority component is under the influence of an effective box-like potential

$$V_{\rm eff}(n') = 2G_C n' - \frac{\sqrt{f_+ mg^3}}{2\hbar\pi} f_G\sqrt{n'}, \tag{10}$$

similarly to the two-component particle imbalanced droplet mixture discussed in Ref. [40]. Apparently, this is created by the majority droplet and depends on the intercomponent interaction (G_C) between the droplet and component C but also on the interaction parameters (g, g_{AB}) of the droplet. Recall that similar effective potentials in highly particle imbalanced mixtures have been successfully used in completely different contexts such as polarons [65], rogue waves [66, 67], and the Townes soliton [68, 69].

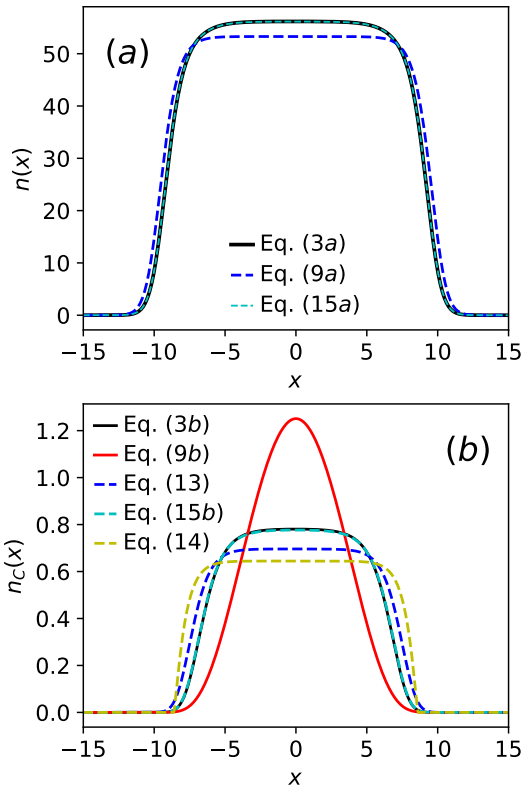

FIG. 5. Comparison between the predictions of different reduced eGPE models introduced in Sec. IV (see legends) and the full numerical solution of the eGPEs of Eq. (3). Ground-state density of (a) the majority droplet and (b) the minority C component. Clearly the predictions of the coupled model of Eq. (15) are in excellent agreement with the exact solutions. Neglecting the MF coupling results in noticeable deviations, however the model of an interacting minority component (Eq. (13)) dressed by and immersed in the symmetric two-component droplet (Eq. (9a)) is fairly close to the exact results. A highly particle imbalanced three-component system is considered with $N = 10^3$, $N_C = 10$ atoms, as well as $g = g_C = g$, $g_{AB} = -0.96g$, and $G_C = -0.04g$ interaction strengths.

This simplified approach motivates us to search for stationary solutions, by setting $\Psi' = e^{-i\mu' t/\hbar}\Phi'$ and $\Psi'_C = e^{-i\mu'_C t/\hbar}\Phi'_C$. Accordingly, Eq. (9a) describing the majority droplet admits the standard droplet solution [6, 7] being valid in the thermodynamic limit

$$\Phi'(x) = \frac{A}{1+\Gamma\cosh\lambda x}, \tag{11}$$

where the involved parameters correspond to

$$A = \frac{-6\hbar\pi\mu'}{\sqrt{mg^3}(f_-^{3/2}+f_+^{3/2})} = \frac{\sqrt{n^s}\mu'}{\mu^s}, \tag{12a}$$

$$\lambda = \sqrt{\frac{-2m\mu'}{\hbar^2}}, \tag{12b}$$

$$\Gamma = \sqrt{1 + \frac{36\hbar^2\pi^2\mu'}{mg^3(f_-^{3/2} + f_+^{3/2})^2}} = \sqrt{1 - \frac{\mu'}{\mu^s}}. \tag{12c}$$

In these expressions, the droplet saturation density $n^s = \frac{mg^3(f_-^{3/2}+f_+^{3/2})^2}{9\hbar^2\pi^2(g+g_{AB})^2}$, with associated saturation value of the chemical potential $\mu^s = -n^s(g+g_{AB})/2$. Note that n^s and μ^s in Eq. (12) coincide with the values at the decoupled limit G_C. This solution is valid within the interval $\mu^s < \mu' < 0$ [7, 8]. For sufficiently large particle imbalance and relatively weak coupling G_C, this solution adequately captures the exact ground-state obtained by numerically solving the exact eGPEs of Eq. (3), as shown in Fig. 5(a). The observed discrepancies in the peak amplitude and width of the droplet distribution are traced back to the neglected MF intercomponent coupling (G_C) with the minority component. Indeed, as it will be showcased below re-introducing the MF coupling in Eq. (9a) leads to an excellent agreement with the full eGPEs predictions. We remark, on the other hand, that for larger atom numbers in the droplet e.g. $N = 10^4$ the deviations reduce (not shown) even in the absence of G_C. This is a consequence of the fact that the terms $\sim |\Psi'|^2$ and $\sim |\Psi'|$ in Eq. (9a) dominate.

Substituting the exact droplet solution given by Eq. (11) (along with Eq. (12)) into Eq. (9b) describing the minority component, we can readily, numerically diagonalize the linear system $H\Phi_n^{'C} = -\frac{\hbar^2}{2m}\frac{\partial^2\Phi_n^{'C}}{\partial x^2} + V_{\rm eff}(n)\Phi_n^{'C} = E_n^C\Phi_n^{'C}$, and find its eigenstates. The latter are similar to the ones of a single-particle trapped in a finite box potential with depth dictated by $V_{\rm eff}(n^s)$, due to the FT shape of the majority droplet density. Hence, they prominently deviate from the full eGPE predictions for the shape of the minority component, see Fig. 5(b). Thus, it becomes clear that this level of approximation is too restrictive for approaching the distribution of the minority component. Indeed, the MF and the LHY nonlinear terms, albeit having a smaller magnitude compared to $V_{\rm eff}(n^s)$, are responsible for giving rise to qualitatively different structures. As such, in order to improve the accuracy of our model, even in the decoupled limit, we take into account the MF intracomponent repulsion ($g_C|\Psi_C|^2\Psi_C$) and the LHY term $\sim |\Psi_C|\Psi_C$ in Eq. (9b). This leads to the effective single-component eGPE governing the minority component

$$\begin{aligned} i\hbar\frac{\partial\Psi_C''}{\partial t} = &-\frac{\hbar^2}{2m}\frac{\partial^2\Psi_C''}{\partial x^2} + V_{\rm eff}(n')\Psi_C'' + g_C|\Psi_C''|^2\Psi_C'' \\ &- \frac{\sqrt{mg^3}}{\hbar\pi}\Big(\frac{g_C}{g} - \frac{f_G}{2}\Big)^{3/2}|\Psi_C''|\Psi_C'', \end{aligned} \tag{13}$$

where, $\rho'(x) = n'(x)/N = \Psi''(x)/N$ and $\rho_C''(x) = n_C''(x)/N = \Psi_C''(x)/N_C$.

It is important to notice that the symmetric droplet is influencing the minority component in three distinct ways. Indeed, within the effective potential $V_{\rm eff}(n')$ there is i) the direct MF intercomponent coupling ($2G_C|\Psi'|^2$) and ii) the beyond MF intercomponent coupling ($\sim |\Psi'|$) stemming from the genuinely three-component LHY energy Eq. (8). Moreover, iii) the beyond MF intracomponent coupling of the minority species is modified by the presence of the majority droplet resulting in a different multiplicative factor $\sqrt{mg^3}(g_C/g - f_G/2)^{3/2}/(\hbar\pi)$ compared to the genuinely single-component LHY factor [$\sim \sqrt{mg_C^3}/(\pi\hbar)$]. The numerical solution of Eq. (13) is shown in Fig. 5(b) against the outcome of the full eGPEs of Eq. (3). It qualitatively captures the distribution of the minority component but with a smaller peak density and slightly larger width. Despite these deviations the prediction of this model is clearly improved compared to the previous case where the nonlinear terms are absent, compare in particular red solid and blue dashed lines against the black solid one in Fig. 5(b).

To obtain analytical insights on the behavior of the minority component, we next consider the Thomas-Fermi limit reached by neglecting the kinetic term in Eq. (13). This solution takes the form

$$\Phi_C^{\rm TF} = \frac{\sqrt{2mg^3}}{8\hbar\pi g_C}(2\frac{g_C}{g} - f_G)^{3/2}\Big[1 - U\Big], \tag{14}$$

where $U = (1 + 32\frac{\hbar^2\pi^2 g_C(\mu_C - V_{\rm eff})}{mg^3(2\frac{g_C}{g} - f_G)^3})^{\frac{1}{2}}$. Following the standard calculation in the Thomas-Fermi limit, we can find the associated density boundary (dubbed here x_b) by demanding $\Phi_C^{\rm TF} = 0 \to \mu_C^{\rm TF} = V_{\rm eff}(x_b)$, while the density is taken to be zero outside this boundary. The chemical potential μ_C is fixed by the normalization condition $N_C = \int_{-x_b}^{x_b}|\Phi_C^{\rm TF}|^2\,dx$. The boundary is given by $x_b = \frac{1}{\lambda}\cosh^{-1}\frac{A-|K|}{\Gamma|K|}$, where $|K| = \frac{\sqrt{f_+mg^3}f_G}{8\hbar\pi G_C}\Bigg[1 - \sqrt{1 + \frac{32G_C\mu_C^{\rm TF}\hbar^2\pi^2}{f_+mg^3f_G^2}}\Bigg]$ and A, λ, Γ are the same as in Eq. (12). The maximum density of the minority component is given by substituting $V_{\rm eff} = V_{\rm eff}(x=0) = V_{\rm eff}(n^s)$. Note that $\Phi_C^{\rm TF}$ is negative and real for $\mu_C^{\rm TF} > V_{\rm eff}$, while its real part becomes positive and it obtains a negative imaginary part as well for $\mu_C^{\rm TF} < V_{\rm eff}$, i.e. outside the density boundaries $|x| > x_b$. The Thomas-Fermi profile of Eq. (14) has a qualitatively similar shape to the exact density [Eq. 3] of the minority component but exhibits a reduced (larger) peak amplitude (width), see yellow dashed line in Fig. 5(b). Notice that its deviation from the exact eGPE result is somewhat larger compared to the one of the model of Eq. (13) which in addition incorporates the kinetic term. This implies that the kinetic energy contribution is important for describing the minority component.

B. Re-introducing mean-field coupling

The term that we have so far neglected in the approximate eGPE for the two-component droplet of Eq. (9a) which doesn't scale with negative powers of N but with N_C is the direct intercomponent MF coupling $\propto G_C n_C$. To incorporate this term we employ the variational treatment of the energy density $\mathcal{E}'$ resulting in the following coupled set of approximate eGPEs

$$\begin{aligned} i\hbar\frac{\partial\tilde{\Psi}}{\partial t} =& -\frac{\hbar^2}{2m}\frac{\partial^2\tilde{\Psi}}{\partial x^2} + \Big((g+g_{AB})\left|\tilde{\Psi}\right|^2 + G_C\left|\tilde{\Psi}_C\right|^2 \\ & - \frac{\sqrt{m}}{2\hbar\pi}(f_-^{3/2}+f_+^{3/2})g^{3/2}\left|\tilde{\Psi}\right|\Big)\tilde{\Psi}, \qquad (15a) \\ i\hbar\frac{\partial\tilde{\Psi}_C}{\partial t} =& -\frac{\hbar^2}{2m}\frac{\partial^2\tilde{\Psi}_C}{\partial x^2} + g_C\left|\tilde{\Psi}_C\right|^2\tilde{\Psi}_C \\ & + \Big(2G_C\left|\tilde{\Psi}\right|^2 - \frac{\sqrt{f_+ mg^3}}{2\hbar\pi}f_G\left|\tilde{\Psi}\right|\Big)\tilde{\Psi}_C \qquad (15b) \\ & - \frac{\sqrt{2mg^3}}{4\hbar\pi}\Big(2\frac{g_C}{g}-f_G\Big)^{3/2}\left|\tilde{\Psi}_C\right|\tilde{\Psi}_C. \end{aligned}$$

In these expressions, $\tilde{\rho}(x) = \tilde{n}(x)/N = \left|\tilde{\Psi}(x)\right|^2/N$ and $\tilde{\rho}_C(x) = \tilde{n}_C(x)/N = \left|\tilde{\Psi}_C(x)\right|^2/N_C$. Note here that Eq. (15b) is identical to that of Eq. (13), while Eq. (15a) differs from Eq. (9a) by a single term, namely $G_C|\tilde{\Psi}_C|^2$. This difference, however, results in a coupled set of equations, meaning that the majority droplet density cannot be considered as a static effective potential and the two equations need to be solved concurrently and self-consistently. In this sense, the intercomponent MF coupling, introduces the back-action of the minority component onto the majority droplet.

The numerical solution of these coupled approximate eGPEs is found to be in near perfect agreement with the solutions of the exact eGPEs described by Eq. (3), for weak intercomponent attractions ($G_C < 0$), compare the dashed and solid lines in Fig. 5 and in Fig. 3(a)-(c). Note that in the decoupled limit $G_C = 0$ [Fig. 3(f)] the standard droplet solution [Eq. (11)] describes the majority droplet and the minority component C with the appropriate parameter (e.g., $\mu \to \mu_C$, $\lambda \to \lambda_C$) modifications for the latter case. For larger attractions, as the ones depicted in Fig. 3(d)-(f), we know that within the full eGPEs [Eqs. (3)] structural deformations of the majority droplet density take place due to the presence of component C, yielding a locally modulated FT profile of the majority droplet in the vicinity of component C which has a Gaussian shape. While these distorted states cannot be captured by the standard droplet solution of Eq. (11), they can be fairly well reproduced by the coupled set of approximate eGPEs [Eq. (15)], as can be readily seen in Fig. 3(d)-(f). Notice the relatively small deviations between the predictions of the reduced model of Eq. (15) and the exact eGPEs in the minority component density for such stronger attractions, where the former estimates a slightly smaller maximum density around $x = 0$ and correspondingly slightly larger width (hardly visible in the scales of Fig. 3(d)-(f)). This is attributed to the fact that the minority component density develops a Gaussian profile upon increasing $|G_C|$, hence imprinting a progressively sharper density hump at the majority droplet distribution. Thus, the neglected energy terms, proportional e.g. to $\sim n_C^{5/2}/n$, become enhanced in-spite of the large particle number imbalance among the droplet and component C.

V. SUMMARY AND PERSPECTIVES

We studied the stability and phases of 1D three-component bosonic mixtures composed of two symmetric species and a third, independent, component within the LHY framework. The two components with repulsive (attractive) intracomponent (intercomponent) interactions form a strongly self-bound symmetric droplet which is coupled to the third species. To assess the composite phases of the three-component mixture we compute the ground-state densities, the chemical potentials and the low-amplitude excitation spectrum (using BdG analysis) as a function of the atom number of the symmetric droplet or the intercomponent interaction between the symmetric droplet and the third component. Three main phases arise referring to an un-trapped, partially trapped and fully trapped third component by the droplet.

First, the particle balanced setup between the symmetric droplet and the third component was briefly addressed. In this case, the third component configures in a spatially extended FT structure lying mainly outside the arguably more localized symmetric droplet and being significantly perturbed by the presence of the latter featuring a pronounced density peak in the overlap region. The system is found to be relatively weakly bound, with the chemical potential increasing as the intercomponent attraction is reduced. Meanwhile, the low-amplitude collective modes gradually cross the particle-emission threshold from below as the intercomponent attraction increases.

Focusing on the particle imbalanced mixture within the weakly attractive regime, we find that upon increasing the atom number of the symmetric droplet, the minority component becomes progressively fully trapped by the droplet, and eventually both species acquire comparable spatial extents. This transition is accompanied by a decrease in the (negative) chemical potentials, indicating the formation of stronger self-bound configurations. This crossover is also clearly imprinted in the excitation spectrum. All modes (except the lowest-lying one) cross the particle-emission threshold from below as the system approaches the transition region and afterwards re-emerge from above, featuring a characteristic pairing tendency in the trapped regime.

We also address the impact of the intercomponent coupling in the states of particle imbalanced mixtures considering variations within the attractive interaction MF

stability regime to the decoupled limit. For strong attractions, the minority component assembles in a Gaussian configuration being fully trapped by the (two-component) droplet, which in turn displays localized undulations in its FT profile at the vicinity of the third component. For moderate attractions, the densities of all components transition into FT configurations of comparable spatial extent. Close to the decoupled limit, the minority component becomes loosely trapped and gradually delocalizes into an extended, low density FT droplet, reminiscent to the one of the particle balance case. As expected, the system becomes less self-bound with decreasing attraction, and the collective modes in the weakly interacting regime exhibit a transition, crossing the particle emission threshold, similarly to the behavior observed for different particle number. Interestingly, for stronger attractions the excitation spectrum possesses a complex interaction-dependent behavior with the ensuing modes experiencing multiple avoided-crossings.

To understand better the numerically identified droplet states, we derive different effective models based on a reduction of the LHY energy density in the limit of large particle imbalance between the majority droplet and the third component. It turns out that the reduced model accounting for the MF interactions and an effective potential to the minority species created by the majority droplet yields excellent agreement with the predictions of the complete LHY theory described by the full eGPEs. Other most simplified models, e.g. neglecting the MF coupling or based on the Thomas-Fermi approximation lead to noticeable deviations with the full system behavior.

Our results open several intriguing directions for future studies especially for particle imbalanced droplet configurations, while providing an initial overview of their ground-state phases and spectrum. Certainly, exploring the effect of an external harmonic trap in the discussed configurations represents an avenue of experimental interest. An immediate extension is to investigate the dynamical response of the particle imbalanced configurations following a quench or a sweep of the intercomponent coupling exploiting the observed avoided-crossings between the collective modes across different localization regimes. Another interesting possibility is to explore the characteristics and properties of composite nonlinear excitations, as it was done for their single-component droplet counterpart [29], where the effective models developed herein may assist in extracting relevant analytical waveforms. Additionally, benchmarking the predictions of the LHY theory presented herein against ab-initio many-body methods [24, 46, 70] aiming also to understand the underlying correlation patterns remains a completely open question for three-component mixtures. Finally, our setup can be utilized to explore Bose polaron physics [56] with droplets to estimate, for instance, the lifetime, residue and induced interaction between the dressed minority atoms.

ACKNOWLEDGMENTS

E.G.C. is supported by the U.S. National Science Foundation under Grant No. DMS-2204782 and DMS-2527314. S.I.M. acknowledges support from the University of Missouri Science and Technology, Department of Physics, Startup fund. S.I.M. thanks P.G. Kevrekidis, G.C. Katsimiga and G.A. Bougas for fruitful discussions on the topic of droplets.

Appendix A: Stability matrix of the three-component mixture

In the main text, we have used BdG analysis to infer the stability and the behavior of the collective excitations of the three-component mixture comprising of two components forming a symmetric droplet and a third component C. To do so, we have linearized the original eGPEs [Eq. (3)] as outlined in Section II B to obtain the system of BdG equations containing the 4×4 stability matrix, dubbed $\mathcal{A}$. The elements of the latter, in dimensionless units, are given by

$$\mathcal{A}_{11} = -\frac{1}{2}\frac{\partial^2}{\partial x^2} - \mu + 2(g+g_{AB})\left|\Psi\right|^2 + G_C\left|\Psi_C\right|^2 + \frac{1}{2}\Big(\frac{\partial \mathcal{E}_{\rm LHY}}{\partial n} + \frac{\partial^2 \mathcal{E}_{\rm LHY}}{\partial n^2}\left|\Psi\right|^2\Big), \tag{A1a}$$

$$\mathcal{A}_{12} = (g + g_{AB} + \frac{1}{2}\frac{\partial^2 \mathcal{E}_{\rm LHY}}{\partial n^2})\Psi^2, \tag{A1b}$$

$$\mathcal{A}_{13} = (G_C + \frac{1}{2}\frac{\partial^2 \mathcal{E}_{\rm LHY}}{\partial n \partial n_C})\Psi\Psi_C^*, \tag{A1c}$$

$$\mathcal{A}_{14} = (G_C + \frac{1}{2}\frac{\partial^2 \mathcal{E}_{\rm LHY}}{\partial n \partial n_C})\Psi\Psi_C, \tag{A1d}$$

$$\mathcal{A}_{21} = (g + g_{AB} + \frac{1}{2}\frac{\partial^2 \mathcal{E}_{\rm LHY}}{\partial n^2})(\Psi^*)^2 = \mathcal{A}_{12}^*, \tag{A1e}$$

$$\mathcal{A}_{22} = -\frac{1}{2}\frac{\partial^2}{\partial x^2} - \mu + 2(g+g_{AB})\left|\Psi\right|^2 + G_C\left|\Psi_C\right|^2 + \frac{1}{2}\Big(\frac{\partial \mathcal{E}_{\rm LHY}}{\partial n} + \frac{\partial^2 \mathcal{E}_{\rm LHY}}{\partial n^2}\left|\Psi\right|^2\Big) = A_{11}, \tag{A1f}$$

$$\mathcal{A}_{23} =(G_C + \frac{\partial^2 \mathcal{E}_{\rm LHY}}{\partial n \partial n_C})\Psi^* \Psi_C^* = \mathcal{A}_{14}^*, \tag{A1g}$$

$$\mathcal{A}_{24} =(G_C + \frac{1}{2}\frac{\partial^2 \mathcal{E}_{\rm LHY}}{\partial n \partial n_C})\Psi^* \Psi_C = \mathcal{A}_{13}^*, \tag{A1h}$$

$$\mathcal{A}_{31} =(2G_C + \frac{\partial^2 \mathcal{E}_{\rm LHY}}{\partial n \partial n_C})\Psi^* \Psi_C, \tag{A1i}$$

$$\mathcal{A}_{32} =(2G_C + \frac{\partial^2 \mathcal{E}_{\rm LHY}}{\partial n \partial n_C})\Psi \Psi_C, \tag{A1j}$$

$$\mathcal{A}_{33} =-\frac{1}{2}\frac{\partial^2}{\partial x^2} - \mu_C + 2g_C |\Psi_C|^2 + 2G_C |\Psi|^2 + \frac{\partial \mathcal{E}_{\rm LHY}}{\partial n_C} + \frac{\partial^2 \mathcal{E}_{\rm LHY}}{\partial n_C^2} |\Psi_C|^2, \tag{A1k}$$

$$\mathcal{A}_{34} =(g_C + \frac{\partial^2 \mathcal{E}_{\rm LHY}}{\partial n_C^2})\Psi_C^2, \tag{A1l}$$

$$\mathcal{A}_{41} =(2G_C + \frac{\partial^2 \mathcal{E}_{\rm LHY}}{\partial n \partial n_C})\Psi^* \Psi_C^* = \mathcal{A}_{32}^*, \tag{A1m}$$

$$\mathcal{A}_{42} =(2G_C + \frac{\partial^2 \mathcal{E}_{\rm LHY}}{\partial n \partial n_C})\Psi \Psi_C^* = \mathcal{A}_{31}^*, \tag{A1n}$$

$$\mathcal{A}_{43} =(g_C + \frac{\partial^2 \mathcal{E}_{\rm LHY}}{\partial n_C^2})(\Psi_C^*)^2 = \mathcal{A}_{34}^*, \tag{A1o}$$

$$\mathcal{A}_{44} =-\frac{1}{2}\frac{\partial^2}{\partial x^2} - \mu_C + 2g_C |\Psi_C|^2 + 2G_C |\Psi|^2 + \frac{\partial \mathcal{E}_{\rm LHY}}{\partial n_C} + \frac{\partial^2 \mathcal{E}_{\rm LHY}}{\partial n_C^2} |\Psi_C|^2 = \mathcal{A}_{22}. \tag{A1p}$$

In the above expressions, the second derivatives with respect to the same densities take the form

$$\frac{\partial^2 \mathcal{E}_{\rm LHY}}{\partial n^2} =-\frac{\sqrt{2m}}{4\pi h}\Bigg(\sqrt{2}\frac{(g-g_{AB})^{\frac{3}{2}}}{\sqrt{n}} + \frac{\left(g+g_{AB}+\frac{\partial Q}{\partial n}\right)^2}{2\sqrt{W+Q}} + \frac{\left(g+g_{AB}-\frac{\partial Q}{\partial n}\right)^2}{2\sqrt{W-Q}} + \frac{\partial^2 Q}{\partial n^2}\left(\sqrt{W+Q}-\sqrt{W-Q}\right)\Bigg), \tag{A2a}$$

$$\frac{\partial^2 \mathcal{E}_{\rm LHY}}{\partial n_C^2} =-\frac{\sqrt{2m}}{4\pi h}\left(\frac{\left(g_C+\frac{\partial Q}{\partial n_C}\right)^2}{2\sqrt{W+Q}} + \frac{\left(g_C-\frac{\partial Q}{\partial n_C}\right)^2}{2\sqrt{W-Q}} + \frac{\partial^2 Q}{\partial n_C^2}\left(\sqrt{W+Q}-\sqrt{W-Q}\right)\right). \tag{A2b}$$

Here, the W, Q parameters are the ones introduced in the main text [see also Eq. (2)] participating in the full LHY energy density [Eq. (1)] of the considered three-component mixture. The second derivatives of Q with respect to the majority droplet density n and the one of component C read

$$\frac{\partial^2 Q}{\partial n^2} = \frac{(g+g_{AB})^2}{Q} - \frac{[(g+g_{AB})^2 n - (g g_C + g_{AB} g_C - 4G_C^2) n_C]^2}{Q^3} = \frac{1}{Q}[(g+g_{AB})^2 - (\frac{\partial Q}{\partial n})^2], \tag{A3a}$$

$$\frac{\partial^2 Q}{\partial n_C^2} = \frac{g_C^2}{Q} - \frac{[g_C^2 n_C - (g g_C + g_{AB} g_C - 4G_C^2) n]^2}{Q^3} = \frac{1}{Q}[(g_C)^2 - (\frac{\partial Q}{\partial n_C})^2]. \tag{A3b}$$

Finally, the mixed derivative term of the LHY energy density appearing in the matrix elements of the linearized system of equations is found to be

$$\frac{\partial^2 \mathcal{E}_{\rm LHY}}{\partial n \partial n_C} = \frac{\partial^2 \mathcal{E}_{\rm LHY}}{\partial n_C \partial n} =-\frac{\sqrt{2m}}{4\pi h}\Bigg(\frac{\left(g_C+\frac{\partial Q}{\partial n_C}\right)\left(g+g_{AB}+\frac{\partial Q}{\partial n}\right)}{2\sqrt{W+Q}} + \frac{\left(g_C-\frac{\partial Q}{\partial n_C}\right)\left(g+g_{AB}-\frac{\partial Q}{\partial n}\right)}{2\sqrt{W-Q}} + \frac{\partial^2 Q}{\partial n \partial n_C}\left(\sqrt{W+Q}-\sqrt{W-Q}\right)\Bigg), \tag{A4}$$

where the relevant expression of the mixed derivative of the Q parameter becomes

$$\frac{\partial^2 Q}{\partial n \partial n_C} = \frac{\partial^2 Q}{\partial n_C \partial n} = \frac{1}{Q}[(4G_C^2 - g g_C - g_{AB} g_C) - \frac{\partial Q}{\partial n}\frac{\partial Q}{\partial n_C}], \tag{A5a}$$

15

$$\frac{\partial Q}{\partial n} = \frac{(g+g_{AB})^2 n - (g g_C + g_C g_{AB} - 4G_C^2) n_C}{Q}, \tag{A5b}$$

$$\frac{\partial Q}{\partial n_C} = \frac{g_C^2 n_C - (g g_C + g_C g_{AB} - 4G_C^2) n}{Q}. \tag{A5c}$$

Appendix B: LHY energy density for large particle imbalances

Applying directly a Taylor expansion to Eq. (1) in terms of $n_C/n \approx 0$ (highly particle imbalance limit), results in a divergent second derivative $\partial^2 \mathcal{E}_{\rm LHY}/\partial (n_C/n)^2\Big|_0$. As such, we cannot rely on the direct Taylor expansion of the LHY energy density in the case of highly particle imbalance between the majority (two-component) droplet and component C. Moreover, inspecting the form of the LHY energy density given by Eq. (B1) below, it is clear that we should expect some terms with rational, but not integer, exponents to be included in our expansion, which cannot be captured by the direct Taylor expansion. Formally, this suggests that the expansion should be based on a Puiseux series [64, 71], instead of a Taylor series. For our purposes, we simply proceed by applying the Taylor expansion in Eq. (1) term-by-term as follows. First we recast the LHY energy density of Eq. (1) into the following form

$$\begin{aligned}\mathcal{E}_{\rm LHY} = -\frac{\sqrt{2m}}{6\hbar\pi}(gn)^{3/2}\Bigg(&\sqrt{8} f_-^{\frac{3}{2}} + \left[(f_+ + \frac{g_C}{g}\frac{n_C}{n}) + \left(f_+^2 - 2f_C\frac{n_C}{n} + \frac{g_C^2}{g^2}(\frac{n_C}{n})^2\right)^{1/2}\right]^{\frac{3}{2}} \\ &+ \left[(f_+ + \frac{g_C}{g}\frac{n_C}{n}) - \left(f_+^2 - 2f_C\frac{n_C}{n} + \frac{g_C^2}{g^2}(\frac{n_C}{n})^2\right)^{1/2}\right]^{\frac{3}{2}}\Bigg),\end{aligned} \tag{B1}$$

where $f_\pm = 1 \pm g_{AB}/g$, and $f_C = g_C/g + g_{AB}g_C/g^2 - (2G_C/g)^2$. Note that in relation to Eq. (1) and Eq. (2) the square root terms in Eq. (B1) correspond to Q/gn, the term inside the small parentheses to W/gn, and the expression inside the square brackets to $(W \pm Q)/gn$. Expanding the square root term appearing in Eq. (B1) yields

$$\frac{Q}{gn} = \left(f_+^2 - 2f_C\frac{n_C}{n} + \frac{g_C^2}{g^2}(\frac{n_C}{n})^2\right)^{1/2} \approx f_+ - \frac{f_C}{f_+}\frac{n_C}{n} + \Big[\frac{g_C^2}{2g^2 f_+} - \frac{f_C^2}{2f_+^3}\Big](\frac{n_C}{n})^2 + \mathcal{O}\Big((\frac{n_C}{n})^3\Big). \tag{B2}$$

From this expression, it is clear that the term corresponding to $(W-Q)/(gn)$ becomes proportional to n_C/n. Hence, the term $\Big((W-Q)/(gn)\Big)^{3/2}$ gives rise to rational powers of n_C/n in the form of $(n_C/n)^{\nu+3/2}$, with $\nu \in N^*$. For this reason, as a next step, we factor out n_C/n and expand the resulting expression in the brackets with respect to n_C/n, obtaining

$$\Big(\frac{W-Q}{gn}\Big)^{3/2} \approx \Big[(\frac{g_C}{g} + \frac{f_C}{f_+})\frac{n_C}{n} - \Big[\frac{g_C^2}{2g^2 f_+} - \frac{f_C^2}{2f_+^3}\Big](\frac{n_C}{n})^2\Big]^{3/2} = (\frac{n_C}{n})^{3/2}\left[(\frac{g_C}{g} + \frac{f_C}{f_+}) - \Big[\frac{g_C^2}{2g^2 f_+} - \frac{f_C^2}{2f_+^3}\Big]\frac{n_C}{n}\right]^{3/2} \tag{B3a}$$

$$\approx (\frac{g_C}{g} + \frac{f_C}{f_+})^{3/2}(\frac{n_C}{n})^{3/2} - \frac{3}{2}\sqrt{\frac{g_C}{g} + \frac{f_C}{f_+}}\left(\frac{g_C^2}{2g^2 f_+} - \frac{f_C^2}{2f_+^3}\right)(\frac{n_C}{n})^{5/2} + \mathcal{O}\Big((\frac{n_C}{n})^{7/2}\Big),$$

$$\begin{aligned}(\frac{W+Q}{gn})^{3/2} &\approx \Big[2f_+^2 + (\frac{g_C}{g} - \frac{f_C}{f_+})\frac{n_C}{n} + \Big[\frac{g_C^2}{2g^2 f_+} - \frac{f_C^2}{2f_+^3}\Big](\frac{n_C}{n})^2\Big]^{3/2} \\ &\approx (2f_+)^{3/2} + \frac{3\sqrt{2f_+}}{2}(\frac{g_C}{g} - \frac{f_C}{f_+})\frac{n_C}{n} + \\ &\left(\frac{3\sqrt{2f_+}}{2}\Big[\frac{g_C^2}{2g^2 f_+} - \frac{f_C^2}{2f_+^3}\Big] + \frac{3}{8\sqrt{2f_+}}\Big[\frac{g_C}{g} - \frac{f_C}{f_+}\Big]^2\right)(\frac{n_C}{n})^2 + \mathcal{O}\Big((\frac{n_C}{n})^3\Big).\end{aligned} \tag{B3b}$$

Substituting all the above terms into the LHY energy density of Eq. (B1) and setting $f_G = (2\frac{G_C}{g})^2/f_+$ results in

$$\mathcal{E}_{\rm LHY} \approx -\frac{2\sqrt{mg^3}}{3\hbar\pi}\left[(f_-^{3/2} + f_+^{3/2})n^{3/2} + (\frac{g_C}{g} - \frac{f_G}{2})^{3/2} n_C^{3/2} + \frac{3\sqrt{f_+}}{4} f_G \sqrt{n} n_C + \mathcal{O}(\frac{1}{\sqrt{N}})\right]. \tag{B4}$$

[1] F. Böttcher, J.-N. Schmidt, J. Hertkorn, K. S. H. Ng, S. D. Graham, M. Guo, T. Langen, and T. Pfau, Rep. Progr. Phys. **84**, 012403 (2020).

[2] B. A. Malomed, Front. Phys. **16**, 22504 (2021).
[3] Z.-H. Luo, W. Pang, B. Liu, Y.-Y. Li, and B. A. Malomed, Front. Phys. **16**, 32201 (2020).
[4] S. I. Mistakidis, A. G. Volosniev, R. E. Barfknecht, T. Fogarty, T. Busch, A. Foerster, P. Schmelcher, and N. T. Zinner, Phys. Rep. **1042**, 1 (2023).
[5] T. D. Lee, K. Huang, and C. N. Yang, Phys. Rev. **106**, 1135 (1957).
[6] D. S. Petrov, Phys. Rev. Lett. **115**, 155302 (2015).
[7] D. S. Petrov and G. E. Astrakharchik, Phys. Rev. Lett. **117**, 100401 (2016).
[8] I. A. Englezos, P. Schmelcher, and S. I. Mistakidis, SciPost Phys. **19**, 133 (2025).
[9] I. Ferrier-Barbut, H. Kadau, M. Schmitt, M. Wenzel, and T. Pfau, Phys. Rev. Lett. **116**, 215301 (2016).
[10] L. Chomaz, S. Baier, D. Petter, M. J. Mark, F. Wächtler, L. Santos, and F. Ferlaino, Phys. Rev. X **6**, 041039 (2016).
[11] L. Chomaz, I. Ferrier-Barbut, F. Ferlaino, B. Laburthe-Tolra, B. L. Lev, and T. Pfau, Rep. Prog. Phys. **86**, 026401 (2022).
[12] C. R. Cabrera, L. Tanzi, J. Sanz, B. Naylor, P. Thomas, P. Cheiney, and L. Tarruell, Science **359**, 301 (2018).
[13] P. Cheiney, C. R. Cabrera, J. Sanz, B. Naylor, L. Tanzi, and L. Tarruell, Phys. Rev. Lett. **120**, 135301 (2018).
[14] G. Semeghini, G. Ferioli, L. Masi, C. Mazzinghi, L. Wolswijk, F. Minardi, M. Modugno, G. Modugno, M. Inguscio, and M. Fattori, Phys. Rev. Lett. **120**, 235301 (2018).
[15] C. D'Errico, A. Burchianti, M. Prevedelli, L. Salasnich, F. Ancilotto, M. Modugno, F. Minardi, and C. Fort, Phys. Rev. Res. **1**, 033155 (2019).
[16] Z. Guo, F. Jia, L. Li, Y. Ma, J. M. Hutson, X. Cui, and D. Wang, Phys. Rev. Res. **3**, 033247 (2021).
[17] L. Cavicchioli, C. Fort, F. Ancilotto, M. Modugno, F. Minardi, and A. Burchianti, Phys. Rev. Lett. **134**, 093401 (2025).
[18] T. A. Flynn, L. Parisi, T. P. Billam, and N. G. Parker, Phys. Rev. Research **5**, 033167 (2023).
[19] T. A. Flynn, N. A. Keepfer, N. G. Parker, and T. P. Billam, Phys. Rev. Res. **6**, 013209 (2024).
[20] L. He, H. Li, W. Yi, and Z.-Q. Yu, Phys. Rev. Lett. **130**, 193001 (2023).
[21] J. C. Pelayo, G. A. Bougas, T. Fogarty, T. Busch, and S. I. Mistakidis, Quant. Sci. Technol. **10**, 045074 (2025).
[22] G. E. Astrakharchik and B. A. Malomed, Phys. Rev. A **98**, 013631 (2018).
[23] M. Tylutki, G. E. Astrakharchik, B. A. Malomed, and D. S. Petrov, Phys. Rev. A **101**, 051601 (2020).
[24] S. I. Mistakidis, T. Mithun, P. G. Kevrekidis, H. R. Sadeghpour, and P. Schmelcher, Phys. Rev. Research **3**, 043128 (2021).
[25] I. A. Englezos, S. I. Mistakidis, and P. Schmelcher, Phys. Rev. A **107**, 023320 (2023).
[26] Z. Zhao, G. Li, Z. Chen, H.-B. Luo, B. Liu, B. A. Malomed, and Y. Li, arXiv:2511.02394 (2025).
[27] L. Dong, D. Liu, and B. A. Malomed, Chaos, Solitons & Fractals **203**, 117676 (2026).
[28] G. Ferioli, G. Semeghini, L. Masi, G. Giusti, G. Modugno, M. Inguscio, A. Gallemí, A. Recati, and M. Fattori, Phys. Rev. Lett. **122**, 090401 (2019).
[29] G. C. Katsimiga, S. I. Mistakidis, G. N. Koutsokostas, D. J. Frantzeskakis, R. Carretero-González, and P. G. Kevrekidis, Phys. Rev. A **107**, 063308 (2023).
[30] M. Edmonds, Phys. Rev. Res. **5**, 023175 (2023).
[31] Y. Li, Z. Chen, Z. Luo, C. Huang, H. Tan, W. Pang, and B. A. Malomed, Phys. Rev. A **98**, 063602 (2018).
[32] G. Bougas, G. C. Katsimiga, P. G. Kevrekidis, and S. I. Mistakidis, Phys. Rev. A **110**, 033317 (2024).
[33] M. N. Tengstrand, P. Stürmer, E. O. Karabulut, and S. M. Reimann, Phys. Rev. Lett. **123**, 160405 (2019).
[34] T. A. Yoğurt, U. Tanyeri, A. Keleş, and M. O. Oktel, Phys. Rev. A **108**, 033315 (2023).
[35] S. Chandramouli, S. I. Mistakidis, G. C. Katsimiga, and P. G. Kevrekidis, Phys. Rev. A **110**, 023304 (2024).
[36] Y. V. Kartashov, V. M. Lashkin, M. Modugno, and L. Torner, New J. Phys. **24**, 073012 (2022).
[37] G. C. Katsimiga, S. I. Mistakidis, B. A. Malomed, D. J. Frantzeskakis, R. Carretero-Gonzalez, and P. G. Kevrekidis, Condensed Matter **8**, 67 (2023).
[38] S. I. Mistakidis, G. Bougas, G. C. Katsimiga, and P. G. Kevrekidis, Phys. Rev. Lett. **134**, 123402 (2025).
[39] S. Chandramouli, S. I. Mistakidis, G. C. Katsimiga, D. J. Ratliff, D. J. Frantzeskakis, and P. G. Kevrekidis, arXiv:2510.03063 (2025).
[40] I. A. Englezos, P. Schmelcher, and S. I. Mistakidis, Phys. Rev. A **110**, 023324 (2024).
[41] S. Gangwar, R. Ravisankar, S. Mistakidis, P. Muruganandam, and P. K. Mishra, Phys. Lett. A **542**, 130426 (2025).
[42] Y. V. Kartashov and D. A. Zezyulin, Phys. Rev. A **110**, L021304 (2024).
[43] J. Vallès-Muns, I. Morera, G. E. Astrakharchik, and B. Juliá-Díaz, SciPost Phys. **16**, 074 (2024).
[44] M. N. Tengstrand, P. Stürmer, E. O. Karabulut, and S. M. Reimann, Phys. Rev. Lett. **123**, 160405 (2019).
[45] E. G. Charalampidis and S. I. Mistakidis, Phys. Rev. A **111**, 013318 (2025).
[46] L. Parisi and S. Giorgini, Phys. Rev. A **102**, 023318 (2020).
[47] L. Parisi, G. E. Astrakharchik, and S. Giorgini, Phys. Rev. Lett. **122**, 105302 (2019).
[48] A. Debnath, A. Khan, and B. Malomed, Commun. Nonlinear Sci. Numer. Simul. **126**, 107457 (2023).
[49] F. Bristy, G. Bougas, G. Katsimiga, and S. Mistakidis, Chaos, Solitons & Fractals **201**, 117383 (2025).
[50] J. Jogania, S. Das, A. Nath, and J. Bera, Physica Scripta **100**, 085212 (2025).
[51] Y. Ma, C. Peng, and X. Cui, Phys. Rev. Lett. **127**, 043002 (2021).
[52] Y. Ma and X. Cui, Phys. Rev. Lett. **134**, 043402 (2025).
[53] G. Bighin, A. Burchianti, F. Minardi, and T. Macrì, Phys. Rev. A **106**, 023301 (2022).
[54] J. C. Pelayo, T. Fogarty, T. Busch, and S. I. Mistakidis, Phys. Rev. Res. **6**, 033219 (2024).
[55] S. Sinha, S. Biswas, L. Santos, and S. Sinha, Phys. Rev. A **108**, 023311 (2023).
[56] F. Grusdt and E. Demler, in *Quantum matter at ultralow temperatures* (IOS Press, 2016) pp. 325–411.
[57] F. Scazza, M. Zaccanti, P. Massignan, M. M. Parish, and J. Levinsen, Atoms **10**, 55 (2022).
[58] R. Schmidt, M. Knap, D. A. Ivanov, J.-S. You, M. Cetina, and E. Demler, Rep. Prog. Phys. **81**, 024401 (2018).
[59] C. Chin, R. Grimm, P. Julienne, and E. Tiesinga, Rev. Mod. Phys. **82**, 1225 (2010).
[60] F. K. Abdullaev and R. Galimzyanov, J. Phys. B: At., Mol. Opt. Phys. **53**, 165301 (2020).

[61] C. T. Kelley, *Solving nonlinear equations with Newton's method* (SIAM, 2003).
[62] H. Uecker, *Numerical Continuation and Bifurcation in Nonlinear PDEs* (SIAM (Philadelphia), 2021).
[63] T. Kapitula and K. Promislow, *Spectral and Dynamical Stability of Nonlinear Waves* (Springer-Verlag (New York), 2013).
[64] N. J. Willis, A. K. Didier, and K. M. Sonnanburg, arXiv:0807.4674 (2008).
[65] S. I. Mistakidis, G. C. Katsimiga, G. M. Koutentakis, T. Busch, and P. Schmelcher, Phys. Rev. Lett. **122**, 183001 (2019).
[66] A. Romero-Ros, G. Katsimiga, S. I. Mistakidis, S. Mossman, G. Biondini, P. Schmelcher, P. Engels, and P. G. Kevrekidis, Phys. Rev. Lett. **132**, 033402 (2024).
[67] G. Bougas, G. Katsimiga, S. Mossman, P. Engels, P. Kevrekidis, and S. Mistakidis, arXiv:2510.24917 (2025).
[68] B. Bakkali-Hassani, C. Maury, Y.-Q. Zou, E. Le Cerf, R. Saint-Jalm, P. C. M. Castilho, S. Nascimbene, J. Dalibard, and J. Beugnon, Phys. Rev. Lett. **127**, 023603 (2021).
[69] B. Bakkali-Hassani and J. Dalibard, arXiv:2210.14045 (2022).
[70] L. Cao, V. Bolsinger, S. I. Mistakidis, G. M. Koutentakis, S. Krönke, J. M. Schurer, and P. Schmelcher, J. Chem. Phys. **147**, 044106 (2017).
[71] R. J. Walker, *Algebraic curves*, Vol. 58 (Springer, 1950).

Chapter 5

Conclusions and Outlook

The present cumulative thesis deals with correlated one-dimensional ultracold bosonic mixtures featuring short range interactions. A particular focus is placed on the investigation of the ground state and dynamical properties of the recently discovered quantum droplets. First, we employed a two-component mixture, featuring attractive intercomponent interactions, trapped in harmonic oscillators. We utilized the *ab-initio* ML-MCTDHX method to solve the corresponding variant of the full many-body nonlinear Schrödinger equation, for both the ground state, and the dynamical response of the system following a quench of the external geometry. Second, we address the multi-component one-dimensional bosonic mixture, by applying the perturbative Bogoliubov theory, to obtain analytical results for the impact of quantum fluctuations on two- three- and four-component mixtures. In this section we provide a brief summary of the main findings which resulted from the above-mentioned investigations and outline relevant future perspectives.

5.1 Many-Body Harmonically Trapped Quantum Droplets in One - Dimension

In [IE1, IE2] harmonically confined quantum droplet configurations have been investigated in homonuclear (interaction balanced or imbalanced) and heteronuclear (mass-imbalanced) two-component bosonic mixtures, utilizing the *ab-initio* ML - MCTDHX approach. The main focus has been to benchmark and investigate the accuracy of the recently proposed LHY theory beyond its formal validity regime, as well as in previously less explored settings. Namely, early investigations were mainly focused on the symmetric droplet configurations, where the two components are either characterized by identical parameters or these parameters are fine tuned to specific values such that their densities ratio is fixed to a value determined by their intracomponent interaction strengths [162, 180]. While this condition is crucial for the stability of quantum droplets in 3D geometries [183], our works were among the first to illustrate that 1D droplets remain remarkably stable even beyond this symmetric configuration [184, 189, 190, 193]. In addition, the question of quantum droplets under confinement is particularly intriguing in its own right,

since the LHY theory is not formally valid in this case. Understanding the impact of confinement in quantum droplets is of great importance in terms of the realization of low-dimensional settings, in improving our ability to control and exploit quantum droplet structures, and in engineering more complex mixed structures and phases [207–209]. Finally, comparisons with the so-called eGPE, as well as the standard MF approximation, provided also indications for the role of LHY and beyond-LHY correlations, as the different theoretical approaches incorporate the impact of correlations at different levels.

5.1.1 Correlated Dynamics of One-Dimensional Droplets in a Harmonic Trap

In [IE1] the ground state properties and the out-of-equilibrium dynamics following a quench, of 1D droplet configurations confined in a harmonic trap, were studied. Homonuclear, as well as heteronucluar bosonic mixtures for which the corresponding eGPEs have not been derived, were addressed.

Focusing on the ground state configurations of the symmetric (i.e. interaction, mass and particle balanced) mixture, a transition from Gaussian shaped to FT droplet density profile was identified for sufficiently large atom numbers, or for weaker intercomponent attraction [469]. Moreover, in the case of mixtures featuring intracomponent interaction imbalance, the genuinely two-component nature of the system becomes evident, as the components become spatially mixed. In particular, interaction-imbalanced settings can be realized, where the more strongly repulsive component exhibits FT density configurations, while the other component remains in a Gaussian-like density profile. The genuinely two-component nature of the system is similarly evident in heteronuclear (i.e. mass-imbalanced) mixtures, where the heavier component develops FT signatures upon reducing the intercomponent attraction. Furthermore, the use of the *ab-initio* many-body ML - MCTDHX method allows for the identification of droplet observables beyond the particle density. Namely, in all cases, the examination of the two-body density matrix reveals that a characteristic anti-bunching behavior can be identified for particles of the same component. In contrast, two bosons belonging to different components are slightly correlated when placed at the same location inside the droplet.

Breathing dynamics of the droplet are seeded by quenches of the harmonic trap frequency. For homonuclear mixtures and for sufficiently strong quenches, aside from the stable breathing contraction and expansion of the cloud, the droplet can also undergo more involved excitation processes. Namely, a progressive spatial delocalization of the droplet and expulsion of atoms from its density tails, was shown to occur, accompanied by the build-up of excitations around its center. This process is, reminiscent of the self-evaporation process, which is known in 3D droplets [139, 183], but absent in 1D settings [179, 180]. From the many-body perspective, this excitation mechanism is associated with enhanced intercomponent entanglement

and long-range two-body correlations. During the stable part of the dynamics, the breathing frequency was found to be close to the ideal gas limit close to the attractive MF stability edge, while it is reduced for weaker attraction. Heteronuclear mixtures are characterized by in-phase breathing for stronger attractions, while a phase difference emerges towards the decoupling limit. Interestingly, while in the absence of correlations the dynamics are dominated by intercomponent collisions, a pronounced dephasing develops within the many-body picture for species selective quench frequencies.

In contrast to the involved breathing motion, the droplet dipole motion, which can be seeded by a sudden displacement of the center of the trap, was found to be remarkably stable and insensitive to the system parameters for homonuclear mixtures. For heteronuclear mixtures a transition from phase-locked to dephasing dynamics takes place upon reducing intercomponent attraction. Finally, species selective displacement quenches were found to result in irregular dipole patterns characterized by component collisions and intercomponent energy transfer.

An intriguing extension of the quench dynamics is to consider time-dependent rampings of the intercomponent attraction across the identified phases, in order to reveal mixed droplet states or the spontaneous emergence of nonlinear structures. Moreover, the genuinely two-component nature of the system can be further explored by considering particle imbalanced droplet settings, and in particular the crossover from particle balanced configurations to the highly particle imbalanced or impurity limit [IE2, 190, 193]. This would give access to the concept of quasiparticles in quantum droplets, which is still highly unexplored. In addition, an explicit derivation of the impact of quantum fluctuations in the presence of external confinement would be greatly desirable from the theoretical side. In the meantime, such trapped configurations under various geometries can also be addressed by *ab-initio* numerical methods as was done for a flat box geometry [184–186], or in an optical lattice [468]. Finally, exploring the LHY or beyond - LHY correlations and entanglement in three-component mixtures is also a promising direction [IE3, IE4, 197, 477].

5.1.2 Particle Imbalanced Droplets in an One-Dimensional Harmonic Trap

In [IE2] the formation of two-component bosonic droplet configurations in the limit of large particle imbalance between the components was studied. The qualitative behavior of the system was analytically predicted by employing a reduction of the two-component eGPEs, based on the LHY theory [162, 189], in the limit of large particle imbalance. Under these conditions, the system was shown to approximately decouple into a FT droplet configuration for the majority component, and a bright-like soliton structure occupied by the minority component. Moreover, this behavior was verified and extended to the presence of an 1D harmonic trap, using many-body *ab-initio* simulations obtained with the ML-MCTDHX method. It was found that the majority component becomes arranged in a FT droplet profile, exhibiting

also localized modulations of its density at the overlap region with the minority component. The amplitude of these modulations can be tuned. For instance, they become more pronounced by increasing the intercomponent attraction, but also, interestingly, by increasing the intracomponent repulsion of the minority atoms, or for larger masses of the minority species. Notably, the transition from droplet-like minority configurations to soliton-like ones upon reducing their number is also evident in the intra-component two-body density profile. The later was found to transition from the characteristic anti-correlation signature at the same spatial point to a correlated one. Finally, examining the case of fermionic impurities, the FT signatures in the bosonic bath readily vanish, in agreement with the predicted suppression of droplet configurations in Bose-Fermi mixtures [168–170].

A direct extension based on the results mentioned above, is to study the dynamical response of these particle imbalanced structures, utilizing for example quenches of the coupling strengths [478]. The significant differences between genuinely two-component droplet configurations in 1D, compared to their 3D counterparts [194–196], further emphasize the importance of characterizing the dimensional crossover and exploring the validity region of the 1D droplet phenomenology. Some important steps have been taken in this direction [182, 471, 479]. However, further work is required to understand the impact of quantum fluctuations under confinement throughout the dimensional crossover and especially beyond the restriction to symmetric droplets. Hence, fully characterizing the dimensional crossover is a highly desirable, but far from trivial task, which would likely require the combination of analytical techniques and sophisticated many-body methods, such as the ML-MCTDHX employed herein, exact diagonalization approaches [480], quantum Monte-Carlo [185, 186] or DMRG [193, 468]. All of these methods have already been shown to provide intriguing results in the context of quantum droplets. Finally, another interesting direction is to address the stability of these imbalanced droplet configurations [191, 481].

5.2 LHY Theory of Multi-Component One-Dimensional Bosonic Mixtures

In [IE3, IE4] one dimensional quantum droplets have been addressed in free space, subject to periodic boundary conditions, where analytical results can be obtained, utilizing the perturbative Bogoliubov theory [25, 26]. The first order perturbative correction to the MF energy, commonly referred to as the LHY energy, yields the impact of first-order quantum fluctuations at zero temperature [163]. This LHY energy correction was shown to prevent the MF collapse in 3D binary mixtures [139] and later also in three-component 3D mixtures [197], by contributing an additional repulsion. Since the LHY energy, however, obtains an imaginary part outside the MF stability region (where droplet formation occurs), the theoretical calculation is

carried-out at its attractive edge, which makes the treatment formally valid only at perturbatively small deviations of the interaction strengths from this edge [139]. Motivated by the 3D case, the same assumption was made in the derivation of the 1D LHY correction for binary mixtures [162]. In [IE3], motivated by the investigations of 1D quantum droplets discussed above, which drew attention to the significant differences between the 1D and 3D droplets, we revisited the calculation of the LHY energy in 1D mixtures. In particular, we focused on making the minimal assumptions required explicitly for the 1D setup. Taking advantage of the fact that the 1D droplet regime coincides with MF stability regime, we derived the LHY correction and corresponding eGPEs for two-, three- and four-component 1D bosonic mixtures featuring short-range contact interactions, which are formally valid throughout the MF stability regime. In [IE4] we focused on the three-component mixture, and addressed in detail the transition from a particle balanced mixture to a highly particle imbalanced one. In both cases, the unique phenomenology and enhanced stability of 1D quantum droplets are emphasized, highlighting them as an ideal setting to explore novel correlated phases and gain further insights on the impact of quantum fluctuations on the system.

5.2.1 Multi-Component One-Dimensional Quantum Droplets

In [IE3] the LHY correction and associated eGPEs were systematically derived for two-, three- and four-component 1D bosonic mixtures featuring short-range contact interactions, throughout the MF stability regime. This work provided an exact perturbative derivation of beyond-mean-field corrections for multi-component 1D mixtures, and it generalized the quantum-droplet regime to include weakly attractive, as well as repulsive intercomponent interactions, both of which had previously been unavailable. Whenever possible, closed form expressions were also explicitly given. We note in passing, that the LHY energy cannot be analytically derived for more than four components in the general case.

For the two-component mixture, the LHY energy and the corresponding coupled set of eGPEs can be derived in closed form for the homonuclear system, while numerical results can be obtained for the heteronuclear mixture. The original two-component LHY treatment can be derived from our results, as a limiting case at the edge of the MF stability regime. As the system is taken further from this stability edge, by reducing the intercomponent attraction, quantitative deviations from the original treatment emerge, reflected in the width and saturation density of the droplet. Further decreasing the intercomponent attraction or turning to repulsive interactions, significant qualitative differences emerge for genuinely two-component mixtures. Namely, self-bound configurations with decreasing saturation densities persist regardless of the magnitude and sign of the intercomponent interaction. In addition, a previously unexplored early onset of phase-separation occurs as a result of quantum

fluctuations on the repulsive homonuclear or heteronuclear mixture. Notably, this phase-separation is not captured within the the original treatment.

Moreover, exact closed form expressions are provided for the three-component mixture in the cases where all three or only two of the three components are assumed to be symmetric. An interesting observation is that the LHY energy increases (in absolute value) faster than linearly with the number of components. In addition, in the case where one component is taken to be independent, a multitude of droplet phases were identified ranging from Gaussian, to mixed FT, and to phase-separated configurations depending on the system parameters. Finally, the LHY energy of the fully symmetric four-component mixture was also provided in a closed form. The transition from Gaussian to FT configurations upon decreasing the intercomponent attraction was illustrated for the four-component mixture as well. Note, that all these configurations were shown to be self-bound and emerging solely under the impact of quantum fluctuations, while the MF prediction corresponds simply to a uniform solution in all cases discussed.

Our work provides an initial point for several intriguing extensions in the exploration of ground state configurations and out-of-equilibrium dynamics of multicomponent 1D droplets. In the two-component mixture the most straightforward pathway is an in-depth study of the phase-separated states and the transitions towards them, under the impact of quantum fluctuations. For the three- and four-component mixtures, there is a very strong possibility to unveil unseen exotic droplet phases, since they offer a highly extended and almost entirely unexplored parameter space. Our work already suggests the existence of deformed and mixed droplet configurations that are promising to host droplet-soliton [482] or droplet-vortex [208] configurations in higher dimensions. Of course, dynamical transitions between these droplet phases can also be expected to provide valuable insights in their collective excitations and creation of nonlinear excitations, or potentially shock-waves [483, 484]. The connection between droplet phases and the few-body regime of embedded interacting impurities [485–487] is also particularly interesting in these higher-component settings. This is because, the two- or three-component bath offers a more stable and higher density background to host the impurities, compared to the corresponding limit of the binary mixture [IE2, 193]. Some initial efforts in this direction either from the macroscopic limit [IE4] or from the limit of a single impurity [200, 202, 475] are already being undertaken. Finally, a highly relevant direction is the extension of our treatment to arbitrary external geometries. Especially since, it would also constitute an important step towards the full quantum-mechanical treatment of quasi-1D systems and eventually towards fully characterizing the dimensional crossover [182, 471, 479].

5.2.2 Particle Imbalanced Three-Component Quantum Droplets

In [IE4] the ground state configurations of 1D three-component bosonic mixtures, consisting of two symmetric species attractively coupled to a third unconstrained one were addressed. Their dynamical stability and excitation spectrum with respect to low-amplitude perturbations was also explored using BdG analysis. Upon investigating the impact of the atom number in the two symmetric components and the strength of their intercomponent attraction with the third component, three main phases were found to arise. Namely, the third component is either un-trapped, partially trapped or fully trapped by the two-component droplet respectively.

In the particle balanced configuration, the third component arranges itself in a wide FT structure extending significantly beyond the arguably more localized symmetric components. Upon increasing the attraction, the third component becomes increasingly perturbed forming a pronounced density peak in the overlap region. The chemical potential reveals a relatively weakly bound system regardless of the attraction strength, while the low-amplitude modes tend to cross the particle-emission threshold from below for increasing intercomponent attraction.

Turning our attention to the weakly attractive particle imbalanced mixture, it was found that as the atom number in the symmetric components increases, the minority component localizes. In particular, it gradually transitions towards becoming fully trapped by the majority components, at which point it acquires a similar and slightly smaller spatial extent. During this transition the (negative) chemical potentials significantly decrease, indicating progressively more tightly self-bound structures. Interestingly, all but the lowest-lying excitation modes cross the particle-emission threshold from below during this transition. Once the transition is completed several excitation modes reappear from above, arranged now in quasi - degenerate pairs. As a next step, we fix the atom numbers to a highly particle imbalanced configuration and we tune the intercomponent coupling from the decoupled limit to the attractive edge of the MF stability regime. A similar transition, from an un-trapped to a fully trapped minority component, was found to occur for weaker attractions. Upon further increasing the attraction, the system transitions to a regime where the trapped minority component induces localized undulations on top of the FT configuration of the majority components. Naturally, the system becomes increasingly self-bound with increasing attraction. In addition, the collective modes exhibit a similar transition to the one mentioned above, as the intercomponent interaction is tuned from zero to moderately attractive values. Interestingly, stronger attractions induce a complex interaction-dependence on the excitation spectrum, characterized by multiple avoided-crossings between the collective mode branches.

The numerical solutions of the eGPEs were also bolstered by the derivation of a series of effective models based on an analytical reduction of the LHY energy in the limit of large particle imbalance. The simplest models, which neglect all but the most

dominant terms, allowed for the development of physical intuition regarding the impact of each term as they were systematically re-introduced. Moreover, the derivation of approximate analytical solutions valid in the corresponding limits were possible in some cases. A slightly more involved model, taking into account both the effective potential experienced by the minority species due to the two-component bath and the back-action of the minority component to the bath, was found to be in excellent agreement with the results of the complete LHY theory.

A promising path for future research would be to explore the impact of harmonic confinement to the configurations identified above, especially due to the experimental importance of the harmonically trapped setting. Moreover, exploring the dynamical response of the system upon a quench or sweep of the intercomponent interaction strength between the majority components and the minority one is an intriguing direction, especially across the different trapping regimes. One could also consider exploiting the minority component to seed composite nonlinear excitations, while the effective models could be used to derive approximate analytical forms of the relevant excitations [204]. In addition, validating the LHY theory of three-component mixtures by ab-initio many-body methods [184, 186, 427, 468] and exploring the underlying many-body character of the resulting structures is an important, and so far completely unexplored question. Finally, the highly particle imbalanced setting naturally invokes a connection with Bose polaron physics [152], while the droplet character of the bath in the three-component case provides an additional intriguing aspect regarding questions of induced interactions between the dressed impurities or their lifetimes.

Acknowledgements

First and foremost, I would like to thank the supervisor of my thesis, Professor Peter Schmelcher, for introducing me to the field of Ultracold atoms, and providing me with ample challenge to learn and grow, and for providing me the means to do so.

I am also very grateful to Professor Simeon Mistakidis for his guidance and support throughout the years, and for our fruitful collaboration. I would also like to thank Andreas Katsaris, Professor Fotios Diakonos, Professor Christof Weitenberg, and Professor Stathis Charalampidis for several discussions and for the lively collaboration that we had. I would like to additionally thank my professor in the University of Athens, Professor Fotios Diakonos, for giving me the opportunity to contribute to my first research project and motivating me to continue my journey into physics research. Special thanks to Professor Henning Moritz for his support and advice.

It has also been a great pleasure to exchange knowledge and moments of levity with the other members of Professor Schmelcher's group including Giorgis, Lia, Simos, Christian, George, Fanis, Dimitris, Zeki, Rohan, Kapil, Friethjof, Mirko, Frederic, Alejandro, Rick, Maxim, Kevin, Malte, Fabian, Jie, Ansgar, Felipe, Dan, André, Judith, Samir, Aditya, Gagan, Mathis, Henry, Frank, David, Nader, and Tomasz. Special thanks go to Anja, for consistently soldering the crashing weight of bureaucracy with an admirable positive attitude.

I am also grateful for generous financial support from the University of Hamburg under the Deutsche Forschungsgemeinschaft (DFG) in the framework of the SFB 925 "Light induced dynamics and control of correlated quantum" systems.

Outside of my scientific environment, I am grateful for the people I have met and for their friendship. Finally, but most importantly, I would like to thank my parents for their support and encouragement, which allowed for my entire education.

Bibliography

[1] M. H. Anderson, J. R. Ensher, M. R. Matthews, C. E. Wieman, and E. A. Cornell, Science **269**, 198 (1995).

[2] C. C. Bradley, C. A. Sackett, J. J. Tollett, and R. G. Hulet, Phys. Rev. Lett. **75**, 1687 (1995).

[3] K. B. Davis, M. O. Mewes, M. R. Andrews, N. J. van Druten, D. S. Durfee, D. M. Kurn, and W. Ketterle, Phys. Rev. Lett. **75**, 3969 (1995).

[4] B. DeMarco and D. S. Jin, Science **285**, 1703 (1999).

[5] A. G. Truscott, K. E. Strecker, W. I. McAlexander, G. B. Partridge, and R. G. Hulet, Science **291**, 2570 (2001).

[6] E. L. Raab, M. Prentiss, A. Cable, S. Chu, and D. E. Pritchard, Phys. Rev. Lett. **59**, 2631 (1987).

[7] H. Ludvigsen, A. Aeijaelae, A. Pietilaeinen, H. Talvitie, and E. Ikonen, Physica Scripta **49:4**, 10.1088/0031-8949/49/4/007 (1994).

[8] R. S. Williamson and T. Walker, J. Opt. Soc. Am. B **12**, 1393 (1995).

[9] S. Grego, M. Colla, A. Fioretti, J. Müller, P. Verkerk, and E. Arimondo, Optics Communications **132**, 519 (1996).

[10] U. Schünemann, H. Engler, M. Zielonkowski, M. Weidemüller, and R. Grimm, Optics Communications **158**, 263 (1998).

[11] T. Kuwamoto, K. Honda, Y. Takahashi, and T. Yabuzaki, Phys. Rev. A **60**, R745 (1999).

[12] H. J. Metcalf and P. Straten, *Laser cooling and trapping* (Springer New York, NY, 1999).

[13] H. Katori, T. Ido, Y. Isoya, and M. Kuwata-Gonokami, Phys. Rev. Lett. **82**, 1116 (1999).

[14] J. Grünert and A. Hemmerich, Phys. Rev. A **65**, 041401 (2002).

[15] F. Y. Loo, A. Brusch, S. Sauge, M. Allegrini, E. Arimondo, N. Andersen, and J. W. Thomsen, Journal of Optics B: Quantum and Semiclassical Optics **6**, 81 (2003).

[16] J. J. McClelland and J. L. Hanssen, Phys. Rev. Lett. **96**, 143005 (2006).

[17] S. H. Youn, M. Lu, U. Ray, and B. L. Lev, Phys. Rev. A **82**, 043425 (2010).

[18] W. Vassen, C. Cohen-Tannoudji, M. Leduc, D. Boiron, C. I. Westbrook, A. Truscott, K. Baldwin, G. Birkl, P. Cancio, and M. Trippenbach, Rev. Mod. Phys. **84**, 175 (2012).

[19] T. Hänsch and A. Schawlow, Optics Communications **13**, 68 (1975).

[20] W. D. Phillips and H. Metcalf, Phys. Rev. Lett. **48**, 596 (1982).
[21] S. Chu, L. Hollberg, J. E. Bjorkholm, A. Cable, and A. Ashkin, Phys. Rev. Lett. **55**, 48 (1985).
[22] S. Stenholm, Rev. Mod. Phys. **58**, 699 (1986).
[23] W. Ketterle and M. W. Zwierlein, La Rivista del Nuovo Cimento **31**, Published online 21 July 2008, 247 (2008).
[24] M. Inguscio and L. Fallani, *Atomic physics: precise measurements and ultracold matter* (OUP Oxford, 2013).
[25] C. J. Pethick and H. Smith, *Bose–einstein condensation in dilute gases*, 2nd ed. (Cambridge University Press, 2008).
[26] L. Pitaevskii and S. Stringari, *Bose-einstein condensation and superfluidity* (Oxford University Press, Jan. 2016).
[27] I. Bloch, Nature Physics **1**, 23 (2005).
[28] I. Bloch, J. Dalibard, and W. Zwerger, Rev. Mod. Phys. **80**, 885 (2008).
[29] I. Bloch, J. Dalibard, and S. Nascimbéne, Nature Phys. **8**, 267 (2012).
[30] L. Wolswijk, L. Cavicchioli, G. Vinelli, M. Chiarotti, L. Donati, M. F. Fernandez, D. H. Rajkov, C. Mancini, P. Vezio, T. Zhou, G. D. Pace, C. Mazzinghi, N. Antolini, L. Salvi, and V. Gavryusev, *Trapping, manipulating and probing ultracold atoms: a quantum technologies tutorial*, 2025.
[31] S. Inouye, M. R. Andrews, J. Stenger, H.-J. Miesner, D. M. Stamper-Kurn, and W. Ketterle, Nature **392**, 151 (1998).
[32] J. I. Kim, V. S. Melezhik, and P. Schmelcher, Phys. Rev. Lett. **97**, 193203 (2006).
[33] T. Köhler, K. Góral, and P. S. Julienne, Rev. Mod. Phys. **78**, 1311 (2006).
[34] C. Chin, R. Grimm, P. Julienne, and E. Tiesinga, Rev. Mod. Phys. **82**, 1225 (2010).
[35] P. Giannakeas, V. S. Melezhik, and P. Schmelcher, Phys. Rev. Lett. **111**, 183201 (2013).
[36] J. von Stecher and C. H. Greene, Phys. Rev. Lett. **99**, 090402 (2007).
[37] W. Zwerger, ed., *The bcs-bec crossover and the unitary fermi gas*, 1st ed., Vol. 836, Lecture Notes in Physics, Published: 21 October 2011 (eBook), 22 October 2011 (softcover); 154 b/w illustrations (Springer, Berlin, Heidelberg, 2012), XVI+532.
[38] C. H. Greene, P. Giannakeas, and J. Pérez-Ríos, Rev. Mod. Phys. **89**, 035006 (2017).
[39] M. Holten, L. Bayha, K. Subramanian, S. Brandstetter, C. Heintze, P. Lunt, P. M. Preiss, and S. Jochim, Nature **606**, 287 (2022).
[40] L. D. Landau and E. M. Lifshitz, *Quantum mechanics: non-relativistic theory, vol. 3* (Elsevier, 1977).
[41] L. Bayha, M. Holten, R. Klemt, K. Subramanian, J. Bjerlin, S. M. Reimann, G. M. Bruun, P. M. Preiss, and S. Jochim, Nature **587**, 583 (2020).
[42] O. Morsch and M. Oberthaler, Rev. Mod. Phys. **78**, 179 (2006).

[43] D. Jaksch, C. Bruder, J. I. Cirac, C. W. Gardiner, and P. Zoller, Phys. Rev. Lett. **81**, 3108 (1998).

[44] M. Greiner, O. Mandel, T. Esslinger, T. W. Hänsch, and I. Bloch, Nature **415**, 39 (2002).

[45] V. I. Yukalov, Laser Physics **19**, 1 (2009).

[46] F. Serwane, G. Zürn, T. Lompe, T. B. Ottenstein, A. N. Wenz, and S. Jochim, Science **332**, 336 (2011).

[47] G. Zürn, F. Serwane, T. Lompe, A. N. Wenz, M. G. Ries, J. E. Bohn, and S. Jochim, Phys. Rev. Lett. **108**, 075303 (2012).

[48] A. N. Wenz, G. Zürn, S. Murmann, I. Brouzos, T. Lompe, and S. Jochim, Science **342**, 457 (2013).

[49] A. M. Kaufman, B. J. Lester, M. Foss-Feig, M. L. Wall, A. M. Rey, and C. A. Regal, Nature **527**, 208 (2015).

[50] S. I. Mistakidis, A. G. Volosniev, R. E. Barfknecht, T. Fogarty, T. Busch, A. Foerster, P. Schmelcher, and N. T. Zinner, Phys. Rep. **1042**, 1 (2023).

[51] M. Endres, H. Bernien, A. Keesling, H. Levine, E. R. Anschuetz, A. Krajenbrink, C. Senko, V. Vuletic, M. Greiner, and M. D. Lukin, Science **354**, 1024 (2016).

[52] D. Barredo, S. de Léséleuc, V. Lienhard, T. Lahaye, and A. Browaeys, Science **354**, 1021 (2016).

[53] A. Browaeys and T. Lahaye, Nature Physics **16**, 132 (2020).

[54] A. M. Kaufman and K.-K. Ni, Nature Physics **17**, 1324 (2021).

[55] N. R. Cooper, J. Dalibard, and I. B. Spielman, Rev. Mod. Phys. **91**, 015005 (2019).

[56] C. Weitenberg and J. Simonet, Nature Phys. **17**, 1342 (2021).

[57] J. Léonard, S. Kim, J. Kwan, P. Segura, F. Grusdt, C. Repellin, N. Goldman, and M. Greiner, Nature **619**, 495 (2023).

[58] O. Boada, A. Celi, J. I. Latorre, and M. Lewenstein, Phys. Rev. Lett. **108**, 133001 (2012).

[59] M. Mancini, G. Pagano, G. Cappellini, L. Livi, M. Rider, J. Catani, C. Sias, P. Zoller, M. Inguscio, M. Dalmonte, and L. Fallani, Science **349**, 1510 (2015).

[60] B. K. Stuhl, H. I. Lu, L. M. Aycock, D. Genkina, and I. B. Spielman, Science **349**, 1514 (2015).

[61] T. Chalopin, T. Satoor, A. Evrard, V. Makhalov, J. Dalibard, R. Lopes, and S. Nascimbene, Nature Phys. **16**, 1017 (2020).

[62] S. K. Kanungo, J. D. Whalen, Y. Lu, M. Yuan, S. Dasgupta, F. B. Dunning, K. R. A. Hazzard, and T. C. Killian, Nature Comm. **13**, 972 (2022).

[63] A. Görlitz, J. M. Vogels, A. E. Leanhardt, C. Raman, T. L. Gustavson, J. R. Abo-Shaeer, A. P. Chikkatur, S. Gupta, S. Inouye, T. Rosenband, and W. Ketterle, Phys. Rev. Lett. **87**, 130402 (2001).

[64] H. Moritz, T. Stöferle, M. Köhl, and T. Esslinger, Phys. Rev. Lett. **91**, 250402 (2003).

[65] Z. Hadzibabic and J. Dalibard, La Rivista del Nuovo Cimento **34**, 389 (2011).

[66] Z. Hadzibabic, P. Krüger, M. Cheneau, B. Battelier, and J. Dalibard, Nature **441**, 1118 (2006).

[67] B. Paredes, A. Widera, V. Murg, S. Fölling, I. Cirac, G. V. Shlyapnikov, and I. Bloch, Nature, 10.1038/nature02530 (2004).

[68] E. Haller, M. Gustavsson, M. J. Mark, J. G. Danzl, R. Hart, G. Pupillo, and H.-C. Nägerl, Science **325**, 1224 (2009).

[69] C. Baroni, G. Lamporesi, and M. Zaccanti, Nature Reviews Physics **6**, 736 (2024).

[70] C. J. Myatt, E. A. Burt, R. W. Ghrist, E. A. Cornell, and C. E. Wieman, Phys. Rev. Lett. **78**, 586 (1997).

[71] G. Modugno, M. Modugno, F. Riboli, G. Roati, and M. Inguscio, Phys. Rev. Lett. **89**, 190404 (2002).

[72] K. Pilch, A. D. Lange, A. Prantner, G. Kerner, F. Ferlaino, H.-C. Nägerl, and R. Grimm, Phys. Rev. A **79**, 042718 (2009).

[73] M. Egorov, B. Opanchuk, P. Drummond, B. V. Hall, P. Hannaford, and A. I. Sidorov, Phys. Rev. A **87**, 053614 (2013).

[74] A. Burchianti, C. D'Errico, S. Rosi, A. Simoni, M. Modugno, C. Fort, and F. Minardi, Phys. Rev. A **98**, 063616 (2018).

[75] G. Roati, F. Riboli, G. Modugno, and M. Inguscio, Phys. Rev. Lett. **89**, 150403 (2002).

[76] C. A. Regal, M. Greiner, and D. S. Jin, Phys. Rev. Lett. **92**, 040403 (2004).

[77] M. W. Zwierlein, C. A. Stan, C. H. Schunck, S. M. F. Raupach, A. J. Kerman, and W. Ketterle, Phys. Rev. Lett. **92**, 120403 (2004).

[78] S. Tojo, Y. Taguchi, Y. Masuyama, T. Hayashi, H. Saito, and T. Hirano, Phys. Rev. A **82**, 033609 (2010).

[79] Y. Eto, M. Takahashi, M. Kunimi, H. Saito, and T. Hirano, New J. Phys. **18**, 073029 (2016).

[80] S. I. Mistakidis, G. C. Katsimiga, P. G. Kevrekidis, and P. Schmelcher, New J. Phys. **20**, 043052 (2018).

[81] I. V. Barashenkov and E. Y. Panova, Phys. D: Non. Phen. **69**, 114 (1993).

[82] T. Karpiuk, M. Brewczyk, S. Ospelkaus-Schwarzer, K. Bongs, M. Gajda, and K. Rzazewski, Phys. Rev. Lett. **93**, 100401 (2004).

[83] F. K. Abdullaev and J. Garnier, "Bright solitons in bose-einstein condensates: theory", in *Emergent nonlinear phenomena in bose-einstein condensates: theory and experiment*, edited by P. G. Kevrekidis, D. J. Frantzeskakis, and R. Carretero-González (Springer Berlin Heidelberg, Berlin, Heidelberg, 2008), pp. 25–43.

[84] R. V. Mishmash and L. D. Carr, Phys. Rev. Lett. **103**, 140403 (2009).

[85] B. Malomed, L. Torner, F. Wise, and D. Mihalache, J. Phys. B: At. Mol. and Opt. Phys. **49**, 170502 (2016).

[86] G. C. Katsimiga, S. I. Mistakidis, G. M. Koutentakis, P. G. Kevrekidis, and P. Schmelcher, New J. Phys. **19**, 123012 (2017).

[87] S. Krönke and P. Schmelcher, Phys. Rev. A **91**, 053614 (2015).
[88] T. M. Bersano, V. Gokhroo, M. A. Khamehchi, J. DÁmbroise, D. J. Frantzeskakis, P. Engels, and P. G. Kevrekidis, Phys. Rev. Lett. **120**, 063202 (2018).
[89] B. Bakkali-Hassani, C. Maury, Y. Q. Zou, É. Le Cerf, R. Saint-Jalm, P. C. M. Castilho, S. Nascimbene, J. Dalibard, and J. Beugnon, Phys. Rev. Lett. **127**, 023603 (2021).
[90] C. N. Weiler, T. W. Neely, D. R. Scherer, A. S. Bradley, M. J. Davis, and B. P. Anderson, Nature **455**, 948 (2008).
[91] A. del Campo, A. Retzker, and M. B. Plenio, New Journal of Physics **13**, 083022 (2011).
[92] S. Serafini, M. Barbiero, M. Debortoli, S. Donadello, F. Larcher, F. Dalfovo, G. Lamporesi, and G. Ferrari, Phys. Rev. Lett. **115**, 170402 (2015).
[93] A. Romero-Ros, G. Katsimiga, S. I. Mistakidis, S. Mossman, G. Biondini, P. Schmelcher, P. Engels, and P. G. Kevrekidis, Phys. Rev. Lett. **132**, 033402 (2024).
[94] V. M. Pérez-García and J. B. Beitia, Phys. Rev. A **72**, 033620 (2005).
[95] M. Lewenstein, D. Bruss, J. I. Cirac, B. Kraus, M. Kus, J. Samsonowicz, A. Sanpera, and R. Tarrach, Journal of Modern Optics **47**, 2481 (2000).
[96] M. Horodecki, P. Horodecki, and R. Horodecki, Physics Letters A **283**, 1 (2001).
[97] A. Peres, *Quantum theory: concepts and methods*, 1st ed., Vol. 57, Fundamental Theories of Physics, Springer Science+Business Media B.V., 2002 (Springer Dordrecht, 2006), p. 450.
[98] K. M. Mertes, J. W. Merrill, R. Carretero-González, D. J. Frantzeskakis, P. G. Kevrekidis, and D. S. Hall, Phys. Rev. Lett. **99**, 190402 (2007).
[99] R. Horodecki, P. Horodecki, M. Horodecki, and K. Horodecki, Rev. Mod. Phys. **81**, 865 (2009).
[100] M. Roncaglia, A. Montorsi, and M. Genovese, Phys. Rev. A **90**, 062303 (2014).
[101] S. Krönke, J. Knörzer, and P. Schmelcher, New Journal of Physics **17**, 053001 (2015).
[102] G. C. Katsimiga, G. M. Koutentakis, S. I. Mistakidis, P. G. Kevrekidis, and P. Schmelcher, New Journal of Physics **19**, 073004 (2017).
[103] T. Busch, B.-G. Englert, K. Rzażewski, and M. Wilkens, Foundations of Physics **28**, 549 (1998).
[104] Z. Idziaszek and T. Calarco, Phys. Rev. A **71**, 050701 (2005).
[105] F. Werner and Y. Castin, Phys. Rev. Lett. **97**, 150401 (2006).
[106] Z. Idziaszek and T. Calarco, Phys. Rev. A **74**, 022712 (2006).
[107] G. Bougas, S. I. Mistakidis, and P. Schmelcher, Phys. Rev. A **100**, 053602 (2019).
[108] G. Bougas, S. I. Mistakidis, G. M. Alshalan, and P. Schmelcher, Phys. Rev. A **102**, 013314 (2020).
[109] G. Bougas, S. I. Mistakidis, P. Giannakeas, and P. Schmelcher, New Journal of Physics **23**, 093022 (2021).
[110] G. Bougas, "Stationary properties and dynamical response of few-body systems at low temperatures", PhD thesis (University of Hamburg, 2023).

[111] L. Santos, G. V. Shlyapnikov, P. Zoller, and M. Lewenstein, Phys. Rev. Lett. **85**, 1791 (2000).

[112] A. Griesmaier, Journal of Physics B: Atomic, Molecular and Optical Physics **40**, R91 (2007).

[113] I. Ferrier-Barbut, H. Kadau, M. Schmitt, M. Wenzel, and T. Pfau, Phys. Rev. Lett. **116**, 215301 (2016).

[114] F. Böttcher, J.-N. Schmidt, M. Wenzel, J. Hertkorn, M. Guo, T. Langen, and T. Pfau, Phys. Rev. X **9**, 011051 (2019).

[115] T. Gallagher, *Rydberg atoms*, Cambridge Monographs on Atomic, Molecular and Chemical Physics (Cambridge University Press, 1994).

[116] T. F. Gallagher and P. Pillet, in *Advances in atomic, molecular, and optical physics*, Vol. 56, Advances In Atomic, Molecular, and Optical Physics (Academic Press, 2008), pp. 161–218.

[117] S. L. Cornish, M. R. Tarbutt, and K. R. A. Hazzard, Nature Physics **20**, 730 (2024).

[118] N. Bigagli, W. Yuan, S. Zhang, B. Bulatovic, T. Karman, I. Stevenson, and S. Will, Nature **631**, 289 (2024).

[119] L. Chomaz, I. Ferrier-Barbut, F. Ferlaino, B. Laburthe-Tolra, B. L. Lev, and T. Pfau, Rep. Prog. Phys. **86**, 026401 (2022).

[120] A. J. Daley, Nature Reviews Physics **5**, 702 (2023).

[121] N. Goldman, G. Juzeliūnas, P. Öhberg, and I. B. Spielman, Reports on Progress in Physics **77**, 126401 (2014).

[122] M. Mancini, G. Pagano, G. Cappellini, L. Livi, M. Rider, J. Catani, C. Sias, P. Zoller, M. Inguscio, M. Dalmonte, and L. Fallani, Science **349**, 1510 (2015).

[123] N. Goldman, J. C. Budich, and P. Zoller, Nature Physics **12**, 639 (2016).

[124] M. Aidelsburger, S. Nascimbene, and N. Goldman, Comptes Rendus Physique **19**, Quantum simulation / Simulation quantique, 394 (2018).

[125] M. Arndt, A. Bassi, D. Giulini, A. Heidmann, and J.-M. Raimond, Procedia Computer Science **7**, Proceedings of the 2nd European Future Technologies Conference and Exhibition 2011 (FET 11), 77 (2011).

[126] A. M. Kaufman, B. J. Lester, and C. A. Regal, Phys. Rev. X **2**, 041014 (2012).

[127] D. Bluvstein, H. Levine, G. Semeghini, T. T. Wang, S. Ebadi, M. Kalinowski, A. Keesling, N. Maskara, H. Pichler, M. Greiner, V. Vuletić, and M. D. Lukin, Nature **604**, 451 (2022).

[128] P. Lipka-Bartosik, H. Wilming, and N. H. Y. Ng, Rev. Mod. Phys. **96**, 025005 (2024).

[129] M. Lewenstein and L. You, Phys. Rev. Lett. **77**, 3489 (1996).

[130] S. Will, T. Best, U. Schneider, L. Hackermüller, D.-S. Lühmann, and I. Bloch, Nature **465**, 197 (2010).

[131] T. Zhou, K. Yang, Z. Zhu, X. Yu, S. Yang, W. Xiong, X. Zhou, X. Chen, C. Li, J. Schmiedmayer, X. Yue, and Y. Zhai, Phys. Rev. A **99**, 013602 (2019).

[132] L. Tonks, Phys. Rev. **50**, 955 (1936).

[133] M. Girardeau, Journal of Mathematical Physics **1**, 516 (1960).
[134] P. Devillard, D. Chevallier, P. Vignolo, and M. Albert, Phys. Rev. A **101**, 063604 (2020).
[135] G. E. Astrakharchik, J. Boronat, J. Casulleras, and S. Giorgini, Phys. Rev. Lett. **95**, 190407 (2005).
[136] P. Massignan, M. Zaccanti, and G. M. Bruun, Rep. Prog. Phys. **77**, 034401 (2014).
[137] R. Schmidt, M. Knap, D. A. Ivanov, J.-S. You, M. Cetina, and E. Demler, Rep. Prog. Phys. **81**, 024401 (2018).
[138] F. Grusdt, N. Mostaan, E. Demler, and L. A. P. Ardila, Reports on Progress in Physics **88**, 066401 (2025).
[139] D. S. Petrov, Phys. Rev. Lett. **115**, 155302 (2015).
[140] F. Böttcher, J.-N. Schmidt, J. Hertkorn, K. S. H. Ng, S. D. Graham, M. Guo, T. Langen, and T. Pfau, Rep. Progr. Phys. **84**, 012403 (2020).
[141] Z.-H. Luo, W. Pang, B. Liu, Y.-Y. Li, and B. A. Malomed, Front. Phys. **16**, 32201 (2020).
[142] B. A. Malomed, Front. Phys. **16**, 22504, 22504 (2021).
[143] J. Catani, G. Barontini, G. Lamporesi, F. Rabatti, G. Thalhammer, F. Minardi, S. Stringari, and M. Inguscio, Phys. Rev. Lett. **103**, 140401 (2009).
[144] T. Fukuhara, A. Kantian, M. Endres, M. Cheneau, P. Schauss, S. Hild, D. Bellem, U. Schollwöck, T. Giamarchi, C. Gross, I. Bloch, and S. Kuhr, Nature Physics **9**, 235 (2013).
[145] M.-G. Hu, M. J. Van de Graaff, D. Kedar, J. P. Corson, E. A. Cornell, and D. S. Jin, Phys. Rev. Lett. **117**, 055301 (2016).
[146] N. B. Jørgensen, L. Wacker, K. T. Skalmstang, M. M. Parish, J. Levinsen, R. S. Christensen, G. M. Bruun, and J. J. Arlt, Phys. Rev. Lett. **117**, 055302 (2016).
[147] Z. Z. Yan, Y. Ni, C. Robens, and M. W. Zwierlein, Science **368**, 190 (2020).
[148] C. Kohstall, M. Zaccanti, M. Jag, A. Trenkwalder, P. Massignan, G. M. Bruun, F. Schreck, and R. Grimm, Nature **485**, 615 (2012).
[149] M. Koschorreck, D. Pertot, E. Vogt, B. Fröhlich, M. Feld, and M. Köhl, Nature **485**, 619 (2012).
[150] F. Scazza, G. Valtolina, P. Massignan, A. Recati, A. Amico, A. Burchianti, C. Fort, M. Inguscio, M. Zaccanti, and G. Roati, Phys. Rev. Lett. **118**, 083602 (2017).
[151] S. P. Rath and R. Schmidt, Phys. Rev. A **88**, 053632 (2013).
[152] E. Demler and F. Grusdt, arXiv:1510.04934 (2015).
[153] M. Bruderer, A. Klein, S. R. Clark, and D. Jaksch, Phys. Rev. A **76**, 011605 (2007).
[154] L. A. P. Ardila and S. Giorgini, Phys. Rev. A **92**, 033612 (2015).
[155] F. Grusdt, R. Schmidt, Y. E. Shchadilova, and E. Demler, Phys. Rev. A **96**, 013607 (2017).

[156] A. S. Dehkharghani, A. G. Volosniev, and N. T. Zinner, Phys. Rev. Lett. **121**, 080405 (2018).
[157] T. Ichmoukhamedov and J. Tempere, Phys. Rev. A **100**, 043605 (2019).
[158] A. G. Volosniev, H.-W. Hammer, and N. T. Zinner, Phys. Rev. A **92**, 023623 (2015).
[159] F. Grusdt, K. Seetharam, Y. Shchadilova, and E. Demler, Phys. Rev. A **97**, 033612 (2018).
[160] S. I. Mistakidis, G. C. Katsimiga, G. M. Koutentakis, T. Busch, and P. Schmelcher, Phys. Rev. Lett. **122**, 183001 (2019).
[161] S. I. Mistakidis, A. G. Volosniev, N. T. Zinner, and P. Schmelcher, Phys. Rev. A **100**, 013619 (2019).
[162] D. S. Petrov and G. E. Astrakharchik, Phys. Rev. Lett. **117**, 100401 (2016).
[163] T. D. Lee, K. Huang, and C. N. Yang, Phys. Rev. **106**, 1135 (1957).
[164] A. R. P. Lima and A. Pelster, Phys. Rev. A **84**, 041604 (2011).
[165] L. Chomaz, S. Baier, D. Petter, M. J. Mark, F. Wächtler, L. Santos, and F. Ferlaino, Phys. Rev. X **6**, 041039 (2016).
[166] R. N. Bisset, L. A. P. Ardila, and L. Santos, Phys. Rev. Lett. **126**, 025301 (2021).
[167] J. C. Smith, D. Baillie, and P. B. Blakie, Phys. Rev. Lett. **126**, 025302 (2021).
[168] X. Cui, Phys. Rev. A **98**, 023630 (2018).
[169] D. Rakshit, T. Karpiuk, M. Brewczyk, and M. Gajda, SciPost Phys. **6**, 79 (2019).
[170] J. B. Wang, J. S. Pan, X. Cui, and W. Yi, Chin. Phys. Lett. **37**, 076701 (2020).
[171] Y. Sekino and Y. Nishida, Phys. Rev. A **97**, 011602 (2018).
[172] I. Morera, B. Juliá-Díaz, and M. Valiente, Phys. Rev. Res. **4**, L042024 (2022).
[173] C. R. Cabrera, L. Tanzi, J. Sanz, B. Naylor, P. Thomas, P. Cheiney, and L. Tarruell, Science **359**, 301 (2018).
[174] P. Cheiney, C. R. Cabrera, J. Sanz, B. Naylor, L. Tanzi, and L. Tarruell, Phys. Rev. Lett. **120**, 135301 (2018).
[175] C. D'Errico, A. Burchianti, M. Prevedelli, L. Salasnich, F. Ancilotto, M. Modugno, F. Minardi, and C. Fort, Phys. Rev. Research **1**, 033155 (2019).
[176] F. Ancilotto, M. Barranco, M. Guilleumas, and M. Pi, Phys. Rev. A **98**, 053623 (2018).
[177] G. Ferioli, G. Semeghini, L. Masi, G. Giusti, G. Modugno, M. Inguscio, A. Gallemí, A. Recati, and M. Fattori, Phys. Rev. Lett. **122**, 090401 (2019).
[178] C. Fort and M. Modugno, Appl. Sci. **11(2)**, 866 (2021).
[179] M. Tylutki, G. E. Astrakharchik, B. A. Malomed, and D. S. Petrov, Phys. Rev. A **101**, 051601 (2020).
[180] G. E. Astrakharchik and B. A. Malomed, Phys. Rev. A **98**, 013631 (2018).
[181] G. E. Astrakharchik and S. Giorgini, J. Phys. B: At. Mol. and Opt. Phys. **39**, S1 (2006).
[182] L. Lavoine and T. Bourdel, Phys. Rev. A **103**, 033312 (2021).

[183] G. Semeghini, G. Ferioli, L. Masi, C. Mazzinghi, L. Wolswijk, F. Minardi, M. Modugno, G. Modugno, M. Inguscio, and M. Fattori, Phys. Rev. Lett. **120**, 235301 (2018).

[184] S. I. Mistakidis, T. Mithun, P. G. Kevrekidis, H. R. Sadeghpour, and P. Schmelcher, Phys. Rev. Research **3**, 043128 (2021).

[185] L. Parisi, G. E. Astrakharchik, and S. Giorgini, Phys. Rev. Lett. **122**, 105302 (2019).

[186] L. Parisi and S. Giorgini, Phys. Rev. A **102**, 023318 (2020).

[187] Z. Guo, F. Jia, L. Li, Y. Ma, J. M. Hutson, X. Cui, and D. Wang, Phys. Rev. Res. **3**, 033247 (2021).

[188] L. Cavicchioli, C. Fort, F. Ancilotto, M. Modugno, F. Minardi, and A. Burchianti, Phys. Rev. Lett. **134**, 093401 (2025).

[189] T. Mithun, A. Maluckov, K. Kasamatsu, B. A. Malomed, and A. Khare, Symmetry **12**, 32201 (2020).

[190] M. N. Tengstrand and S. M. Reimann, Phys. Rev. A **105**, 033319 (2022).

[191] E. G. Charalampidis and S. I. Mistakidis, Phys. Rev. A **111**, 013318 (2025).

[192] I. Morera, G. E. Astrakharchik, A. Polls, and B. Juliá-Díaz, Phys. Rev. Lett. **126**, 023001 (2021).

[193] J. Vallés-Muns, I. Morera, G. E. Astrakharchik, and B. Juliá-Díaz, SciPost Phys. **16**, 074 (2024).

[194] L. He, H. Li, W. Yi, and Z.-Q. Yu, Phys. Rev. Lett. **130**, 193001 (2023).

[195] T. A. Flynn, L. Parisi, T. P. Billam, and N. G. Parker, Phys. Rev. Research **5**, 033167 (2023).

[196] T. A. Flynn, N. A. Keepfer, N. G. Parker, and T. P. Billam, Phys. Rev. Res. **6**, 013209 (2024).

[197] Y. Ma, C. Peng, and X. Cui, Phys. Rev. Lett. **127**, 043002 (2021).

[198] Y. Ma and X. Cui, Phys. Rev. Lett. **134**, 043402 (2025).

[199] F. K. Abdullaev and R. M. Galimzyanov, J. Phys. B: At. Mol. Opt. Phys. **53**, 165301 (2020).

[200] G. Bighin, A. Burchianti, F. Minardi, and T. Macrí, Phys. Rev. A **106**, 023301 (2022).

[201] D. Edler, L. A. P. Ardila, C. R. Cabrera, and L. Santos, Phys. Rev. Res. **4**, 033017 (2022).

[202] S. Sinha, S. Biswas, L. Santos, and S. Sinha, Phys. Rev. A **108**, 023311 (2023).

[203] P. Naidon and D. S. Petrov, Phys. Rev. Lett. **126**, 115301 (2021).

[204] G. C. Katsimiga, S. I. Mistakidis, G. N. Koutsokostas, D. J. Frantzeskakis, R. Carretero-González, and P. G. Kevrekidis, Phys. Rev. A **107**, 063308 (2023).

[205] M. Edmonds, Phys. Rev. Res. **5**, 023175 (2023).

[206] P. Examilioti and G. M. Kavoulakis, J. Phys. B: At. Mol. and Opt. Phys. **53**, 175301 (2020).

[207] Y. Li, Z. Chen, Z. Luo, C. Huang, H. Tan, W. Pang, and B. A. Malomed, Phys. Rev. A **98**, 063602 (2018).

[208] G. Bougas, G. C. Katsimiga, P. G. Kevrekidis, and S. I. Mistakidis, Phys. Rev. A **110**, 033317 (2024).

[209] M. N. Tengstrand, P. Stürmer, E. Ö. Karabulut, and S. M. Reimann, Phys. Rev. Lett. **123**, 160405 (2019).

[210] T. A. Yo ğurt, U. Tanyeri, A. Kele ş, and M. Ö. Oktel, Phys. Rev. A **108**, 033315 (2023).

[211] T. Giamarchi, *Quantum physics in one dimension*, Vol. 121 (Clarendon press, 2003).

[212] A. Bambini and A. Agresti, Phys. Rev. A **56**, 3040 (1997).

[213] D. Hernandez-Rajkov, J. E. Padilla-Castillo, M. Mendoza-Lopez, R. Colin-Rodriguez, A. Gutierrez-Valdes, S. A. Morales-Ramirez, R. A. Gutierrez-Arenas, C. A. Gardea-Flores, R. Jauregui-Renaud, J. A. Seman, F. J. Poveda-Cuevas, and G. Roati, Revista Mexicana de Física **66**, 388 (2020).

[214] A. Burchianti, G. Valtolina, J. A. Seman, E. Pace, M. De Pas, M. Inguscio, M. Zaccanti, and G. Roati, Phys. Rev. A **90**, 043408 (2014).

[215] C. J. Cooper, G. Hillenbrand, J. Rink, C. G. Townsend, K. Zetie, and C. J. Foot, Europhysics Letters **28**, 397 (1994).

[216] J. Dalibard and C. Cohen-Tannoudji, J. Opt. Soc. Am. B **6**, 2023 (1989).

[217] P. D. Lett, R. N. Watts, C. I. Westbrook, W. D. Phillips, P. L. Gould, and H. J. Metcalf, Phys. Rev. Lett. **61**, 169 (1988).

[218] C. Adams and E. Riis, Progress in Quantum Electronics **21**, 1 (1997).

[219] H. Perrin, P. Lemonde, F. Pereira dos Santos, V. Josse, B. Laburthe Tolra, F. Chevy, and D. Comparat, Comptes Rendus Physique **12**, Quantum Hall Effect and Metrology, 417 (2011).

[220] F. Schreck and K. v. Druten, Nature Physics **17**, 1296 (2021).

[221] C. N. Cohen-Tannoudji and W. D. Phillips, Physics Today **43**, 33 (1990).

[222] Z. Lin, K. Shimizu, M. Zhan, F. Shimizu, and H. T. Hiroshi Takuma, Japanese Journal of Applied Physics **30**, L1324 (1991).

[223] C. Salomon, J. Dalibard, W. D. Phillips, A. Clairon, and S. Guellati, Europhysics Letters **12**, 683 (1990).

[224] G. Sprouse, L. Orozco, J. Simsarian, W. Shi, and W. Zhao, Nuclear Instruments and Methods in Physics Research Section B: Beam Interactions with Materials and Atoms **126**, International Conference on Electromagnetic Isotope Separators and Techniques Related to Their Applications, 370 (1997).

[225] B. Sheehy, S.-Q. Shang, P. van der Straten, S. Hatamian, and H. Metcalf, Phys. Rev. Lett. **64**, 858 (1990).

[226] X. Xu, T. H. Loftus, J. W. Dunn, C. H. Greene, J. L. Hall, A. Gallagher, and J. Ye, Phys. Rev. Lett. **90**, 193002 (2003).

[227] N. Kostylev, E. Ivanov, M. E. Tobar, and J. J. McFerran, J. Opt. Soc. Am. B **31**, 1614 (2014).

[228] A. J. Berglund, S. A. Lee, and J. J. McClelland, Phys. Rev. A **76**, 053418 (2007).

[229] S. H. Youn, M. Lu, and B. L. Lev, Phys. Rev. A **82**, 043403 (2010).

[230] A. T. Grier, I. Ferrier-Barbut, B. S. Rem, M. Delehaye, L. Khaykovich, F. Chevy, and C. Salomon, Phys. Rev. A **87**, 063411 (2013).

[231] D. Rio Fernandes, F. Sievers, N. Kretzschmar, S. Wu, C. Salomon, and F. Chevy, Europhysics Letters **100**, 63001 (2012).

[232] M. Landini, S. Roy, L. Carcagní, D. Trypogeorgos, M. Fattori, M. Inguscio, and G. Modugno, Phys. Rev. A **84**, 043432 (2011).

[233] F. Sievers, N. Kretzschmar, D. R. Fernandes, D. Suchet, M. Rabinovic, S. Wu, C. V. Parker, L. Khaykovich, C. Salomon, and F. Chevy, Phys. Rev. A **91**, 023426 (2015).

[234] S. E. Hamann, D. L. Haycock, G. Klose, P. H. Pax, I. H. Deutsch, and P. S. Jessen, Phys. Rev. Lett. **80**, 4149 (1998).

[235] V. Vuleti ć, C. Chin, A. J. Kerman, and S. Chu, Phys. Rev. Lett. **81**, 5768 (1998).

[236] D.-J. Han, S. Wolf, S. Oliver, C. McCormick, M. T. DePue, and D. S. Weiss, Phys. Rev. Lett. **85**, 724 (2000).

[237] A. J. Kerman, V. Vuleti ć, C. Chin, and S. Chu, Phys. Rev. Lett. **84**, 439 (2000).

[238] T. Weber, J. Herbig, M. Mark, H.-C. Nägerl, and R. Grimm, Science **299**, 232 (2003).

[239] F. Lison, P. Schuh, D. Haubrich, and D. Meschede, Phys. Rev. A **61**, 013405 (1999).

[240] C. V. Heer, Review of Scientific Instruments **34**, 532 (1963).

[241] D. E. Pritchard, Phys. Rev. Lett. **51**, 1336 (1983).

[242] A. L. Migdall, J. V. Prodan, W. D. Phillips, T. H. Bergeman, and H. J. Metcalf, Phys. Rev. Lett. **54**, 2596 (1985).

[243] M. Lu, S. H. Youn, and B. L. Lev, Phys. Rev. Lett. **104**, 063001 (2010).

[244] W. Ketterle, K. B. Davis, M. A. Joffe, A. Martin, and D. E. Pritchard, Phys. Rev. Lett. **70**, 2253 (1993).

[245] N. Radwell, G. Walker, and S. Franke-Arnold, Phys. Rev. A **88**, 043409 (2013).

[246] J. Pérez-Ríos and A. S. Sanz, American Journal of Physics **81**, 836 (2013).

[247] C. V. Sukumar and D. M. Brink, Phys. Rev. A **56**, 2451 (1997).

[248] T. Bergeman, G. Erez, and H. J. Metcalf, Phys. Rev. A **35**, 1535 (1987).

[249] T. Esslinger, I. Bloch, and T. W. Hänsch, Phys. Rev. A **58**, R2664 (1998).

[250] E. W. Streed, A. P. Chikkatur, T. L. Gustavson, M. Boyd, Y. Torii, D. Schneble, G. K. Campbell, D. E. Pritchard, and W. Ketterle, Review of Scientific Instruments **77**, 023106 (2006).

[251] T. Wang, S. F. Yelin, R. Côté, E. E. Eyler, S. M. Farooqi, P. L. Gould, M. Ko štrun, D. Tong, and D. Vrinceanu, Phys. Rev. A **75**, 033802 (2007).

[252] W. Petrich, M. H. Anderson, J. R. Ensher, and E. A. Cornell, Phys. Rev. Lett. **74**, 3352 (1995).

[253] R. Grimm, M. Weidemüller, and Y. B. Ovchinnikov, in , Vol. 42, edited by B. Bederson and H. Walther, Advances In Atomic, Molecular, and Optical Physics (Academic Press, 2000), pp. 95–170.

[254] J. D. Miller, R. A. Cline, and D. J. Heinzen, Phys. Rev. A **47**, R4567 (1993).

[255] G. Gauthier, T. A. Bell, A. B. Stilgoe, M. Baker, H. Rubinsztein-Dunlop, and T. W. Neely, in , Vol. 70, edited by L. F. Dimauro, H. Perrin, and S. F. Yelin, Advances In Atomic, Molecular, and Optical Physics (Academic Press, 2021), pp. 1–101.

[256] M. Duocastella, S. Surdo, A. Zunino, A. Diaspro, and P. Saggau, Journal of Physics: Photonics **3**, 012004 (2020).

[257] A. P. Goutzoulis, *Design and fabrication of acousto-optic devices (1st ed.)*. (CRC Press, 1994).

[258] P. Ricci, M. Marchetti, M. Sorelli, L. Turrini, F. Resta, V. Gavryusev, G. de Vito, G. Sancataldo, F. Vanzi, L. Silvestri, and F. S. Pavone, Journal of Biophotonics **15**, e202100256 (2022).

[259] P. Ricci, G. Sancataldo, V. Gavryusev, F. S. Pavone, P. Saggau, and M. Duocastella, Journal of Physics: Photonics **6**, 022001 (2024).

[260] L. R. B. Picard and M. Endres, *A three-dimensional acousto-optic deflector*, 2025.

[261] Y.-H. Lu, N. Song, T. Xiang, J. Ho, T.-C. Lee, Z. Yan, and D. M. Stamper-Kurn, *Astigmatism-free 3d optical tweezer control for rapid atom rearrangement*, 2025.

[262] L. Chen, M. Ghilardi, J. J. C. Busfield, and F. Carpi, Frontiers in Robotics and AI **Volume 8 - 2021**, 10.3389/frobt.2021.678046 (2021).

[263] Y. Pang, K. Zhang, and L. Lang, Frontiers in Physics **Volume 10 - 2022**, 10.3389/fphy.2022.1102996 (2022).

[264] G. B. Esmer, Opt. Express **23**, 12636 (2015).

[265] M. Ammenwerth, H. Timme, V. Giardini, R. Tao, F. Gyger, O. Lib, D. Berndt, D. Kourkoulos, T. Rom, I. Bloch, and J. Zeiher, Phys. Rev. Appl. **24**, 034031 (2025).

[266] J. Sebby-Strabley, M. Anderlini, P. S. Jessen, and J. V. Porto, Phys. Rev. A **73**, 033605 (2006).

[267] T. Zhou, K. Yang, Y. Zhai, X. Yue, S. Yang, J. Xiang, Q. Huang, W. Xiong, X. Zhou, and X. Chen, Opt. Express **26**, 16726 (2018).

[268] W. S. Bakr, J. I. Gillen, A. Peng, S. Fölling, and M. Greiner, Nature **462**, 74 (2009).

[269] J. F. Sherson, C. Weitenberg, M. Endres, M. Cheneau, I. Bloch, and S. Kuhr, Nature **467**, 68 (2010).

[270] R. Jördens, N. Strohmaier, K. Günter, H. Moritz, and T. Esslinger, Nature **455**, 204 (2008).

[271] A. Mazurenko, C. S. Chiu, G. Ji, M. F. Parsons, M. Kanász-Nagy, R. Schmidt, F. Grusdt, E. Demler, D. Greif, and M. Greiner, Nature **545**, 462 (2017).

[272] T. Nicholson, S. Campbell, R. Hutson, G. Marti, B. Bloom, R. McNally, W. Zhang, M. Barrett, M. Safronova, G. Strouse, W. Tew, and J. Ye, Nature Communications **6**, 6896 (2015).

[273] P. Cladé, E. de Mirandes, M. Cadoret, S. Guellati-Khélifa, C. Schwob, F. ç. Nez, L. Julien, and F. ç. Biraben, Phys. Rev. Lett. **96**, 033001 (2006).

[274] U. Schneider, L. Hackermüller, S. Will, T. Best, I. Bloch, T. A. Costi, R. W. Helmes, D. Rasch, and A. Rosch, Science **322**, 1520 (2008).

[275] D. Greif, T. Uehlinger, G. Jotzu, L. Tarruell, and T. Esslinger, Science **340**, 1307 (2013).

[276] D. Tusi, L. Franchi, L. F. Livi, K. Baumann, D. B. Orenes, L. D. Re, R. E. Barfknecht, T.-W. Zhou, M. Inguscio, G. Cappellini, M. Capone, J. Catani, and L. Fallani, Nature Physics **18**, 1201 (2022).

[277] C. S. Chiu, G. Ji, A. Bohrdt, M. Xu, M. Knap, E. Demler, F. Grusdt, M. Greiner, and D. Greif, Science **365**, 251 (2019).

[278] G. Jotzu, M. Messer, R. Desbuquois, M. Lebrat, T. Uehlinger, D. Greif, and T. Esslinger, Nature **515**, 237 (2014).

[279] E. Haller, J. Hudson, A. Kelly, D. A. Cotta, B. Peaudecerf, G. D. Bruce, and S. Kuhr, Nature Physics **11**, 738 (2015).

[280] D. G. Grier, Nature **424**, 810 (2003).

[281] T. Grünzweig, A. Hilliard, M. McGovern, and M. F. Andersen, Nature Physics **6**, 951 (2010).

[282] F. Nogrette, H. Labuhn, S. Ravets, D. Barredo, L. Béguin, A. Vernier, T. Lahaye, and A. Browaeys, Phys. Rev. X **4**, 021034 (2014).

[283] V. Giardini, L. Guariento, A. Fantini, S. Storm, M. Inguscio, J. Catani, G. Cappellini, V. Gavryusev, and L. Fallani, Atoms **14**, 10.3390/atoms14010001 (2026).

[284] D. Schäffner, T. Preuschoff, S. Ristok, L. Brozio, M. Schlosser, H. Giessen, and G. Birkl, Opt. Express **28**, 8640 (2020).

[285] M. Schlosser, S. Tichelmann, D. Schäffner, D. O. de Mello, M. Hambach, J. Schütz, and G. Birkl, Phys. Rev. Lett. **130**, 180601 (2023).

[286] L. Pause, L. Sturm, M. Mittenbühler, S. Amann, T. Preuschoff, D. Schäffner, M. Schlosser, and G. Birkl, Optica **11**, 222 (2024).

[287] T.-W. Hsu, W. Zhu, T. Thiele, M. O. Brown, S. B. Papp, A. Agrawal, and C. A. Regal, PRX Quantum **3**, 030316 (2022).

[288] X. Huang, W. Yuan, A. Holman, M. Kwon, S. J. Masson, R. Gutierrez-Jauregui, A. Asenjo-Garcia, S. Will, and N. Yu, Progress in Quantum Electronics **89**, 100470 (2023).

[289] R. Huang, F. Zhou, X. Li, P. Xu, Y. Wang, and M. Zhan, Opt. Express **32**, 21293 (2024).

[290] A. Ashkin, Proceedings of the National Academy of Sciences **94**, 4853 (1997).

[291] M. F. Andersen, Advances in Physics: X **7**, 2064231 (2022).

[292] J. Gieseler, J. R. Gomez-Solano, A. Magazzù, I. P. Castillo, L. P. García, M. Gironella-Torrent, X. Viader-Godoy, F. Ritort, G. Pesce, A. V. Arzola, K. Volke-Sepúlveda, and G. Volpe, Adv. Opt. Photon. **13**, 74 (2021).

[293] D. Frese, B. Ueberholz, S. Kuhr, W. Alt, D. Schrader, V. Gomer, and D. Meschede, Phys. Rev. Lett. **85**, 3777 (2000).

[294] N. Schlosser, G. Reymond, I. Protsenko, and P. Grangier, Nature **411**, 1024 (2001).
[295] N. Schlosser, G. Reymond, and P. Grangier, Phys. Rev. Lett. **89**, 023005 (2002).
[296] S. Kuhr, W. Alt, D. Schrader, M. Müller, V. Gomer, and D. Meschede, Science **293**, 278 (2001).
[297] B. J. Lester, N. Luick, A. M. Kaufman, C. M. Reynolds, and C. A. Regal, Phys. Rev. Lett. **115**, 073003 (2015).
[298] Y. H. Fung and M. F. Andersen, New Journal of Physics **17**, 073011 (2015).
[299] M. O. Brown, T. Thiele, C. Kiehl, T.-W. Hsu, and C. A. Regal, Phys. Rev. X **9**, 011057 (2019).
[300] A. L. Shaw, P. Scholl, R. Finklestein, I. S. Madjarov, B. Grinkemeyer, and M. Endres, Phys. Rev. Lett. **130**, 193402 (2023).
[301] J. Beugnon, C. Tuchendler, H. Marion, A. Gaëtan, Y. Miroshnychenko, Y. R. P. Sortais, A. M. Lance, M. P. A. Jones, G. Messin, A. Browaeys, and P. Grangier, Nature Physics **3**, 696 (2007).
[302] Y. Miroshnychenko, W. Alt, I. Dotsenko, L. Förster, M. Khudaverdyan, D. Meschede, D. Schrader, and A. Rauschenbeutel, Nature **442**, 151 (2006).
[303] M. Schlosser, J. Kruse, C. Gierl, S. Teichmann, S. Tichelmann, and G. Birkl, New Journal of Physics **14**, 123034 (2012).
[304] S. Kim, S. W. Seo, H.-R. Noh, and Y. Shin, Phys. Rev. A **94**, 023625 (2016).
[305] D. Barredo, V. Lienhard, S. de Léséleuc, T. Lahaye, and A. Browaeys, Nature **561**, 79 (2018).
[306] A. Cooper, J. P. Covey, I. S. Madjarov, S. G. Porsev, M. S. Safronova, and M. Endres, Phys. Rev. X **8**, 041055 (2018).
[307] D. Ohl de Mello, D. Schäffner, J. Werkmann, T. Preuschoff, L. Kohfahl, M. Schlosser, and G. Birkl, Phys. Rev. Lett. **122**, 203601 (2019).
[308] K.-N. Schymik, V. Lienhard, D. Barredo, P. Scholl, H. Williams, A. Browaeys, and T. Lahaye, Phys. Rev. A **102**, 063107 (2020).
[309] A. Glicenstein, G. Ferioli, L. Brossard, Y. R. P. Sortais, D. Barredo, F. Nogrette, I. Ferrier-Barbut, and A. Browaeys, Phys. Rev. A **103**, 043301 (2021).
[310] K.-N. Schymik, B. Ximenez, E. Bloch, D. Dreon, A. Signoles, F. Nogrette, D. Barredo, A. Browaeys, and T. Lahaye, Phys. Rev. A **106**, 022611 (2022).
[311] D. Bloch, B. Hofer, S. R. Cohen, A. Browaeys, and I. Ferrier-Barbut, Phys. Rev. Lett. **131**, 203401 (2023).
[312] Y. Wang, S. Shevate, T. M. Wintermantel, M. Morgado, G. Lochead, and S. Whitlock, npj Quantum Information **6**, 54 (2020).
[313] X. Qiu, P. Zoller, and X. Li, PRX Quantum **1**, 020311 (2020).
[314] M. Kim, Y. Song, J. Kim, and J. Ahn, PRX Quantum **1**, 020323 (2020).
[315] M. Kim, K. Kim, J. Hwang, E.-G. Moon, and J. Ahn, Nature Physics **18**, 755 (2022).
[316] T. Kusano, Y. Nakamura, R. Yokoyama, N. Ozawa, K. Shibata, T. Takano, Y. Takasu, and Y. Takahashi, Phys. Rev. Res. **7**, L022045 (2025).

[317] V. Gavryusev, L. Guariento, V. Giardini, A. Fantini, S. Storm, J. Catani, M. Inguscio, L. Fallani, and G. Cappellini, in Quantum 2.0 conference and exhibition (2024), QTh2A.2.

[318] R. Lin, H.-S. Zhong, Y. Li, Z.-R. Zhao, L.-T. Zheng, T.-R. Hu, H.-M. Wu, Z. Wu, W.-J. Ma, Y. Gao, Y.-K. Zhu, Z.-F. Su, W.-L. Ouyang, Y.-C. Zhang, J. Rui, M.-C. Chen, C.-Y. Lu, and J.-W. Pan, Phys. Rev. Lett. **135**, 060602 (2025).

[319] I. H. A. Knottnerus, Y. C. Tseng, A. Urech, R. J. C. Spreeuw, and F. Schreck, SciPost Phys. **19**, 118 (2025).

[320] H. M. Rivy, S. A. Aljunid, E. Lassalle, N. I. Zheludev, and D. Wilkowski, Communications Physics **6**, 155 (2023).

[321] D. Schäffner, T. Schreiber, F. Lenz, M. Schlosser, and G. Birkl, PRX Quantum **5**, 010311 (2024).

[322] S. Ebadi, T. T. Wang, H. Levine, A. Keesling, G. Semeghini, A. Omran, D. Bluvstein, R. Samajdar, H. Pichler, W. W. Ho, S. Choi, S. Sachdev, M. Greiner, V. Vuletić, and M. D. Lukin, Nature **595**, 227 (2021).

[323] H. Labuhn, D. Barredo, S. Ravets, S. de Léséleuc, T. Macrì, T. Lahaye, and A. Browaeys, Nature **534**, 667 (2016).

[324] H. Bernien, S. Schwartz, A. Keesling, H. Levine, A. Omran, H. Pichler, S. Choi, A. S. Zibrov, M. Endres, M. Greiner, V. Vuletić, and M. D. Lukin, Nature **551**, 579 (2017).

[325] I. Lesanovsky and H. Katsura, Phys. Rev. A **86**, 041601 (2012).

[326] P. Scholl, M. Schuler, H. J. Williams, A. A. Eberharter, D. Barredo, K.-N. Schymik, V. Lienhard, L.-P. Henry, T. C. Lang, T. Lahaye, A. M. Läuchli, and A. Browaeys, Nature **595**, 233 (2021).

[327] R. Samajdar, W. W. Ho, H. Pichler, M. D. Lukin, and S. Sachdev, Proceedings of the National Academy of Sciences **118**, e2015785118 (2021).

[328] S. Ebadi, A. Keesling, M. Cain, T. T. Wang, H. Levine, D. Bluvstein, G. Semeghini, A. Omran, J.-G. Liu, R. Samajdar, X.-Z. Luo, B. Nash, X. Gao, B. Barak, E. Farhi, S. Sachdev, N. Gemelke, L. Zhou, S. Choi, H. Pichler, S.-T. Wang, M. Greiner, V. Vuletić, and M. D. Lukin, Science **376**, 1209 (2022).

[329] M. Saffman, T. G. Walker, and K. Mølmer, Rev. Mod. Phys. **82**, 2313 (2010).

[330] D. Bluvstein, S. J. Evered, A. A. Geim, S. H. Li, H. Zhou, T. Manovitz, S. Ebadi, M. Cain, M. Kalinowski, D. Hangleiter, J. P. B. Ataides, N. Maskara, I. Cong, X. Gao, P. S. Rodriguez, T. Karolyshyn, G. Semeghini, M. J. Gullans, M. Greiner, V. Vuletić, and M. D. Lukin, Nature **626**, 58 (2024).

[331] H. F. Hess, Phys. Rev. B **34**, 3476 (1986).

[332] N. Masuhara, J. M. Doyle, J. C. Sandberg, D. Kleppner, T. J. Greytak, H. F. Hess, and G. P. Kochanski, Phys. Rev. Lett. **61**, 935 (1988).

[333] K. B. Davis, M.-O. Mewes, M. A. Joffe, M. R. Andrews, and W. Ketterle, Phys. Rev. Lett. **74**, 5202 (1995).

[334] O. J. Luiten, M. W. Reynolds, and J. T. M. Walraven, Phys. Rev. A **53**, 381 (1996).

[335] C. C. Bradley, C. A. Sackett, J. J. Tollett, and R. G. Hulet, Phys. Rev. Lett. **75**, 1687 (1995).

[336] H.-J. Miesner, D. M. Stamper-Kurn, M. R. Andrews, D. S. Durfee, S. Inouye, and W. Ketterle, Science **279**, 1005 (1998).

[337] L. Wolswijk, C. Mordini, A. Farolfi, D. Trypogeorgos, F. Dalfovo, A. Zenesini, G. Ferrari, and G. Lamporesi, Phys. Rev. A **105**, 033316 (2022).

[338] G. Lamporesi, S. Donadello, S. Serafini, F. Dalfovo, and G. Ferrari, Nature Physics **9**, 656 (2013).

[339] S. Donadello, S. Serafini, T. Bienaimé, F. Dalfovo, G. Lamporesi, and G. Ferrari, Phys. Rev. A **94**, 023628 (2016).

[340] I.-K. Liu, S. Donadello, G. Lamporesi, G. Ferrari, S.-C. Gou, F. Dalfovo, and N. P. Proukakis, Communications Physics **1**, 24 (2018).

[341] A. Farolfi, D. Trypogeorgos, G. Colzi, E. Fava, G. Lamporesi, and G. Ferrari, Review of Scientific Instruments **90**, 115114 (2019).

[342] C. Rogora, R. Cominotti, C. Baroni, D. Andreoni, G. Lamporesi, A. Zenesini, and G. Ferrari, Phys. Rev. A **110**, 013319 (2024).

[343] C. S. Adams, H. J. Lee, N. Davidson, M. Kasevich, and S. Chu, Phys. Rev. Lett. **74**, 3577 (1995).

[344] S. Chaudhuri, S. Roy, and C. S. Unnikrishnan, Journal of Physics: Conference Series **80**, 012036 (2007).

[345] C. Li, T. Zhou, Y. Zhai, J. Xiang, T. Luan, Q. Huang, S. Yang, W. Xiong, and X. Chen, Review of Scientific Instruments **88**, 053104 (2017).

[346] M. D. Barrett, J. A. Sauer, and M. S. Chapman, Phys. Rev. Lett. **87**, 010404 (2001).

[347] R. Cominotti, A. Berti, C. Dulin, C. Rogora, G. Lamporesi, I. Carusotto, A. Recati, A. Zenesini, and G. Ferrari, Phys. Rev. X **13**, 021037 (2023).

[348] A. Zenesini, A. Berti, R. Cominotti, C. Rogora, I. G. Moss, T. P. Billam, I. Carusotto, G. Lamporesi, A. Recati, and G. Ferrari, Nature Physics **20**, 558 (2024).

[349] C. J. Fot, *Atomic physics* (Oxford University Press, 2005).

[350] L. Allen and J. Eberly, *Optical resonance and two-level atoms* (Dover Publications, 1975).

[351] M. O. Scully and M. S. Zubairy, *Quantum optics* (Cambridge University Press, 1997).

[352] C. Cohen-Tannoudji, J. Dupont-Roc, and G. Grynberg, *Atom-photon interactions: basic processes and applications* (Wiley-VCH, Jan. 2008), 678 pp.

[353] T. Caneva, T. Calarco, and S. Montangero, Phys. Rev. A **84**, 022326 (2011).

[354] M. A. Nielsen and I. L. Chuang, *Quantum computation and quantum information: 10th anniversary edition* (Cambridge University Press, 2010).

[355] M. Kasevich and S. Chu, Phys. Rev. Lett. **67**, 181 (1991).

[356] N. F. Ramsey, Phys. Rev. **78**, 695 (1950).

[357] E. L. Hahn, Phys. Rev. **80**, 580 (1950).

[358] K. Moler, D. S. Weiss, M. Kasevich, and S. Chu, Phys. Rev. A **45**, 342 (1992).

[359] F. Sorrentino, Q. Bodart, L. Cacciapuoti, Y.-H. Lien, M. Prevedelli, G. Rosi, L. Salvi, and G. M. Tino, Phys. Rev. A **89**, 023607 (2014).
[360] M. A. Norcia and F. Ferlaino, Nature Phys. **17**, 1745 (2021).
[361] J. Dalibard, in Volume 140: bose-einstein condensation in atomic gases (2002).
[362] J. O. Andersen, Rev. Mod. Phys. **76**, 599 (2004).
[363] H. T. C. Stoof, M. Bijlsma, and M. Houbiers, Journal of Research of the National Institute of Standards and Technology **101**, 443 (1996).
[364] N. P. Proukakis and B. Jackson, Journal of Physics B: Atomic, Molecular and Optical Physics **41**, 203002 (2008).
[365] J. Dalibard, *Collisional dynamics of ultra-cold atomic gases (bose-einstein condensation in gases)* (IOS Press, 1999).
[366] J. T. M. Walraven, *Quantum gases lectures, university of amsterdam* (Online, 2019).
[367] C. Joachain, *Quantum collision theory* (North-Holland., Dec. 2024).
[368] H. Friedrich, *Scattering theory*, Lecture Notes in Physics (Springer Berlin Heidelberg, 2013).
[369] H. Bethe and R. Peierls, Proceedings of the Royal Society of London. Series A - Mathematical and Physical Sciences **148**, 146 (1935).
[370] E. Fermi, Il Nuovo Cimento (1924-1942) **11**, 157 (1934).
[371] K. Huang and C. N. Yang, Phys. Rev. **105**, 767 (1957).
[372] C. Chin, R. Grimm, P. Julienne, and E. Tiesinga, Rev. Mod. Phys. **82**, 1225 (2010).
[373] A. Farrell and B. P. van Zyl, Journal of Physics A: Mathematical and Theoretical **43**, 015302 (2009).
[374] M. Li, H. Fu, Y.-Z. Wang, J. Chen, L. Chen, and C. Chen, Phys. Rev. A **66**, 015601 (2002).
[375] V. E. Barlette, M. M. Leite, and S. K. Adhikari, European Journal of Physics **21**, 435 (2000).
[376] J. P. Corson and J. L. Bohn, Phys. Rev. A **94**, 023604 (2016).
[377] S. K. Adhikari, W. G. Gibson, and T. K. Lim, The Journal of Chemical Physics **85**, 5580 (1986).
[378] T. K. Lim and P. A. Maurone, Phys. Rev. B **22**, 1467 (1980).
[379] K. Wódkiewicz, Phys. Rev. A **43**, 68 (1991).
[380] M. Olshanii and L. Pricoupenko, Phys. Rev. Lett. **88**, 010402 (2001).
[381] K. Kanjilal and D. Blume, Phys. Rev. A **73**, 060701 (2006).
[382] L. Pricoupenko and M. Olshanii, Journal of Physics B: Atomic, Molecular and Optical Physics **40**, 2065 (2007).
[383] J. Levinsen and M. M. Parish, "Strongly interacting two-dimensional fermi gases", in *Annual review of cold atoms and molecules* (2015) Chap. CHAPTER 1, pp. 1–75.
[384] D.S. Petrov, D.M. Gangardt, and G.V. Shlyapnikov, J. Phys. IV France **116**, 5 (2004).

[385] D. S. Petrov and G. V. Shlyapnikov, Phys. Rev. A **64**, 012706 (2001).
[386] L. Pricoupenko, Phys. Rev. Lett. **100**, 170404 (2008).
[387] S. R. Beane and M. Jafry, Journal of Physics B: Atomic, Molecular and Optical Physics **52**, 035001 (2019).
[388] B. M. Faigle-Cedzich, J. M. Pawlowski, and C. Wetterich, Phys. Rev. A **103**, 033320 (2021).
[389] S. Lammers, I. Boettcher, and C. Wetterich, Phys. Rev. A **93**, 063631 (2016).
[390] M. Olshanii, Phys. Rev. Lett. **81**, 938 (1998).
[391] T. Bergeman, M. G. Moore, and M. Olshanii, Phys. Rev. Lett. **91**, 163201 (2003).
[392] I. S. Gradshteyn and I. M. Ryzhik, *Table of integrals, series, and products* (Academic press, Boston, 2014).
[393] T. Kinoshita, T. Wenger, and D. S. Weiss, Science **305**, 1125 (2004).
[394] V. A. Yurovsky, M. Olshanii, and D. S. Weiss, in , Vol. 55, edited by E. Arimondo, P. R. Berman, and C. C. Lin, Advances In Atomic, Molecular, and Optical Physics (Academic Press, 2008), pp. 61–138.
[395] E. Haller, M. J. Mark, R. Hart, J. G. Danzl, L. Reichsöllner, V. Melezhik, P. Schmelcher, and H.-C. Nägerl, Phys. Rev. Lett. **104**, 153203 (2010).
[396] V. S. Melezhik and P. Schmelcher, Phys. Rev. A **84**, 042712 (2011).
[397] P. Giannakeas, F. K. Diakonos, and P. Schmelcher, Phys. Rev. A **86**, 042703 (2012).
[398] M. Holten, L. Bayha, A. C. Klein, P. A. Murthy, P. M. Preiss, and S. Jochim, Phys. Rev. Lett. **121**, 120401 (2018).
[399] R. Duine and H. Stoof, Physics Reports **396**, 115 (2004).
[400] U. Fano, Phys. Rev. **124**, 1866 (1961).
[401] H. Feshbach, Annals of Physics **5**, 357 (1958).
[402] H. Feshbach, Annals of Physics **19**, 287 (1962).
[403] E. Tiesinga, B. J. Verhaar, and H. T. C. Stoof, Phys. Rev. A **47**, 4114 (1993).
[404] C. E. Klauss, X. Xie, C. Lopez-Abadia, J. P. D'Incao, Z. Hadzibabic, D. S. Jin, and E. A. Cornell, Phys. Rev. Lett. **119**, 143401 (2017).
[405] E. Nicklas, H. Strobel, T. Zibold, C. Gross, B. A. Malomed, P. G. Kevrekidis, and M. K. Oberthaler, Phys. Rev. Lett. **107**, 193001 (2011).
[406] P. Engels, C. Atherton, and M. A. Hoefer, Phys. Rev. Lett. **98**, 095301 (2007).
[407] M. Theis, G. Thalhammer, K. Winkler, M. Hellwig, G. Ruff, R. Grimm, and J. H. Denschlag, Phys. Rev. Lett. **93**, 123001 (2004).
[408] P. A. Ruprecht, M. J. Holland, K. Burnett, and M. Edwards, Phys. Rev. A **51**, 4704 (1995).
[409] A. G. D. Maestro and M. J. P. Gingras, Journal of Physics: Condensed Matter **16**, 3339 (2004).
[410] M. A. Cazalilla, R. Citro, T. Giamarchi, E. Orignac, and M. Rigol, Rev. Mod. Phys. **83**, 1405 (2011).
[411] M. A. García-March, B. Juliá-Díaz, G. E. Astrakharchik, J. Boronat, and A. Polls, Phys. Rev. A **90**, 063605 (2014).

[412] M. A. Garcia-March and T. Busch, Phys. Rev. A **87**, 063633 (2013).
[413] M. A. Garcia-March, B. Juliá-Díaz, G. E. Astrakharchik, T. Busch, J. Boronat, and A. Polls, Phys. Rev. A **88**, 063604 (2013).
[414] M. A. García-March, B. Juliá-Díaz, G. E. Astrakharchik, T. Busch, J. Boronat, and A. Polls, New Journal of Physics **16**, 103004 (2014).
[415] L. A. P. Ardila and S. Giorgini, Phys. Rev. A **92**, 033612 (2015).
[416] G. E. Astrakharchik and S. Giorgini, Phys. Rev. A **66**, 053614 (2002).
[417] S. R. White, Phys. Rev. Lett. **69**, 2863 (1992).
[418] S. R. White, Phys. Rev. B **48**, 10345 (1993).
[419] U. Schollwöck, Rev. Mod. Phys. **77**, 259 (2005).
[420] U. Schollwöck, Annals of Physics **326**, January 2011 Special Issue, 96 (2011).
[421] S. P. Rath and R. Schmidt, Phys. Rev. A **88**, 053632 (2013).
[422] A. G. Volosniev, H.-W. Hammer, and N. T. Zinner, Phys. Rev. A **92**, 023623 (2015).
[423] G. Kordas, S. I. Mistakidis, and A. I. Karanikas, Phys. Rev. A **90**, 032104 (2014).
[424] W. Li and S. Das Sarma, Phys. Rev. A **90**, 013618 (2014).
[425] S. Krönke, L. Cao, O. Vendrell, and P. Schmelcher, New J. Phys. **15**, 063018 (2013).
[426] L. Cao, S. Krönke, O. Vendrell, and P. Schmelcher, J. Chem. Phys. **139**, 134103 (2013).
[427] L. Cao, V. Bolsinger, S. I. Mistakidis, G. M. Koutentakis, S. Krönke, J. M. Schurer, and P. Schmelcher, J. Chem. Phys. **147**, 044106 (2017).
[428] V. J. Bolsinger, S. Krönke, and P. Schmelcher, Journal of Physics B: Atomic, Molecular and Optical Physics **50**, 034003 (2017).
[429] H.-D. Meyer, U. Manthe, and L. Cederbaum, Chemical Physics Letters **165**, 73 (1990).
[430] M. Beck, A. Jäckle, G. Worth, and H.-D. Meyer, Physics Reports **324**, 1 (2000).
[431] H. Wang, The Journal of Physical Chemistry A **119**, 7951 (2015).
[432] H. R. Larsson, The Journal of Chemical Physics **151**, 204102 (2019).
[433] H. R. Larsson, Molecular Physics **122**, e2306881 (2024).
[434] H. Wang and M. Thoss, The Journal of Chemical Physics **131**, 024114 (2009).
[435] U. Manthe and T. Weike, The Journal of Chemical Physics **146**, 064117 (2017).
[436] F. Köhler, R. Mukherjee, and P. Schmelcher, Phys. Rev. Res. **5**, 023135 (2023).
[437] A. I. Streltsov, O. E. Alon, and L. S. Cederbaum, Phys. Rev. Lett. **99**, 030402 (2007).
[438] O. E. Alon, A. I. Streltsov, and L. S. Cederbaum, Phys. Rev. A **77**, 033613 (2008).
[439] A. I. Streltsov, O. E. Alon, and L. S. Cederbaum, Phys. Rev. A **81**, 022124 (2010).
[440] A. I. Streltsov, O. E. Alon, and L. S. Cederbaum, Phys. Rev. A **73**, 063626 (2006).

[441] A. I. Streltsov, O. E. Alon, and L. S. Cederbaum, Phys. Rev. Lett. **100**, 130401 (2008).

[442] A. I. Streltsov, O. E. Alon, and L. S. Cederbaum, Phys. Rev. Lett. **106**, 240401 (2011).

[443] A. I. Streltsov, K. Sakmann, O. E. Alon, and L. S. Cederbaum, Phys. Rev. A **83**, 043604 (2011).

[444] K. Sakmann, A. I. Streltsov, O. E. Alon, and L. S. Cederbaum, Phys. Rev. Lett. **103**, 220601 (2009).

[445] K. Sakmann, A. I. Streltsov, O. E. Alon, and L. S. Cederbaum, Phys. Rev. A **82**, 013620 (2010).

[446] K. Sakmann, A. I. Streltsov, O. E. Alon, and L. S. Cederbaum, Phys. Rev. A **89**, 023602 (2014).

[447] G. M. Koutentakis, S. I. Mistakidis, and P. Schmelcher, New Journal of Physics **21**, 053005 (2019).

[448] L. Cao, S. I. Mistakidis, X. Deng, and P. Schmelcher, Chemical Physics **482**, Electrons and nuclei in motion - correlation and dynamics in molecules (on the occasion of the 70th birthday of Lorenz S. Cederbaum), 303 (2017).

[449] G. C. Katsimiga, G. M. Koutentakis, S. I. Mistakidis, P. G. Kevrekidis, and P. Schmelcher, New Journal of Physics **19**, 073004 (2017).

[450] S. I. Mistakidis, L. Cao, and P. Schmelcher, Journal of Physics B: Atomic, Molecular and Optical Physics **47**, 225303 (2014).

[451] S. I. Mistakidis, L. Hilbig, and P. Schmelcher, Phys. Rev. A **100**, 023620 (2019).

[452] S. I. Mistakidis, G. C. Katsimiga, G. M. Koutentakis, T. Busch, and P. Schmelcher, Phys. Rev. Research **2**, 033380 (2020).

[453] K. M. Mittal, S. I. Mistakidis, P. G. Kevrekidis, and P. Schmelcher, Phys. Rev. A **102**, 013302 (2020).

[454] Y. Gwak, O. V. Marchukov, and U. R. Fischer, Annals of Physics **434**, 168592 (2021).

[455] G. M. Koutentakis, S. I. Mistakidis, and P. Schmelcher, Atoms **10**, 10.3390/atoms10010003 (2022).

[456] F. Brauneis, T. G. Backert, S. I. Mistakidis, M. Lemeshko, H.-W. Hammer, and A. G. Volosniev, New Journal of Physics **24**, 063036 (2022).

[457] G. M. Koutentakis, S. I. Mistakidis, and P. Schmelcher, New Journal of Physics **21**, 053005 (2019).

[458] S. Krönke, J. Knörzer, and P. Schmelcher, New Journal of Physics **17**, 053001 (2015).

[459] A. Peres, *Quantum theory: concepts and methods*, Vol. 57 (Springer Science & Business Media, 2006).

[460] J. Broeckhove, L. Lathouwers, E. Kesteloot, and P. Van Leuven, Chemical Physics Letters **149**, 547 (1988).

[461] A. McLachlan, Molecular Physics **8**, 39 (1964).

[462] J. Frenkel, *Wave mechanics*, Bd. 1 (Clarendon Press, 1932).

[463] P. A. M. Dirac, Mathematical Proceedings of the Cambridge Philosophical Society **26**, 376 (1930).

[464] G. Ferioli, G. Semeghini, S. Terradas-Briansó, L. Masi, M. Fattori, and M. Modugno, Phys. Rev. Research **2**, 013269 (2020).

[465] A. Cappellaro, T. Macrí, and L. Salasnich, Phys. Rev. A **97**, 053623 (2018).

[466] X. Cui and Y. Ma, Phys. Rev. Research **3**, L012027 (2021).

[467] S. R. Otajonov, E. N. Tsoy, and F. K. Abdullaev, Phys. Lett. A **383**, 125980 (2019).

[468] I. Morera, G. E. Astrakharchik, A. Polls, and B. Juliá-Díaz, Phys. Rev. Research **2**, 022008 (2020).

[469] A. Debnath, A. Khan, and S. Basu, Phys. Lett. A, 128137 (2022).

[470] A. U. J. Lode, C. Lévêque, L. B. Madsen, A. I. Streltsov, and O. E. Alon, Rev. Mod. Phys. **92**, 011001 (2020).

[471] T. Ilg, J. Kumlin, L. Santos, D. S. Petrov, and H. P. Büchler, Phys. Rev. A **98**, 051604 (2018).

[472] J. C. Pelayo, G. Bougas, T. Fogarty, T. Busch, and S. I. Mistakidis, SciPost Phys. **18**, 129 (2025).

[473] M. Wenzel, T. Pfau, and I. Ferrier-Barbut, Physica Scripta **93**, 104004 (2018).

[474] X. Zhang, X. Xu, Y. Zheng, Z. Chen, B. Liu, C. Huang, B. A. Malomed, and Y. Li, Phys. Rev. Lett. **123**, 133901 (2019).

[475] J. C. Pelayo, T. Fogarty, T. Busch, and S. I. Mistakidis, Phys. Rev. Res. **6**, 033219 (2024).

[476] M. N. Tengstrand, P. Stürmer, E. Ö. Karabulut, and S. M. Reimann, Phys. Rev. Lett. **123**, 160405 (2019).

[477] K. Keiler, S. I. Mistakidis, and P. Schmelcher, Phys. Rev. A **104**, L031301 (2021).

[478] F. Ancilotto, M. Barranco, and M. Pi, Phys. Rev. A **107**, 063312 (2023).

[479] P. Zin, M. Pylak, T. Wasak, M. Gajda, and Z. Idziaszek, Phys. Rev. A **98**, 051603 (2018).

[480] L. Chergui, J. Bengtsson, J. Bjerlin, P. Stürmer, G. M. Kavoulakis, and S. M. Reimann, Phys. Rev. A **108**, 023313 (2023).

[481] G. C. Katsimiga, S. I. Mistakidis, G. N. Koutsokostas, D. J. Frantzeskakis, R. Carretero-González, and P. G. Kevrekidis, Phys. Rev. A **107**, 063308 (2023).

[482] G. C. Katsimiga, S. I. Mistakidis, B. A. Malomed, D. J. Frantzeskakis, R. Carretero-Gonzalez, and P. G. Kevrekidis, Condensed Matter **8**, `https://doi.org/10.3390/condmat8030067` (2023).

[483] V. Cikojevi ć, L. V. š. Marki ć, M. Pi, M. Barranco, F. Ancilotto, and J. Boronat, Phys. Rev. Res. **3**, 043139 (2021).

[484] S. Chandramouli, S. I. Mistakidis, G. C. Katsimiga, and P. G. Kevrekidis, Phys. Rev. A **110**, 023304 (2024).

[485] T. Duong Anh-Tai, M. A. García-March, T. Busch, and T. Fogarty, New Journal of Physics **27**, 073201 (2025).

[486] T. D. Anh-Tai, T. Fogarty, S. de María-García, T. Busch, and M. A. García-March, Phys. Rev. Res. **6**, 043042 (2024).

[487] F. Theel, S. I. Mistakidis, and P. Schmelcher, SciPost Phys. **16**, 023 (2024).

Eidesstattliche Versicherung / Declaration of oath

I hereby declare and affirm that this doctoral dissertation is my own work and that I have not used any aids and sources other than those indicated.

If electronic resources based on generative artificial intelligence (gAI) were used in the course of writing this dissertation, I confirm that my own work was the main and value-adding contribution and that complete documentation of all resources used is available in accordance with good scientific practice. I am responsible for any erroneous or distorted content, incorrect references, violations of data protection and copyright law or plagiarism that may have been generated by the gAI.

Hamburg,

June 26, 2026

Date

Ilias ENGLEZOS